EPFL

Numerical and Experimental Investigations on Non-Contacting Seals for Small-Scale Applications

Suresh KATUWAL CHHETRI

■ École
polytechnique
fédérale
de Lausanne

2020

"When a man dwells on the pleasure of sense, attraction for them arises in him.
From attraction arises desire, the lust of possession, and this leads to passion, to anger.

From passion comes confusion of mind, then loss of remembrance, the forgetting of duty.
From this loss comes the ruin of reason, and the ruin of reason leads man to destruction."

— Bhagavad Gita

" Dedicated to my beloved late father *Nanda Bahadur Katuwal Chhetri* and beloved
late grandfather *Chandra Bahadur Katuwal Chhetri* "

Acknowledgements

Firstly I would like to express my sincere gratitude and a very big thank you to my supervisor Prof. Jürg Schiffmann for allowing me to do PhD at LAMD - EPFL, all the support, and encouragement he gave me during my PhD work. Without his guidance, constant feedback and work freedom this PhD would not have been achievable.

I'm grateful to Prof. Jean-Claude Badoux and Prof. John Cannell for all the continuous supports, motivations, and guidance not only on technical but also on a personal level for more than 15 years of my life journey. Both of you are and will be a true source of inspiration for me. Furthermore, I would like to thank my jury members Prof. Steven Chatterton, Prof. Daniel Weiss, Dr. Peter Ott and Dr. Jan Van Herle for their valuable suggestions on my thesis.

How can I forget my Boros Dr. Markus Diehl and Dr. Philipp Bättig. You guys are simply awesome (my gurus, Swiss bank, motivators, best friends, and brothers from another mother). In short, I had a wonderful time with both of you. Also a big thank you goes to Nikola Huguelet for your help, yummy food and of course playing 'JACKPOT'.

Thank you so much, Dr. Christoph Schreiber and Dr. Karim Shalash for pushing me out of the comfort zone and helping me with your constructive suggestions. Furthermore, I would like to thank Dr. Patrick Wagner and Dr. Lili Gu for helping me out in my hardest phase of life. I'm indebted to your help and support for my whole life. Many thanks go to Dr. Julie Lenoble for taking care of administrative work. Without your help, my stay in Switzerland would not be comfortable.

I like to thank Christophe Pham for his professional help in the design and building of the test-rig. Thank you for listening to me and being my translator in the workshop. Without your help, test-rig would not be in the present state. Also, many thanks to Marcel who helped to build the electrical cabinet of the test-rig. Also, a big thank you goes to Thierry Mesot who helped me with the LabVIEW user interface for tracking, recording, and controlling the test-rig. Big thanks to the former and current lab members (Adeel, Ansgar, Antonio, Bi, Ceyhun, Cyril, Eliott, Eric, Kévin, Kossi, Luis, Nathaniel, Sajjad, Soheyl, Tomohiro, Victoria, and Wanhui) for their help and company during my stay in the lab.

Acknowledgements

Neuchâtel, June 2020
Suresh Katuwal Chhetri

Abstract

Dynamic non-contacting seals have been identified as the most appropriate sealing technology for reduced-scale and high-speed turbomachinery applications since they provide a clearance gap preventing rotor-to-seal contact during operation. Yet, any clearance, however small, between rotor and seal permits the passage to fluid flow across regions of unequal pressure as a leakage which penalize the overall system efficiency.

A thorough theoretical and experimental investigation of these types of gas seal at a reduced scale, however, is missing today. Furthermore, in thermodynamic cycles, fluids often operate within the vicinity of the saturation line where the well-known ideal gas law is not valid. For reduced-scale turbomachinery seals operating close to the fluid saturation line, validated models to capture the real gas effects are not available yet. The aim of this thesis is to address these shortcomings.

Initially, a qualitative research approach has been used for the selection of the ideal seals for reduced-scale applications. Using the qualitative data available from the literature of large-scale seals, a weighted decision matrix has been implemented. For assessing the robustness of the selection process, the sensitivity analysis has been carried out by using different weight distributions. The top two ranked seals, namely, Hole Pattern Seal (HPS) and Pocket Damper Seal (PDS), have been identified as the most promising seals for reduced-scale turbomachinery applications due to their low leakage rates and their low influence on the rotordynamic system.

In order to predict the seal performance, the commonly used bulk-flow approach has been used for the numerical modeling approach. The seal models developed by the author considering the real gas properties along with the governing equations, assumptions, empirical factors and the solving scheme have been discussed. Furthermore, for the comparison purpose, three different state-of-the-art models have been implemented. As a benchmark, the predicted results from the different models are compared with the experimental data of well-established literature. A good agreement between the different seal models and the experimental data has been observed.

A dedicated hermetic test-rig for the experimental investigations on the reduced-scale seal has been designed and built. A modular test section design has been adopted to

Abstract

test different types and sizes of seals. The salient features of the test-rig are tunable inlet and outlet pressure, tunable inlet temperature for the identification of real gas effects, fluid changeability, leakage measurement, as well as pressure and temperature measurement within individual seal cavities.

Six different reduced-scale seals, both on cylindrical and conical cross-section, have been investigated experimentally at different inlet boundary conditions with R134a and air. The experimental data for different seals were compared between the predicted results from the developed models as a validation process. Compared to the-state-of-the-art models, the author's model demonstrates a superior prediction quality in terms of leakage, cavity pressure, and temperature distribution in all test cases. The author's model shows an overall maximum deviation of $< 2\%$ and 5% in leakage on cylindrical and conical seals respectively with R134a at all tested inlet pressure and over the entire range of pressure ratios. For the air test, a maximum deviation of 4% can be observed with the author's model. This corresponds to a significant improvement compared to the state-of-the-art models (up to 20% deviation) since the author's model cuts the deviation to experimental data by 10 to 15%. The cavity pressure distribution showed an overall average deviation of 3% and 6% on the cylindrical and conical seals respectively. The cavity temperature distribution indicated up to 1 and 1.5 K overall average deviation on the cylindrical and the conical seals respectively. The Hole Pattern Seal (HPS) has been identified as the most effective seal for reduced-scale applications with 20% and 10% relatively lower leakage rates with R134a and air respectively compared to the baseline Smooth Seal (SS). The four-teeth Labyrinth seal with varying cavity pitch (LSVP4T) yields less leakage compared to the five-teeth Labyrinth seal with constant cavity pitch (LSCP5T). Thus, the existence of the optimum geometrical features on the seal with identical length and identical clearance has been highlighted.

Finally, experimental data suggests a strong impact of the real gas effects on leakage. Compared to a high degree of superheat the leakage increases by up to 10% for an operation close to the saturation line. The author's model shows better prediction quality at different degrees of superheat compared to state-of-the-art models and demonstrates its ability to capture the real gas effect.

Keywords: Reduced-scale seal, Real gas effect, Seal model, Leakage, Cavity Pressure, Cavity temperature, Experimental investigation, Model validation, Superheat, R134a

iv

Zusammenfassung

Dynamische, berührungslose Dichtungen wurden als die am meisten geeignete Dichtungslösung für die Anwendung in Miniatur und Hochgeschwindigkeits-Turbomaschinen identifiziert, da sie über radiales Spiel verfügen, welches eine Berührung zwischen Rotor und Dichtung im Betrieb verhindert. Jedes noch so kleine radiale Spiel in der Dichtung erlaubt jedoch das Durchströmen von Fluid, getrieben durch Druckdifferenzen, was zu einer Verminderung des Gesamt-System-Wirkungsgrades führt.

Eine ausführliche theoretische und experimentelle Untersuchung dieser Art von berührungslosen Gas-Dichtungen im Miniatur-Bereich fehlt zum heutigen Zeitpunkt. Des Weiteren befindet sich ein Fluid, welches einen thermodynamischen Zyklus durchläuft, oftmals nahe der Sättigungsgrenze, was dazu führt, dass die Bedingungen zur Anwendung des Idealgasgesetzes nicht erfüllt sind. Validierte Modelle zur Bestimmung der Realgas-Effekte bei Miniatur-Turbomaschinen-Dichtungen, welche nahe der Sättigungsgrenze betrieben werden, existieren zum heutigen Zeitpunkt noch nicht. Diese Dissertation hat zum Ziel, sich diesen Mängeln anzunehmen.

Der Einstieg in diese Arbeit beinhaltete die Anwendung einer qualitativen Forschungsmethode, um den idealen Dichtungstyp für Miniaturanwendungen zu identifizieren. Die Benutzung der in der Literatur verfügbaren qualitativen Daten für Grossanwendungen erlaubte die Implementierung einer gewichteten Entscheidungsmatrix. Eine Variation der Gewichtungsparameter erlaubte die Durchführung einer Sensitivitätsanalyse des Selektierungsprozesses. Die beiden bestbewerteten Dichtungstypen, die Hole Pattern Seal (HPS) und die Pocket Damper Seal (PDS), wurden augrund ihrer geringen Leckagemassenströme und ihres geringen Einflusses auf die Rotordynamik des Systems als die vielversprechendsten Kandidaten für die Anwendung in Miniatur-Turbomaschinen identifiziert.

Ein hermetisch abgedichteter Prüfstand wurde speziell für die experimentelle Untersuchung der berührungslosen Miniatur-Dichtungen konzipiert und gebaut. Das modulare Design der Testsektion erlaubte die Untersuchung von unterschiedlichen Dichtungstypen und -grössen. Die herausstechenden Eigenschaften dieses eigens für die Untersuchung von Miniatur-Dichtungen konzipierten Prüfstandes sind die frei einstellbaren Werte für Einlass- und Auslassdruck, der einstellbaren Einlasstemperatur zur Identifizierung von Realgas-Effekten, der Möglichkeit verschiedene Fluide zu testen, die Messung des Leckagemassenstromes sowie der Messung von Druck und

Zusammenfassung

Temperatur in den einzelnen Kavitäten der Dichtung.

Die Eigenschaften von sechs unterschiedlichen Miniatur-Dichtungstypen mit jeweils zylindrischem sowie konischem Querschnitt wurden bei unterschiedlichen Randbedingungen mit R134a und Luft als Fluid experimentell untersucht. Die experimentellen Resultate der verschiedenen Dichtungen wurden zu Validierungszwecken mit den Berechnungsresultaten der in dieser Arbeit entwickelten numerischen Modelle verglichen. Im Vergleich mit den bekannten, dem Stand der Technik entsprechenden, Modellen zeigt das vom Autor vorgestellte Modell eine verbesserte Qualität in der Vorhersage der Leckagemassenströme sowie der Druck- und der Temperaturverteilung in den Kavitäten der Dichtung für alle untersuchten Fälle. Das vom Autor entwickelte Modell zeigt eine maximale Gesamtabweichung für die Vorhersage des Leckagemassenstromes von <2% für zylindrische und <5% für konische Dichtungsquerschnitte mit R134a als Fluid über den gesamten getesteten Bereich von Einlassdrücken und Druckverhältnissen. Bei den experimentellen Untersuchungen mit Luft als Fluid konnte eine maximale Abweichung von 4% mit dem vom Autor vorgestellten Modell bezeichnet werden. Dies entspricht einer signifikanten Verbesserung der Vorhersagequalität verglichen mit den bisher bekannten Modellen. Das in dieser Arbeit vorgestellte Modell reduziert die Abweichung zu den experimentellen Daten um 10% bis 15% verglichen mit den bisher bekannten Modellen (bis zu 20% Abweichung). Die Druckverteilung in den Kavitäten zeigte eine durchschnittliche Gesamtabweichung von 3% für die zylindrischen und 6% für die konischen Dichtungsquerschnitte. Die Abweichung der Temperaturverteilung in den Kavitäten konnte mit 1K für die zylindrischen respektive 1.5K für die konischen Dichtungsquerschnitte beziffert werden. Die Hole Pattern Seal (HPS) konnte mit einem verringerten Leckagemassenstrom von 20% für den zylindrischen respektive 10% für den konischen Dichtungsquerschnitt in R134a sowie in Luft, verglichen mit der als Referenz dienenden Smooth Seal (SS), als effektivster Dichtungstyp identifiziert werden. Des Weiteren konnte in dieser Arbeit gezeigt werden, dass die 4-Zahn Labyrinth-Dichtung mit variierendem Zahn-Abstand (LSVP4T) weniger Leckage aufweist als eine 5-Zahn Labyrinth-Dichtung mit konstantem Zahn-Abstand (LSCP5T). Dies verdeutlicht, dass für Dichtungen mit identischen Längen und Radialspielen eine optimale Geometrie existiert.

Die experimentellen Daten weisen auf einen starken Einfluss der Realgas-Effekte auf die Leckagemassenströme hin. Verglichen mit einem stark überhitzten Fluid, der Einsatz des Fluids nahe der Sättigungslinie führt zu einer Erhöhung der Leckagemassenströme um bis zu 10%. Das vom Autor dieser Arbeit vorgestellte Modell verfügt über bessere Vorhersagequalität für überhitzte Zustände unterschiedlichen Grades verglichen mit den aktuell verfügbaren Modellen und verdeutlicht daher seine Eignung zur Erfassung von Realgas-Effekten.

Schlüsselworte: Miniatur-Dichtung, Realgas-Effekt, Dichtungsmodell, Leckage, Druck in Kavität, Temperatur in Kavität, Experimentelle Untersuchung, Modellvalidierung, Überhitzung, R134a

Résumé

Les joints dynamiques sans contact ont été identifiés comme la technologie d'étanchéité la plus appropriée pour les applications de turbomachines à échelle réduite et grande vitesse, car ils permettent un dégagement empêchant le contact entre le rotor et le joint en fonctionnement. Pour l'instant, tout dégagement aussi petit soit-il entre le rotor et le joint permet le passage du fluide à travers les régions de pression inégale, comme une fuite qui pénalise l'efficacité globale du système.

Cependant, une étude théorique et expérimentale approfondie des différents types de joints à gaz d'échelle réduite fait défaut aujourd'hui. De plus, dans les cycles thermodynamiques, les fluides opèrent souvent à proximité de la ligne de saturation où la loi des gaz parfaits n'est pas valable. Pour les joints de turbomachines à échelle réduite fonctionnant à proximité de la ligne de saturation du fluide, aucun modèle valide pour saisir les effets réels des gaz n'est disponible pour le moment. L'objectif de cette thèse est de remédier à ces lacunes.

Au départ, une approche de recherche qualitative a été utilisée pour la sélection d'un joint idéal pour les applications d'échelle réduite. En utilisant les données qualitatives disponibles dans la littérature sur les joints à grande échelle, une matrice de décision pondérée a été mise en place. Pour l'évaluation de la robustesse du processus de sélection, l'analyse de sensibilité a été réalisée en utilisant différentes pondérations. Les deux joints les mieux classés, à savoir le type Hole Pattern Seal (HPS) et Pocket Damper Seal (PDS), ont été identifiés comme les joints les plus prometteurs pour les applications de turbomachines à échelle réduite, en raison de leur faible taux de fuite et de leur faible influence sur le comportement dynamique du rotor.

Afin de prédire la performance des joints, l'approche en vrac a été utilisée pour la modélisation numérique. Les modèles de joints développés par l'auteur, en considérant les propriétés réelles du gaz, les équations qui le régissent, Les hypothèses, les facteurs empiriques ainsi que le schéma de résolution ont été remis en question. En outre, à des fins de comparaison, trois modèles de pointe différents ont été mis en œuvre. À titre de test, les résultats attendus des différents modèles ont été comparés par rapport aux données expérimentales de la littérature bien établie. Un bon accord a été observé entre les différents modèles de joints et les données expérimentales.

Un banc d'essai hermétique dédié aux études expérimentales à échelle réduite a été

développé et fabriqué. Une conception modulaire de la section d'essai a été adoptée afin de tester différents types et tailles de joints. Les principales caractéristiques du banc d'essai sont réglables telles que la pression à l'entrée et à la sortie, la température à l'entrée est ajustable pour l'identification des effets réels du gaz ainsi que la variabilité du fluide et la mesure des fuites. La pression et la température sont également mesurées dans les cavités individuelles des joints.

Six différents joints d'échelle réduite, de section cylindrique et conique, ont été étudiés expérimentalement à différentes conditions d'entrées du système avec du gaz R134a et de l'air. Les données expérimentales pour les différents joints ont été comparées avec les résultats obtenus des modèles développés en tant que processus de validation. Par rapport aux modèles de la littérature, le modèle de l'auteur démontre une qualité de prédiction supérieure en termes de fuite, de pression dans la cavité et de répartition de la température dans tous les cas d'essai. Le modèle de l'auteur montre un écart maximum global inférieur à 2% et 5% de fuite sur les joints cylindriques et respectivement coniques avec du gaz R134a pour toutes les pressions d'entrée testées, et également sur toute la gamme de rapports de pression. Pour l'essai dans l'air, un écart maximal de 4% a été observé. Avec le modèle de l'auteur cela correspond à une amélioration significative par rapport aux modèles de la littérature (jusqu'à 20% d'écart) puisqu'il réduit l'écart global de 10 à 15%. La distribution de pression dans la cavité montre une déviation moyenne de 3% et 6% pour les joints cylindriques, respectivement coniques. La distribution de température à l'intérieur de la cavité indique un écart moyen de 1 et 1,5 K pour un joint cylindrique, respectivement conique. Le type Hole Pattern Seal (HPS) a été identifié comme le type de joint le plus efficace pour les applications à échelle réduite, en comparaison au type de joint Smooth Seal (SS) avec 20% et 10% de fuite en moins en utilisant du gaz R134a, respectivement de l'air. Pour le joint labyrinthe à quatre dents et avec un pas de cavité variable (LSVP4T), il en résulte moins de fuite par rapport au joint labyrinthe avec un pas de cavité constant (LSCP5T) et 5 dents. Ainsi, l'existence de caractéristiques géométriques optimales pour un joint avec des longueurs et jeux identiques ont été mis en évidence.

Enfin, les données expérimentales suggèrent un important impact des effets réels du gaz sur les fuites. En comparaison à un degré élevé de surchauffe, le débit de fuite augmente jusqu'à 10% pour un fonctionnement proche de la ligne de saturation. Le modèle de l'auteur montre une meilleure qualité de prédiction à différents niveaux de surchauffe, par rapport aux modèles de la littérature et démontre sa capacité à capter l'effet réel du gaz.

Mots-clés : Joint d'échelle réduite, Effet réel des gaz, Modèles de joints, Fuite, Pression dans la cavité, Température dans la cavité, Recherche expérimentale, Validation de modèles, Surchauffe, Gaz R134a

Contents

Contents

Contents

List of Figures

List of Figures

List of Tables

Nomenclature

Acronyms

1D   One-dimensional

2D   Two-dimensional

3D   Three-dimensional

Adiab Adiabtic

CFD   Computational fluid dynamics

CTU   Compressor and turbine unit

CV   Control volume

EDM   Electrical discharge machining

HCS   Honeycomb seal

HP-ORCS Heat pump-organic rankine cycle

HPS   Hole pattern seal

HVAC Heating ventilation and air conditioning

ID   Inner diameter

LSCP4T Labyrinth seal constant pitch four teeth

LSCP5T Labyrinth seal constant pitch five teeth

LSVP4T Labyrinth seal varying pitch four teeth

NT   Number of teeth

OD   Outer diameter

PDS   Pocket damper seal

QRM   Qualitative research method

Nomenclature

RDev   Relative deviation

Rel   Relative

RHS   Right hand side

SA   Sensitivity analysis

SS   Smooth seal

VFD   Variable frequency drive

Greek Symbols

γ Specific heat capacity ratio $\frac{c_p}{c_v}$, [-]

μ Kinetic energy carry-over coefficient, [-]

ν Kinematic viscosity, $\left[\frac{m^2}{s}\right]$

Ω Whirl speed, $\left[\frac{rad}{s}\right]$

ω Rotational speed, $\left[\frac{rad}{s}\right]$

ρ Density, $\left[\frac{kg}{m^3}\right]$

τ Shear stress, [Pa]

θ Circumferential coordinate, [-]

Υ Asperity ratio, [-]

Roman Symbols

$\dot{m}$ Leakage mass flowrate, $\left[\frac{kg}{s}\right]$

$\dot{m}_{nonD}$ Non-dimensional leakage, [-]

$\dot{V}$ Volume flow, $\left[\frac{m^3}{s}\right]$

A Cross-sectional area, $[m^2]$

a_r Rotor dimensionless cavity length, [-]

a_s Seal dimensionless cavity length, [-]

B Cavity / hole depth, $[m]$

C_d Discharge coefficient, [-]

C_{in} Speed of sound at seal inlet, $\left[\frac{m}{s}\right]$

C_{XX} Direct damping coefficient in x direction, $\left[\frac{Ns}{m}\right]$

C_{XY} Cross-coupled damping coefficient in x direction, $\left[\frac{Ns}{m}\right]$

C_{YX} Cross-coupled damping coefficient in y direction, $\left[\frac{Ns}{m}\right]$

C_{YY} Direct damping coefficient in y direction, $\left[\frac{Ns}{m}\right]$

D_r Diameter of rotor, $[m]$

D_s Specific diameter, [-]

D_{imp} Diameter of an impeller, $[m]$

Dh Hydraulic diameter, $[m]$

e Total energy, $\left[\frac{J}{kg}\right]$

e_s, e_r Absolute seal and rotor roughness, $[m]$

f_s, f_r Seal and rotor friction factor, $[m]$

h Enthalpy, $\left[\frac{J}{kg}\right]$

L Cavity pitch, $[m]$

L_s Seal axial length, $[m]$

M Mach number, [-]

N_s Specific speed, [-]

P Pressure, $[Pa]$

P_r Power of rotor, $[kW]$

R Specific gas constant, $\left[\frac{J}{kgK}\right]$

R_{clr} Steady radial clearance, $[m]$

R_r Rotor radius, $[m]$

Re Reynolds number, [-]

S Entropy, $\left[\frac{J}{kgK}\right]$

s Teeth pitch, $[m]$

T Temperature, $[K]$

t_w Teeth width, $[m]$

Nomenclature

w Tooth width, $[m]$

U Circumferential velocity, $\left[\frac{m}{s}\right]$

u Internal energy, $\left[\frac{J}{kg}\right]$

V_{rel} Relative velocity, $\left[\frac{m}{s}\right]$

V Axial velocity, $\left[\frac{m}{s}\right]$

W Radial velocity, $\left[\frac{m}{s}\right]$

Subscripts

cav   Cavity

exp   Experiment

i $i^{th}cavity$

in   Inlet

isen   Isentropic

out   Outlet

r   Rotor

rel   Relative

s   Seal

st   Static

T   Teeth

tot   Total

1 Introduction

The downscaling trend of turbomachinery has been in the focus of research for the last decade driven by various applications in different fields. Reduced-scale turbo-machinery has been identified as a promising key technology for highly efficient decentralized energy conversion. Downscaled turbomachinery may be implemented for example as compressors for residential heating and cooling [1, 2], for air conditioning in electric and hybrid vehicles, for fuel cell air supply and pressurization in transport application [3] or low scale decentralized electrical power generation [4]. Scaling laws for turbomachinery impose small tip diameters leading to smaller rotor diameters and higher rotational speeds needed to achieve reasonable efficiencies at reduced-scale. Due to the high rotor speeds and high life-time expectations, classical bearings such as roller element bearings are not suitable due to their contacting nature, hence contact-less gas-lubricated bearings are used instead. The advantages of this type of bearing technology are the oilfreeness, low losses, higher life-time and fewer components making them an ideal candidate for reduced-scale high-speed turbo-machinery applications. However, one issue related to the down-scaling of current technology is the relative leakage by-passing the turbomachinery, which is significantly higher compared to large-scale machines, mainly due to relatively low clearance required to mitigate leakage which is in the range of gas-bearing clearance leading to manufacturing limitations.

Seals are widely used in turbomachinery applications to control leakage flow. For high rotor speeds, contacting seals like radial lip or brush seals are not appropriate due to the frictional heat generated by the surface contact. Dynamic non-contacting seals have been identified as the most appropriate sealing technology for high-speed turbomachinery applications since they provide a clearance gap preventing rotor-to-stator contact during operation. Any clearance between rotor and seal permits the passage to fluid flow across regions of unequal pressure as a leakage which penalize the overall system efficiency.

1

Non-contacting gas seals like labyrinth seal, pocket damper seal, hole pattern seal etc. play a crucial role in the turbomachinery system by reducing or controlling leakage of fluid by creating a pressure loss through throttling. For high-speed turbomachinery applications, these seals have proven invaluable due to their leakage reduction characteristics and their non-contacting nature, which allows rotor speeds to be increased significantly [5]. A summary of different types of state-of-the-art non-contacting seals for gaseous fluids used in turbomachinery applications have been presented by Floyd [6] and by Flitney [7].

The primary function of non-contacting seal is to reduce leakage and hence increase system thermodynamic efficiency of the turbomachines. Despite the aforementioned advantage, field experience have clearly shown that these seals also affects the critical speeds and stability limits of a rotordynamic system [8, 9]. Non-contacting gas seals possess negligible added mass terms and seal forces for small rotor motion about centered position are generally represented by the reaction force model [10] as shown in equation (1.1).

$$-\begin{bmatrix} F_X \\ F_Y \end{bmatrix} = \begin{bmatrix} K_{XX} & K_{XY} \\ K_{YX} & K_{YY} \end{bmatrix} \cdot \begin{bmatrix} X \\ Y \end{bmatrix} + \begin{bmatrix} C_{XX} & C_{XY} \\ C_{YX} & C_{YY} \end{bmatrix} \cdot \begin{bmatrix} \dot{X} \\ \dot{Y} \end{bmatrix} \tag{1.1}$$

This equation (1.1) relates the seal forces due to rotor motion and velocity through direct (K_{XX}, K_{YY}, C_{XX}, C_{YY}) and cross-coupled (K_{XY}, K_{YX}, C_{XY}, C_{YX}) linear force coefficients [11]. For an accurate prediction of critical speeds and rotordynamic stability of rotating machinery, accurate values of seal force coefficient are necessary. From a rotordynamics point of view, seals with large positive direct damping coefficients (C_{XX}, C_{YY}) and low or null cross-coupled stiffness coefficients (K_{XY}, K_{YX}) are desired to reduce rotor vibration amplitudes and to improve the dynamic stability of high-speed rotors [12]. Figure 1.1 shows the geometry and interacting forces between the seal and rotor assembly. The forces which acts on the rotor from seals are categorized into radial (F_r) and tangential (F_t) components. The radial force component in gas seals arises from direct stiffness and cross-coupled damping coefficients which can be represented by an effective stiffness (K_{eff}) as shown in equation (1.2).

$$K_{eff} = K_{XX} + C_{XY} \cdot \Omega \tag{1.2}$$

The effective stiffness has a weak effect on rotordynamic stability but has a strong effect on the natural frequency and hence on critical speed of rotor [13]. For the gas seals cross-coupled damping coefficients are very small and its contribution to radial force is almost negligible [10, 13]. The tangential force arising from gas seal is de-stabilizing in nature. This force is a combination of direct damping and cross-coupled stiffness force coefficients which is characterized by effective damping and evaluated using
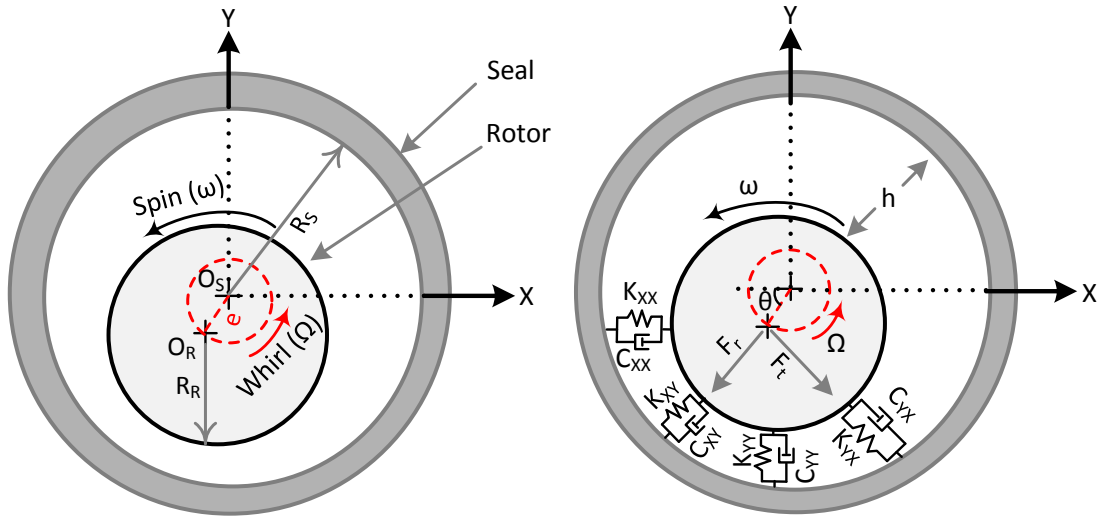
Figure 1.1 – Schematic representation of a seal and a rotor in a dynamic system: Spin and whirl motion of a rotor (right) and seal force coefficients (left)

equation (1.3).

$$C_{\text{eff}} = C_{\text{XX}} - \frac{K_{\text{XY}}}{\Omega} \qquad (1.3)$$

The tangential force is calculated by multiplying effective damping coefficient times the whirl orbit velocity. From the rotordynamic viewpoint, a positive value of effective damping is stabilizing while a negative value is de-stabilizing.

The undesirable effect on the dynamic stability of rotor systems can mainly be attributed to destabilizing cross-coupling stiffness that arises from circumferential flow in the annular cavities within the seals, which is driven by the rotor tip speed. This rotation of fluid amplifies rotor vibration by feeding energy into the whirl orbit resulting in instability [9, 10].

1.1 Overview of non-contacting gas seals

Non-contacting gas seals are dynamic seals that maximize pressure loss and minimize leakage by creating a barrier between moving and stationary surfaces. Although these types of seals are used to reduce leakage in turbomachinery applications, some leakage is inevitable due to the presence of a clearance gap together with pressure gradient. An

overview of the different types of the-state-of-the-art non-contacting seals for gaseous fluids used in large-scale turbomachinery application is illustrated in Figure 1.2.
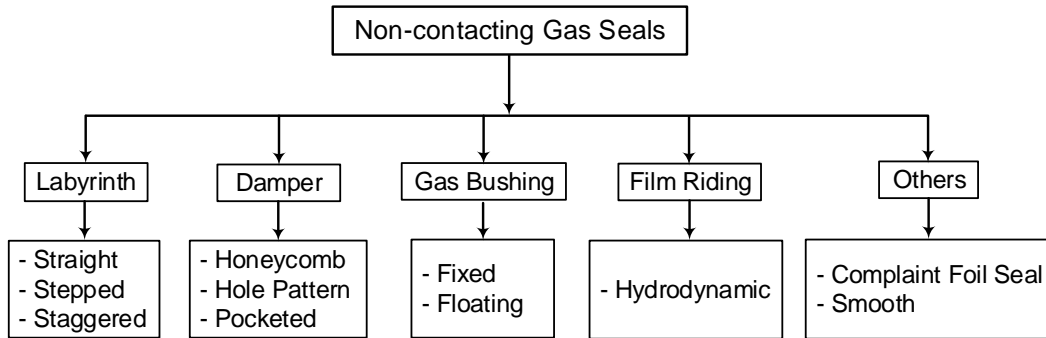
Figure 1.2 – Classification of the-state-of-the-art non-contacting gas seals

1.1.1 Labyrinth seal

Among many non-contacting seals, labyrinth seal offers advantages of simplicity but also yields the moderate leakage and lowest effective damping. Amongst varieties of non-contacting seals, labyrinth seals (LS) are the most widely used seals in turbomachinery applications due to their design simplicity and long past industrial knowledge. Although very effective in reducing leakage they possess undesirable rotordynamic characteristics, like, limited or even negative direct-damping and high cross-coupled stiffness coefficients that may lead to rotordynamic instability [14, 15]. This type of seal is composed of many grooves or teeth and can be of straight, stepped or staggered type (refer to figure 1.3) depending upon their geometrical appearance. Staggered type offers lowest leakage compared to other types of labyrinth seal at same length to diameter (L/D) ratio and radial clearance due to its long characteristic flow length [16, 17].
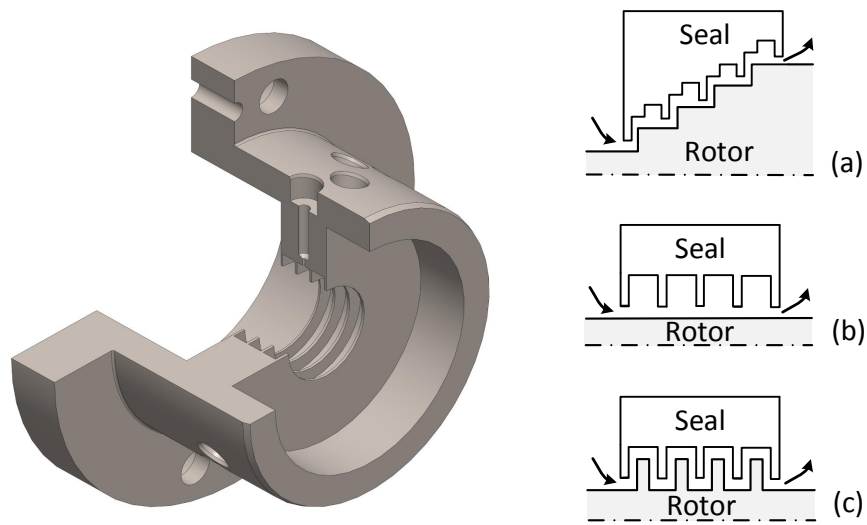
Figure 1.3 – Different types of labyrinth seal: (a) Stepped, (b) Straight or see-through and (c) Staggered or interlocking

1.1.2 Damper seal

Damper seals are incorporated with unique geometrical shapes along and around the seal inner surface, which tend to limit the development of circumferential flow patterns, nearly eliminating cross-coupled stiffness and thus attenuating rotor vibration response [18]. This type of seals are categorized as pocket damper seal (PDS), hole-pattern seal (HPS) and honeycomb seal (HCS) as shown in figure 1.4. Unlike labyrinth seals, damper seal exhibits limited cross-coupled behavior and offers considerable amount of radial damping [14, 19, 20, 21], and hence making the system rotordynamically more stable.
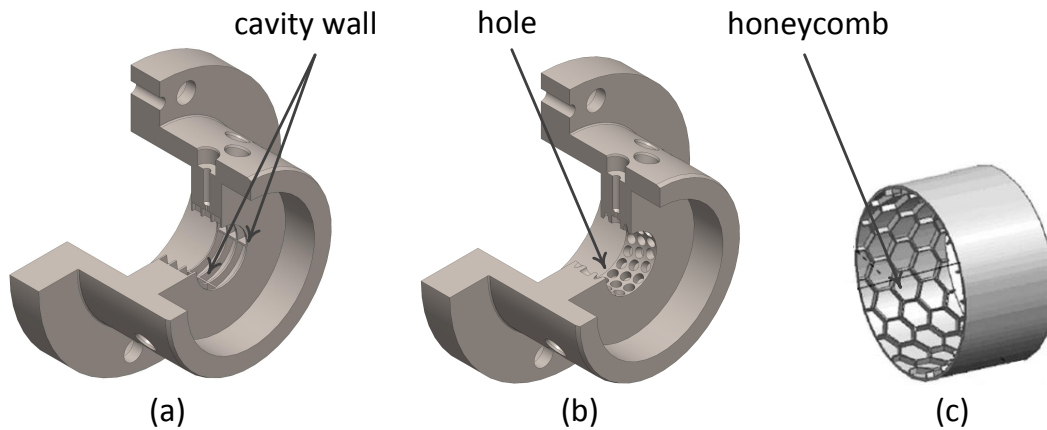
Figure 1.4 – Different types of damper seal: (a) Pocket damper seal, (b) Hole-pattern seal and (c) Honeycomb seal [22]

1.1.3 Gas bushing seal

The bushing seal is a sleeve that forms a small clearance between the rotor and seal where leakage is limited by flow resistance. A bushing can be a ring of metal or composite material, which is softer than the rotor material, inserted inside the seal housing. There are two configuration of this seal type, namely floating and fixed bushing (refer to figure 1.5). Fixed bushing seal has stationary bush while floating type has spring loaded flexible bush. These types of seals yield higher leakage than the other type of seals for same boundary conditions and same radial clearance [23].
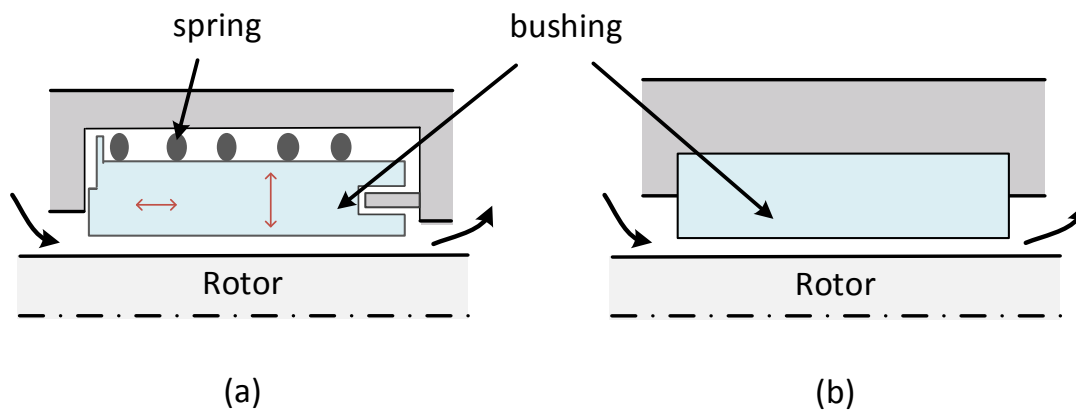
Figure 1.5 – Schematic diagram of different types of bushing seal: (a) Floating and (b) Fixed

1.1.4 Film riding seal

Based upon their working principle, they are categorized as hydrostatic seal (refer to figure 1.6 (a)[1]) and hydrodynamic seal (refer to figure 1.6 (b)[2]). In a hydrostatic film riding seal external pressurized gas is injected which controls the opening and closing of sealing gap which is independent of rotor speed [23, 24, 25]. Although this type of seal offers good leakage performance and simplicity in design, it needs auxiliary external pressurization and its control system. In hydrodynamic seal, the lifting forces are generated by the viscous shear effect of the gas film due to the rotor speed [23]. The sealing effect are accomplished by the reverse pumping effect generated by spiral grooves engraved either on a rotating disk or on the seal stationary faces [24, 25]. This type of seal has best leakage resistance characteristic but requires high operational speed to generate hydrodynamic lift and also complex to design leading to high manufacturing cost.
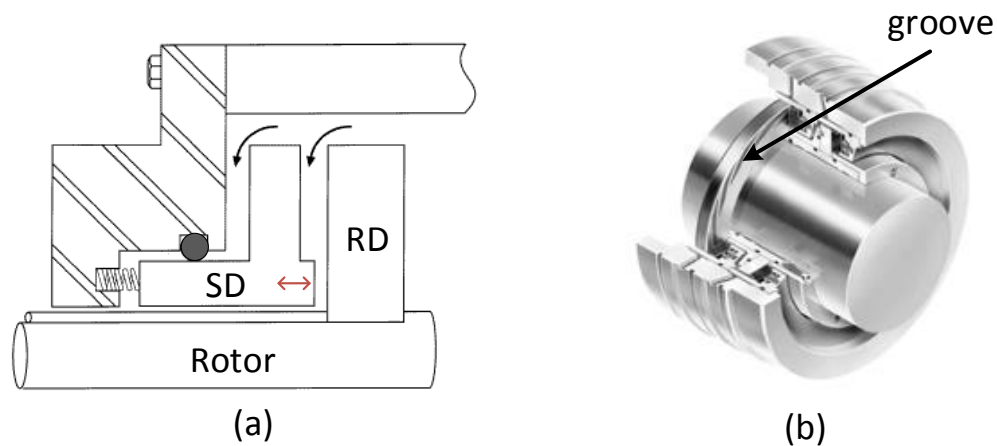
Figure 1.6 – Types of film riding seal: (a) Hydrostatic and (b) Hydrodynamic

1.1.5 Complaint foil seal

This seal, as shown in figure 1.7 (a), is an expanded version of leaf seal concept proposed by Salehi and Hesmat as an extension of their foil bearing work for aerospace application [26]. This seal operates similar to compliant foil bearing based on developing a high pressure thin gas film between the rotor and the top foil. The top foil is supported by spatially variable complaint elements called spring bumps and extends both axially and radially to restrict axial flow.

---

[1]www.mcnallyinstitute.com/12-html/12-02.html
[2]www.johncrane.com/products/mechanical-seals/dry-gas/type-28at
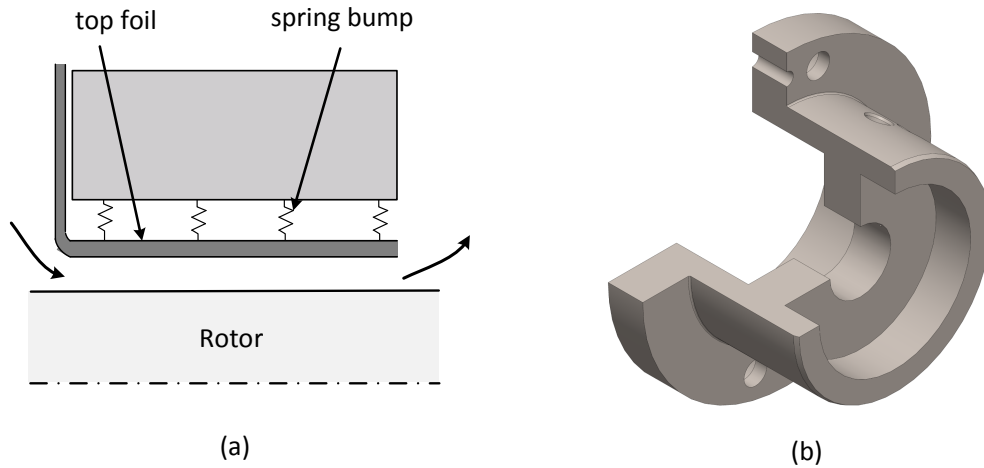
Figure 1.7 – Complaint foil seal (a) and Smooth seal (b)

1.1.6 Smooth seal

The smooth seal is the simplest type of gas seal, which has a smooth cylindrical sealing surface (refer to figure 1.7 (b)). This type of seal offers large direct stiffness due to Lomakin effect but has highest leakage compared to other seal counterparts for similar clearance and boundary conditions [10].

1.2 Selection of seals

To identify the most promising seal technology for reduced-scale applications and since no work has been reported in sealing technologies for reduced-scale applications, the selection procedure has been carried out using qualitative data of different non-contacting gas seals. The qualitative parameters of seals include leakage resistance, rotordynamic performance (stiffness and damping), size, manufacturability, adaptability with the system, design simplicity, cost, durability, and simplicity. For the sake of simplicity, these parameters were reduced to four characteristic features: leakage resistance, rotordynamics, overall size, and other factors, which include all the remaining parameters. Each of these features was provided with their own range of weights based on the priority level (refer to Table 1.1). Different weight configurations have been analyzed to assess the robustness of the selection process.

The weightage decision matrix (refer Table A.1, A.2 & A.3 in Appendix) and sensitivity analysis (refer Table 1.2) was performed on state-of-the-art non-contacting gas seals using the different weighting scenarios summarized in Table 1. With the grading of seals, the overall ranking of different seals was accomplished. The sensitivity analysis performed by using different weight distributions tests the robustness of the selection process. Finally, the top two ranked seals (hole pattern and pocket damper) have been

Table 1.1 – *Range of weightage value for core characteristics features of non-contacting gas seals*

Variables	Weight (*W*)						
	W1	*W2*	*W3*	*W4*	*W5*	*W6*	*W7*
Leakage	0.45	0.45	0.45	0.4	0.35	0.45	0.4
Rotordynamic	0.3	0.35	0.4	0.4	0.4	0.3	0.35
Axial length	0.2	0.15	0.1	0.15	0.2	0.2	0.2
Others	0.05	0.05	0.05	0.05	0.05	0.05	0.05
Total	1	1	1	1	1	1	1

identified as the most promising seals for reduced scale turbomachinery applications.

Table 1.2 – *Sensitivity analysis of the-state-of-the-art non-contacting gas seals*

Weightage (*W*)	Rank				
	1	2	3	4	5
W1	Hole pattern	Pocket damper	Hydrodynamic	Hydrostatic	Honeycomb
Score	4.21	4.19	3.81	3.7	3.56
W2	Hole pattern	Pocket damper	Hydrodynamic	Hydrostatic	Honeycomb
Score	4.23	4.19	3.81	3.7	3.61
W3	Hole pattern	Pocket damper	Hydrodynamic	Hydrostatic	Honeycomb
Score	4.24	4.19	3.81	3.7	3.66
W4	Pocket damper	Hole pattern	Hydrodynamic	Hydrostatic	Honeycomb
Score	4.27	4.26	3.82	3.67	3.63
W5	Pocket damper	Hole pattern	Hydrodynamic	Hydrostatic	Honeycomb
Score	4.36	4.27	3.83	3.65	3.6
W6	Hole pattern	Pocket damper	Hydrodynamic	Hydrostatic	Honeycomb
Score	4.22	4.19	3.81	3.7	3.6
W7	Pocket damper	Hole pattern	Hydrodynamic	Hydrostatic	Honeycomb
Score	4.27	4.24	3.82	3.68	3.58

1.3 Scaling analysis of non-contacting gas seals

In order to highlight the evolution of the specific leakage when downscaling turbomachinery, a simple scaling analysis has been performed using 1D seal model with non-ideal fluid properties assumption. The investigation is done using the Balje diagrams [27] for radial flow turbine. For an efficiency of 80% a specific speed (N_s) of 0.2 and specific diameter (D_s) of 7.8 have been selected for the calculation while the

shaft power (P_{shaft}) was varied from 0.5 to 100 kW. The following equations are used to determine total inlet mass flow rate ($\dot{m}_{tot}$), inlet volume flow rate ($\dot{V}$), rotational speed (ω) and diameter of the impeller (D_{imp}).

$$P_{\text{shaft}} = \eta_{\text{isen}} \cdot \dot{m}_{\text{tot}} \cdot \Delta h_{\text{isen}} \tag{1.4}$$

$$\dot{V} = \frac{\dot{m}_{\text{tot}}}{\rho} \tag{1.5}$$

$$N_{\text{s}} = \omega \cdot \frac{\left(\dot{V}\right)^{0.5}}{\left(\Delta h_{\text{isen}}\right)^{0.75}} \tag{1.6}$$

$$D_{\text{s}} = D_{\text{imp}} \cdot \frac{\left(\Delta h_{\text{isen}}\right)^{0.25}}{\left(\dot{V}\right)^{0.5}} \tag{1.7}$$

For the the scaling of shaft diameter, following relation between impeller and shaft has been used.

$$D_{\text{shaft}} = \frac{1}{1.8} \cdot D_{\text{imp}} \tag{1.8}$$

As for the seal two cases are investigated: (1) A constant clearance of 30 μm that is independent on the rotor dimensions. (2) A clearance that evolves linearly with the rotor diameter ($R_{\text{clr}}/D_{\text{sh}}$ = 0.0005). Figure 1.8 represents the relative leakage, rotational speed, radial clearance and shaft diameter as a function of shaft power. The analysis suggests that for reduced-scale machines with smaller shaft diameters the relative leakage loss increases for a constant radial seal clearance. For a shaft diameter of 10 mm (0.5 kW-turbine) and a radial seal clearance of 30 μm, the leakage loss corresponds to almost 22% of the turbine inlet mass flow, while for a machine with a rotor diameter of 32 mm (5 kW-machine), the relative leakage drops below to 7%.

In order to minimize this significant loss in reduced-scale turbomachinery to the acceptable limits the radial clearance has to be significantly reduced (around 4 μm for this particular case). However, seals with such low radial clearances are expensive to manufacture and also depreciate rotordynamic performance as seal radial clearance approaches to gas-bearing clearance. A tradeoff between manufacturing cost, leakage, and rotordynamic performance is therefore identified.

Figure 1.8 – Scaling effect on leakage mass flow rate, shaft diameter, radial clearance and rotor speed as a function of shaft power at P_{in} = 18 bar, P_{out} = 6 bar, T_{in} = 82 °C, C_d = 0.716, single tooth seal and R134a as working fluid

1.4 Effect of real gas properties on seal leakage

In thermodynamic cycles, fluids often operate close to the saturation curve (curve which separates two-phase state). A typical *PH* diagram, which is often used to represent the thermodynamic cycles of vapor compression and organic rankine cycles is illustrated in figure 1.9 to give an overview of thermodynamic state variables of a fluid. For gas seals with fluids working near saturation point, the perfect gas assumption is far from valid and real gas effects need to be taken into account [28, 29]. To justify this statement, a static model (no shaft vibration) has been implemented with ideal and non-ideal gas assumptions. For the thermodynamic properties of gas, *REFPROP* database [30] has been used. For the sake of comparison a single tooth seal with a shaft diameter of 14 mm and a clearance of 30 and 40 μm has been chosen and the result for ideal and real gases plotted in figure 1.10 as a function of the degree of superheat, which indicates the distance to the saturation line.

Near saturation temperature with 3 K superheat a discrepancy of almost 9% in leakage flow rate is suggested for both radial clearance value. The difference decreases with the degree of superheat. Similar trends have been published by Wang et al. [28] and Fairuz
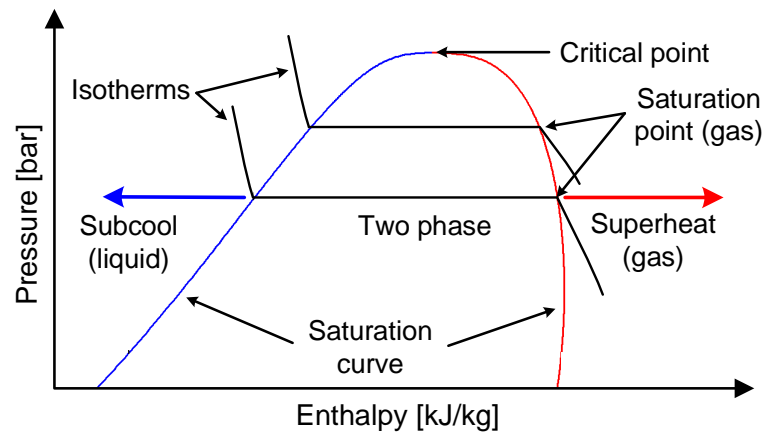
Figure 1.9 – Schematic representation of *PH* diagram with thermodynamic state of fluid

et al. [29]. This clearly demonstrates that the perfect gas assumption is not valid for the fluid operating near saturation point and therefore highlights the need to account for the real gas effect.
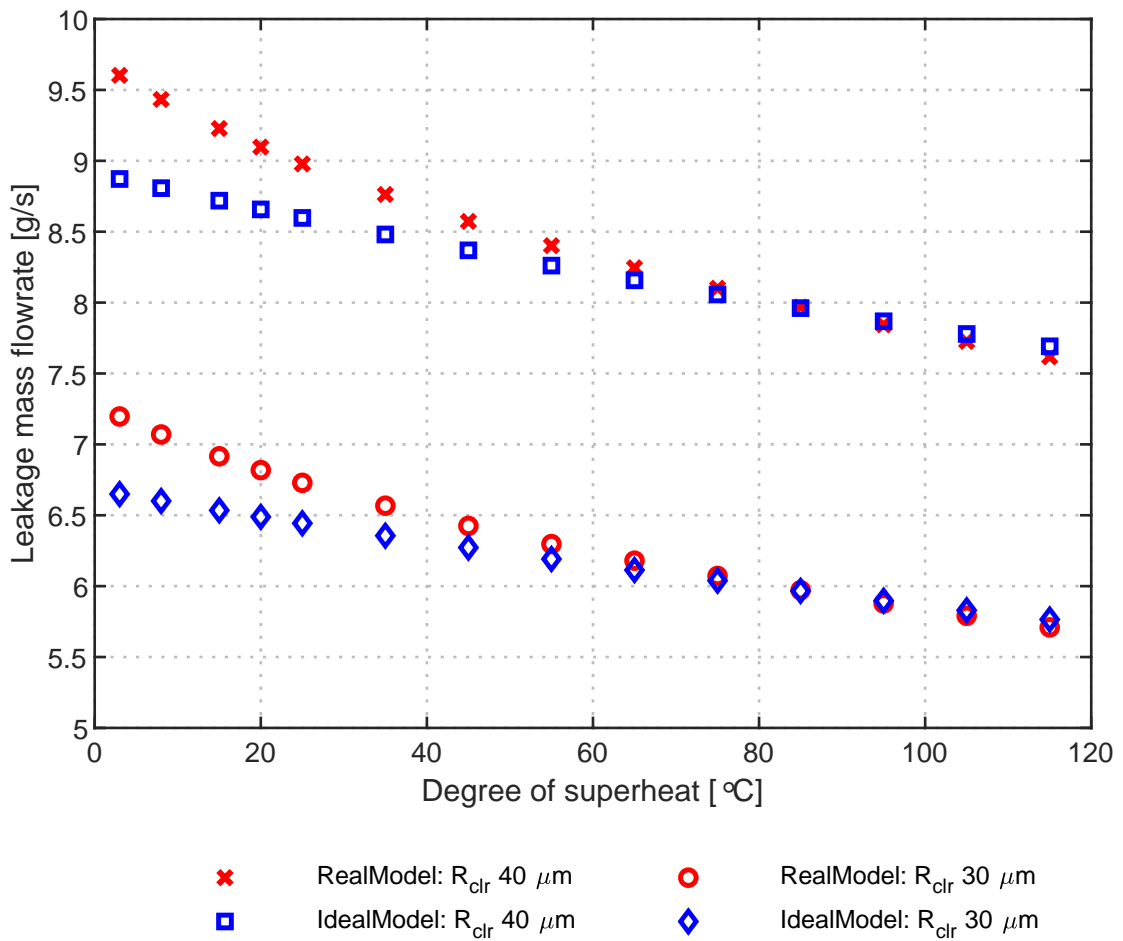
Figure 1.10 – Leakage mass flow prediction using perfect gas and real gas model at P_{in} = 18 bar, P_{out} = 6 bar, C_d = 0.716, T_{sat} = 65.85 $°C$ and R134a as working fluid

1.5 Problem statement

Seals are commonly used in all kinds of turbomachinery applications to minimize secondary leakage losses and hence to increase system thermodynamic efficiency. Besides the leakage reduction characteristics, seals are also known to have their influence on rotor critical speeds, and most importantly, on rotordynamic stability of the turbomachinery [8], [9]. The prediction of seal performance is mainly evaluated using the bulk-flow models, and more recently via three-dimensional CFD software. However, the reliability of the models can only be gauged by the experimental validation.

In 1935, Egli [31] performed an analytical and experimental analysis on labyrinth seals leakage, where he defined and determined kinetic carry-over in seals experimentally. Benckert and Wachter [32] experimentally investigated seal performance due to destabilizing force at low inlet pressures (1.42 bar). Although they performed the test at such low-pressures their experimental data have been used by many scholars as a

13

benchmarking tool to their numerical models. Childs and Scharrer [33] measured direct damping force in a labyrinth seal reporting, however, a poor prediction quality of their theoretical bulk-flow model compared to the experimental results. Picardo et al. [34] performed measurements on labyrinth and hole pattern seal at elevated inlet pressure of 70 bar and rotor speed up to 20.2 krpm at two radial clearances, and different inlet pre-swirl ratios. Comparisons of measured leakage and rotordynamic force coefficients were made with the predicted results from one-control-volume and two-control-volume bulk-flow models. The predicted results suggested poor agreement with the measured data, however, the one-control-volume model showed better performance compared to the two-control-volume model.

Recently, Cangioli et al. have published their experimental data on labyrinth seals [35, 36] and pocket damper seals [37] which were performed on a high-pressure seal test-rig [38] with nitrogen as working fluid. In their papers, they compared the experimental results with the predicted results from their modified mathematical bulk-flow model coupled with energy equation displaying satisfactorily matching results.

So far, literature is rich in theoretical and experimental investigations on different types of non-contacting gas seals for large-scale turbomachinery systems while at reduced-scale like the one shown in figure 1.11 (taken from [39]), such investigation is missing. Further, almost all of these studies considers working fluids as perfect gas. Recently, some research works on effect of real gas on seal performance have been published for large-scale turbomachinery application [29, 40]. However, the trends towards down-scaled turbomachinery and its use with working fluids operated close to the saturation line calls for new approaches in the seal selection and the implementation of real gas effects into existing seal models for predicting leakage and the rotordynamic properties. The scaling analysis (refer to Figure 1.8) highlights leakage as a significant source of losses in a reduced-scale turbomachinery system. For shaft diameter less than 20 mm, the percentage of leakage mass flow is significantly higher depending upon the clearance gap. More efficient seals require reduced clearances, which in turn are expensive and also depreciate rotordynamic performance as seals start to acts like plain cylindrical air bearings [10]. This highlights the fact that a seal is not dissociable from the bearings and rotordynamics, especially at a reduced-scale.

Furthermore, reduced-scale turbomachinery are generally compact in size. More number of constriction in seal increases both manufacturing cost and an overall length of rotor, which complicates rotordynamics. Hence, the first step in seal design phase is to identify the optimum number of constrictions. For this purpose, one of the working point of a reduced-scale turbo-compressor with a rotor diameter of 14 mm running on R134a fluid is used to present the results. A seal with a radial clearance of 30 μm is hypothesized and leakage mass flow is calculated for increasing number of constrictions which is shown in figure 1.12. The results were obtained by simple
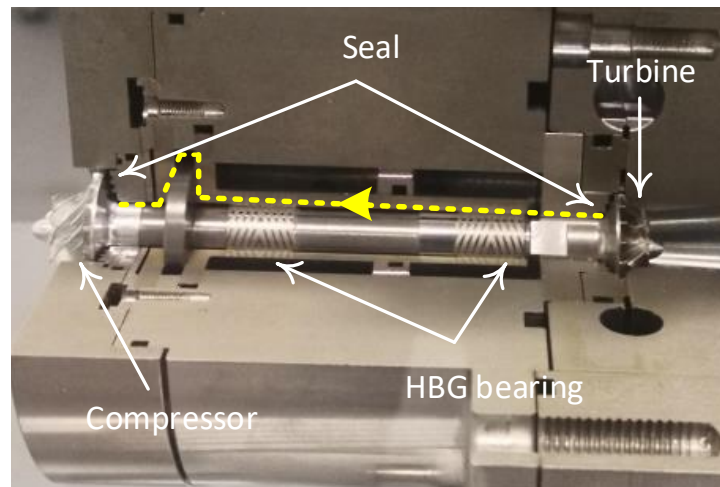
Figure 1.11 – Picture of heat pump organic rankine cycle (HP-ORC) compressor and turbine unit (CTU) showing leakage flow path highlighted by yellow dotted line

one-dimensional models, one considers the real gas properties based on flow representing Fanno curve [23] and the other using the St. Venant leakage equation [14] with perfect gas assumption. Figure 1.12 shows a clear trend of leakage with respect to the number of seal constrictions, which highlights the existence of the optimum number of constrictions beyond which effective leakage characteristics of seals drops. For instance, a seal with two constrictions reveals 16.6% less leakage compared to the seal with single constriction and with an increment of constrictions the result shows an asymptotic behavior.

The next step in the seal design process is to finalize the overall length of the seals. The commonly practiced method is to select the ratio of seal axial length to the diameter of the rotor (L_s/D_r) depending upon the requirement of seal overall influence on the turbomachinery system. For shorter seal ($L_s/D_r < 0.333$), the literature [10] suggests implementing labyrinth seal as an effective solution offering optimum leakage and rotordynamic performance. Furthermore, literature [10] recommends to use roughened seals with geometrical features like holes, pockets or honeycomb for longer seals ($L_s/D_r \geq 0.333$) instead of labyrinth seal to avoid rotordynamic problems.
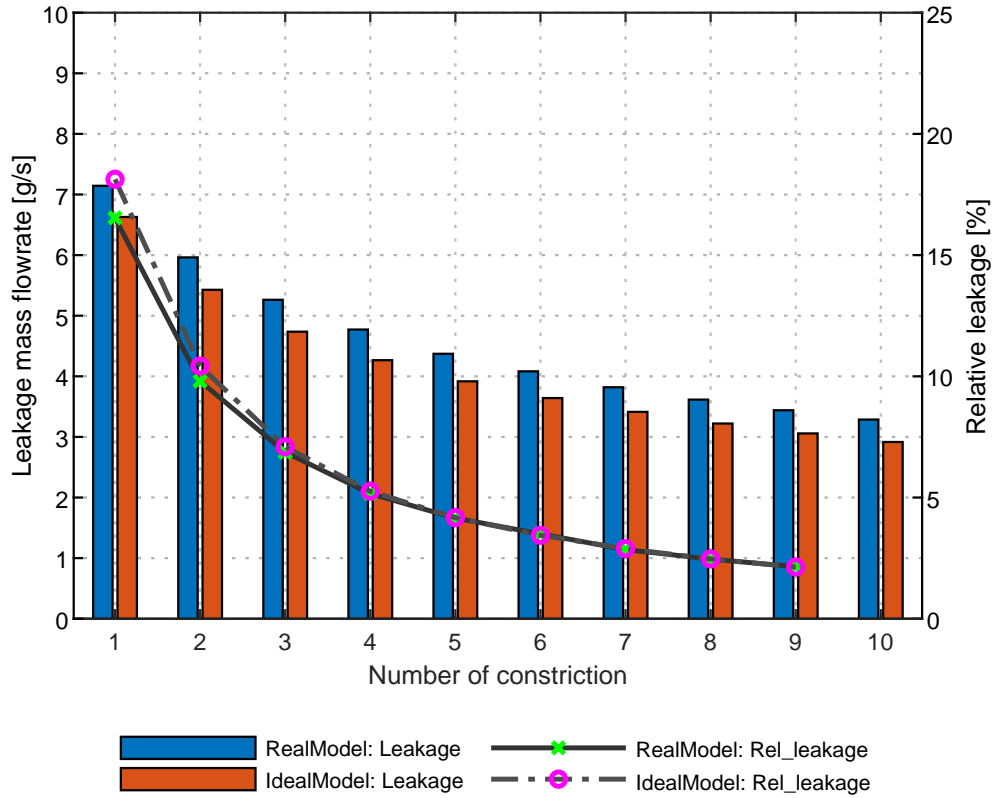
Figure 1.12 – Leakage mass flow prediction using perfect gas and real gas model for varying number of constriction at P_{in} = 18 bar, P_{out} = 6 bar, T_{in} = 67.85 °C, C_d = 0.716 [41] and R134a as working fluid

1.6 Research goal and objectives

The goal of this thesis is to identify the most promising seals and highlight the challenges related to the downscaling of seals. Furthermore, perform numerical and experimental investigations on selected seals geometry to increase thermodynamic efficiency of reduced-scale turbomachinery systems. In order to achieve this goal the following objectives are established:

- Identify the most promising seal topologies for reduced-scale high-speed turbomachinery applications.

- Reduce leakage in down-scale turbomachines with relatively high clearance to shaft diameter ratio operating near fluid saturation curve.

The methodology adapted in this thesis to accomplish research objectives are summarized as follows:

- Selection of promising seals with the help of qualitative data of seals available in

literature using weightage decision matrix and sensitivity analysis.

- Development of mathematical model to predict seal performance taking consideration of real gas effects. Implementation of the conventional models for the comparison purpose between the author model and the experimental results on reduced-scale seals.

- Design and development of test-rig for the experimental investigation of selected seals for reduced-scale application and validation of in-house developed seal model.

The aim of this thesis is to provide better understanding and design guidelines of non-contacting seals with minimum leakage and improved rotordynamic performance for downsized turbomachinery application.

1.7 Organization of thesis

This thesis is composed of six chapters. An overview of each chapter is summarized below:

Chapter 2 This chapter introduces the theoretical aspects of non-contacting gas seals. The-state-of-the-art numerical models to predict seal performance and used terminologies are also highlighted. Furthermore, the description of the developed seal models including the comparison of results with well-established literature is presented.

Chapter 3 This chapter describes the design and development of a test-rig dedicated to the experimental investigation of selected non-contacting seals for reduced-scaled turbomachinery applications. The test procedure along with a description of used instrumentation is illustrated.

Chapter 4 This chapter is dedicated to the experimental study of selected test seals at different operating conditions. Further, the comparison between the different seal models and the experimental results is presented and discussed. Finally, selected test seals are categorized on their performance level in order to identify the best seals for reduced-scale turbomachinery applications.

Chapter 5 This chapter summarizes the conclusions of the thesis including the recommendations for future work.

1.8 Specific aspects of novelty

The specific aspects of novelty of this thesis are summarized in the following points.

- Identification of most promising seals for reduced-scale turbomachinery application using the qualitative approach.

- Design and development of a test-rig dedicated to the experimental investigation on different types of reduced-scale turbomachinery seal operated close to the fluid saturation line.

- Development of 2D seal model to predict the seal performance. Comparison of the author model and the-state-of-the-art seal models with the available literature as well as experimental results. The author model shows good agreement with the existing literature at large-scale. At reduced-scale the author model has superior prediction quality of leakage, cavity pressure and temperature distribution compared to the-state-of-the-art models.

- Measurement of leakage, cavity pressure and cavity temperature in different types of reduced-scale test seals with air and R134a as a working fluid.

- Experimental proof of real gas effect in seal and the ability of the author model to capture this effect with higher accuracy.

2 Seal theory and modeling

This chapter provides an overview of the different approaches used in seal analysis. The governing equations and the empirical factors applied for non-contacting gas seal theoretical investigation are presented. Furthermore, the models developed by the author and the-state-of-the-art seal models along with the assumptions and limitations are discussed. Besides, the results of the author models are compared with well-established data of seal literature as a benchmarking process.

2.1 Introduction

The rotordynamic coefficients of seals are highly dependent on the leakage rates through the seals, circumferential velocity and the pressure in the seal cavities [5]. The procedures to predict these variables involve solving the governing fluid flow equations within the seal either numerically, analytically or in combination. With the technological advancements in computing power, the computational fluid dynamics (CFD) approach is presently popular in the investigation of seal performance. Nevertheless, CFD is still considered to be time and cost expensive. On the other hand, bulk-flow models offer the most-time efficient and acceptable prediction accuracy to estimate the seal performance [42, 43]. Thereby, almost all the existing theoretical analysis on seals uses bulk-flow model to predict the seal behavior in the turbomachinery applications [10, 44]. To visualize the different flow phenomena and the variables used in this chapter, a schematic representation of a single cavity seal is shown in figure 2.1.
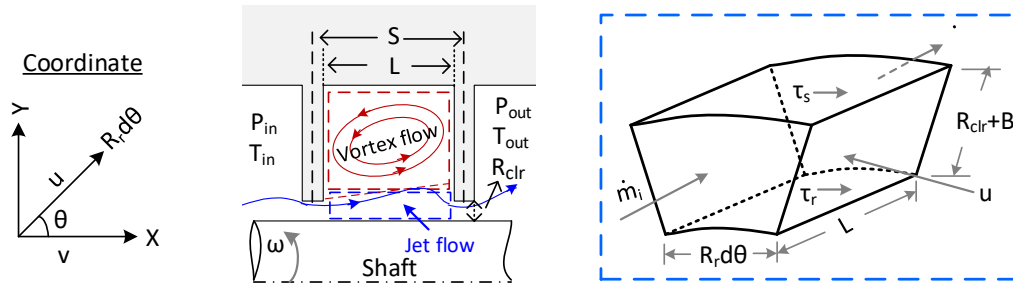
Figure 2.1 – Schematic illustration of a single cavity seal under operation

2.2 Brief evolution on seal modeling and analysis

The relatively large clearance together with the pressure gradient indicates turbulent flow regimes in seals. Hence, the Reynolds lubrication equation is inapplicable for annular seals due to the high Reynolds numbers [10]. The earliest attempt to model the seals was conducted by Black in 1969 [45] and, Black and Jenssen in 1970 [46] using the bulk-flow model for centrifugal pump applications. The bulk-flow model neglects the variation of fluid velocity components across the clearance and employs averaged velocity components [10, 47]. Furthermore, shear stress is considered only at the surface of the seal and the rotor, and is a function of the local Reynolds number. Thus, the bulk-flow model can be considered as a simplified version of the Navier-Stokes equation governing the complex three-dimensional and turbulent flow within the seal. By nature, the governing equations of the bulk-flow model represent the continuity, the momentum and the energy conservations in the seal flow domain. The bulk-flow models established so far can be categorized as a single and multi control-volume analysis.

Kostyuk [48] performed an extensive analysis of labyrinth seals using the conservation of energy and momentum in each seal cavity for compressible flow. His work is still regarded as the basis for most of the present seal analysis. However, he did not consider the change in the flow cross-section area due to rotor eccentricity, hence his model cannot predict de-stabilizing cross-coupled stiffness [44]. Iwatsubo [44] wrote the circumferential-momentum and continuity equations considering one control volume to define the average (bulk-flow) circumferential velocity within a seal cavity. Further, he introduced the time dependency of change in flow area in the model but he ignored the area derivative in the circumferential direction leading to the inaccurate result of the momentum equation [49]. Kurohashi [50] included the dependency of flow coefficient on eccentricity into his analysis, but assumed the constant circumferential velocity in all seal cavities [49]. Childs and Scharrer [49] modified the Iwatsubo one control-volume model [44] and incorporated the Neumann leakage equation [51] with

the Chaplygin discharge coefficient [52] to define the axial velocity for the leakage mass flow rate. The Blasius [53] shear stress definition coupled with the Yamada empirical coefficients [54] was used to model the turbulent flow. To date, this model is commonly used as a design tool to predict the seal performance. In the one control-volume as shown in figure 2.2 (a), the analysis only accounts for the circumferential velocity in the seal cavity and the effect of the axial velocity is neglected. However, the experiment by Iwatsubo et al. [55], calculated result by Rhode [56] and Stoff [57], and the CFD result by Cangioli et al.[42] and Saba et al.[58], suggest the existence of both circumferential flow (core flow) and the jet flow regions in the seal cavities [59] (see figure 2.3).

Wyssmann et al. [60] first introduced a two control-volume model where they separated the core flow region into one control-volume and the axial jet flow as the second one (see figure 2.2 (b)). For each control-volume, continuity and momentum equations were defined. For the shear stress between the jet flow and the core flow, a 2D CFD solution of the Navier-stoke equation was performed. However, they assumed incompressible flow and neglected re-circulation velocity in the cavity due to the formation of vortices. Scharrer [61] expanded the theory of Childs and Scharrer [49] by employing the two control-volume concept of Wyssmann et al. [60] along with the re-circulation velocity and compressible flow in the seal analysis [62]. For the calculation of cavity shear stresses, he used the jet theory to determine the re-circulation velocity. Later Klauk [63] developed a three control-volume model for a labyrinth seal analysis for compressible fluids, where he assigns one control-volume to the vortex flow region and two control-volumes for jet flow region, one below the teeth and one in the seal cavity (see figure 2.2 (c)). Later, Weiser [64] extended the work of Klauk in his Ph.D. work.

Nordmann and Weiser [65] introduced a three-control-volume model in addition to the continuity, momentum and energy balance for each control volume. For the turbulence modeling, they used semi-empirical wall shear stress by Moody [66]. Their approach does not use any turbulence model, instead, it uses the wall shear stress correlation by Wyssmann et al. [60]. As the friction factor directly influences shear forces and hence the seal performance, the correct estimation of the friction factors are crucial. The commonly used models to determine the friction factors are Blasius [53], Moody [66], Colebrook-White [67] and Swamee-Jain [68]. The comparative investigation of the friction factors model on seal performance is described by Dereli [69] and more recently by Cangioli et al. [35]. The close results was reported by Dereli irrespective of the models [69], whereas, the better agreement with the experimental data using the Swamee-Jain model was stated by Cangioli et al. [35].

Initially, Rhode et al. [71] applied finite difference methods to the labyrinth seals analysis. Nordmann et al. [72, 73] used finite difference procedure to solve the compressible Navier-Stokes equations together with the k-ϵ turbulence model of Launder and Spalding [74]. However, the majority of the finite difference analysis of the annular seals has been performed along with the bulk-flow models. Benckert et al. [32] developed
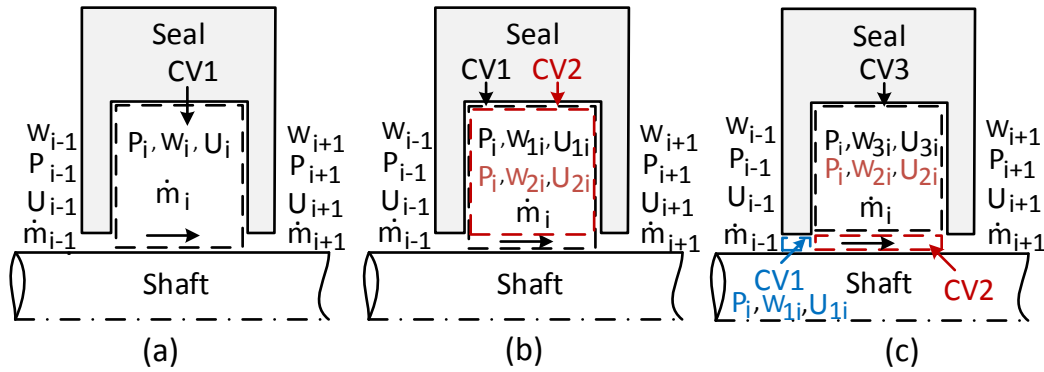
Figure 2.2 – Schematic illustration of types of control-volume in seal analysis: One control-volume (a), two control-volume (b) and three control-volume (c)

a simple one control-volume model where he replaced a three-dimensional flow in the circumferential direction with a single averaged circumferential velocity using a three-dimensional finite-difference model. The main peculiarity of this model is the implementation of a circumferential momentum coefficient describing the amount of circumferential momentum contributed to the seal cavity from the jet flow [62]. However, this model lacks the prediction of damping force coefficients.

The theoretical analyses using the bulk-flow approach and the experimental investigations on annular seals are well documented since the early last century. Even though the bulk-flow model is known for its time and cost-effectiveness, its prediction accuracy relies on the empirical factors, especially on friction factors, shear stresses, and discharge coefficients. Currently, with the advancement of computing power and the availability of the commercial three-dimensional Computational Fluid Dynamics (CFD) software, CFD based solution of the Navier-Stokes equations governing the flow physics in seals is gaining in popularity. However, a proper mesh generation, solving and post-processing of the data requires a significant amount of time for a seal full CFD simulation. As a consequence, a hybrid CFD/Bulk-flow method was proposed by Migliorini et al. [75]. At first, a 3D CFD was used to calculate the steady-state variables. In a second step, the CFD solution was implemented in the bulk-flow model as averaged values over the seal cavity for the identification of seal reaction forces. In their paper, the hybrid model showed good agreement with the experimental results compared to the reference bulk-flow model and reference CFD results in a much reduced computational time. In their second paper [76], they assumed non-isothermal flow. Comparison with previous results, suggest better prediction quality with the modified model. Cangioli et al. [42] performed the design and analysis of CFD experiments to develop the leakage correlation for one control-volume bulk-flow model. Their model with CFD infused correlation showed accurate prediction results to the experiment
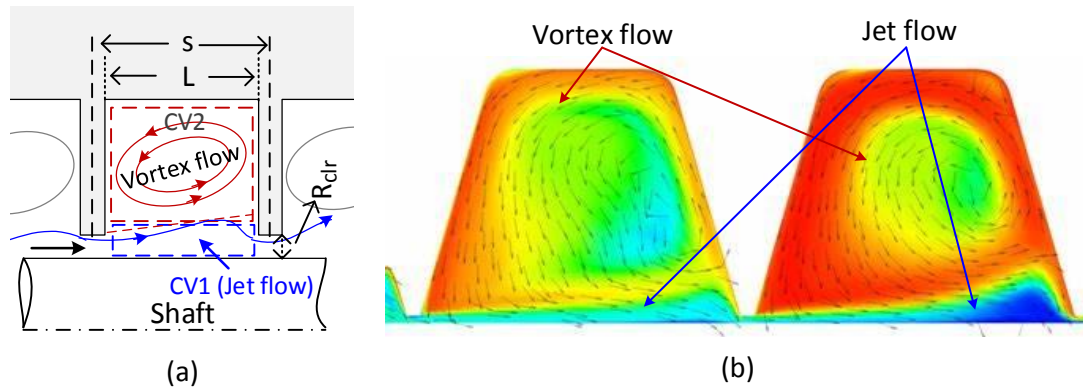
Figure 2.3 – Illustration of vortex flow and jet flow region in seal cavity with the respective control-volume used in seal analysis: Schematic representation (a) and CFD visualization (b) [70]

result compared to the other bulk-flow models. Recently, Wu and San Andrés [77] presented a CFD investigation on seal and rotor friction factors (crucial for dynamic analysis) concerning the seal geometry and operating conditions. Their work aimed at finding the dominant factors influencing the wall shear stress with the help of CFD simulation to improve the prediction quality of the bulk-flow model.

Literature suggests that the bulk-flow model is the most widely used method as a design tool to predict seal performance. Although CFD approaches claim better prediction accuracy, they are time consuming compared to bulk-flow model, and do not offer the same level of flexibility for parametric analysis.

So far, literature is rich in experimental and theoretical investigations of large-scale seals operated with fluids where perfect gas laws are applicable. The so-called bulk-flow model and its prediction accuracy have been well documented for the large-scale applications. However, with the trends towards down-scaled turbomachinery and its working fluids operated close to the saturation line, the validity of the-state-of-the-art seal models with the existing empirical correlations is questionable.

The aims of this chapter are highlighted as follows:

- To develop own mathematical models for gas seals with the implementation of real gas properties based on two control-volume bulk-flow model.

- To develop the most commonly used models in large-scale seal applications using the existing literature knowledge as the baseline models.

- To compare own models and the baseline models with the existing well-established literature at large-scale seals as a benchmarking process.

2.3 Seal theory

The theoretical analysis employed in this thesis is the adaptation of the commonly used bulk-flow model. The governing equations for the complex turbulent compressible flow in the seal cavities are continuity, circumferential momentum, and energy conservation. As the governing equations are coupled to each other and complex in nature, a direct analytical solution is hard to achieve and hence simplification is essential. As a first step, the leakage mass flow rate in the governing equations is simplified by the empirical leakage equation. The resulting set of the governing partial differential equations is linearized using the perturbation method around a centered position. The zeroth-order solution yields the leakage rate, cavity pressures, and circumferential velocities. The temporal and the convective terms in the first-order equations are eliminated by assuming an elliptical or circular orbit of the rotor [10]. Finally, with the perturbed pressures and perturbed circumferential velocities in the seal, seal reaction forces are determined. As this chapter is dedicated to the steady-state solution, the first-order equations, and their solutions to determine seal force coefficients are not discussed here. A detailed background on different leakage model used in seal analysis is presented by Gamal [14]. For the sake of brevity, the relevant leakage equations with their empirical correlations are highlighted below.

2.3.1 Correlations used in bulk-flow model

The fundamental leakage equations in the bulk-flow model comprises two correlations, namely, the discharge coefficient and the kinetic carry-over coefficient.

Discharge coefficient

The discharge coefficient describes the vena contracta effect which relates the flow and the pressure loss in the seal teeth. It is defined as the ratio of actual mass flow rate to the theoretical mass flow rate in seals and denoted by a dimensionless number C_d (see equation 2.1). Due to the presence of rotor, there is only half vena contracta effect in the seal teeth. The value of the discharge coefficient is always < 1. In seal analysis, the common practice is to use Chaplygin's equation [78] or a constant value proposed by Eser and Kazakia [41].

$$C_d = \frac{\dot{m}_{real}}{\dot{m}_{ideal}} \tag{2.1}$$

• **Chaplygin's equation** Chaplygin [78] studied the vena contracta effect and postulated an analytical formula (equation 2.2) to calculate the discharge coefficient, which is a function of the pressure ratio and the specific heat capacity.

$$C_{d,i} = \frac{\pi}{\pi + 2 - 5 \cdot \beta_i + 2 \cdot \beta_i^2} \tag{2.2}$$

where, β_i is calculated as:

$$\beta_i = \left(\frac{P_{i-1}}{P_i} \right)^{\gamma - 1/\gamma} - 1 \tag{2.3}$$

- **Eser and Kazakia**   To evaluate the validity of Chaplygin's discharge coefficient, Eser and Kazakia [41] performed two-dimensional CFD simulation on a rectangular strip rather than an annular orifice. They compared their CFD results and the analytical solution of Chaplygin's equation with the experimental value. After extrapolation of the CFD results, they concluded a constant value of 0.716 shows a better agreement with the experimental data. Even though their analysis showed better accuracy, the applicability of this constant value of discharge coefficient is questionable for most of the seal operating conditions as their study focused only on two teeth seal at a very low inlet pressure.

Kinetic energy carry-over coefficient

In a non-contact seal the kinetic energy developed due to the flow acceleration in the orifice ideally fully dissipates in the seal following cavity. It is known, however, that such an ideal case does not hold, as a portion of undissipated kinetic energy is carried over to the following cavity [14, 35, 79]. This phenomenon was first demonstrated by Egli [31] in 1935 and has a detrimental effect on leakage, especially on the short-pitched seals. Unlike, the discharge coefficient, this coefficient has a negative effect on the seal's leakage performance as it's value is always > 1. However, there is a numerical limit of this coefficient since if the clearances continue to increase, the fluid will blow straight through the seal acting as a seal with large single constriction [80]. In literature, there exist many correlations for the kinetic carry-over coefficient (refer to [31, 50, 80, 81]). The relevant ones are presented below.

- **Vermes carry-over coefficient**   Based on the fluid mechanics' approach of boundary layer theory, Vermes [82] developed his own kinetic energy carry-over coefficient. He computed the flow in the cavity as one half of a flat symmetrical jet originated from an infinitesimally small hole [35].

$$\mu_i = \sqrt{\frac{1}{(1 - \alpha_i)}} \tag{2.4}$$

where,

$$\alpha_i = \frac{8.52}{\frac{L_i}{R_{clr,i}} + 7.23} \tag{2.5}$$

• **Neumann carry-over coefficient** Unlike, Vermes carry-over coefficient which considers only the ratio of cavity length (L) to the radial clearance (R_{clr}), Neumann [51] used a semi-empirical carry-over coefficient in his empirical leakage equation which consists of the ratio of radial clearance to the tooth pitch (S) as well as the number of seal constrictions (NT).

$$\mu_i = \sqrt{\frac{NT}{NT \cdot (1 - \alpha_i) + \alpha_i}} \tag{2.6}$$

where,

$$\alpha_i = 1 - \frac{1}{\left(1 + 16.6 \cdot \frac{R_{clr,i}}{S_i}\right)^2} \tag{2.7}$$

Shear stress correlation

To calculate the shear stresses in seal (τ_{si}) and rotor (τ_{ri}), the Darcy friction factors for both seal (f_{si}) and rotor (f_{ri}) are estimated using the explicit correlation formulas. Figure 2.4 provides a visual impression of the terminology used in the shear stress definition. The shear stresses are calculated as:
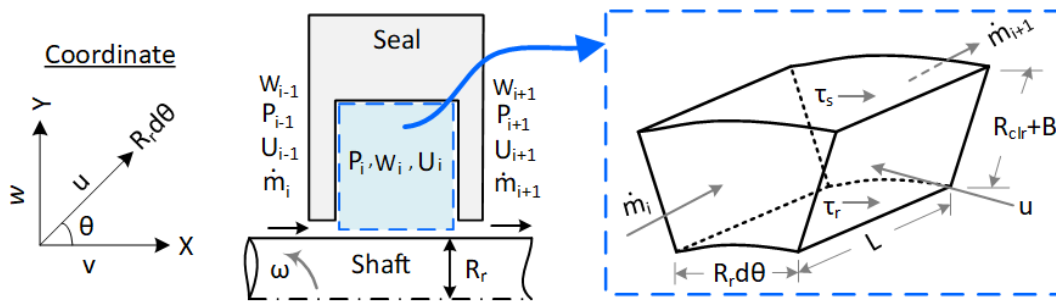
Figure 2.4 – Schematic illustration of bulk velocity and shear stress in one-control-volume

$$\tau_{si} = \frac{\rho_i}{2} f_{si} U_i^2 \, \text{sign} \, (U_i) \tag{2.8}$$

$$\tau_{ri} = \frac{\rho_i}{2} f_{ri} \left(R_r \omega - U_i\right)^2 \text{sign} \left(R_r \omega - U_i\right) \tag{2.9}$$

For the calculation of the Darcy friction factors, two commonly used equations are used in this work.

• **Blasius equation** [53] is regarded as the straightforward way to calculate the Darcy friction factor. It does not considers pipe roughness and is valid for smooth pipes with Reynolds number upto 10^5 [35, 83].

$$f_{si} = n \cdot \left(\frac{U_i Dh_i}{\nu}\right)^m \tag{2.10}$$

$$f_{ri} = n \cdot \left(\frac{(R_r \omega - U_i) Dh_i}{\nu}\right)^m \tag{2.11}$$

where, the coefficients n = 0.079, and m = -0.25 are the empirical values from Yamada [84]. The hydraulic diameter Dh_i is defined as:

$$Dh_i = \frac{2 \left(R_{clr,i} + B_i\right) L_i}{\left(R_{clr,i} + B_i + L_i\right)} \tag{2.12}$$

• **Swamee-Jain equation** The friction factor correlation proposed by Swamme and Jain [68] is valid for rough surfaces and is claimed to be more accurate than the Blasius equation [83].

$$f_{si} = \frac{1}{4} \left(\log_{10} \left(\frac{e_s}{3.7 Dh_i} + \frac{5.74}{(Re_{si})^{0.9}}\right)\right)^{-2} \tag{2.13}$$

$$f_{ri} = \frac{1}{4} \left(\log_{10} \left(\frac{e_r}{3.7 Dh_i} + \frac{5.74}{(Re_{ri})^{0.9}}\right)\right)^{-2} \tag{2.14}$$

where, the hydraulic diameter Dh_i is calculated by using equation 2.12. The Reynolds numbers for seal (Re_{si}) and rotor (Re_{ri}) are calculated as:

$$Re_{si} = \frac{U_i Dh_i}{\nu} \qquad\qquad Re_{ri} = \frac{(R_r \omega - U_i) Dh_i}{\nu} \tag{2.15}$$

2.3.2 The St. Venant leakage equation

The St. Venant equation [14] is the modified version of one-dimensional flow equation developed by Vennard and Street [85]. Vennard and Street performed an energy balance on a flow element to derived the Euler equation. After integrating the Euler equation with the isentropic flow and no change in height, the flow velocity was expressed in terms of density and pressure. St. Venant used the equation by Vennard and Street with the perfect gas assumption and therefore eliminated the density term from the equation. The resulting final equation is termed as the St. Venant equation as shown in 2.16. He used this equation to calculate leakage for labyrinth seals with the assumption of isentropic throttling process in seal teeth and followed by an isobaric dissipation in the cavity.

$$\dot{m}_i = \frac{C_{d,i} \cdot \mu_i \cdot P_i \cdot A_i}{\sqrt{\gamma \cdot R \cdot T_i}} \cdot \sqrt{\frac{2 \cdot \gamma^2}{\gamma - 1} \cdot \left[\left(\frac{P_{i+1}}{P_i} \right)^{2/\gamma} - \left(\frac{P_{i+1}}{P_i} \right)^{\gamma + 1/\gamma} \right]} \tag{2.16}$$

where, $C_{d,i}$ and μ_i corresponds to the discharge and the kinetic energy carry-over coefficient, for which various correlation can be used.

2.3.3 The Neumann leakage equation

The empirical leakage equation proposed by Neumann [51] is shown in 2.17. In his leakage equation, he used Chaplygin's discharge coefficient to account for the contraction of flow in seal constriction and a semi-empirical kinetic carry-over coefficient to address the undissipated kinetic energy. He assumed the seal flow as isothermal. Many scholars [10, 41, 49] used his leakage equation in their work and still prominent in seal analysis as a basis equation.

$$\dot{m}_i = C_{d,i} \cdot \mu_i \cdot A_i \cdot \sqrt{\frac{P_{i-1}^2 - P_i^2}{R \cdot T_i}} \tag{2.17}$$

2.3.4 The modified Neumann leakage equation

Cangioli et al. [35] modified the leakage equation of Neumann [51] and generalized it to account for the real gas effect (see equation 2.18). Furthermore, they coupled the energy equation in their investigation and published matching results with the experimental data [40]. In one of their papers [36], they also included a heat transfer model and structural-mechanics model to evaluate the radial thermal growth in a seal and rotor assembly. Also, Cangioli et al. [42] published a hybrid CFD infused bulk-flow model with their modified Neumann leakage equation to develop a better correlation for the discharge coefficient. They highlighted accurate prediction results from their

modified model compared to the other numerical models. Recently, Cangioli et al. [37] performed a two control-volume bulk-flow analysis on Pocket damper seal (PDS) using the modified Neumann leakage equation.

$$\dot{m}_i = C_{d,i} \cdot \mu_i \cdot A_i \cdot \sqrt{\rho_{i-1} P_{i-1} - \rho_i P_i} \qquad (2.18)$$

2.4 Development of mathematical seal model

To predict the leakage, cavity pressure and circumferential velocity distribution in non-contacting gas seals, numerical models have been implemented in MatLab for both real and perfect gas fluids. These models are based on the control volume bulk-flow approach. Seals with multiple restrictions are modeled as a series of nozzles followed by expanders.

Figure 2.5 – Fanno curve showing the changes in states across the seal

Figure 2.5 shows an enthalpy-entropy diagram highlighting the change of the state variables in the constrictions and the following cavities. In the constriction the gas accelerates with constant entropy and this acceleration is accompanied by a sharp pressure drop. After the flow acceleration, the gas jet expands and dissipates in complex turbulent vortices at constant pressure within the following cavity. Ideal dissipation would give total recovery of the original enthalpy, at the lower gas pressure in the cavity (Isenthalpic process). However, in a real annular seal, due to heat transfer from or to

the fluid and due to the addition of work through the rotating shaft, the transformation in a seal is not necessarily isenthalpic. Further, there is some recovery of pressure [23] due to residual kinetic energy. The mass flow rate is constant along the seal, and because the density decreases as the pressure drops, the flow velocity becomes higher at each subsequent constriction. Ideally, in each constriction the enthalpy drop would correspond to the isentropically evolving velocity ($\triangle h = V^2/2$). The enthalpy drop for different values of density defines the Fanno curve. This curve represents successive thermodynamic states of a gas flow governed by dissipation of kinetic energy.

2.4.1 Own seal models

The exchange of energy due to the shear forces between the rotor and the seal will result to the enthalpy variation across the seal. To highlight this issue, two different models with isenthalpic flow assumptions and adiabatic flow assumptions have been developed. In summary, The governing equations for turbulent compressible flow are continuity, circumferential momentum, and energy equation in each cavity of the seal. The thermo-physical properties of the working fluid are evaluated using the REFPROP [30] database. The following assumptions are used in the governing equations.

- The working fluid is in a single phase.

- The pressure is constant within a seal cavities.

- The wall shear stress is calculated using circumferential velocity and axial velocity is neglected.

- The isenthalpic model contains energy equation only in seal constriction considering relative velocity.

- The adiabatic model take account of energy equation, both, in seal constriction considering relative velocity and seal cavity considering circumferential velocity.

Governing equations

The derivation of the governing equations is borrowed directly from the book of Childs [10] and White [86]. The schematic representation of the control-volume with flow variables is shown in figure 2.6.

Continuity equation
The continuity equation for the control-volume is taken from [10]:

$$\frac{\partial}{\partial t}(\rho_i A_i) + \frac{\partial}{\partial \theta}\left(\frac{\rho_i A_i U_i}{R_r}\right) + \dot{m}_{i+1} - \dot{m}_i = 0 \tag{2.19}$$
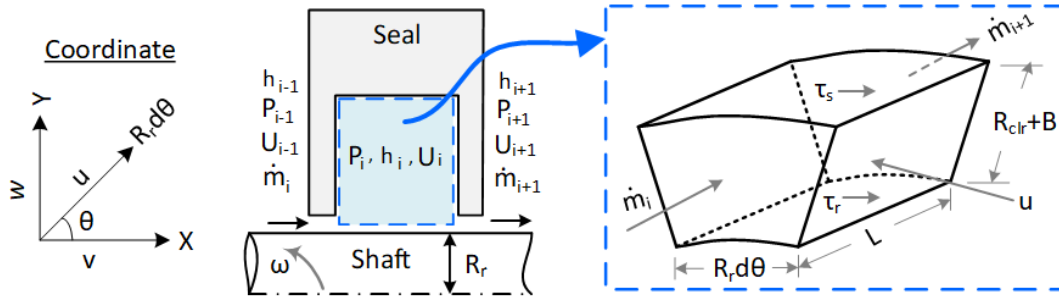
Figure 2.6 – Schematic illustration of the control-volume and flow variables

where, A_i is the cross-sectional area of seal cavity and defined by equation 2.20.

$$A_i = L_i(B_i + R_{clr,i}) \tag{2.20}$$

Circumferential momentum equation

Applying the control-volume in the circumferential direction in the seal cavity, the circumferential momentum equation is obtained as [10]:

$$-\frac{A_i}{R_r}\frac{\partial P_i}{\partial \theta} + (\tau_{ri}a_{ri} - \tau_{si}a_{si})\, L_i = \frac{\partial}{\partial \theta}\left(\frac{\rho_i A_i U_i^2}{R_r}\right) + \frac{\partial}{\partial t}(\rho_i A_i U_i) + \dot{m}_{i+1}U_i - \dot{m}_i U_{i-1} \tag{2.21}$$

where, a_{ri} and a_{si} denote the nondimensional lengths of rotor and seal cavity respectively upon which shear stress acts. The dimensionless lengths are defined by equation 2.22 for tooth-on-rotor and by equation 2.23 for tooth-on-stator seals.

$$a_{si} = 1 \qquad\qquad a_{ri} = \frac{2B_i + L_i}{L_i} \tag{2.22}$$

$$a_{si} = \frac{2B_i + L_i}{L_i} \qquad\qquad a_{ri} = 1 \tag{2.23}$$

Energy equation: Isenthalpic

The energy equation for isenthalpic transformation is used to calculate static enthalpy (h_{st}) in seal constriction and is defined by equation 2.24:

$$h_{st,i} = h_{in} - \frac{V_{rel,i}^2}{2} \qquad\qquad V_i = \frac{\dot{m}_i}{C_{di}R_{clr,i}\rho_{i-1}} \tag{2.24}$$

Energy equation: Adiabatic

Applying the conservation of energy in a control-volume with the adiabatic flow assumption, the energy equation in the seal cavity is expressed as [86]:

$$\frac{\partial}{\partial t}\left(e_i \rho_i A_i\right)+\frac{\partial}{\partial \theta}\left[\left(e_i+\frac{P_i}{\rho_i}\right)\left(\frac{\rho_i U_i A_i}{R_r}\right)\right]+\dot{m}_{i+1}\left(e_{out}+\frac{P_i}{\rho_i}\right)-\dot{m}_i\left(e_{in}+\frac{P_{i-1}}{\rho_{i-1}}\right)=\tau_{ri} R_r L_i \omega$$

(2.25)

The RHS of the equation represents the rotor frictional power loss, e is the total energy of the fluid, and consists of internal energy (u) and kinetic energy ($U^2/2$). Also, enthalpy (h) is denoted as the sum of internal energy and flow work.

$$e = u + \frac{U^2}{2} \qquad\qquad e + \frac{P}{\rho} = h + \frac{U^2}{2}$$

(2.26)

Finally, using the relation of equation 2.26, the energy equation 2.25 can be stated as:

$$\frac{\partial}{\partial t}\left(\left(u_i+\frac{U_i^2}{2}\right)\rho_i A_i\right)+\frac{\partial}{\partial \theta}\left(\left(h_i+\frac{U_i^2}{2}\right)\frac{\rho_i U_i A_i}{R_r}\right)+\dot{m}_{i+1}\left(h_i+\frac{U_i^2}{2}\right)-\dot{m}_i\left(h_{i-1}+\frac{U_{i-1}^2}{2}\right)$$
$$= \tau_{ri} R_r L_i \omega$$

(2.27)

Similarly, the energy equation for the seal constriction is expressed as:

$$h_{st,i} = h_{tot,i-1} - \frac{V_{rel,i}^2}{2} \qquad\qquad V_i = \frac{\dot{m}_i}{C_{di} R_{clr,i} \rho_{i-1}}$$

(2.28)

2.4.2 Solution procedure

The governing equations are solved iteratively to find the solutions for desired thermo-physical fluid properties within each control-volume. The schematic flow algorithm used in the adiabatic model is shown in figure 2.7 and for the isenthalpic model in figure B.1 in appendix. The solutions need to satisfy the following zeroth-order equations:

$$\dot{m}_i = \dot{m}_{i+1} = \dot{m}_0$$

(2.29)

$$\dot{m}_0\left(U_i - U_{i-1}\right) = \left(\tau_{ri} a_{ri} - \tau_{si} a_{si}\right) L_i$$

(2.30)

$$\dot{m}_0 \left(h_i + \frac{U_i^2}{2} \right) - \dot{m}_0 \left(h_{i-1} + \frac{U_{i-1}^2}{2} \right) = \tau_{ri} ar_i L_i R_r \omega \qquad (2.31)$$

Initially, a guess leakage mass flow is calculated assuming seal with single constriction
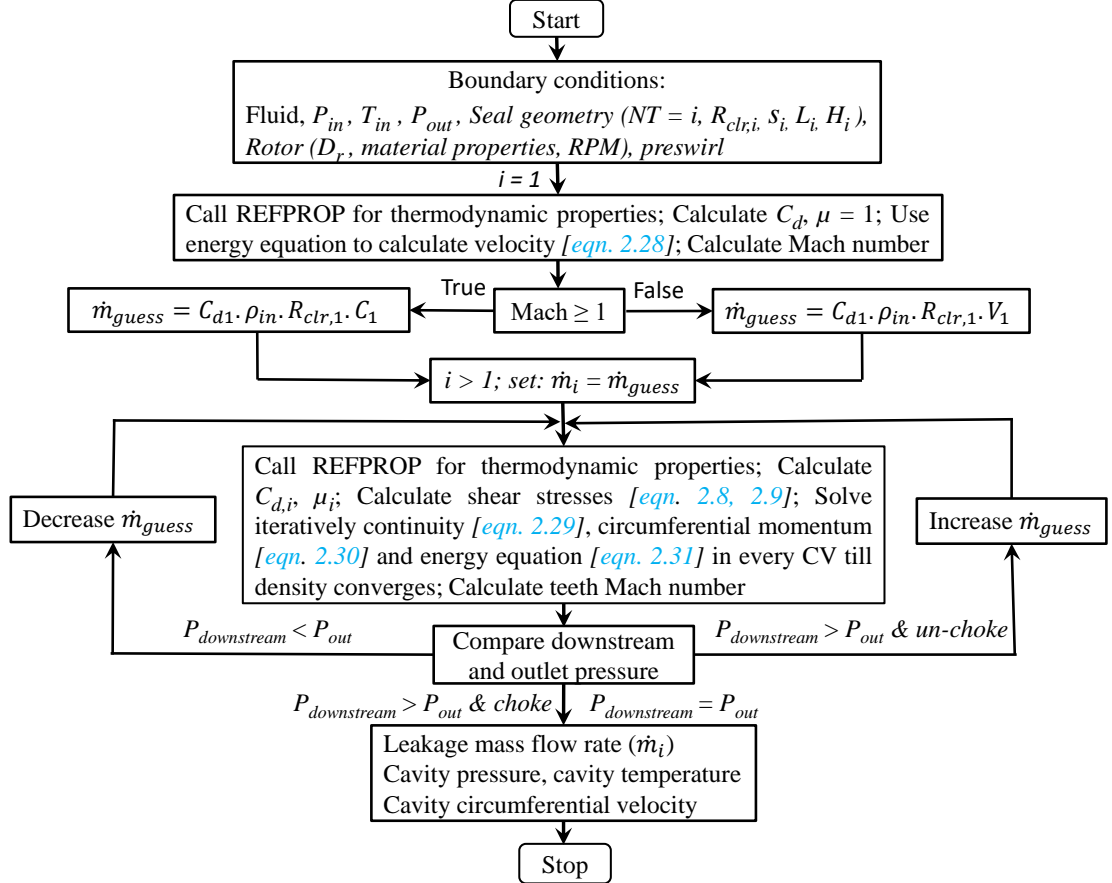
Figure 2.7 – Iterative solution scheme of author two control volume bulk-flow model

taking consideration whether flow is choked or un-choked. For multiple constrictions, this start mass flow rate is used to calculate the axial leakage velocity using equation 2.24 or 2.28, and hence relative velocity in each constriction is calculated using equation 2.32.

$$V_{rel,i} = \sqrt{V_i^2 + U_{i-1}^2} \qquad (2.32)$$

where, U_{i-1} is the circumferential velocity in the prior cavity.

Furthermore, using the energy equation static enthalpy in each constriction is calculated. As the flow in constrictions is assumed to be isentropic, with the known value of entropy in the preceding cavities and calculated static enthalpy in each constric-

tion, static pressure and Mach number distributions are determined using REFPROP database. The discharge coefficient, kinetic carry-over coefficient and shear stress correlation are selected as desired. In the case of the isenthalpic model, each cavity enthalpy remains fixed to the known inlet value. The cavity pressure remains the same as that of teeth pressure due to the isobaric dissipation assumption. With these two flow properties, entropy and other thermodynamic variables are obtained.

For the adiabatic model, similar assumptions to the isenthalpic model holds only in the seal constrictions. Additionally, this model use energy equation with friction effect as mentioned in equation 2.31 to calculate the cavity enthalpy distributions. The cavity pressure distributions are determined taking residual kinetic energy into account. With the calculated cavity pressure and enthalpy values, required thermodynamic gas properties are acquired using the REFPROP database.

In summary, the solution procedure initiates with a first guess mass flow rate. The coupled zeroth-order continuity, circumferential momentum, and the energy equations are solved iteratively in all control-volumes till the density converges to a designated desired value. Further, the calculated downstream pressure is compared with the prescribed outlet pressure. If the calculated pressure is lower than the given outlet pressure, the guess value of mass flow is reduced. Conversely, if the calculated pressure is higher than the given outlet pressure and the flow is un-choke (Mach < 1), the guess value of mass flow is increased. This process is repeated until the proper convergence is achieved.

2.5   Development of the St. Venant mathematical seal model

The governing equations for this model are continuity and circumferential momentum equations (see section 2.4.1 and 2.4.1). The basic assumption of this model is a single-phase working fluid following the ideal gas law. The St. Venant equation [85] is used as a base leakage model in the continuity equation. The zeroth-order solution of the governing equations results in steady-state leakage, cavity pressure, and circumferential velocity distribution.

Initially, guess leakage mass flow rate through the seal is calculated assuming a single constriction using St. Venant equation as shown in equation 2.16 in section 2.3.2. The leakage calculation is initiated with a guess mass flow rate and the known values of the inlet variables. Further, using the St. Venant equation 2.16 and circumferential momentum equation 2.30, the unknown downstream pressure and circumferential velocity are calculated, which will be used as the upstream value for next tooth. The adjacent cavity pressure and circumferential velocity are determined in a similar manner. In this way, the calculation is performed until downstream of the last constriction.

The mass-flow is iterated until the calculated downstream pressure and Mach number corresponds to the imposed boundary condition. In the governing equations, the discharge coefficient, kinetic carry-over coefficient, and shear stress correlation can be adapted as per the requirements.

2.6 Development of the Neumann mathematical seal model

In this model, the governing equations and the assumptions are similar to the St. Venant mathematical model (refer to section 2.5). Furthermore, the solution procedure is analogous to the St. Venant model. The only difference in this model is the implementation of the Neumann leakage equation (refer to section 2.3.3) instead of the St. Venant leakage equation. Similar to the other models, the discharge coefficient, kinetic carry-over coefficient, and shear stress correlation can be adjusted. This model employs the corrective iterative method to solve the governing equations to predict the leakage mass flow rate, cavity pressure and cavity circumferential velocity distributions in the seal.

2.7 Development of the modified Neumann mathematical seal model

Recently, Cangiloi et al. [35] proposed an improvement to the existing state-of-the-art bulk-flow models by introducing the energy equation in their analysis. They considered the effect of the energy equation to better characterize the real gas properties due to the enthalpy variation in the seal cavities. However, they assumed the enthalpy variation in the seal cavities only for the centered rotor (zeroth-order). They performed sensitivity studies on commonly used correlations and compared the results with the experimental data to identify the most accurate combination of correlations to be implemented in the bulk-flow model. Their study concluded that the model with the Neumann leakage equation, Swamee-Jains's friction factor correlation, Chaplygin's discharge coefficient and Kurohashi's kinetic carry-over coefficient [50] showed the best tradeoff in the estimation of seal performance. The modified Neumann equation (refer to the equation 2.18) in this thesis is a generalized form of the Neumann equation by Cangioli et al. [35] and referred as the Neumann model in this work.

The solution procedure is similar to the author models as described in section 2.4.2. Initially, a guess leakage mass flow is introduced. With the known values of mass flow rate, inlet pressure and inlet density, the modified Neumann equation is used to determine the subsequent cavity pressure and density until the density converge. This process continues until the downstream pressure and Mach number matches with the prescribed boundary conditions. Similar to the other models, different kinetic

carry-over coefficient, the discharge coefficient, and the shear stress correlations can be selected. The output are leakage flow rate, cavity pressure, cavity circumferential velocity, and other thermo-physical properties.

2.8   Results and discussions

In this section, the numerical results of the author models and the-state-of-the-art models described in section 2.4 are compared with existing literature to benchmark the seal models. For the sake of comparison, all the seal models employ identical discharge coefficient, carry-over coefficient and shear stress correlation as implemented in the reference model. The seal geometry and the operating conditions of the reference cases are listed in table 2.1. The abbreviations used for the different models to present the results is shown in table 2.2.

Table 2.1 – *Seal geometry and operating conditions of the reference case [35]: Nitrogen*

Boundary conditions	Case A	Case B
Inlet pressure (bar) P_{in}	72.75	35.03
Outlet pressure (bar) P_{out}	50.89	25.14
Inlet temperature (K) T_{in}	287	294
Rotational speed (rpm)	12000	10000
Inlet swirl velocity (m/s) U_{in}	101 (positive)	110 (negative)
Rotor radius (mm) R_r	110	110
Radial clearance (mm) R_{clr}	0.3	0.3
Cavity pitch (mm) L	4.7	4.7
Cavity depth (mm) B	4	4
Tooth width (mm) t_w	0.2	0.2
Number of teeth NT	14	14
Absolute roughness (μm) e	3.2	3.2
Discharge coefficient (-) C_d	Chaplygin	Chaplygin
Carry-over coefficient (-) μ	Neumann	Neumann
Shear stress correlation (Pa) τ	Swamee-Jain	Swamee-Jain

Table 2.2 – Abbreviation of implemented seal models

Acronym	Definition
AdiabModel	Author's model with adiabatic flow assumptions
IsenModel	Author model with isenthalpic flow assumptions
NeumannModel	Based on Cangioli et al. [35] with Neumann leakage equation [51]
IdealModelNeumann	Ideal model based on Neumann leakage equation [51]
IdealModelSt.Venant	Ideal model based on St.Venant leakage equation [14]

Figure 2.8 shows the comparison of leakage between experimental results of Cangioli et al. [35] and the numerical results obtained from different seal models. For the positive inlet pre-swirl (refer to Case A in table 2.1), there is over-prediction of leakage by all the

models. The maximum and the minimum discrepancy of 7.5% and 0.2% have been observed by the ideal St. Venant model and the modified Neumann model respectively. The reference model indicated a minor deviation of 1.2% whereas the adiabatic model and the isenthalpic model showed a deviation of 4.9% and 6% accordingly. In the case of negative pre-swirl (refer to Case B in table 2.1), all the models under-predict leakage. The maximum relative deviation of 10.3%, 9.4%, 7.4%, 7.1%, 7%, 6.9% and 5.7% were monitored by the modified Neumann model, adiabatic model, reference model of Cangioli et al. [35], Thorat and Childs model [35], isenthalpic model, ideal Neumann model and ideal St. Venant model respectively. Despite the existence of deviations in all models, the predicted leakage mass flow rates are within the band of measurement uncertainty, hence justifying the validity of all seal models.
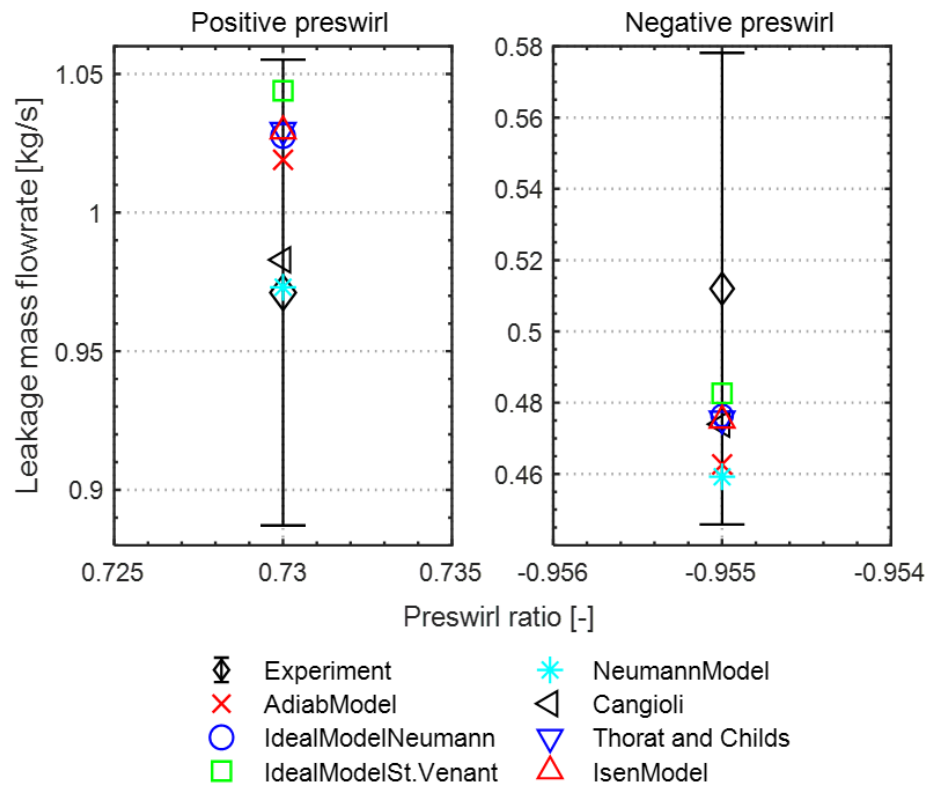
Figure 2.8 – Prediction quality of the leakage mass flow by different seal models compared to the experimental data of Cangioli et al. [35]

Besides the comparison of the seal models with the literature in nitrogen as a working fluid, a similar investigation has been performed in air and the result is presented in table 2.4. The seal geometry and operating conditions are shown in table 2.3. The prediction accuracy of leakage mass flow from the model developed by the author with the adiabatic flow assumption matches well with the reference experimental values at

all operating conditions. However, a significant under-prediction from the author's model has been noticed for the radial clearance of 0.4 mm compared to the experimental result from Scharrer [59] which, in author opinion appears to be measurement or presentation error. This statement is justified when comparing the results with the model from Bradley [87].

Table 2.3 – *Seal geometry and operating conditions of the reference case: Air*

Boundary conditions	Case C [41]	Case D [59]	Case E [59]
Inlet pressure (bar) P_{in}	3.08	8.25	3.08
Outlet pressure (bar) P_{out}	1.01	0.943	0.943
Inlet temperature (K) T_{in}	300	283.15	283.15
Rotational speed (rpm)	-	3000	3000
Inlet swirl velocity (m/s) U_{in}	20 (positive)	60 (positive)	60 (positive)
Rotor radius (mm) R_r	77	75.7	75.7
Cavity pitch (mm) L	3	3.05	3.05
Cavity depth (mm) B	3.2	3.2	3.2
Tooth width (mm) w	0.2	0.15	0.15
Number of teeth NT	16	16	16
Discharge coefficient (-) C_d	Eser and Kazakia (0.716)	Chaplygin	Chaplygin
Carry-over coefficient (-) μ	Neumann	Neumann	Neumann
Shear stress correlation (Pa) τ	Blasius	Blasius	Blasius

Table 2.4 – *Comparison of leakage between author's adiabatic model and reference literature with air as a working fluid*

Case	R_{clr} (mm)	$\dot{m}_{exp}$ [59] (kg/s)	$\dot{m}$ [87] (kg/s)	$\dot{m}_{Adiab}$ (kg/s)	RDev: Adiab & Exp (%)
	0.33	0.11	0.098	0.1064	3.3
D	0.4	0.178	0.12	0.135	24.2
	0.5	0.189	0.16	0.18	4.71
	0.33	0.039	0.036	0.0385	1.3
E	0.4	0.064	0.046	0.049	23.5
	0.5	0.067	0.061	0.065	2.7

For a published result of Cangioli et al. [35] with negative inlet pre-swirl (refer to case B in table 2.1), the comparison of cavity pressure and circumferential velocity distribution are shown in figures 2.9 and 2.11 respectively. All the investigated seal models predict cavity pressure accurately with respect to the reference model of Cangioli et al. [35] with a minor under-prediction. The author's adiabatic model indicated the lowest deviation of 1.3% at seventh cavity compared to the ideal Neumann model and the ideal St. Venant model which, showed almost identical value of 1.6% in the same cavity. Furthermore, in the case of air test (refer to case C in table 2.3), the adiabatic model slightly over-predicts pressure with a relative difference of 2% in the last cavity (see figure 2.10) compared to the reference model of Eser and Kazakia [41]. Unfortunately,

literature lacks the measurement of cavity pressure. On the other hand, numerical results showed good agreement with each other, thus highlighting the reliability of all seal models.
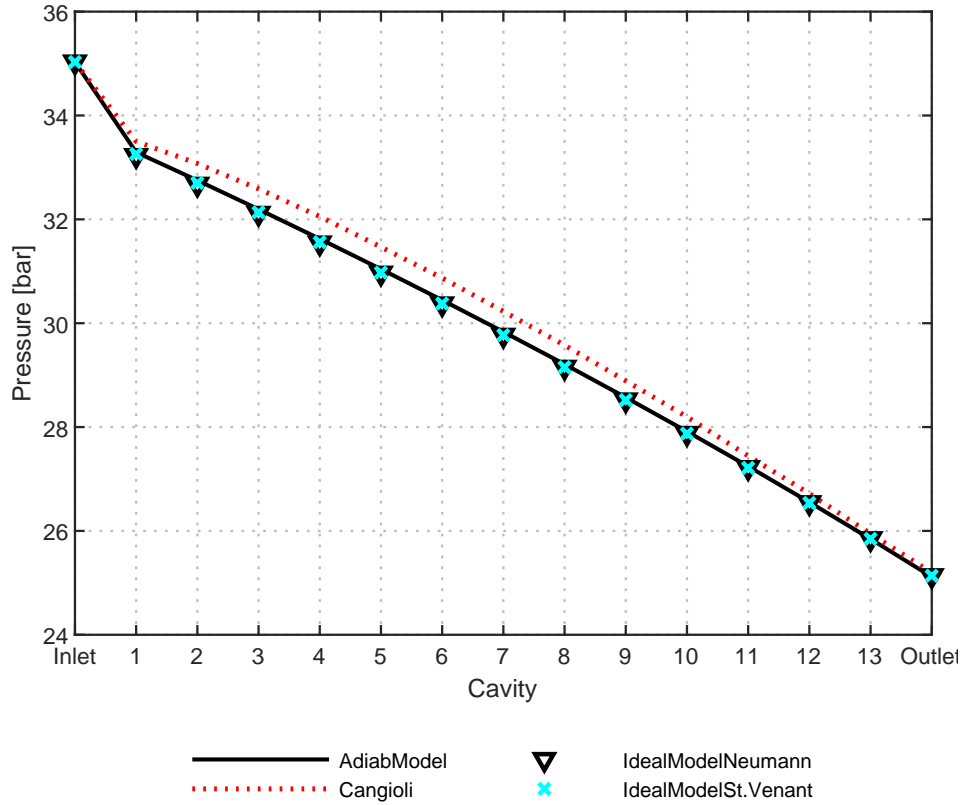
Figure 2.9 – Prediction quality of the cavity pressure distribution by different seal models compared to the experimental data of Cangioli et al. [35]: Case B

Additionally, figure 2.10 displays the cavity circumferential velocity profile estimated by the author's adiabatic model and the reference model of [41] for both rotating and stationary rotor in test case C as mentioned in table 2.3. The implemented adiabatic model under-predicts circumferential velocities for both rotor operating conditions. The maximum relative error for the rotating case is 7% in the seventh cavity while the non-rotating case is 15.1% in the last cavity.

Figure2.11 shows the comparison of the cavity circumferential velocity distribution predicted by different seal models and the reference model of Cangioli et al. [35] for negative inlet pre-swirl ratio. Compared to the other seal models, the adiabatic model demonstrates a better agreement with the reference model. However, the highest relative error of 70.6% has been noticed in the seventh cavity, but at a velocity very close to zero. The adiabatic model shows under-prediction of circumferential velocity in all the cavity whereas the ideal Neumann and the ideal St. Venant model indicated
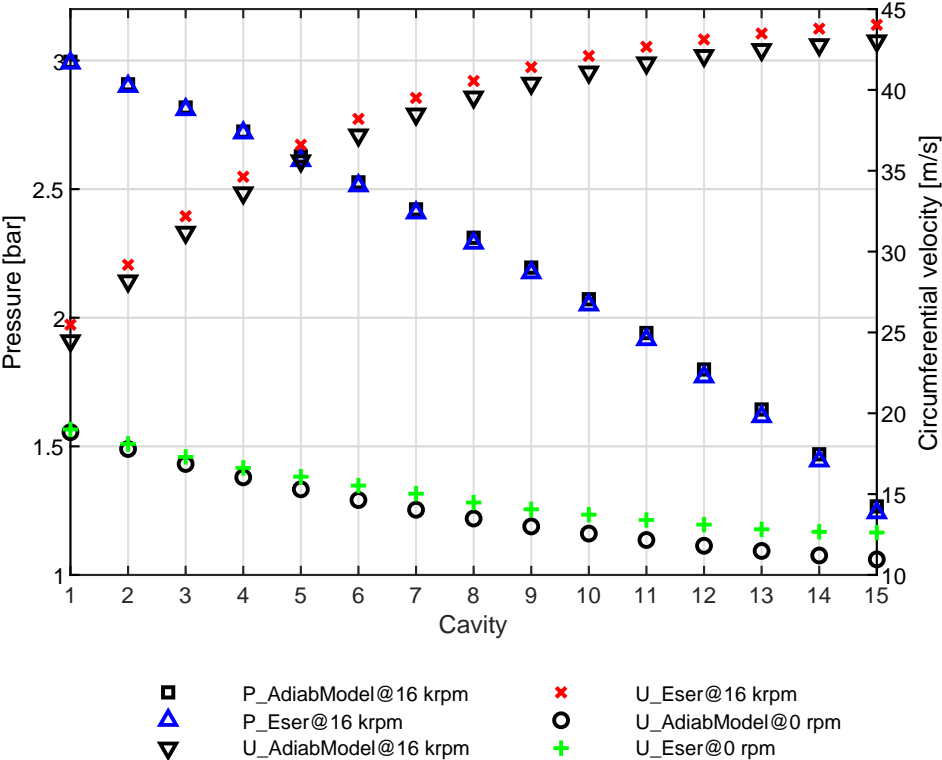
Figure 2.10 – Pressure and circumferential velocity distribution from adiabatic model and reference literature [41]: Case C

similar higher value in over-prediction ranging from 25% till 680%.
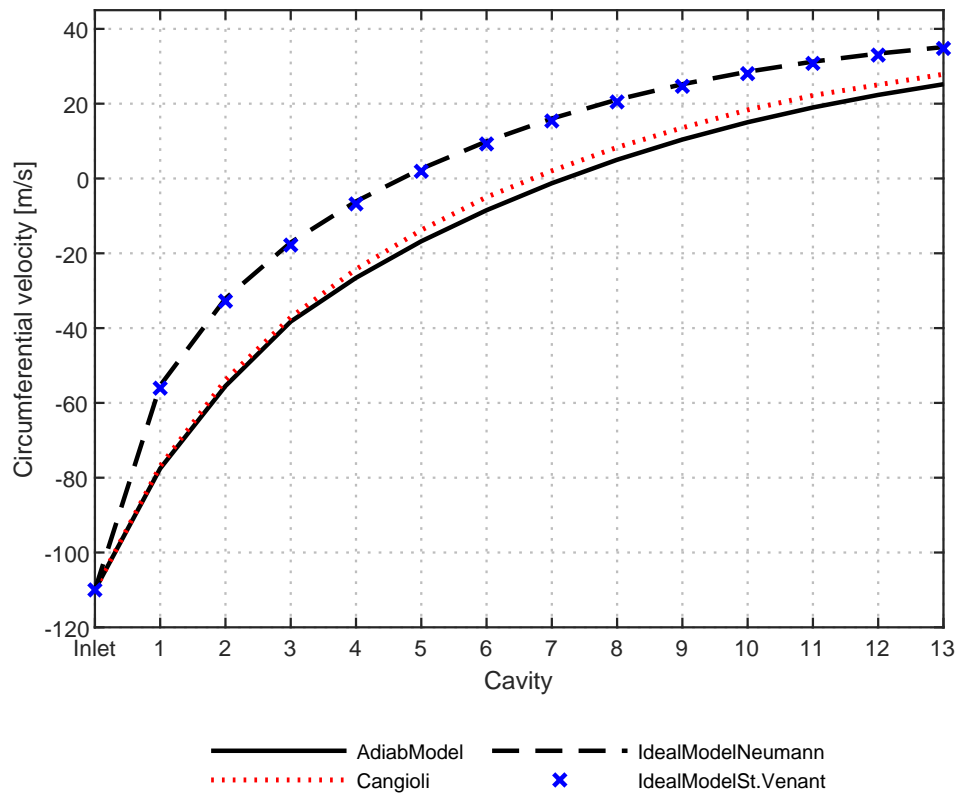
Figure 2.11 – Prediction quality of the cavity circumferential velocity distribution by different seal models and Cangioli et al. [35] model: Case B

2.9 Conclusion

This chapter presents the theoretical background employed in the seal modeling process. The most commonly used Bulk-flow model in seal analysis, its types, the governing equations, assumptions and the different correlations used in this model have been discussed. The lack of validation of the-state-of-the-art bulk-flow models on reduced-scale turbomachinery seals with working fluid operated near to the saturation point has been highlighted. To address these issues, two mathematical seal models, namely, isenthalpic and adiabatic, considering the real gas properties of the fluid have been developed. Further, three different state-of-the-art seal models have been developed for comparison. Finally, the prediction quality of the seal models developed in this work have been compared with the available well-established literature at large-scale seals as a benchmarking process. The following conclusions can be drawn from this chapter:

- The bulk-flow model is the most widely used method as a design tool to predict seal performance. Although CFD approaches claim better prediction accuracy, they are time expensive compared to the bulk-flow models. The prediction

accuracy of the bulk-flow model relies on many correlations that are used to simplify the complex three-dimensional turbulent flow in seals, hence, these correlations need to be properly selected. Furthermore, a hybrid CFD / Bulk-flow model can be used in seal analysis as a trade-off between prediction accuracy and cost.

- The comparison of the predicted leakage has been performed between experimental results available in the literature and numerical results obtained from seals models developed in this work. Overall, four different cases at large-scale seals with air and nitrogen as working fluids, both, positive and negative inlet pre-swirl velocity at high, medium and low-pressure inlet conditions have been investigated. All the implemented seal models showed good agreement within the range of measurement uncertainty.

- Accurate prediction quality of the cavity pressure distributions have been observed in all test cases between the reference literature and the implemented seal models with minor deviations.

- The adiabatic model developed by the author suggests good agreement on the cavity circumferential velocity to the reference literature for both positive and negative pre-swirl case whereas both ideal Neumann model and the ideal St. Venant model showed poor prediction performance with respect to the reference case.

In summary, for large-scale seals, the bulk-flow models developed by the author including the-state-of-the-art bulk-flow models illustrated good agreement to the experimental data for leakage. Furthermore, the numerical results of cavity pressure distribution obtained from all investigated seal models match well with the reference literature. The aforementioned points demonstrate the validity of all models for leakage and cavity pressure prediction in large-scale turbomachinery. On the other hand, the adiabatic model developed by the author showed the lowest deviation with respect to the reference model of Cangioli et al. [35] (so-called generalized Neumann equation for real gases) compared to the both ideal models (Neumann and St. Venant), hence, highlighting the advantage of the energy equation and real gas properties in the seal analysis.

3 | Design of reduced-scale seal and test-rig

This chapter provides a detailed description on the design and development process of test-rig to perform experimental investigations on reduced-scale clearance seals. Also, the design and manufacturing of the selected seals, seal housing and assembly procedure including the mounting of the measurement probes in the seal assembly are discussed. Furthermore, the design specifications, instrumentation, measurement capabilities, and operating procedure is presented.

3.1 Introduction

A large number of numerical and experimental investigation is available on seals for large-scale ($D_r > 0.1\ m$) turbomachinery applications. However, only limited experimental data is available for real gas effects on seals at large-scale application. For reduced-scale seals, to the author's knowledge, no such investigations have been published yet. To predict seal performance at reduced-scale for high-speed turbomachinery application, where the working fluid have non-ideal properties, a new model has been developed and implemented. To validate the model and also to examine seal performance experimentally, a dedicated test-rig for such reduced-scale seals needs to be developed. This chapter summarizes the design and development of the test-rig including the test seals assembly and instrumentation that allow the experimental assessment of reduced-scale seals operated at different boundary conditions serving as a source of validation of the numerical model.

3.2 Objectives of the experimental campaign

The objectives of the experimental campaign are as follows:

- Test and compare the performance of different seals at reduced-scale.

- Gather experimental data for the validation of different seal models.

- Capture real gas effects.

3.3   Design specifications

The first step prior to the conceptual design of the test-rig is to characterize the specifications and requirements of the experimental rig. The technical requirements of the seal-test-rig are summarized as follows:

- Hermetic test-rig up to the pressure level of 30 bar.

- Capability of testing seals at varying inlet and outlet pressure with a maximum seal inlet pressure of 25 bar and a maximum pressure ratio of 4.

- Ability to condition the inlet fluid pressure and temperature to capture the effect of the seal operating close to the saturation line (real gas effects).

- Flexibility of testing different types of seals in a universal seal housing.

- Versatility of test-rig to use different test fluid.

- Adaptability of testing the influence of seals on different rotor and gas-bearing high-speed reduced-scale turbomachinery systems.

- Alignment mechanism between seal and rotor.

- Leakage, pressure, and temperature measurement at the inlet and exhaust as well as within the seal along the leakage path.

3.4   Test loop

Taking into consideration of the design specifications, a dedicated test-rig for reduced-scale seal investigation has been designed and developed. The test-rig is mainly comprised of a reciprocating compressor, heat exchangers, thermostat, seal test section, piping, electrical cabinet and measurement probes. Figure 3.1 shows a photograph of the operational seal test-rig displaying some of the major components which are divided into two main section, namely, test loop and test section. The schematic diagram and position of the test-rig is provided in figure 3.2.

The main purpose of the test loop is to feed the seal test section with a continuous supply of test fluid, mainly refrigerant R134a. Beside R134a, commonly used gases like air, nitrogen, and argon can be easily fed in a loop as a test fluid. The test loop is equipped with a reciprocating compressor, a variable frequency drive to control the
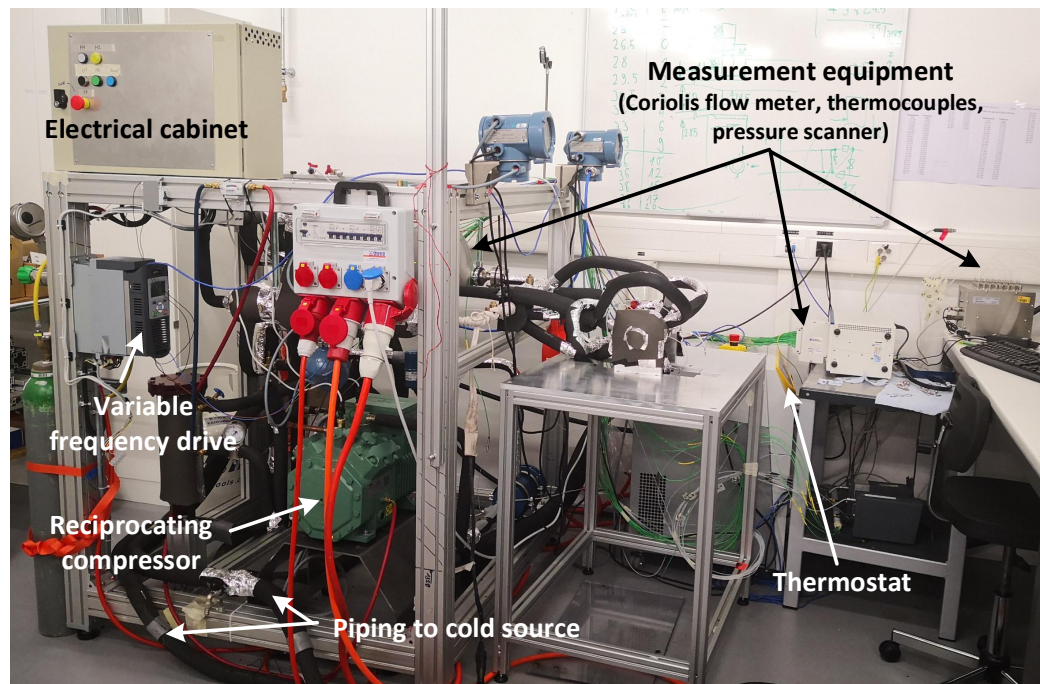
Figure 3.1 – Photograph of the operational seal test-rig showing test loop including compressor assembly (left), and adaptable seal test section (right)

compressor motor, a coalescent type high-grade oil separator, three flat plate type heat exchangers, a Lauda thermostat, supply from a cooling source, two Coriolis mass flow meters, a liquid separator, a filter drier, three pressure regulators, eight manometers, four pressure transducers, a differential pressure sensor, fourteen thermocouples, valves, piping, and an electrical enclosure. A brief overview of the main components of the test loop is presented below.
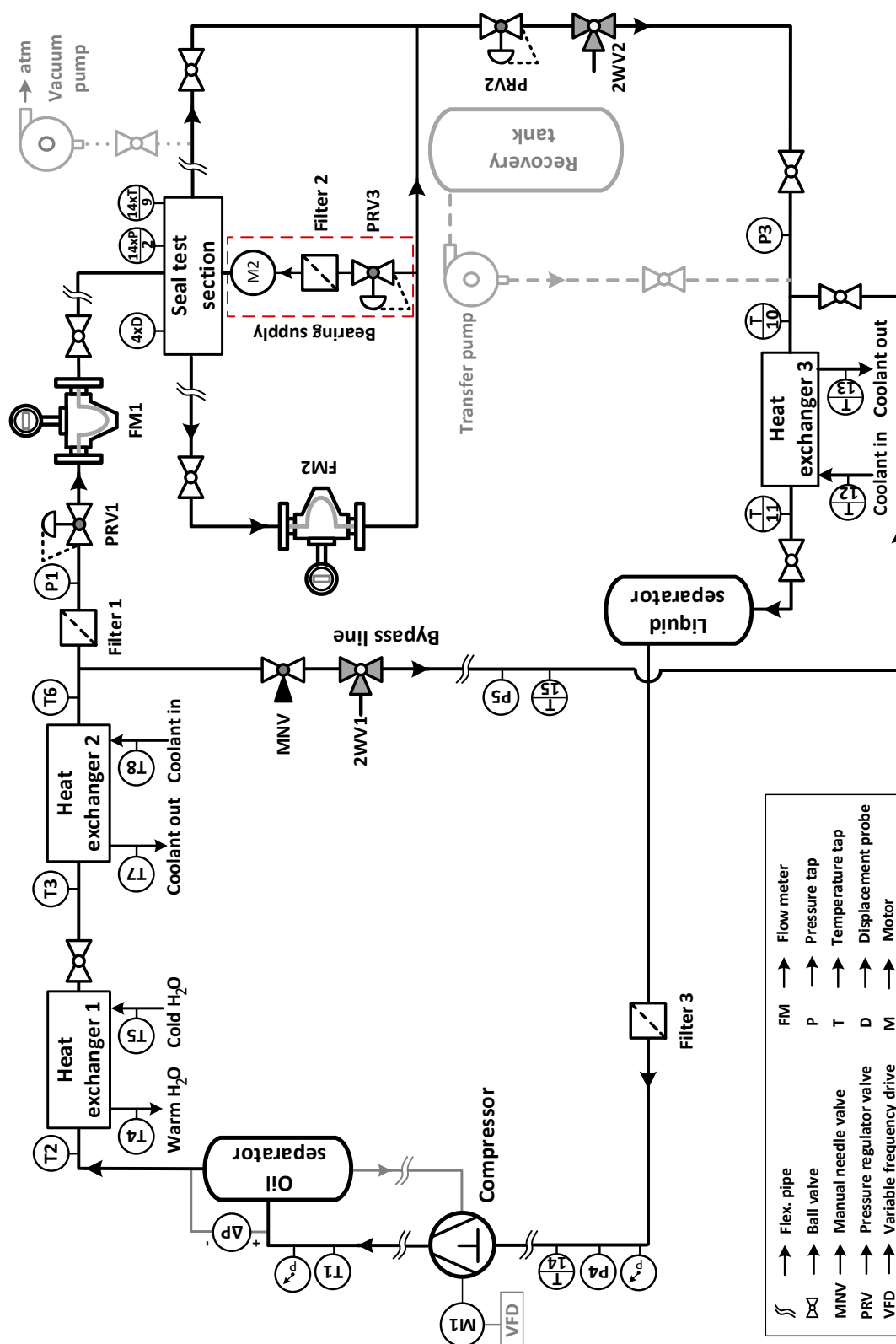
Figure 3.2 – Schematic flow chart of the test-rig

- **Speed controlled compressor**

A semi-hermetic reciprocating four-cylinder compressor, 4FDC-5Y [1] model from Bitzer, with a maximum 6.4 kW input power star-connected motor has been employed in the test loop. The compressor is the backbone of the test loop which raises the pressure level and maintains the continuous flow of refrigerant R134a in a closed loop. Depending upon the inlet condition, the discharge pressure ranges from few bars till 35 bar and refrigerant mass flow varies from a couple of g/s till almost 150 g/s.

To control the speed of the compressor and hence the mass flow rate, the Bitzer VARI-PACK frequency inverter FDU+16 [2] model has been installed in the test-bench. The frequency range varies from a minimum of 25 Hz to a maximum of 70 Hz. For the capacity control of the compressor, an external setpoint signal of 0-10 V has been used to activate minimum and maximum speed of the compressor.

- **Oil separator**

The compressor in the test-rig is a reciprocating piston type, hence, oil is used as a lubrication. A small fraction of the oil escapes with the discharged refrigerant. The oil in a system not only reduces the heat transfer rate in heat exchangers but also the presence of oil droplets in the gas lubricated seal- bearing-rotor assembly may lead to a fatal consequence in high-speed turbomachinery. To avoid this issue, a Temprite coalescent oil separator 922R [3] series model has been implemented. This oil separator is capable to filter contaminants down to 0.3 μm.

- **Heat exchangers**

To maintain the desired seal inlet temperature two flat plate heat exchangers have been used. The first heat exchanger (SWEP B5THx20/1P-SC-M [4]) removes the excess heat of the superheat fluid from the compressor using water as a cooling fluid. The second heat exchanger (SWEP B5THx30/1P-SC-M [5]), serves as a seal inlet temperature regulator and is controlled by a precision thermostat (Lauda Variocool VC 2000 W [6]). Furthermore, to maintain the desired suction pressure to the compressor, another heat exchanger (SWEP B25THx70/1P-SC-M [7]) has been employed. The existing 40 kW cold unit with water/glycol mixture as a heat transfer fluid is used to sub-cool the working refrigerant to maintain the stable desired compressor suction side pressure.

---

[1]https://www.bitzer.de/shared_media/documentation/kb-104-7.pdf
[2]https://www.bitzer.de/shared_media/documentation/cp-100-2.pdf
[3]https://temprite.com/products/coalescent-oil-separators/920r-series-w-reservoir/
[4]https://www.swep.net/products/b5t/
[5]https://www.swep.net/products/b5t/
[6]https://lauda-brinkmann.com/summary/?product_type=variocool&product=Variocool_VC_2000_W
[7]https://europe.swepbusiness.net/residential-heating/heat-pumps/b25t/b25thx70-1p-sc-m-2x28u-20-2x1-22u-20-/prod14147-070.html

- **Pressure regulators**

To reduce the high pressure from the source, such as compressor or pressurized cylinder, to a lower desired value, three different (KPR [8] Swagelok) pressure regulators have been embedded in a test-rig. The maximum inlet pressure is rated as 248 bar and the outlet pressure control ranges from 0 to 34.4 bar. Each pressure regulator is fitted with two manometers to have a visual inspection of the inlet and outlet pressure. Out of three pressure regulators, one is fitted to the seal inlet to set the desired pressure, the second one is installed at the outlet of the seal test section to maintain the desired low-pressure. The third one is fitted to the pressurized cylinder, to perform the leakage test of the whole test-rig.

- **Liquid separator**

As discussed in the previous section 3.4, the low-pressure heat exchanger is maintained in two-phase fluid to establish a stable suction pressure to the compressor. Depending upon the operating conditions, situations can occur when some portions of the liquid refrigerant are carried-over into the compressor and as a consequence liquid-hammer might occur which leads to compressor damage. A liquid separator, (FA-12/15 [9] ESK Schultze), has been selected and installed at the outlet side of the heat exchanger to prevent compressor damage.

- **Filter drier**

To extract the residual moisture and contaminants of the working fluid, a filter drier (FT1-16-CDM [10] ESK Schultze) has been installed between the liquid separator and the compressor suction side.

3.4.1   Seal test section

The seal test section is the heart of the test-rig since it contains the test seals and the relevant instrumentation to measure the seal performance. The back-to-back test approach, two identical seals placed opposite to each other with inlet at the center, is adapted in order to cancel out the axial thrust force of the rotor. A central gas input divided into streams of symmetric flow path towards the two seals. The exit flow of both seals are fed back into the test-rig by two individual outlets. Figure 3.3 shows the seal test section and its relevant components. It is composed of the test seal, the seal outer housing, fluid inlet and outlet housings, and a dummy rotor. The seal and

---

[8]https://www.swagelok.com/downloads/webcatalogs/EN/MS-02-230.PDF
[9]https://www.esk-schultze.de/Produktgruppe.php?Code=FA&p=2&la=en
[10]https://www.esk-schultze.de/Katalog/ESK_Katalog_min.pdf#page=52

its housing are composed of multiple channels to measure pressure and temperature distribution along and around the seal fluid flow. The housing also holds and positions the centering mechanism for the rotor using two orthogonally placed micrometric screws and proximity probes on each side. The assembly steps of the seal test section are illustrated in figure C.6.
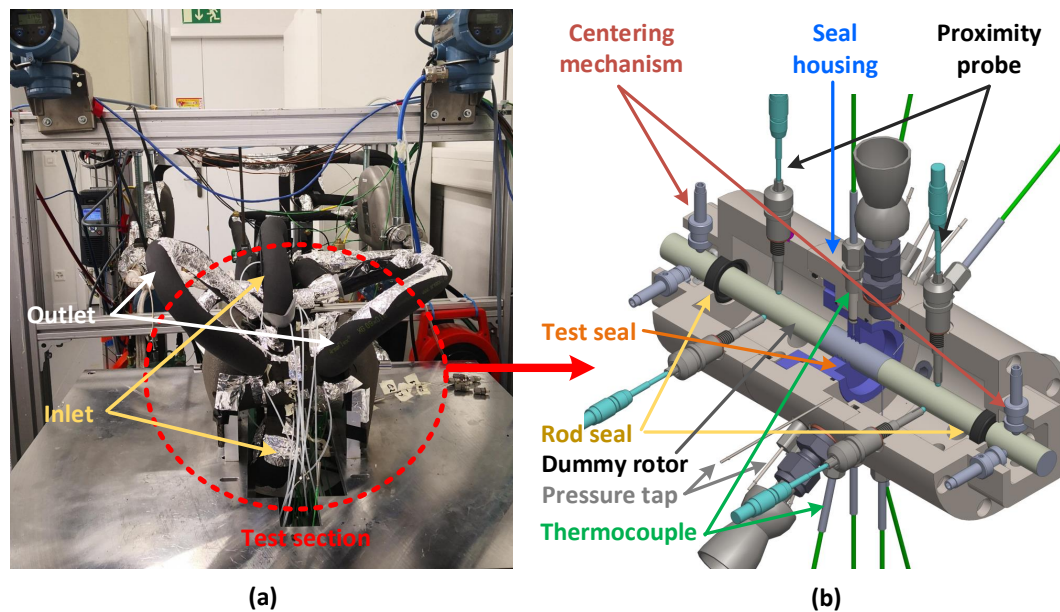
Figure 3.3 – Photograph of the seal test section mounted in a test bench (a); isometric cut view of test section highlighting the components and instrumentation (b)

3.4.2 Instrumentation

The test loop is equipped with pressure, temperature and mass flow measurement probes to monitor the performance of all the relevant components within a test loop.

The absolute pressure at different locations in a test loop is measured via four piezoresistive pressure transducers. Three pressure transducers are installed to monitor the pressure at the inlet of the pressure regulator, bypass pressure at the outlet of the manual needle valve and exit side of the low-pressure heat exchanger respectively. The pressure measurement ranges from 0 to 40 bar with a working temperature ranging from -40 to +125°C. A fourth pressure transducer has been used to measure the compressor suction pressure. The measurement range varies from 0 to 20 bar with an operating temperature ranging from -20 to +50°C. Prior to the installment of pressure transducers in a test loop, each of them were calibrated (refer to section C.1 in appendix) indicating measurement error of ± 500 Pa. Besides the absolute pressure measurement, differential pressure indicator has been installed to monitor the health

of the oil separator.

The temperature of the fluid was measured at inlet and outlet of each heat exchanger, compressor suction and discharge sides including the bypass loop and near the pressure regulating valves using 1.5 mm sheath-diameter type K thermocouples. The immersion depth of each thermocouple is set to around 8 times the diameter of the thermocouple. All the thermocouples were calibrated using a temperature calibrator and a precision resistance temperature detector (RTD) as a reference probe. The calibration result is displayed in figure C.5 in the appendix which shows an average accuracy of ± 0.5 K in the desired range of 0 to +80°C.

The mass flow rate was measured using two Coriolis type mass flow meters supplied by Emerson[11]. The total mass flow rate into the seal was measured by CMFS040 model whose measurement range varies from 0 to 111 g/s. Since the flow is split into two parallel streams, an additional flow meter is used to measure one of the outlets to identify whether the flow distribution is split symmetrically between the two seal sections.

The pressure and temperature measurement at the seal inlet, outlet and inside the seal were carried out using a Scanivalve pressure scanner and thermocouples respectively. At the inlet and outlet side of seal, pressure measurement was conducted at three equally spaced (circumferential) positions and averaged. Also, along the seal length, pressure measurement was performed at four equally spaced positions in each flow cavity. For the pressure measurement, 16 channel temperature compensated Scanivalve pressure scanner, DSA 3217 [12] model, has been used. The temperature measurements within the test section have been carried out using mineral insulated 0.5 mm sheath-diameter type K thermocouples. To measure the seal inlet and outlet temperature, three thermocouples have been installed on each side at an equally spaced position and averaged measurement value was recorded. Regarding the temperature measurement within the seal, two orthogonally placed thermocouples were employed in each seal cavity. Due to the space constraint in the seal flow cavities, the immersion depth of 0.5 mm has been chosen.

An overview of the measurement probes used in the test-rig is provided in table 3.1.

---

[11]https://www.emerson.com/documents/automation/product-data-sheet-elite-series-coriolis-flow-density-meters-micro-motion-en-66748.pdf

[12]https://scanivalve.com/media/28047/dsa3217-18_1604.pdf

Table 3.1 – Lists of measurement probes

Description	Type	Range	Accuracy	Manufacturer
Pressure transducers	Piezoresistive	0-40 bara	$\pm$ 0.25% of span	WIKA
Pressure transducer	Piezoresistive	0-20 bara	$\pm$ 0.5% FSO	Kistler
Pressure scanner (16 ch)	Piezoresistive	0-17.24 bara	$\pm$ 0.05% FSO	Scanivalve
Diff. pressure sensor	-	1 bar	-	Temprite
Thermocouples	K	-40-1000°C	1.5 K	ES
Flowmeter	Coriolis	0-111 g/s	$\pm$ 0.25% of span	Emerson
Flowmeter	Coriolis	0-55 g/s	$\pm$ 0.25% of span	Emerson

3.5 Experimental procedure

The experimental procedure is categorized into three chronological steps, namely experiment protocol, testing, and data acquisition.

3.5.1 Experiment protocol

Prior to the experimental testing of seals, the following steps are performed:

- Mounting of the test seal in the seal housing along with the dummy rotor, inlet and outlet housing, thermocouples and pressure taps fitted with the custom made fittings. The assembly procedure of all the components and instrumentation is provided in figure C.6. The inlet supply and outlet flexible pipes of the test loop are connected to the designated fittings forming a closed flow loop. Finally, the whole test section is mounted on the support table.

- To guarantee a leakage-free system, the test-rig is charged with few grams of R134a refrigerant and pressurized till 30 bar with the argon gas from the pressurized cylinder. Once stable pressure is reached in the test-rig, refrigerant detector is used to physically inspect the leakage. Also, the pressure of the test-rig is monitored at least for 1 hour. After ensuring the leak-free system, the centering of the rotor is performed and the pressurized gas is released from the rig. Furthermore, the seal test section is insulated to reduce the heat transfer between the test fluid and the environment.

- For the R134a test, the rig is vacuumed before it is filled with the right amount of working fluid.

- The desired suction pressure to the compressor is established by cooling down the refrigerant using the 40 kW cold source (refer to point 1 in figure 3.4). Once the desired stable pressure is achieved, the compressor is ready to start.

3.5.2   Testing

After commissioning the test-rig by realizing the experiment protocol, the actual experimental investigation of the test seal begins. The schematic of the thermodynamic cycle of the test-rig under test conditions is illustrated in figure 3.4. The following procedures are carried out during the testing phase:

- Once the compressor is switched on, the discharge pressure and temperature of the refrigerant increases (from point 2 to point 3 in figure 3.4). Initially, the test section is at ambient temperature, to avoid condensation of refrigerant, the inlet pressure needs to be lower than the saturation pressure. This task is accomplished by the pressure regulating valve (refer to PRV1 in figure 3.2). The discharge pressure and temperature are continuously tracked.

- After the compressor discharge pressure and temperature reached a stable condition, the pressure at the seal inlet is slowly increased till the desired value (points 4 and 5 in figure 3.4) via PRV1. The inlet temperature (point 5 in figure 3.4) is controlled from the heat exchanger with the help of thermostat. The intended outlet pressure (point 6 in figure 3.4) is maintained through PRV2 (refer to figure 3.2). Furthermore, PRV2 also reduces the exit pressure (from point 6 to 7 in figure 3.4), and the refrigerant flow is connected to the low-pressure heat exchanger forming the closed flow loop (from point 7 to 1 in figure 3.4). Once the inlet and outlet boundary condition is stable, measurement data is logged and saved.
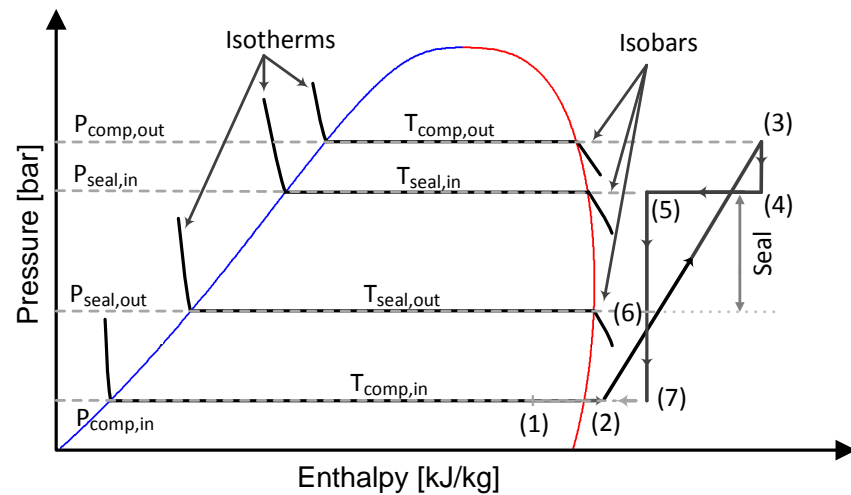
Figure 3.4 – Schematic representation of the thermodynamic cycle of test-rig under test conditions

3.5.3 Data acquisition

National Instrument, NI PXIe - 1078 [13] has been used for acquiring the data. The tracking and recording of the process parameters; especially mass flow rates, pressures, temperatures, and other auxiliary variables were carried out by LabVIEW [88] user interface. The final results were obtained by averaging the 100 data points recorded at a sampling rate of 0.5 Hz.

3.6 Test-rig key feature

The key features of the seal test-rig are summarized as follows:

- Hermetic test-rig ranging from 3 mbar to 30 bar absolute pressure.

- Adaptable to any state-of-the-art fluid used in reduced-scale turbomachinery applications.

- Modular design to test any seal geometrical features at a reduced-scale.

- Leakage mass flow measurement capability up to 55.5 g/s including temperature

---

[13]https://www.ni.com/pdf/manuals/378197a.pdf

and pressure measurement within the seal flow region.

- Seal inlet and outlet fluid pressure independently tunable to obtain test seal leakage map.

- Adjustable inlet fluid temperature to experimentally investigate the real gas effect in seal performance.

- Allows to measure the pressure and temperature evolution inside the seal section to provide more accurate data to validate the different seal models.

3.7 Limitations of test-rig

The identified limitations of the test-rig are as follows:

- The main limitation of the test-rig with a current layout is to perform an experimental investigation at elevated inlet pressure exceeding 15 bar due to the insufficient heating capacity of the used thermostat leading to a formation of two-phase flow at the seal inlet. However, this limitation can be eliminated by installing a thermostat right after the pressure reducing valve which acts as a throttling device and hence drastically reducing the exit side fluid temperature.

- The minimum feasible low-pressure in the test-rig for refrigerant R134a is 2.2 bar, corresponding to the achievable -8°C in the heat exchanger. The cold source temperature can be set to -17°C, equivalent to 1.5 bar for R134a. Nevertheless, mitigating the losses in the cold source supply line would be able to reduce the low-pressure side by some limits.

- In the case of air test, the maximum seal inlet pressure 5 bar was selected for the testing purpose due to the constraints of the supply source. However, using an air compressor or a pressurized air cylinder can avoid this limitation.

- The diameter of the test rotor was fixed to 14 mm for the whole experimental campaign. Nonetheless the rotor diameter can be changed as per the requirement by adapting the seal housing and the rod seals at both ends of the seal test assembly.

- The current test-rig has a fluctuating discharge pressure due to the reciprocating nature of the employed compressor, leading to the non-stable inlet pressure at the seal test section. A pressure settling chamber at the discharge end of the compressor would mitigate this effect.

- For R134a test, the identification of the right amount of fluid is crucial for the safety of the compressor. The general norm employed in HVAC systems was not valid in this test-rig. So, a trial-and-error method has been implemented to

figure out the proper amount of refrigerant, resulting in 1.4 to 1.5 kilograms. The undercharged test-rig demonstrated high discharge temperature and fluctuating suction pressure, whereas, overcharged system was identified by the presence of liquid refrigerant in the suction line and also the high-compression ratio leading to high-discharge temperature.

• So far, the test-rig is capable of measuring pressure, temperature, and leakage mass flow of test seals with a stationary rotor. However, the test section can be easily modulated to the rotating system to perform the experimental investigation of seals rotordynamic properties i.e. stiffness and damping.

3.8 Design of reduced-scale test seals

As stated in section 1.2 of chapter 1, Hole Pattern Seal (HPS) and Pocket Damper Seal (PDS) were identified as the best promising seals for reduced-scale high-speed turbo-machinery application. For the sake of performance comparison between different types of seals, most commonly use Labyrinth Seal (LS) and Smooth Seal (SS) have been opted.

Considering the existence of optimum number of constrictions (refer to figure 1.12), rotordynamic issues and compact nature of the existing high-speed turbo-compressor with a rotor diameter of 14 mm, the ratio L_s/D_r of 0.6 and four number of constrictions have been chosen for the identified promising seal topologies. The design of these seals' geometric features were carried out by applying the scaling laws on the available literature on large-scale seals [14, 89, 90, 91]. For the comparison purpose, the selected seals (HPS and PDS) including Labyrinth Seal and Smooth Seal with identical axial length and radial clearance have been chosen. A schematic diagram is presented in figure 3.5 to provide a visual overview of seal and rotor terminology.
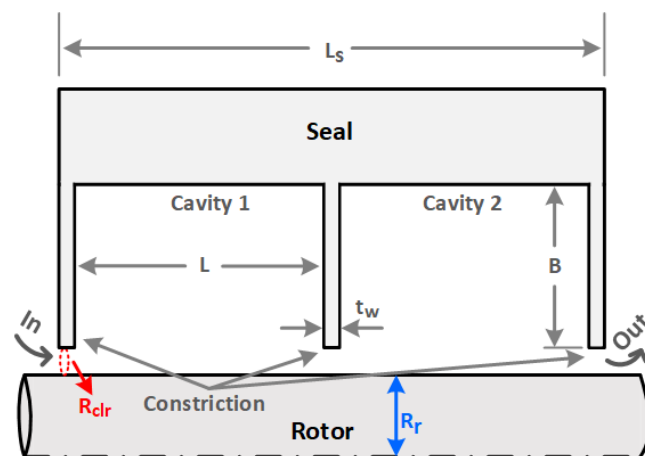
Figure 3.5 – Schematic representation of seal and rotor nomenclature

3.8.1 Design of Hole Pattern Seal

The idea of a roughened seal surface which not only reduces leakage but also enhances the rotordynamic performance of the turbomachinery was proposed by von Pragenau in 1982 [92]. Von Pragenau introduced an iso-grid configuration with concave and convex triangular patterns in his analytical analysis showing an increase in the stability of the system by reducing the undesired cross-coupling stiffness. Later, Childs and Kim [93] experimentally demonstrated that the hole pattern seal (HPS), one with knurled structures and other with diamond-shaped, showed better leakage and rotordynamic performance compared to the other textured seals. Due to the advantages offered by the HPS seal, many investigations have been performed over time to find the optimum geometrical features and reported in literature [90, 91, 93, 94, 95].

Based on the existing literature [90, 96, 97], for large-scale applications, the HPS geometrical features are adapted to the reduced-scale application investigated in this work using the scaling law. The published results [90, 94, 97] suggest an optimum asperity ratio (Υ) of 0.69 as an effective seal configuration, where the asperity ratio (Υ) is defined as follows:

$$\Upsilon = \frac{\text{surface area of holes}}{\text{seal inner surface area}} \qquad (3.1)$$

Furthermore, Childs et al. [96] reported decreased leakage and improved rotordynamic performance with increased diameter and deeper holes compared to small-sized and shallow holes. Taking this into account and considering the number of constrictions including the selected seal length to diameter ratio (L_s/D_r), staggered pattern HPS with 3 holes in axial flow direction has been designed for the tests. Due to the reduced-size and space limitations, which resulted in manufacturing issues, an asperity ratio of 0.41 has been chosen for the HPS seal design. Figure 3.6 displays the general picture of the HPS test seal and the geometry is provided in table 3.2.
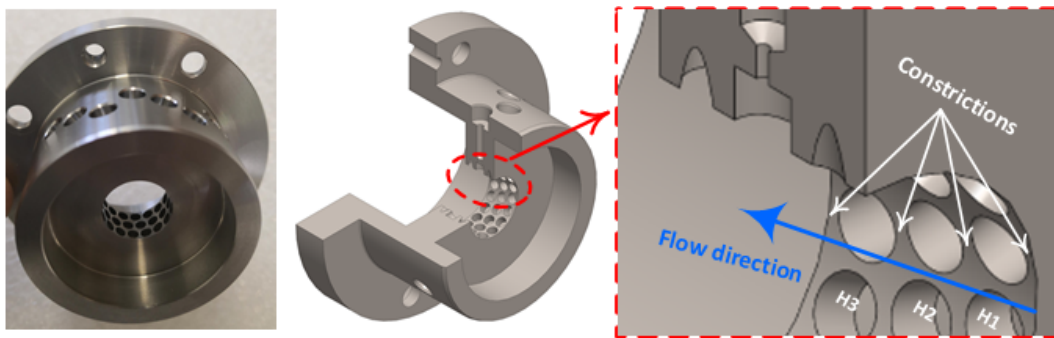
Figure 3.6 – Photograph and cut-view of manufactured Hole Pattern Seal (HPS) used for testing

3.8.2 Design of Pocket Damper Seal

Commonly used labyrinth seals are known to have flow induced destabilizing reaction forces arising due to the circumferential flow within the seal cavity. By restricting the development of circumferential flow within the seal cavity by introducing partition walls, the instability problem of the labyrinth seal can be mitigated. Geometrically, the PDS seal resembles a labyrinth seal with the multiple partition walls in the cavities (refer to figure 3.7). The partition walls divide the circumferential cavities into smaller pockets, which obstructs the circumferential flow and hence increases the effective damping by reducing the destabilizing cross-coupled forces. Experimental results [21, 37, 98] and field experience [99, 100] have demonstrated the beneficial effects of the PDS seals. Gamal [14] performed comprehensive studies on the PDS seal to investigate the effects of geometrical features such as cavity depth, cavity pitch, constriction profile, and constriction thickness. The results showed a reduction in leakage with thick and flat profile constrictions, shallow cavity depth, and increased cavity pitch. The field experience by Li et al. [100] reported higher positive damping and stiffness with a low number of constrictions and increased leakage rates. Hence, these results highlight the existence of a tradeoff between leakage and rotordynamic performance.

Considering the aforementioned literature knowledge, the design of reduced-scale PDS was carried out. Figure 3.7 shows designed and manufactured PDS seal and dimensions are provided in table 3.2.
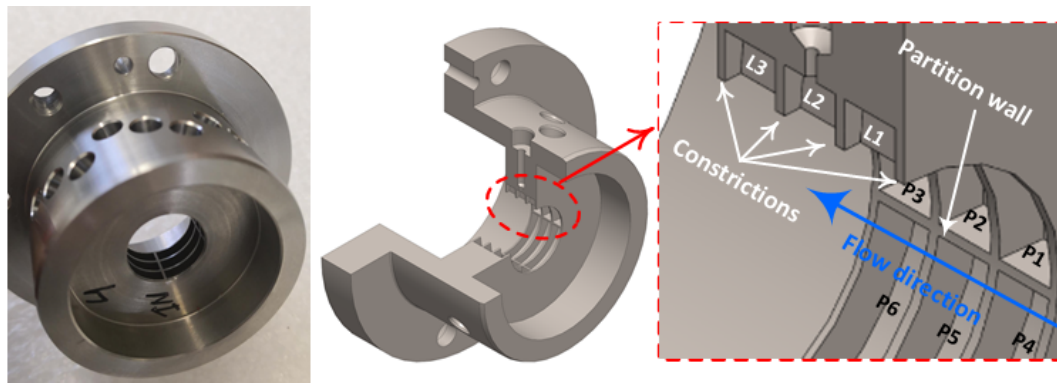
Figure 3.7 – Photograph and cut-view of manufactured Pocket Damper Seal (PDS) used for testing

3.8.3 Design of Baseline Seal

In order to evaluate the performance of HPS and PDS seals, the widely applied Labyrinth Seals (LS) and Smooth Seal (SS) have been chosen as the baseline seals with identical axial length and radial clearance.

• Labyrinth Seals

Literature [14, 100] suggests that seals with short cavity pitch and higher number of teeth have more leakage and lower rotordynamic performance than seal with bigger cavity pitch and less number of teeth for the identical L_s/D_r. To assess the existence of these effects at reduced-scale, 3 types of Labyrinth seals have been designed.

Three different designs of Labyrinth seal have been envisaged, namely, 4 teeth Labyrinth Seal with increasing cavity axial pitch (LSVP4T), 4 teeth Labyrinth Seal with constant cavity axial pitch (LSCP4T) and 5 teeth Labyrinth Seal with constant cavity axial pitch (LSCP5T). Seals dimensions are provided in table 3.2 and figure 3.8 illustrates the feature of the reference Labyrinth seals.
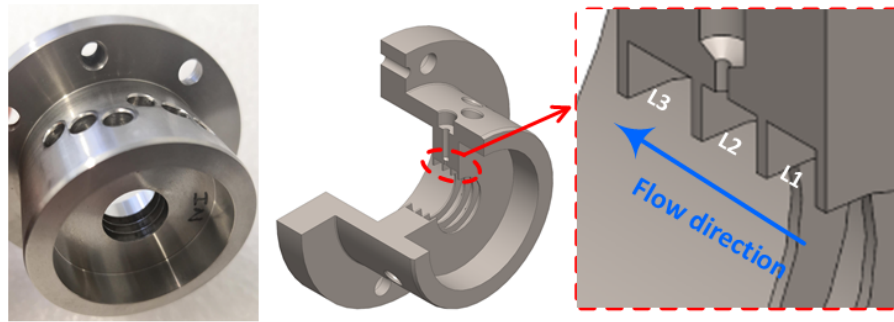
(a) Labyrinth Seal Variable Pitch 4 Teeth: LSVP4T
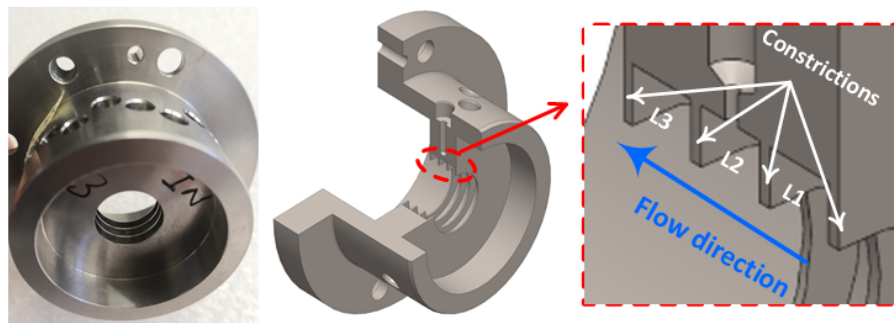
(b) Labyrinth Seal Constant Pitch 4 Teeth: LSCP4T
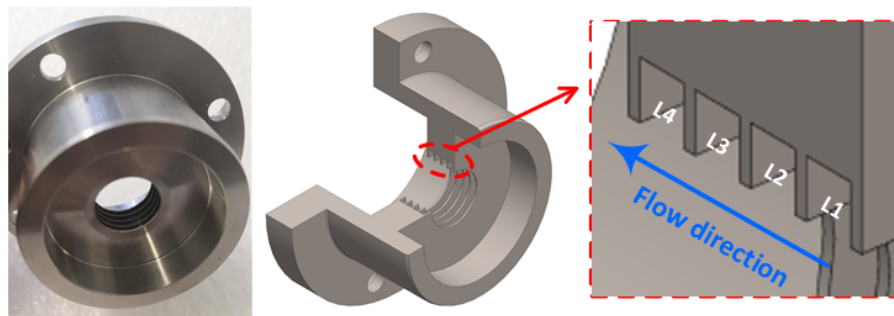
(c) Labyrinth Seal Constant Pitch 5 Teeth: LSCP5T

Figure 3.8 – Photograph and cut-view of manufactured Labyrinth Seals used for testing: (a) 4 teeth with varying cavity pitch (b) 4 teeth with constant cavity pitch (c) 5 teeth with constant cavity pitch

• Smooth Seal

Smooth seals are categorized as annular seals with a smooth inner surface, hence straightforward to manufacture. Due to the smooth surface, these seals yields large cross-coupled destabilizing forces and relatively high leakage compared to the other types of seals with identical clearance and L_s/D_r ratio. On the contrary, these seals offer high centering forces (direct stiffness) [13] due to increased positive Lomakin effect [101].

A Smooth Seal (SS) has been designed and manufactured with similar clearance and L_s/D_r as other test seals. Figure 3.9 shows manufactured smooth seal and its dimension is listed in table 3.2.
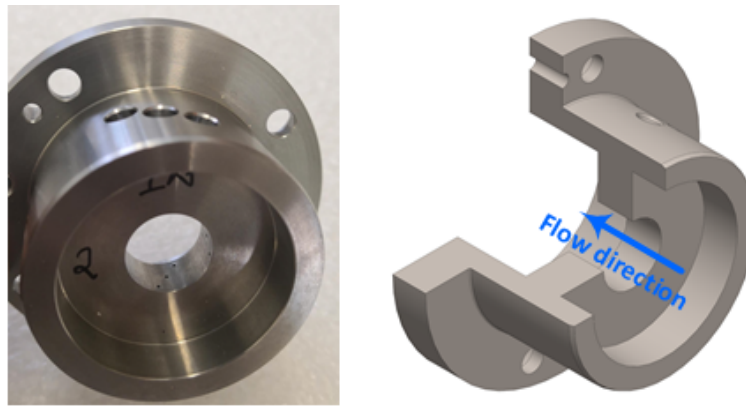
Figure 3.9 – Photograph and cut-view of manufactured Smooth Seal (SS) used for testing

Table 3.2 – Reduced-scale test seals and dimensions

Description	HPS	PDS	LSVP4T	LSCP4T	LSCP5T	SS
Rotor diameter (mm) D_r	14.03	14.03	14.03	14.03	14.03	14.03
Radial clearance (μm) R_{clr}	35	35	35	35	35	35
Length-diameter ratio L_s/D_r	0.6	0.6	0.6	0.6	0.6	0.6
Cavity pitch $L1$ (mm)	-	2.3	2	2.3	1.6	-
Cavity pitch (mm) $L2$	-	2.3	2.2	2.3	1.6	-
Cavity pitch (mm) $L3$	-	2.3	2.6	2.3	1.6	-
Cavity pitch (mm) $L4$	-	-	-	-	1.6	-
Hole diameter (mm) H	2	-	-	-	-	-
Cavity / hole depth (mm) B	2	2	2	2	2	-
Tooth width (mm) t_w	-	3x0.4+1x0.3	4x0.4	3x0.4+1x0.3	5x0.4	-
Number of hole / pocket	48	3x4	-	-	-	-
Asperity ratio (Υ)	0.41	-	-	-	-	-

4 Experimental investigation of test seals and validation of seal model

The experimental results of different types of test seals operated with air and R134a at different boundary conditions are presented in this chapter. The measured leakage, cavity pressure and temperature distributions are compared with the results of different seal models to characterize the prediction quality of the individual model at reduced-scale. Furthermore, selected seals are experimentally tested at different degrees of superheat on R134a, which allows to highlight the real gas effect on seal performance. Finally, the implemented seal model is experimentally validated and best seal topology for reduced-scale turbomachinery applications is identified.

4.1 Introduction

Pocket Damper Seal (PDS), Hole Pattern Seal (HP) and the most commonly used Labyrinth Seal (LS) and Smooth Seal (SS) have been chosen for the experimental investigation and comparison. As described in chapter 3.8, all test seals have been designed with identical inner diameter (ID) and axial length of 14.06 mm μm and 8.4 mm respectively for the sake of comparison. A single dummy rotor of outer diameter (OD) of 14 mm and length of 250 mm has been used for the test purpose. All the numerical results based on the author's model consider adiabatic flow assumptions in the seal cavities and the leakage mass flow rate is made non-dimensional using the relation as shown in equation 4.1.

$$\dot{m}_{nonD} = \frac{\dot{m}_{exp/model}}{\rho_{in} \cdot C_{in} \cdot R_{clr,in}^2} \tag{4.1}$$

where $\dot{m}_{nonD}$ is non-dimensional leakage, $\dot{m}_{exp/model}$ the leakage mass flow rate either from experiment (denoted by exp) or from model in kg/s, ρ_{in} denotes inlet fluid density in kg/m^3, C_{in} is fluid inlet speed of sound in m/s and $R_{clr,in}$ is seal inlet radial clearance

in m.

4.2   Seal characterization: Metrology

After manufacturing of test seals, an assessment of manufacturing deviations of individual seals and dummy rotor has been performed. This step is crucial to determine the actual clearance between the test seals and the dummy rotor. Due to initial manufacturing errors two sets of seals have been used for this investigation. The first set is summarized in table 4.2, where the resulting seal clearances are strongly conical. The second set (summarized in table 4.3) consists of a constant seal clearance. It is noted that the geometrical measurement of test seals have been conducted only on the inlet and outlet seal side due to the miniature seal size. The inlet and outlet clearance is linearly interpolated to determine the dimensions for the inputs of the numerical models. The seal design and their geometrical features are discussed in chapter 3.8 and summarized in table 3.2. The nomenclature of the test seals is summarized in table 4.1. The experimental results are presented separately for the cylindrical and conical seals geometries.   The numerous experiments have been performed on the

Table 4.1 – Abbreviation of test seals

Acronym	Definition
HPS	Hole pattern seal
LSCP4T	Labyrinth seal constant cavity pitch with 4 teeth
LSCP5T	Labyrinth seal constant cavity pitch with 5 teeth
LSVP4T	Labyrinth seal varying cavity pitch with 4 teeth
PDS	Pocket damper seal
R_{clr}	Radial clearance
SS	Smooth seal

Table 4.2 – Manufacturing deviations of conical seals and a dummy rotor

Designation	Measured value [mm]	R_{clr} [μm]
Rotor	13.998 $\pm 1\mu m$	-
LSCP4T	[14.035 (in) - 14.023 (out)] $\pm 1\mu m$	[18.5 (in) - 12.5 (out)] $\pm 1\mu m$
LSCP5T	[14.063 (in) - 14.057 (out)] $\pm 1\mu m$	[32.5 (in) - 29.5 (out)] $\pm 1\mu m$
LSVP4T	[14.066 (in) - 14.054 (out)] $\pm 1\mu m$	[34 (in) - 28 (out)] $\pm 1\mu m$
SS	[14.062 (in) - 14.056 (out)] $\pm 1\mu m$	[32 (in) - 29 (out)] $\pm 1\mu m$

different types of test seals for the characterization and validation purpose of different seal models. The working fluid tested are R134a and air. For R134a, several tests have been performed at various inlet pressures and inlet temperatures to investigate the effect of the proximity of the seal inlet conditions to the saturation curve. An overview on the experimental testing is listed in table 4.4.

Table 4.3 – Manufacturing deviations of cylindrical seals and a dummy rotor

Designation	Measured value [mm]	R_{clr}
Rotor	$14.026 \pm 1\mu m$	–
HPS	$14.102 \pm 1\mu m$	$38 \pm 1\mu m$
LSCP5T	$14.102 \pm 1\mu m$	$38 \pm 1\mu m$
LSVP4T	$14.102 \pm 1\mu m$	$38 \pm 1\mu m$
PDS	$14.102 \pm 1\mu m$	$38 \pm 1\mu m$
SS	$14.102 \pm 1\mu m$	$38 \pm 1\mu m$

Table 4.4 – Summary of the experimental measurements

Leakage	Cavity pressure	Cavity temperature	Degree of superheat
HPS	✓	✓	✓
LSCP4T	✓	✓	✓
LSCP5T	✗	✗	✓
LSVP4T	✓	✓	✓
PDS	✓	✓	✓
SS	✓	✗	✓

4.3 Investigations on cylindrical seals

This section presents the comparison between experimental data and numerical results of different state-of-the-art seal models including the model developed by the author performed on the cylindrical test seals as listed in table 4.3 with R134a and air as a working fluid. Furthermore, the numerical results of leakage obtained from different implemented seal models are compared with the existing experimental and numerical results of Cangioli et al. [35] operating with nitrogen as a benchmarking process on large-scale seal. The state-of-the-art seal models investigated in this work are categorized as the Neumann model (described in ref. [40], [35]), the ideal Neumann model [51] and the ideal St. Venant model [14]. The detailed descriptions of seals models have been discussed in the previous chapter 2.4. The following nomenclature has been used for the different implemented models to present the results (refer to table 4.5).

Table 4.5 – Abbreviation of implemented seal models

Acronym	Definition
AdiabModel	Author's model with adiabatic flow assumptions
NeumannModel	Based on Cangioli et al. [35] with Neumann leakage equation [51]
IdealModelNeumann	Ideal model based on Neumann leakage equation [51]
IdealModelSt.Venant	Ideal model based on St.Venant leakage equation [14]

4.3.1 Comparison of seal models with literature on large-scale seal

The comparison of leakage between the published results of Cangioli et al. [35] and the numerical results obtained from the different seal models (Table 4.5) is shown in

figure 4.1. The geometrical features of the "Cangioli" test seal and rotor including the operating boundary conditions is highlighted in chapter 2.1. For the positive pre-swirl, all models display an over-prediction in leakage. The maximum and the minimum discrepancy of 7.5% and 0.2% have been observed by the ideal St. Venant model and the Neumann model respectively. Likewise, the rest of the models indicated up to 6% deviation. On the contrary, all the seal models under-predicts leakage in the case of negative pre-swirl with a maximum deviation up to 10% by the Neumann model.
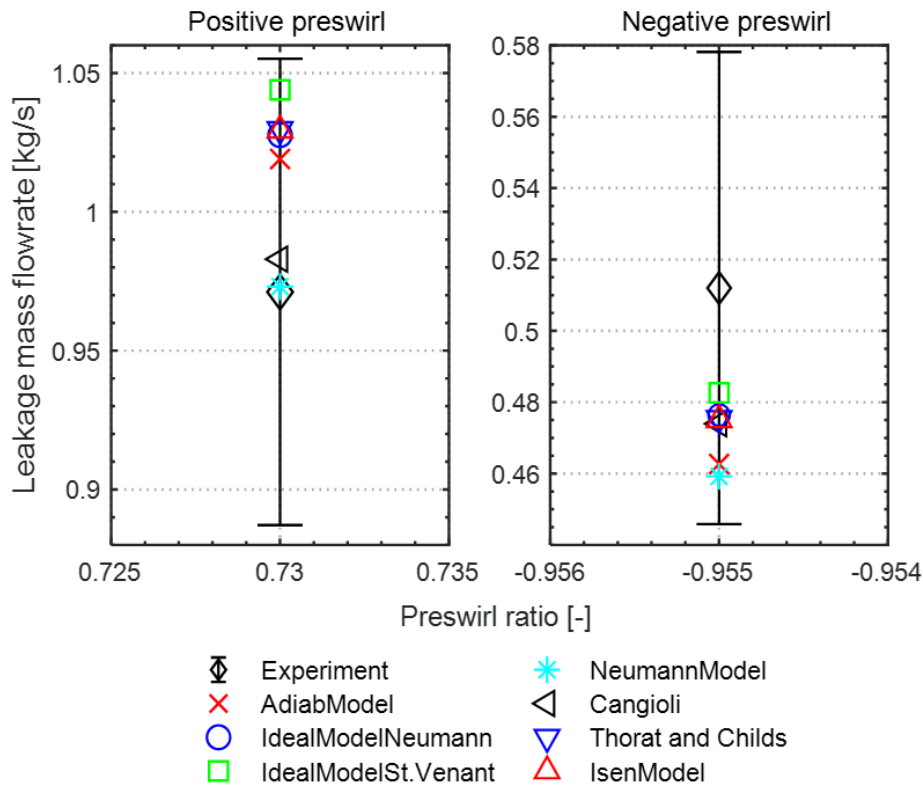
Figure 4.1 – Prediction quality of the leakage mass flow by different seal models compared to the experimental data of Cangioli et al. [35]

Referring to the figure 4.1, all the implemented models showed good agreement with the measured leakage mass flow rates within the range of measurement uncertainty, thus validating all the seal models implemented models in this work for large-scale seals.

4.3.2 Comparison of different seal models on reduced-scale seals with R134a

To evaluate the prediction quality of the-state-of-the-art and the author's model at reduced-scale, numerical results using namely the Vermes [82] and the Neumann [51]

empirical kinetic energy carry-over coefficients, are compared with the experimental measurements. The presentation of the numerical results also include the manufacturing error effects, which highlight the models sensitivity to the seal clearance at reduced-scale. In general, numerical results for all test seals and test conditions suggests a $\pm$ 2.8% deviation in prediction for a geometrical tolerance of $\pm$ 1 μm between seal and rotor. The results are presented mostly at 12 bar and one individual case at 5 bar inlet pressure. The numerical results are shown for high-pressure ratios to evidence the choke flow conditions predicted by different seal models.

Pocket damper seal (PDS)

Figure 4.2 highlights the numerical results obtained using the Vermes and the Neumann carry-over coefficient in different seal models against experimental data for the PDS at an inlet pressure of 5 bar. With the implementation of the Vermes carry-over coefficient in different seal models, the author model demonstrates the highest prediction accuracy compared to the state-of-the-art models at all pressure ratios. A maximum deviation of 1.3% at a pressure ratio of 3.07 and a minimum deviation of 0.2% at a pressure ratio of 1.43 has been monitored in comparison to the author's model. The Neumann model suggests an underprediction in leakage for the entire pressure ratios ranging from 14% to 4% at low and high-pressure ratios respectively. Regarding the ideal Neumann model, numerical results show good agreement with experimental data for low-pressure ratios with a minimum deviation of 0.9% at a pressure ratio of 1.43. However, the deviation increases with pressure ratio and reaches a maximum value of 8.9% at a pressure ratio of 3.07. Likewise, the ideal St. Venant model yields an inferior performance compared to other models for all pressure ratios with a maximum overprediction of 23.3% at a pressure ratio of 3.07.

With the Neumann carry-over coefficient, the author's model suggests a small overprediction in leakage compared to the experimental data for all pressure ratios. The highest deviation of (5%) has been monitored at a low-pressure ratio of 1.43 while the lowest one (3%) occurs at a high-pressure ratio of 3.07. It is noted, however, that the predicted data is still within the bound of the measurement error. The Neumann model shows an underprediction of leakage in all pressure ratios with a maximum discrepancy of 9.1% at a low-pressure of 1.67 and a minimum deviation of 2.3% at a high-pressure ratio of 3.07. The ideal Neumann model shows overprediction in leakage with the lowest variation of 3.9% at a low-pressure ratio of 1.67. However, this variation diverges with increasing pressure ratio and reach a maximum value of 14.3% at a pressure ratio of 3.07. Concerning the ideal St. Venant model, there is an overprediction of leakage for all pressure ratio stretching up to 29% at a pressure ratio of 3.07.

The author's model with the Vermes carry-over coefficient is suggested to offer the better leakage prediction accuracy to the experimental results compared to the-state-of-the-art models over the range of pressure ratios on Pocket damper seal (PDS) at 5

Figure 4.2 – Comparison of leakage between experimental measurements, the author model and the-state-of-the-art models on Pocket damper seal (PDS) at 5 bar inlet pressure, 25°C inlet temperature, varying PR and R134a as a working fluid

bar inlet pressure. Besides leakage, the author's model also captures the choke flow condition as well as the shape of the leakage evolution with pressure ratios.

Figure 4.3 compares the prediction of the state-of-the-art seal models and the author model using the Vermes and the Neumann carry-over coefficients with the experimental results for the PDS operated at an inlet pressure of 12 bar. With the application of the Vermes carry-over coefficient, the author shows minor underprediction in leakage at all pressure ratios with a maximum and minimum deviation of 2.5% and 1.6% at a pressure ratio of 1.43 and 2 respectively. On the other hand, the Neumann model underpredicts up to 10% at a pressure ratio of 1.43 and by 4.1% at high-pressure ratios (3.07). The ideal Neumann model results suggest an underprediction of a maximum 8.2% in leakage at a low-pressure ratio of 1.43 and overprediction up to 4.4% at a high-pressure ratio of 3.07. Regarding the ideal St. Venant model, results show a good agreement at low-pressure ratios, whereas, for increasing pressure ratio, the results diverge up to a maximum discrepancy of 18.4% in overprediction at a pressure ratio of 3.07.

By implementing the Neumann carry-over coefficient in the different seal models, the author's model overpredicts leakage compared to measurement data for all pressure ratios. The maximum and minimum deviation of 3.1% and 2% is noticed at a pressure ratio of 2 and 3.07 respectively. On the contrary, the Neumann model shows an underprediction in leakage by 6.8% at a low-pressure ratio of 1.43, which decreases with increasing pressure ratio yielding a good agreement with experimental result at high-pressure ratios of 3.07. In the case of the ideal Neumann model, leakage is underpredicted at low-pressure ratios with a maximum deviation of 4.1% at a pressure ratio of 1.43. However, an increasing pressure ratio, numerical results turn into overprediction reaching a maximum value of 8.1% at a pressure ratio of 3.07. On the other hand, the ideal St. Venant model demonstrates overprediction in leakage for all pressure ratios with a minimum and maximum difference of 0.4% and 24.3% at a pressure ratio of 1.43 and 3.07 respectively.

At elevated test pressure on pocket damper seal (PDS), the author's model with the Vermes carry-over coefficient is suggested to achieve a better prediction accuracy of leakage over the complete range of pressure ratios compared to other models. Furthermore, using the Neumann carry-over coefficient in the seal models, both the author and the Neumann model show a good prediction accuracy ($< 4.1\%$). For the choke flow prediction, the author's model suggested a good agreement with the experiment compared to the state-of-the-art models.

Figure 4.3 – Comparison of leakage between experimental measurements, the author model and the-state-of-the-art models on Pocket damper seal (PDS) at 12 bar inlet pressure, 50°C inlet temperature, varying PR and R134a as a working fluid

Labyrinth seal (LSVP4T)

The comparison of leakage between different seal models and the experimental results using the Vermes and the Neumann carry-over coefficient is presented in figure 4.4

for the labyrinth seal with 4 teeth and varying axial cavity pitch (LSVP4T). Among the different seal models with the Vermes carry-over coefficient, the author's model shows very good agreement with the experiment for the entire pressure ratios indicating a maximum and a minimum overprediction of 1.7% and 0.02% at pressure ratios of 2.5 and 1.43 respectively. However, the Neumann model underpredicts leakage for the range of pressure ratios under investigation. The highest discrepancy of 9.8% has been noticed at a low-pressure ratio of 1.43. However, this discrepancy reduces with the increasing pressure ratio showing a minimum value of 2.75% at a high-pressure ratio of 3.07. Similarly, the ideal Neumann model suggests an underprediction in leakage at low-pressure ratios indicating an error up to of 6% at a pressure ratio of 1.43, whereas, overpredicting leakage at high-pressure ratios with a maximum deviation of 6.2% at a pressure ratio of 3.07. In the case of the ideal St. Venant model, a matching performance has been observed at low-pressure ratios, meanwhile, the numerical results diverges with the increasing pressure ratios approaching up to 20% at a pressure ratio of 3.07.

The prediction quality of different seal models using the Neumann carry-over coefficient highlights an overprediction in leakage by the author's model at all pressure ratios. A maximum deviation of 6.2% has been observed at a pressure ratio of 2.5. Amongst the other models, the Neumann model shows good agreement with the measured data, especially, at higher pressure ratios. On the other hand, this model underpredicts leakage at low-pressure ratios deviating up to 6% at a pressure ratio of 1.43. The ideal Neumann model indicates 1.6% of underprediction at a low-pressure ratio of 1.43, whereas with increasing pressure ratio, the model overpredicts leakage by up to 11.4% at a pressure ratio of 3.07. Furthermore, the ideal St. Venant model overpredicts leakage for all pressure ratios with a minimum and maximum discrepancy of 2.8% and 26.5% at a pressure ratio of 1.43 and 3.07 respectively.

Regarding the measured leakage value on 4 teeth Labyrinth seal with varying cavity pitch (LSVP4T) at 12 bar inlet pressure, the author model with the Vermes carry-over coefficient offers a higher accuracy than the rest of the seal models. The Neumann model with the Neumann carry-over coefficient showed second-best performance in terms of leakage prediction. As suggested by figure 4.4, the author's model also captures the trend of choking following the pattern of the experimental data, whereas the rest of the models predict this phenomenon to happen at higher pressure ratios.
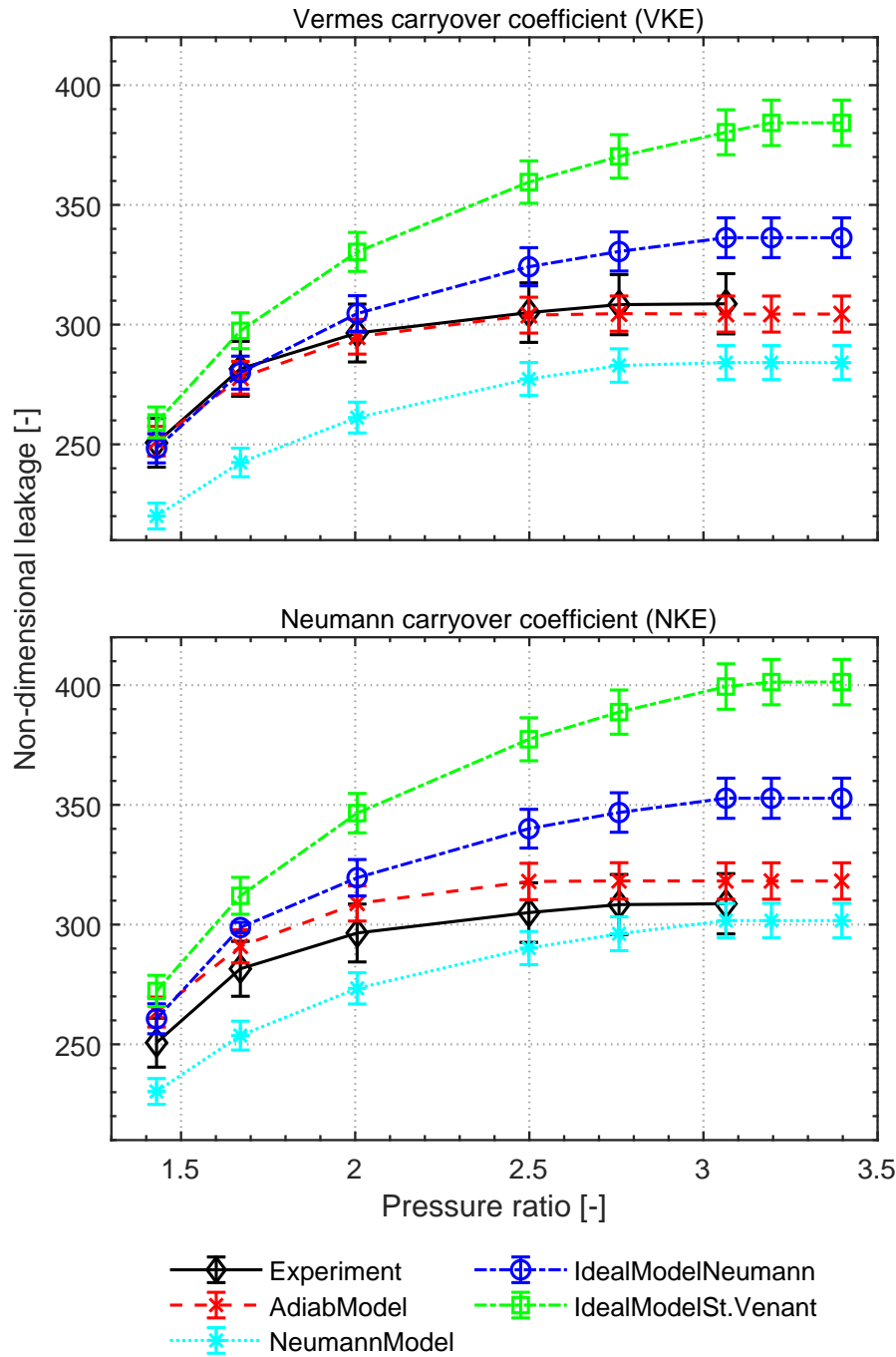
Figure 4.4 – Comparison of leakage between the experimental measurements, the author model and the-state-of-the-art models on Labyrinth seal (LSVP4T) at 12 bar inlet pressure, 50°C inlet temperature, varying PR and R134a as a working fluid

Labyrinth seal (LSCP5T)

Figure 4.5 illustrates the prediction quality of leakage between the different seal models with the Vermes and the Neumann carry-over coefficient on labyrinth seal with 5 teeth

and constant cavity axial pitch (LSCP5T). The implementation of the Vermes carry-over coefficient on the seals models yields an underprediction in leakage at almost all pressure ratios. A maximum and minimum deviation of 6.8% and 5.1% has been observed at the pressure ratio of 1.43 and 3.07 respectively. Similarly, the Neumann model shows underprediction of leakage for all pressure ratios. The highest and lowest discrepancy up to 14.4% and 9.3% have been noticed at low and high pressure ratios respectively. Likewise, the ideal Neumann model displays underprediction of leakage for all pressure ratios. A difference of 13.5% has been noticed at a low-pressure ratio of 1.43. However, this discrepancy decreases with increasing pressure ratios and shows a minimum value of 2.7% at a high-pressure ratio of 3.07. Regarding the ideal St. Venant model, numerical results highlight an underprediction of leakage at low-pressure ratios stating up to 10% at a pressure ratio of 1.43, decreasing to 2.7% at a pressure ratio of 2 and then turning into an overprediction by 8% at a pressure ratio of 3.07.

With the Neumann carry-over coefficient, the author's model demonstrates accurate leakage prediction at all pressure ratios with a maximum overprediction of 1.2% at a pressure ratio of 2.5. The Neumann model underpredicts leakage over the entire pressure ratios by up to 8.8%. In the case of the ideal Neumann model, leakage is underpredicted at low-pressure ratios with a maximum deviation of 7.2% at a pressure ratio of 1.43. However, with the increasing pressure ratio, numerical results intersects experimental data indicating overprediction of leakage with a maximum deviation of 4.5% at a pressure ratio of 3.07. Similarly, the ideal St. Venant model shows up to 3.8% of underprediction in leakage at a pressure ratio of 1.43, however, with the increment in pressure ratios, the deviation reduces and finally intersects the measurement data resulting in overprediction of leakage with a maximum value of 16.2% at a pressure ratio of 3.07.

The comparison of experimental and numerical results on the labyrinth seal with 5 teeth (LSCP5T) at 12 bar inlet pressure highlights the prediction quality of different seal models. The numerical results of all models yield poor performance of the Vermes carry-over coefficient for the 5 teeth Labyrinth seal, suggesting the existence of the optimum number of teeth beyond which the use of the Vermes carry-over coefficient is questionable, and instead, the Neumann carry-over coefficient needs to be employed to achieve a better performance. Besides the seal geometrical features, the Neumann carry-over coefficient also considers the number of teeth in the equation whereas the Vermes correlation does not take this into account (refer to equations 2.4 and 2.6 on chapter 2.3.1). To better understand and highlight this effect in reduced-scale seals, at least two more seals with different number of teeth needs to be manufactured and tested, ideally with 3 and with 6 teeth. With regards to the choke flow prediction, the author's model achieves a better performance compared to the other seal models by illustrating a similar trend with the experimental data, whereas other seal models are suggested to capture this flow phenomenon at higher pressure ratios.
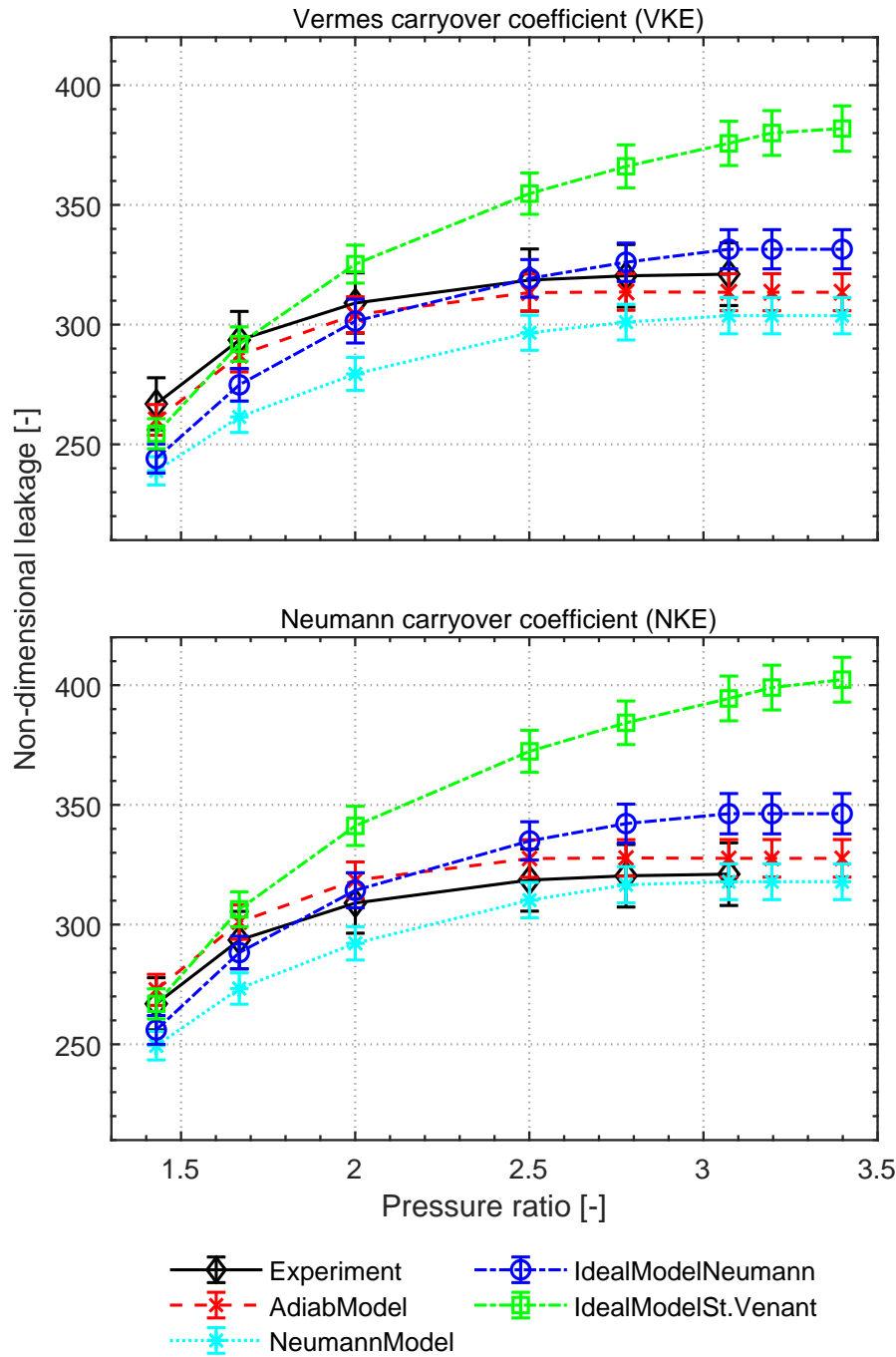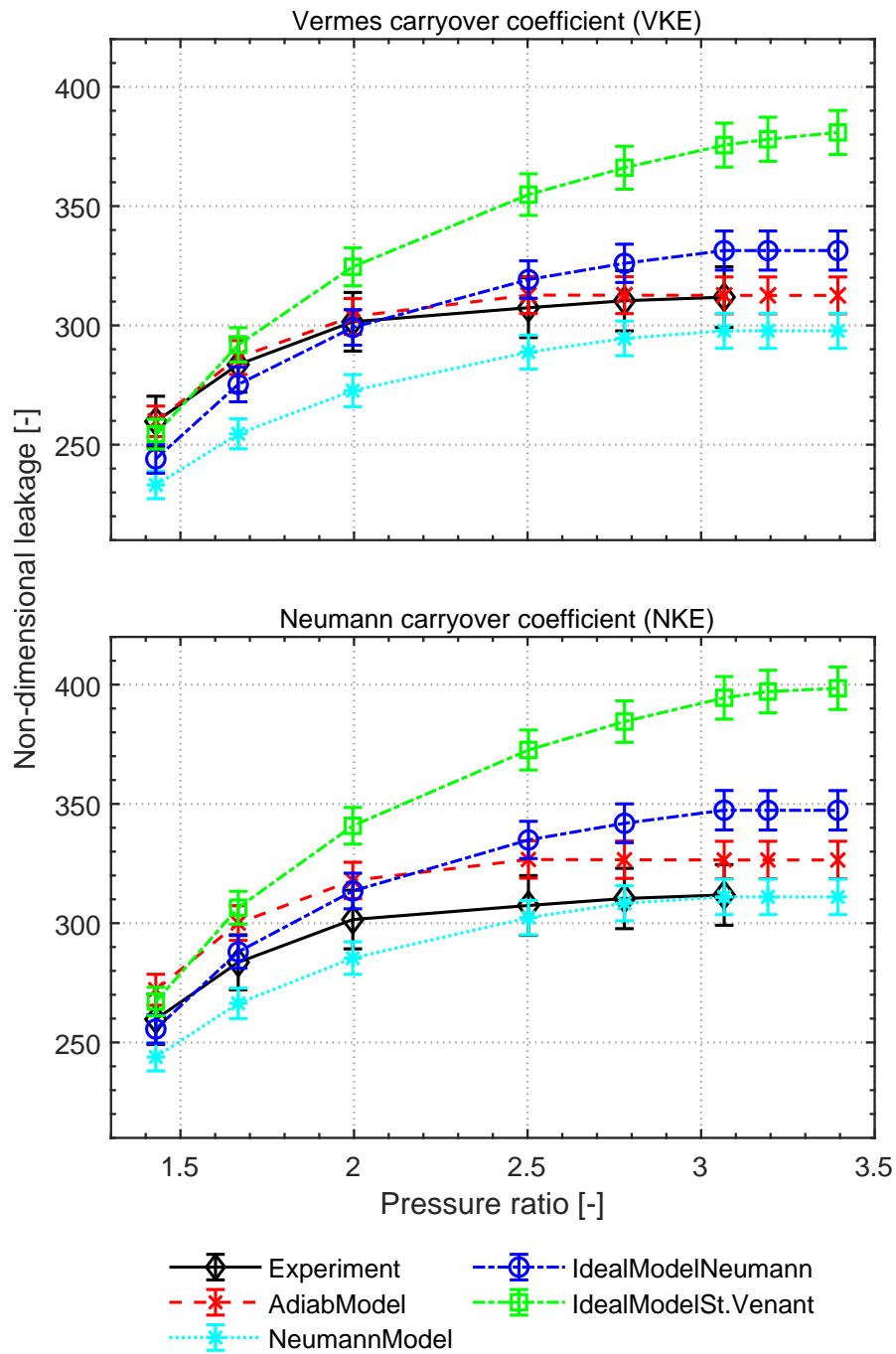
Figure 4.5 – Comparison of leakage between the experimental measurements, the author model and the-state-of-the-art models on Labyrinth seal (LSCP5T) at 12 bar inlet pressure, 50°C inlet temperature, varying PR and R134a as a working fluid

4.3.3   Comparison of different seal models on reduced-scale seals with air

To gauge the prediction accuracy of different seal models at reduced-scale operating on different working fluids, the most commonly used working fluid i.e. air has been selected and experimentally investigated. The numerical results consider manufacturing error to expose the sensitivity of the models with the seal clearance at reduced-scale seal performance. Overall, numerical results for all test seals and test conditions indicate around $\pm$ 2.8% deviation in prediction with the geometrical tolerance of $\pm$ 1 μm between seal and rotor. For the air test, all seals have been investigated at an inlet pressure of 5 bar and inlet temperature of 25°C.

Pocket damper seal (PDS)

Figure 4.6 compares the different seal models using the Vermes and the Neumann carry-over coefficients against the experimental results on Pocket damper seal (PDS). With the application of the Vermes carry-over coefficient, the author model yields an overprediction in leakage for all pressure ratios with a maximum and minimum deviation of 5.7% and 2.5% at a pressure ratio of 4 and 1.67 respectively. Note that all the predicted points are within the measurement errors. Conversely, the Neumann model shows the underprediction of leakage at all pressure ratios ranging from 11.3% and 1.3% at pressure ratios of 1.67 and 4 respectively. The numerical results of the ideal Neumann model suggest an overprediction in leakage by up to 19.5% at a high-pressure ratio of 4 and by 6.6% at a pressure ratio of 1.43. Similarly, the ideal St. Venant model indicates the highest deviation amongst the other models with a minimum and maximum value of 7.8% and 23.6% at a pressure ratio of 1.43 and 4 respectively.

Figure 4.6 – Comparison of leakage between the experimental measurements, the author model and the-state-of-the-art models on Pocket damper seal (PDS) at 5 bar inlet pressure, 25°C inlet temperature, varying PR and air as a working fluid

Using the Neumann carry-over coefficient, the author's model indicates the overprediction of leakage at all pressure ratios. A maximum deviation of 11% has been observed at a pressure ratio of 4. Compared to the other models, the Neumann model illustrates a better prediction quality, suggesting 7.2% underprediction at a pressure ratio of 1.67. With increasing pressure ratio the deviation decreases turning into a 3.2% overprediction at a pressure ratio of 4. In the case of the ideal Neumann model, leakage is overpredicted for all pressure ratios with a minimum and a maximum difference of 11.8% and 25.3% at a pressure ratio of 1.67 and 4 respectively. Similarly, the ideal St. Venant model shows overprediction of leakage at all pressure ratios varying from 13.2% to 29.7% at a pressure ratio of 1.43 and 4 respectively.

Referring to the result in figure 4.6 on pocket damper seal (PDS) with air as a working fluid, the author's model with the Vermes carry-over coefficient demonstrates the highest prediction accuracy compared to the other seal models. Similarly, the Neumann model with the Neumann carry-over coefficient ranked as the second-best model in terms of leakage prediction. On the other hand, the author's model predicts the choke flow pressure ratio, whereas other models capture this effect at higher pressure ratios.

Labyrinth seal (LSVP4T)

Figure 4.7 represents the comparison between the numerical results of different seal models and the experimental data using the Vermes and the Neumann carry-over coefficient on the 4 teeth Labyrinth seal with varying cavity axial pitch (LSVP5T). With the implementation of the Vermes carry-over coefficient, the author's model shows good agreement with the experimental results compared to the-state-of-the-art models over the range of pressure ratios. A minimum and maximum overprediction of 4.5% and 6.5% has been recorded at a pressure ratio of 1.43 and 4 respectively. The Neumann model underpredicts leakage at all pressure ratios with a 9.8% deviation at a low-pressure ratio of 1.43. The error, however, diminishes with increasing pressure ratio and reaches a minimum value of 0.4% of overprediction at a pressure ratio of 4. The ideal Neumann model shows overprediction in leakage for the entire pressure ratios indicating a minimum deviation of 8.7% at a pressure ratio of 1.67, meanwhile, the deviation diverges with pressure ratio up to 21% at a pressure ratio of 4. Likewise, the ideal St. Venant model demonstrates inferior performance compared to other models at all pressure ratios stretching up to 25% in overprediction at high-pressure ratios.

Regarding the employment of the Neumann carry-over coefficient in the seal models, the author's model shows an overprediction of leakage for all pressure ratios. The lower and higher deviation of 9.5% and 11.5% has been noticed at a pressure ratio of 1.67 and 4 respectively. Among the other models, the Neumann model shows good agreement with the measurement data indicating up to 5.7% underprediction at low-pressure ratio (1.67) and 4.2% of overprediction at a pressure ratio of 4. The ideal Neumann model
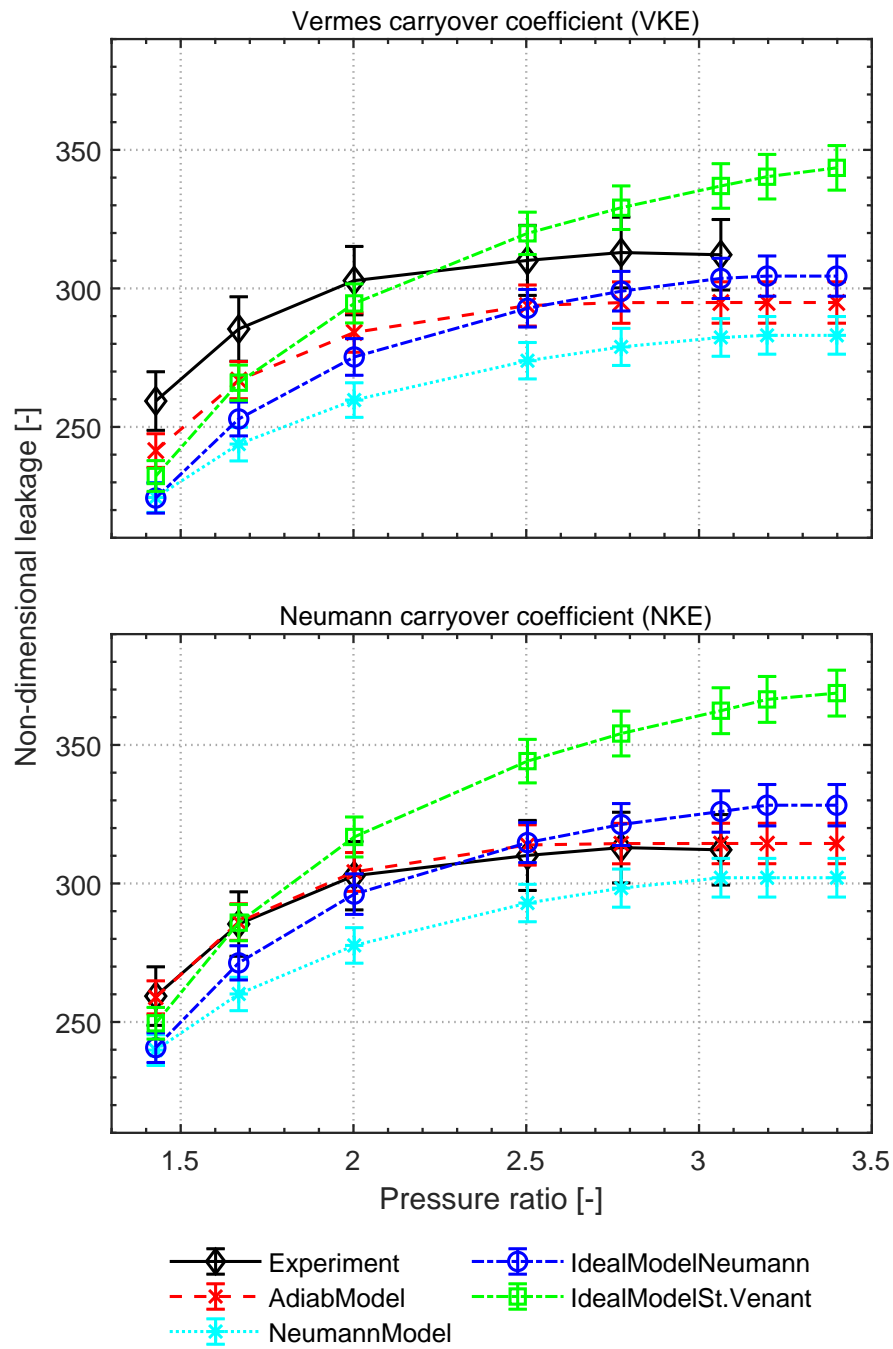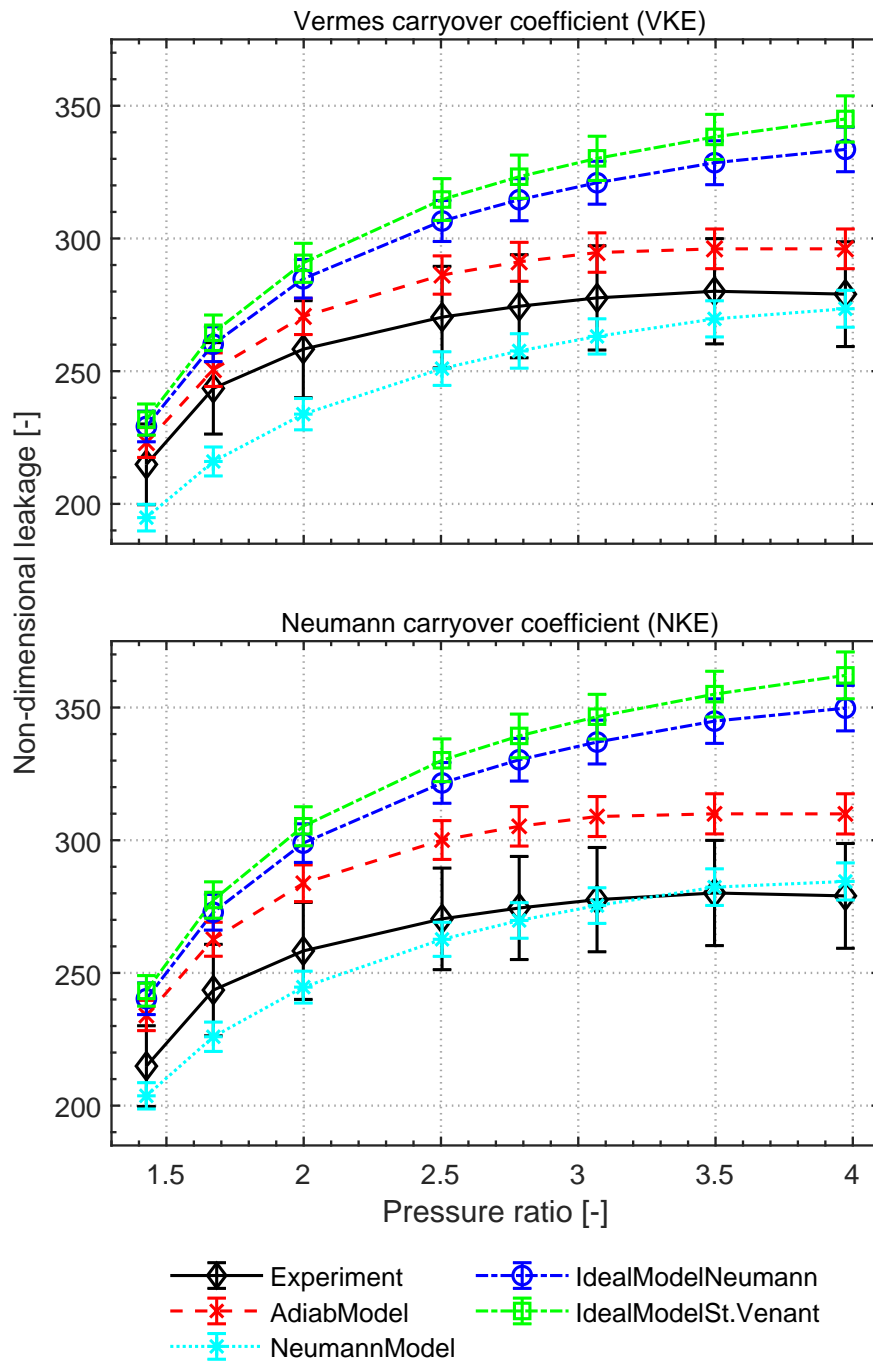
Figure 4.7 – Comparison of leakage between the experimental measurements, the author model and the-state-of-the-art models on Labyrinth seal (LSVP4T) at 5 bar inlet pressure, 25°C inlet temperature, varying PR and air as a working fluid

displays overprediction of leakage over the entire range of pressure ratios extending up to 26% at high-pressure ratios. Likewise, the ideal St. Venant model overpredicts leakage for all pressure ratios with a maximum discrepancy of 30.8% at a pressure ratio of 4.

The leakage test on labyrinth seal with 4 teeth and varying cavity pitch (LSVP4T) with air highlights the better prediction quality of the author's model compared to the experimental results with the use of the Vermes carry-over coefficient. Furthermore, the Neumann model with the Neumann carry-over coefficient suggests matching results with the measured data. For the choke flow prediction, the author's model shows matching results analogous to the experimental data, whereas, other models predict choke at higher pressure ratios.

Labyrinth seal (LSCP5T)

Figure 4.8 shows the prediction quality of different models using the Vermes and Neumann carry-over coefficient for the 5 teeth Labyrinth seal with constant cavity pitch. Considering the Vermes carry-over coefficient, the author's model demonstrates better prediction accuracy at all pressure ratios with a minimum and a maximum overprediction of 0.7% and 6.5% at a pressure ratio of 1.43 and 4 respectively. On the other hand, the Neumann model underpredicts leakage showing a minimum and a maximum deviation of 4% and 12.5% at a pressure ratio of 4 and 1.43 respectively. In the case of the ideal Neumann model, leakage is overpredicted at all pressure ratios with a minimum and a maximum deviation of 2.9% and 17.6% at a pressure ratio of 1.43 and 4 respectively. Similarly, the ideal St. Venant model suggests overprediction in leakage ranging from 3.9% to 20.7% at a pressure ratio of 1.43 and 4 accordingly.

With the implementation of the Neumann carry-over coefficient, the author model overpredicts leakage for all pressure ratios with a minimum and a maximum deviation of 8% and 14% at a pressure ratio of 1.43 and 4 respectively. Among the other models, the Neumann model shows good agreement with the measured data, especially, at higher pressure ratios with a minimum deviation of 0.56%. However, this model underpredicts leakage at low-pressure ratios deviating up to 6.4% at a pressure ratio of 1.43. The ideal Neumann model shows overprediction in leakage at all pressure ratios extending up to 26% at high-pressure ratio. Similarly, the ideal St. Venant model overpredicts leakage for all pressure ratios with a minimum and maximum difference of 11.6% and 29.8% at a pressure ratio of 1.43 and 4 respectively.

The results presented in figure 4.8 demonstrates the validity of the author's model using the Vermes carry-over coefficient. Similarly, the Neumann model with the Neumann carry-over coefficient also suggests a good agreement with leakage prediction. On the other hand, the author model predicts the choke flow with good accuracy, whereas, the other models predict choke flow at higher pressure ratios.
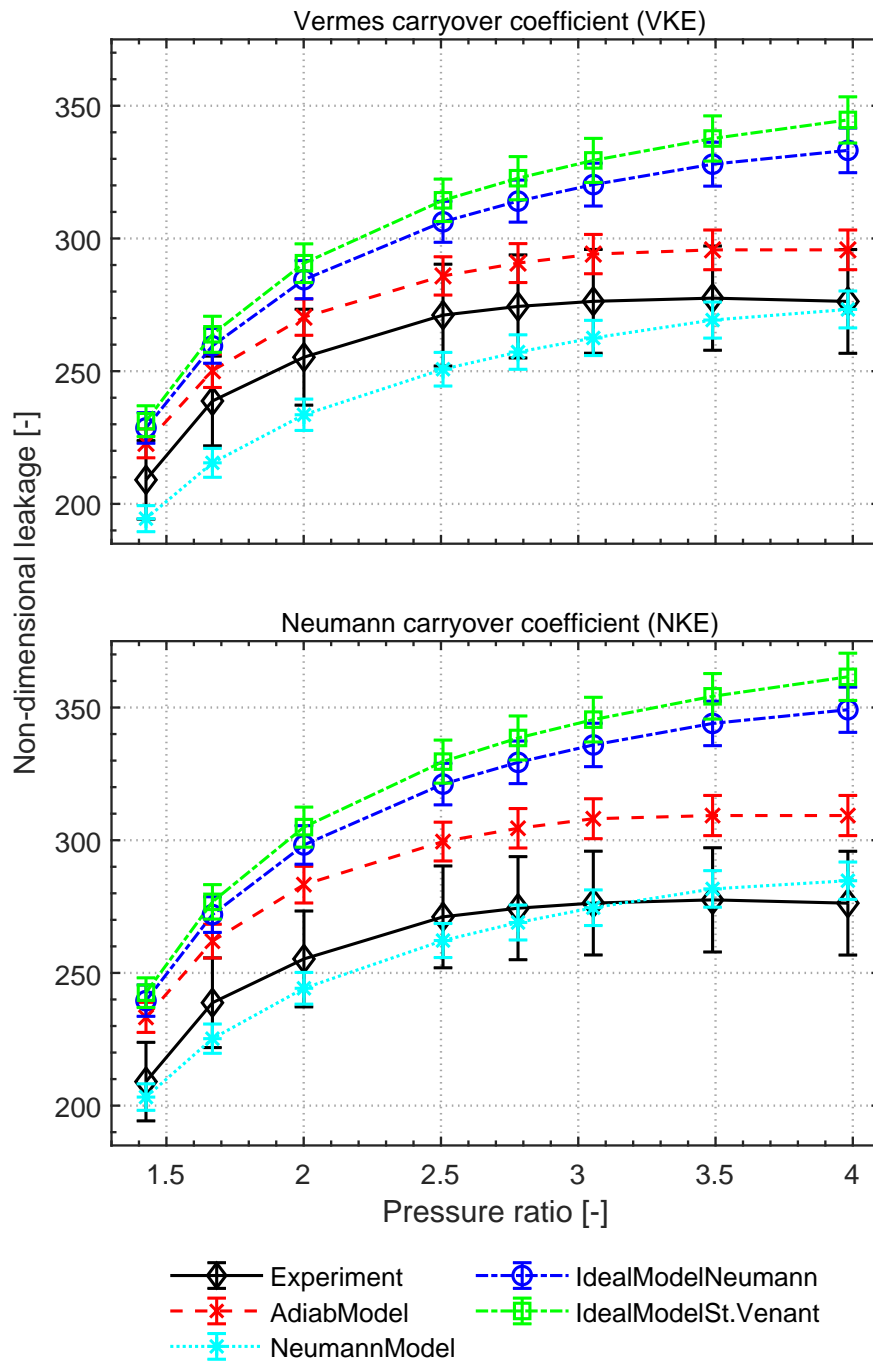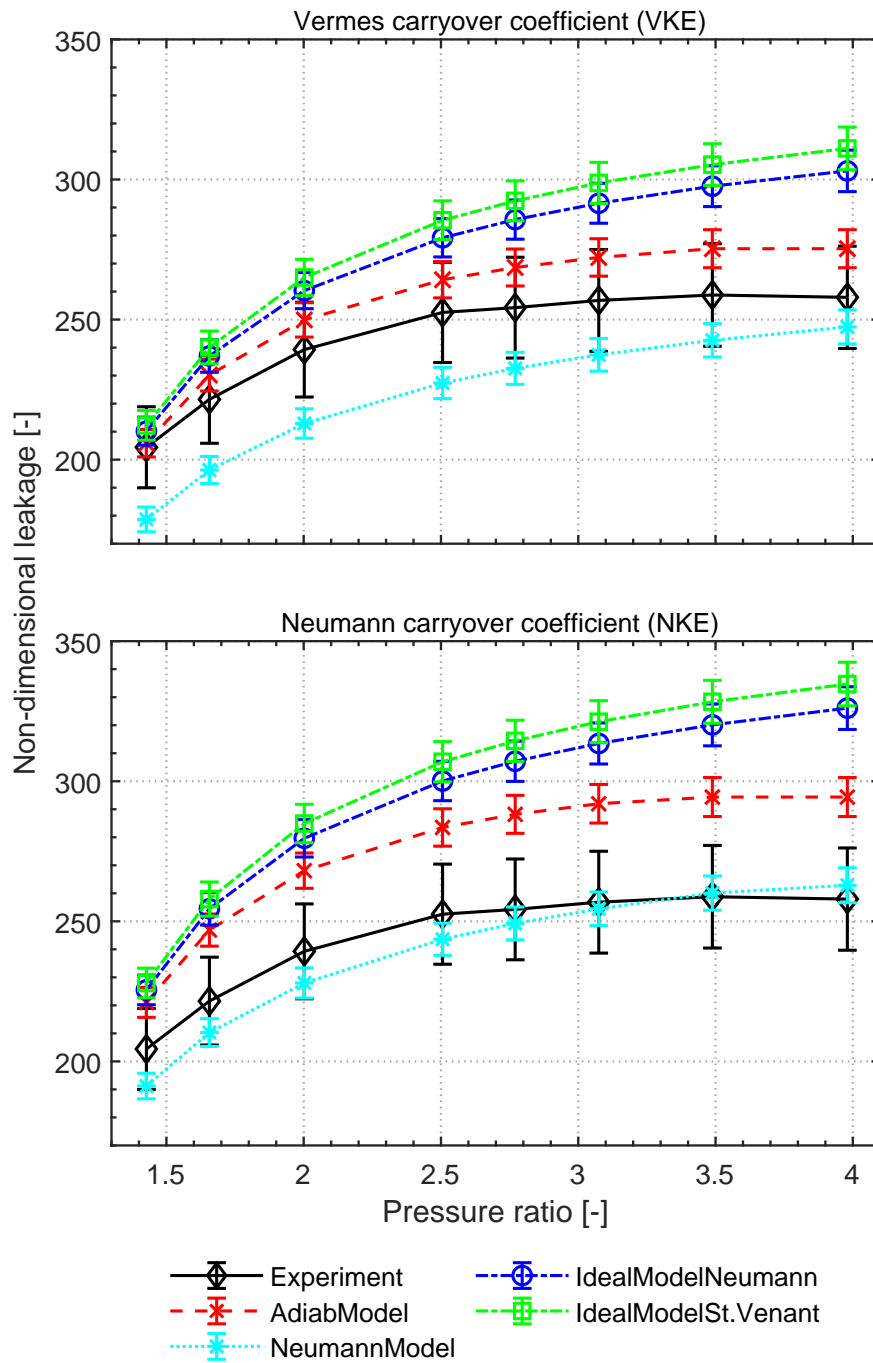
Figure 4.8 – Comparison of leakage between the experimental measurements, the author model and the-state-of-the-art models on Labyrinth seal (LSCP5T) at 5 bar inlet pressure, 25°C inlet temperature, varying PR and air as a working fluid

Referring to the results of R134a and air in different seals, no fundamental difference is detected between the experimental and the numerical data of the author's model. The conclusion drawn from the R134a test applies to air test as well in a qualitative manner.

4.3.4 Comparison between the different seals

In this section the performance of the different seals are compared for R134a and air at 12 and 5 bar inlet pressure respectively. As evidenced by all the previous test results, the author's model is suggested to achieve the best performance in prediction of leakage and choke flow and has therefore been selected for the numerical analysis. The manufacturing error and the measurement errors have been omitted in the presented results for clarity, and average clearance is considered to compare with the experimental data.

Test fluid: R134a

The experimental measurements and numerical prediction of leakage for all test seals at 12 bar inlet pressure is shown in Figure 4.9. For the identical seal clearance and operating conditions, the Hole pattern seal (HPS) demonstrates the lowest leakage overall pressure ratios compared to the other seals. The Smooth seal (SS) shows the highest leakage with up to 17% higher leakage compared to the Hole pattern seal (HPS). Noteworthy, the 4 teeth labyrinth seal with varying cavity axial pitch (LSVP4T) reveals a slightly lower leakage than the 5 teeth labyrinth seal with constant cavity pitch (LSCP5T) at all pressure ratios, thus indicating the existence of optimum seal geometrical features. The minimum and maximum difference of 0.2% and 0.6% at a pressure ratio of 1.43 and 3.07 has been noticed between the LSCP5T seal and the LSVP4T seal. In comparison to the HPS seal, the LSCP5T and the LSVP4T seals indicated up to 8.2% and 7.6% higher leakage respectively. Compared to the HPS seal, the Pocket damper seal (PDS) displays almost 10% higher leakage. It is noted that in this analysis the PDS can be associated to a labyrinth seal with 4 teeth and a constant cavity pitch.

The experimental results suggests the Hole pattern seal (HPS) to be the most effective seal yielding the lowest leakage. Furthermore, improvement in leakage reduction has been experimentally evidenced with 4 teeth Labyrinth seal with varying cavity pitch (LSVP4T) compared to 5 teeth Labyrinth seal with constant cavity pitch (LSCP5T) for the identical clearance and identical seal axial length. Hence, highlighting the existence of optimum seal geometrical features for a given overall seal length, leading not only to an optimum leakage performance (refer figure D.15 in appendix) but also to a reduction of manufacturing cost and time. This unique experimental characteristic
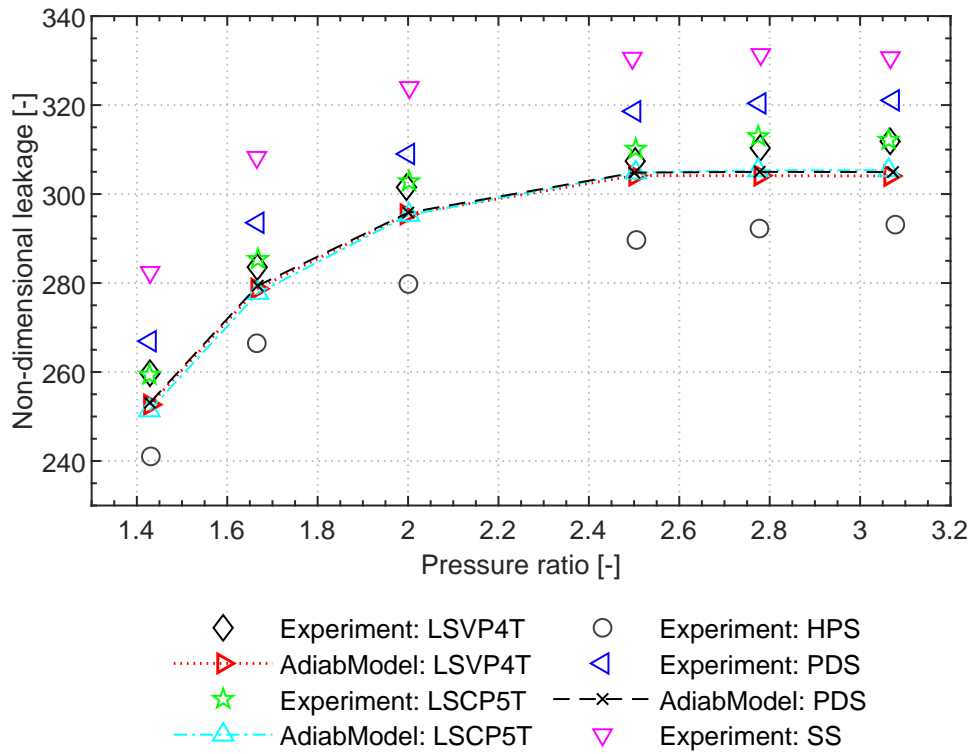
Figure 4.9 – Experimental and numerical comparison between the different seals at 12 bar inlet pressure, 50°C inlet temperature, varying PR and R134a as a working fluid

has been captured by the author's model. The improvement offered by the LSVP4T seal can be better understood by examining the kinetic energy carry-over coefficient (equations 2.4 and 2.6). Both equations highlight the dependency of the kinetic energy carry-over coefficient, which is directly proportional to the cavity axial pitch, hence leading to less dissipation of kinetic energy in the seal cavity with a small pitch.

Test fluid: Air

To grade leakage performance of the different test seals operated with air, the comparison of the experimental data together with numerical results of test seals has been summarized in figure 4.10. Similar to R134a test, Hole pattern seal (HPS) seal demonstrates the highest performance with a minimum leakage compared to the other seals for all pressure ratios. Conversely, Smooth seal (SS) indicates the highest leakage extending up to 24% higher leakage compared to HPS seal. The 4 teeth Labyrinth seal with varying cavity pitch (LSVP4T) revealed 9.6% to 16% high leakage relative to HPS seal, whereas, the LSCP5T seal shows 9.2% to 12% increased relative leakage. In this

case, the LSCP5T seal indicates less leakage compared to the LSVP4T seal (1.6% to 6%). Furthermore, the PDS seal displays 13% to 20% higher leakage compared to the HPS seal.
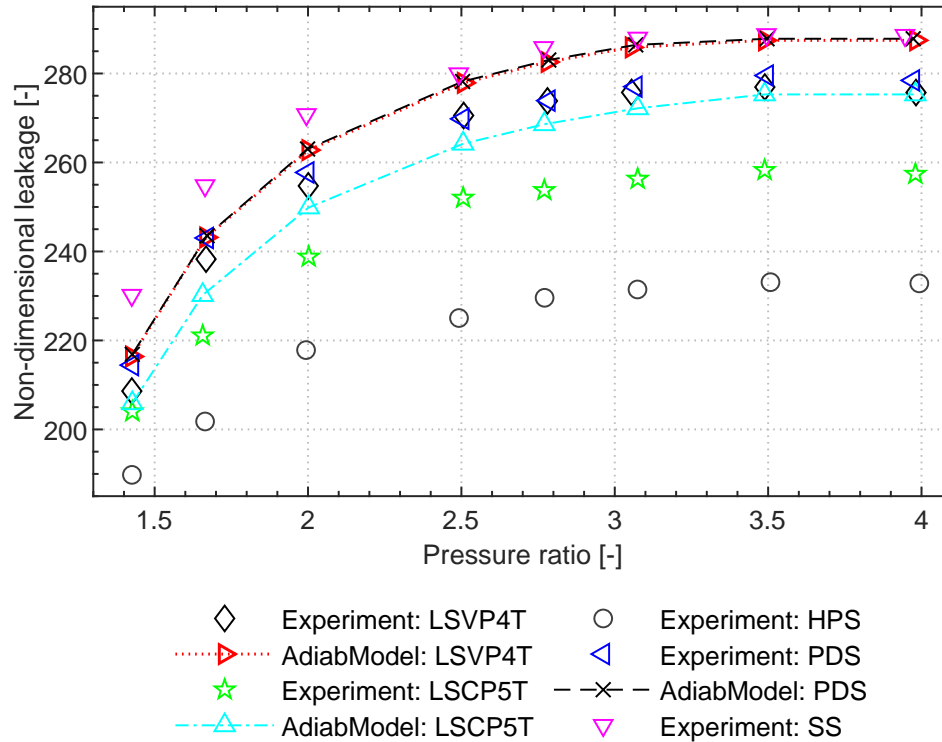
Figure 4.10 – Experimental and numerical comparison between the different seals at 5 bar inlet pressure, 25°C inlet temperature, varying PR and air as a working fluid

For the air test, the hole pattern seal (HPS) demonstrated the lowest leakage over the entire pressure ratios. Both labyrinth seals indicated similar leakage characteristics with a minor improvement for the 5 teeth labyrinth seal. Similar to the R134a test, the existence of optimum seal geometrical features for a given overall seal length has been highlighted (refer figure D.16 in appendix). Nevertheless, author's model shows a similar trend with the experimental results on LSVP4T and LSVP5T.

4.3.5   Comparison of cavity pressure distribution

Besides the accurate prediction of leakage is required to determine the system efficiency, the accurate prediction of the pressure distribution within the seal cavities is crucial to assess the influence of seal on the rotordynamic system. To examine the quality of the author's model in terms of pressure prediction, the experimental data are

compared with the numerical results. The numerical results have been compared with the measured data obtained from different seals at varying boundary conditions and two discrete fluid, namely R134a and air. For the sake of brevity, the numerical results are presented for average seal clearance. The measurement uncertainty of the pressure scanner is rated to be 8.6 mbar, which is negligible compared to the measured values, thus omitted in the results. For the sake of comparison, the predicted numerical results from the Neumann model is presented on the test seals with R134a.

Pocket damper seal (PDS): R134a

Figure 4.11 shows the comparison of seal cavity pressure distribution between the experimental data, the author's model and the Neumann model prediction on the Pocket Damper Seal at 12 bar inlet pressure and varying pressure ratios. The author's model demonstrates good agreement with the measurement data at all pressure ratios. The model underpredicts the cavity pressure with a maximum deviation of 5, 2.7 and 0.6% in the first, second and third cavity respectively at a high-pressure ratio of 3.07. At other pressure ratios, the author model shows underprediction of pressure up to 3% in the first cavity, whereas a negligible deviation can be reported on the other two cavities. A similar trend has been monitored for 5 and 9 bar inlet pressures (refer to figure D.19 and D.20 in the appendix).

The Neumann model shows underprediction of the cavity pressure in the first cavity with a maximum deviation of 4.9% in the first cavity at the pressure ratio of 3.07. On the other hand, it indicates up to 4% overprediction in pressure in the second cavity at the low-pressure ratio. In the case of third cavity, the Neumann model underpredicts pressure up to 8% at the high-pressure ratio of 3.07. At low-pressure ratios, this model yields overprediction in cavity pressure turning into underprediction of the cavity pressure with increasing pressure ratios.

The author's model shows better agreement with the experimental data on the prediction of the seal's cavity pressure distribution compared to the Neumann model at all pressure ratios. For both models, the highest deviation up to 22% overprediction has been noticed at the exit of the seal when the choke flow occurs. The high deviation at the exit of the seal can be attributed to the expansion effects, which have been neglected in the models due to its complexity in nature to implement in the two-dimensional model.
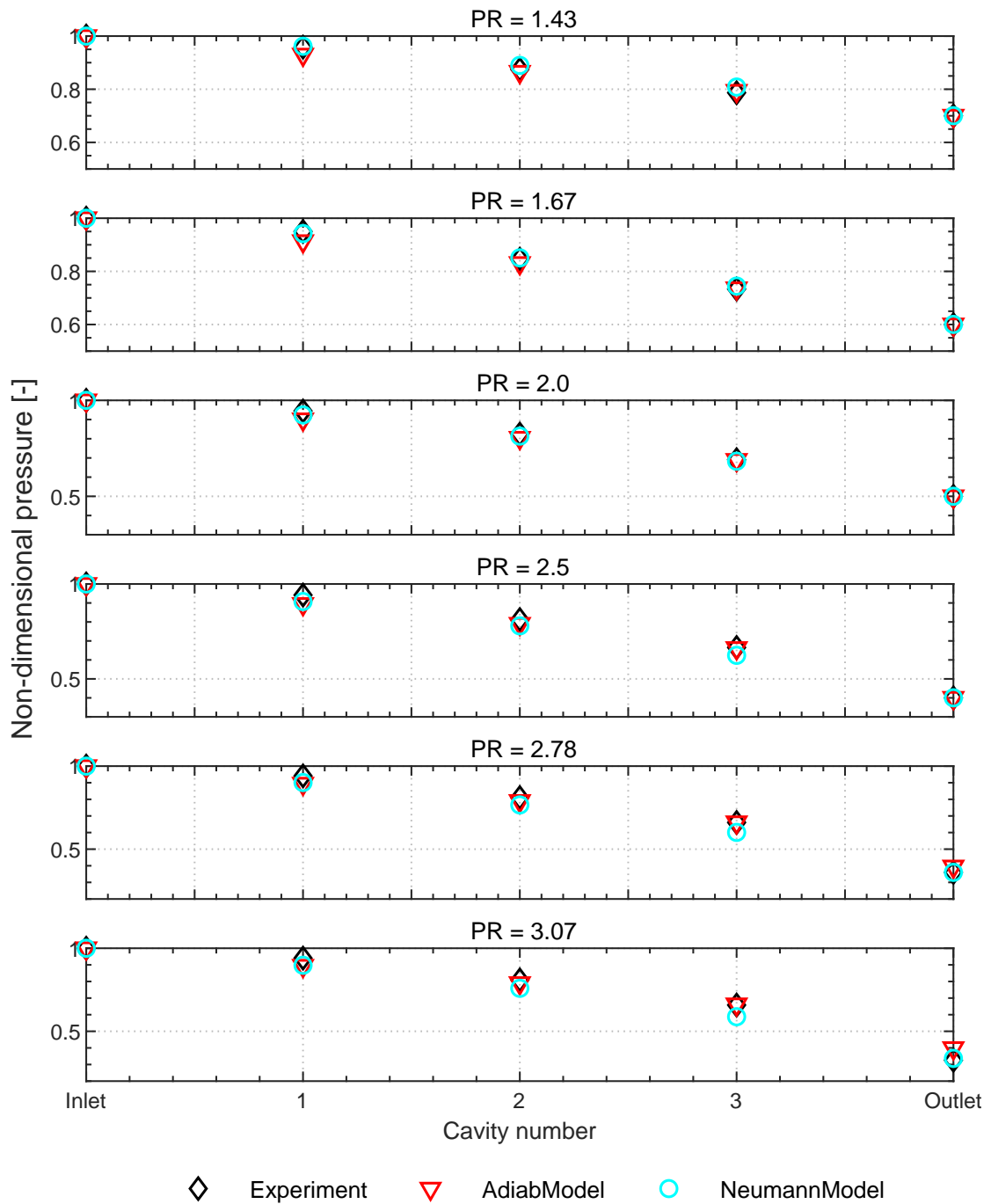
Figure 4.11 – Comparison of cavity pressure distribution between experiment, the author model and the Neumann model on Pocket Damper Seal (PDS) at 12 bar inlet pressure, 50°C inlet temperature and varying PR with R134a as working fluid

Labyrinth seal (LSVP4T): R134a

Figure 4.12 represents the comparison of cavities pressure distribution between the experimental data, the author model and the Neumann model on the 4 teeth labyrinth

seal with varying cavity pitch (LSVP4T) at 12 bar inlet pressure with varying pressure ratios. The predicted results from the author model highlight a fine match with the measured data with a maximum overprediction of 3.2% in the last cavity at a high-pressure ratio of 3.07. For the first and second cavity, author's model indicated a negligible deviation.

Regarding the Neumann model, the numerical results yields an overprediction of pressure in all cavities at a low-pressure ratio by up to 5% in the last cavity. Similarly to the pocket damper seal, this model displays a shift towards an underprediction of pressure in all cavities with a maximum deviation of 8.3% in the last cavity at a high-pressure ratio of 3.07.

Referring to the comparison of cavity pressure distribution between the experimental results and the numerical results from the author's model and the Neumann model, the author's model demonstrates a better prediction accuracy. The good agreement between the cavity pressure distribution of the author's model highlights the reliability of the leakage prediction. Furthermore, both models showed the highest deviation in the prediction of seal exit pressure the choked flow conditions. A similar explanation to the pocket damper seal applies here as well.
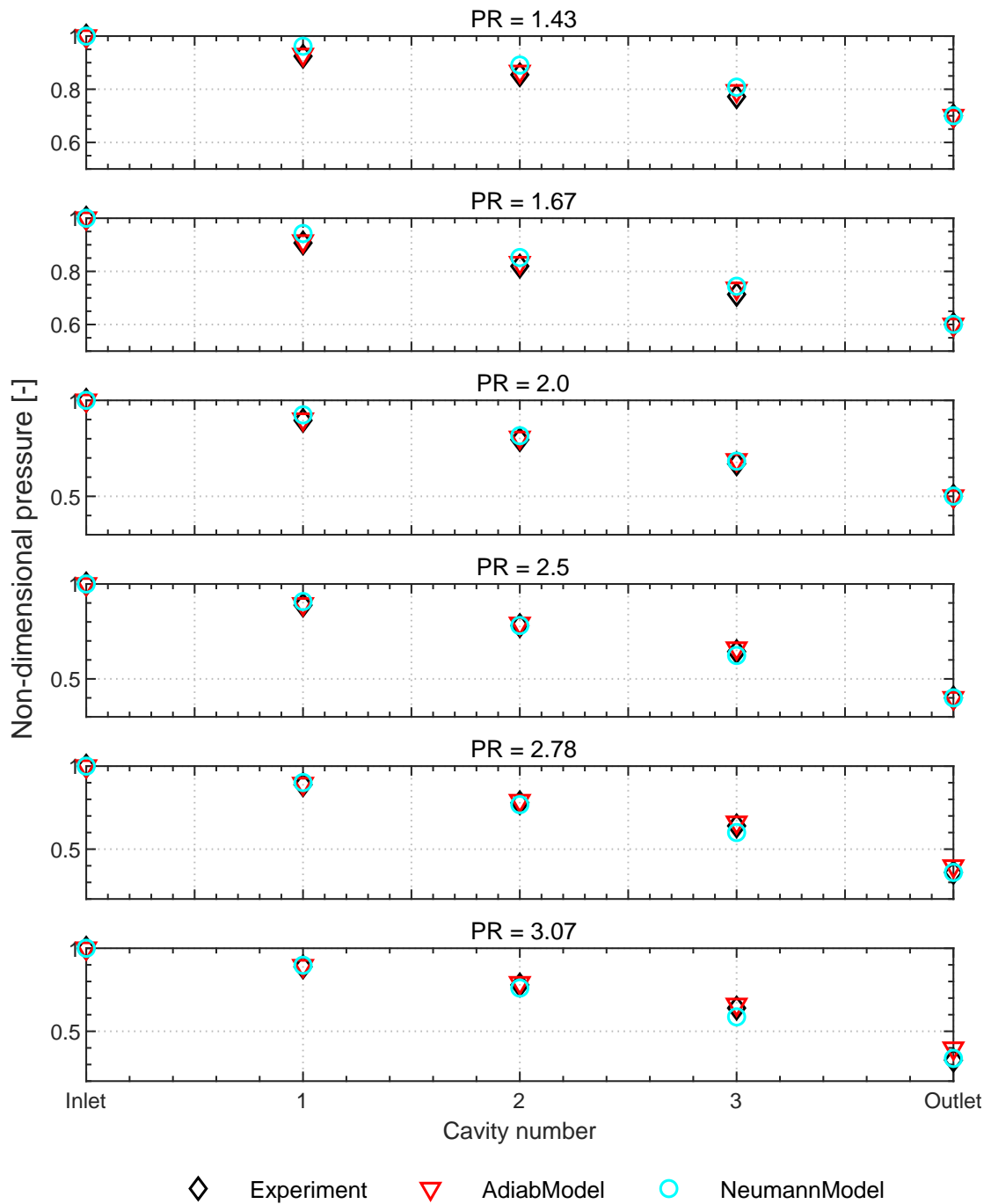
Figure 4.12 – Comparison of cavity pressure distribution between experiment, the author model and the Neumann model on Labyrinth seal (LSVP4T) at 12 bar inlet pressure, 50°C inlet temperature and varying PR with R134a as working fluid

Pocket damper seal (PDS): Air

Figure 4.13 highlights the comparison of cavity pressure distribution between the measurements and the author's model on the Pocket damper seal (PDS). For the range

of tested pressure ratios, the author's model yields an underprediction of the pressure distribution in all cavities. At low-pressure ratios, a maximum deviation of 3% has been observed in the first cavity. However, with increasing pressure ratio, the deviation increases and extends up to 6% at a high-pressure ratio of 4. The highest overprediction of 23.5% has been noticed on the seal outlet at the choke flow region.
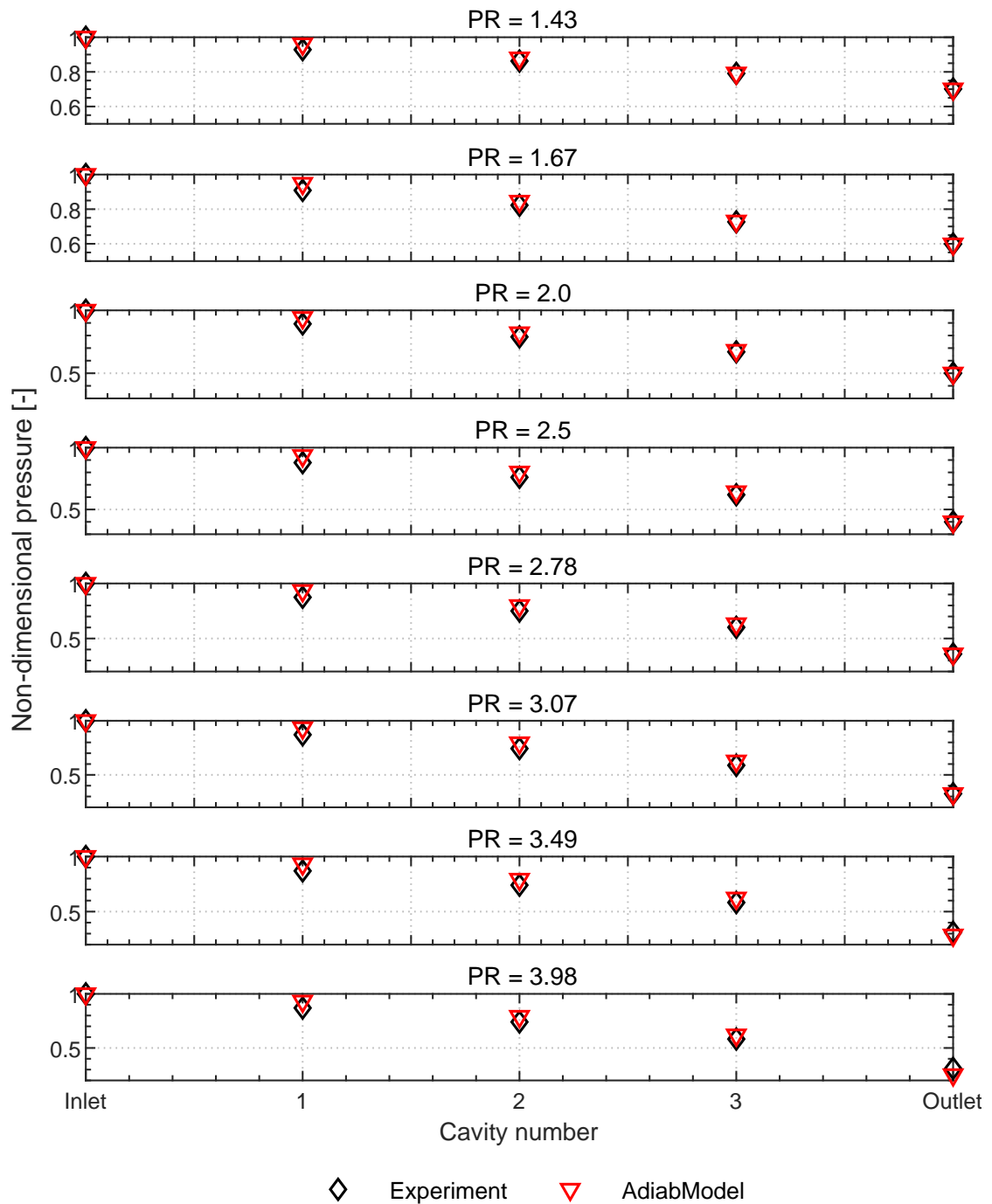
Figure 4.13 – Comparison of cavity pressure distribution between experiment and the author model on Pocket Damper Seal (PDS) at 5 bar inlet pressure, 25°C inlet temperature and varying PR with air as working fluid

Labyrinth seal (LSVP4T): Air

Figure 4.14 highlights the comparison of the cavity pressure distribution between the experimental data and the numerical results based on the author's model on the 4

teeth Labyrinth seal with varying cavity pitch (LSVP4T) operated in air. The predicted cavity pressure distribution matches the experimental data very well at all pressure ratios. At a pressure ratio of 4, the model yields a maximum overprediction of 1.3%, 1.6% and 2.5% in the first, second and third cavity respectively. At choked conditions, the model overpredicts the exit pressure up to 23%.

The outcome of the comparison between the experimental and numerical data of the cavity pressure distribution on two different types of seals with air and R134a demonstrates the good prediction quality of the author's model. The highest deviation of pressure appears on the seal outlet at high-pressure ratios due to the choked flow where uncontrolled expansion occurs, which is not taken into account in the author model.
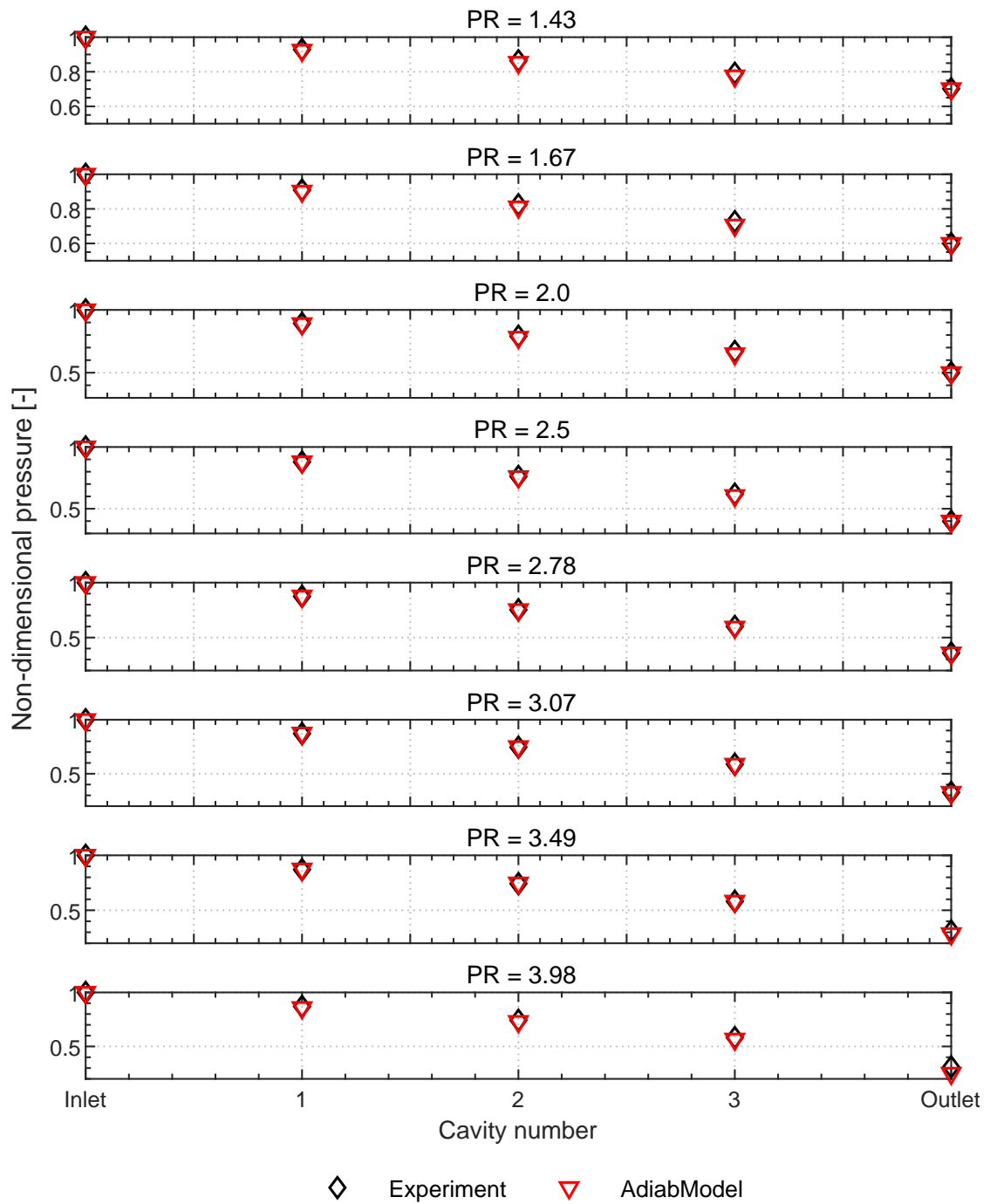
Figure 4.14 – Comparison of cavity pressure distribution between experiment and the author model on Labyrinth seal (LSVP4T) at 5 bar inlet pressure, 25°C inlet temperature and varying PR with air as working fluid

4.3.6 Comparison of cavity temperature distribution

Besides the leakage and cavity pressure measurement, seal cavity temperature measurements have been carried out on different seals with R134a and air. This section presents the comparison of the measured and the predicted seal cavity temperature.

Pocket damper seal (PDS): R134a

Figure 4.15 compares the cavity temperature distribution from the experimental data and from the predicted result based on the author's model and Neumann's model for the Pocket damper seal (PDS) at 12 bar inlet pressure. The author's model overpredicts the cavity temperature over the entire seal pressure ratios with a maximum deviation of 2.4 K and 1.6 K in the first and the following cavities respectively at a pressure ratio of 4. With a decrease in pressure ratio, the deviation in cavity temperature reduces and aligns well with the measured values. The similar prediction accuracy have been observed at 5 and 9 bar inlet pressure (refer to figure D.24 and D.25 in appendix).

The Neumann model also overpredicts the cavity temperature in the first cavity for all pressure ratios with a maximum deviation ranging up to 2.2 K. In the last two cavities, the model underpredicts the temperature distribution at all pressure ratios with a maximum deviation of 2.6 K in the last cavity at high pressure ratios.
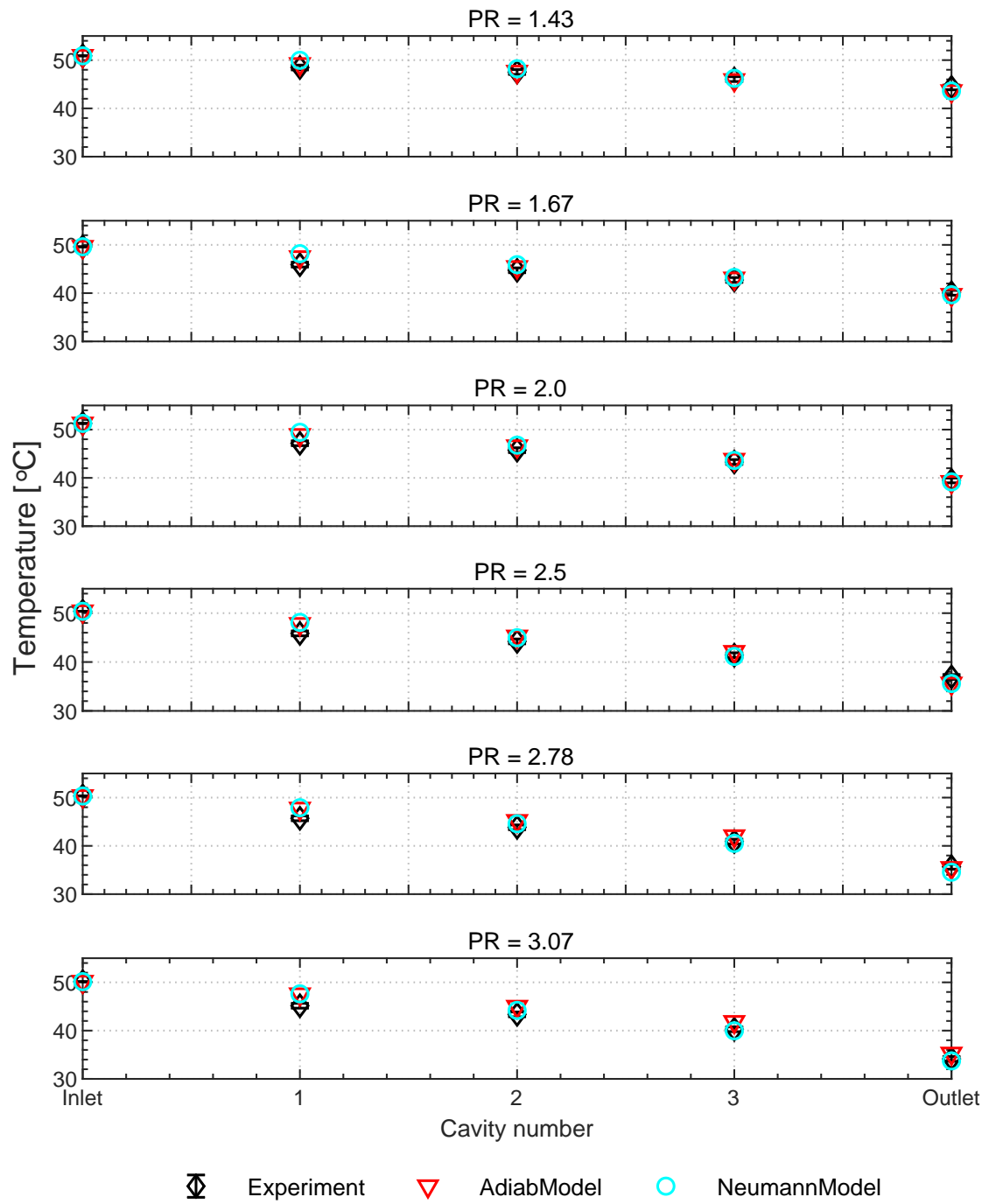
Figure 4.15 – Comparison of cavity temperature distribution between the experiment, the author model and the Neumann model on Pocket Damper Seal (PDS) at 12 bar inlet pressure, 50°C inlet temperature and varying PR with R134a as working fluid

Labyrinth seal (LSVP4T): R134a

Figure 4.16 illustrates the numerical results and the experimental results of the cavity temperature profile on the Labyrinth seal (LSVP4T) at 12 bar inlet pressure. An overprediction of the cavity temperature by the author's model can be observed at all pressure ratios in the first two cavity. The maximum deviation of 2.8 K has been recorded in the first cavity at a pressure ratio of 3.07. The results in the second cavity suggests negligible deviation over the complete range of investigated pressure ratios. In contrast to the first two cavities, the author's model underpredicts the temperature in the last cavity for almost all pressure ratios with a maximum deviation distribution up to 1.1 K.

The Neumann model suggests a similar trend of the temperature distribution as the author's model. The model indicated overprediction in temperature resulting up to 3.5 K and 1.2 K in the first and second cavity respectively at a high-pressure ratio of 4. However, in the last cavity model underpredicts the cavity temperature at all pressure ratios.

Referring to the measured and predicted results of two seal models on two different seals types, both models yields a similar prediction quality in the cavity temperature distribution. However, the author's model reveals a marginally lower deviation compared to the Neumann model.
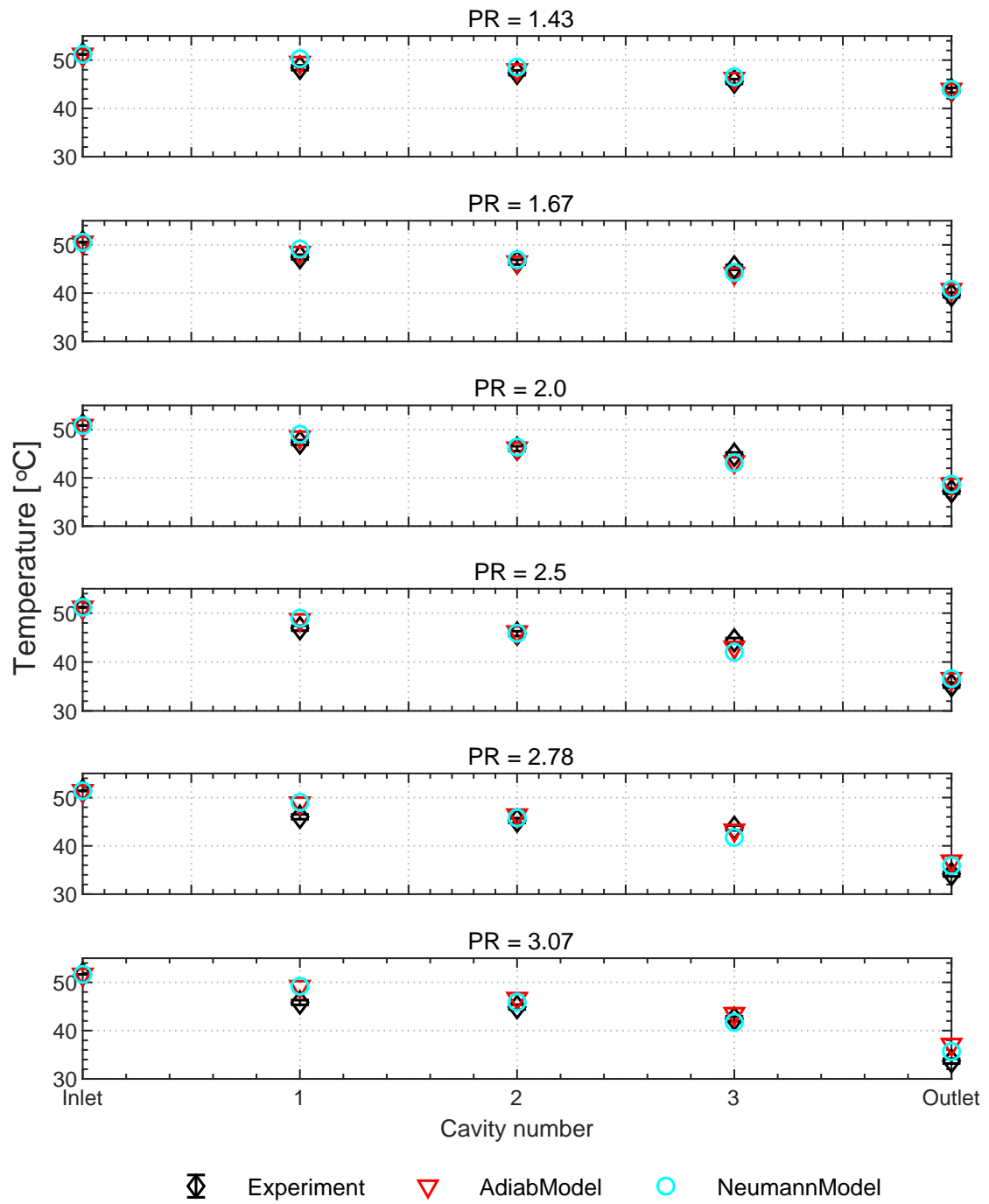
Figure 4.16 – Comparison of cavity temperature distribution between the experiment, the author model and the Neumann model on Labyrinth seal (LSVP4T) at 12 bar inlet pressure, 50°C inlet temperature and varying PR with R134a as working fluid

Cavity temperature distribution: Air

The comparison of the cavity temperature distribution between the measured data and predicted results on the Pocket damper seal (PDS) and the Labyrinth seal (LSVP4T) with air at 5 bar inlet pressure illustrates the superior performance of the author's model. A maximum overprediction of 0.4 and 0.2 K can be observed for the PDS (refer figure D.26 in appendix) and LSVP4T (refer figure D.27 in appendix) respectively at a pressure ratio of 4.

4.4 Investigations on conical seals

In order to examine the robustness of the author's model, irregular and non-identical clearance seals, labyrinth seals with different geometrical features have been experimentally tested with R134a and compared with the author's model using the Vermes kinetic carry-over correlation. For brevity, the results are presented at 5 and 9 bar inlet pressure. Special measure was undertaken to maintain same inlet boundary conditions for all seals in order to have robust data for comparison. An overview of the test seals with their dimensions is listed in table 4.2. The definition of the used abbreviation for test seals is listed in table 4.1.

4.4.1 Comparison of leakage on individual test seals

Labyrinth seal (LSVP4T)

The prediction of leakage by the author model at 5 and 9 bar inlet pressure is presented in figure 4.17 for the 4 teeth Labyrinth seal with varying cavity pitch. The numerical results shows very good agreement with the experimental results for both inlet pressure at all pressure ratios. The model indicates underprediction of leakage at a low-pressure ratio of 1.43 for both inlet pressures with a maximum deviation of 4% and 3.5% respectively.
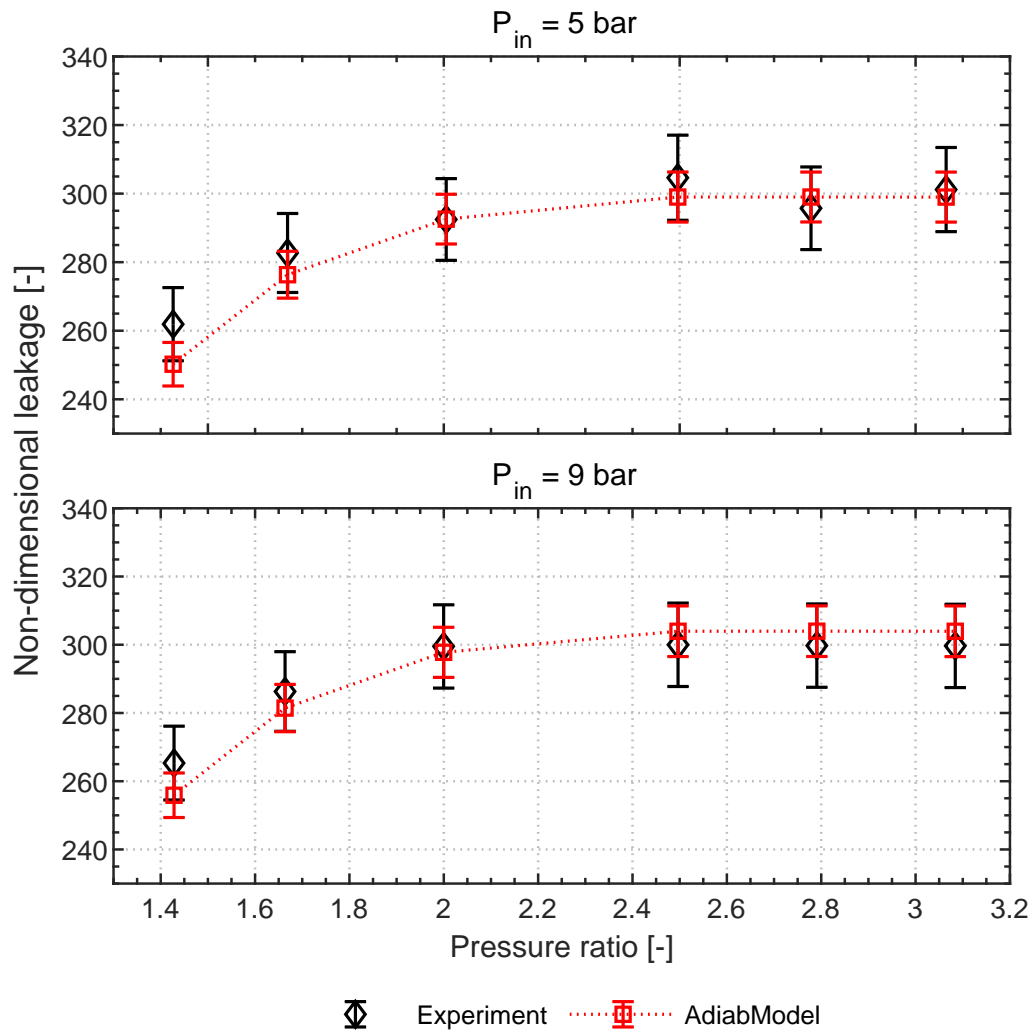
Figure 4.17 – Comparison of non-dimensional leakage between the experiment and the author model on Labyrinth seal (LSVP4T) at inlet pressure of 5 and 9 bar with inlet temperature of 25° and 40° respectively, varying PR and R134a as a working fluid

Labyrinth seal (LSCP5T)

Figure 4.18 displays the comparison between the experimental and the numerically predicted data from the author's model at 5 and 9 bar inlet pressure for the 5 teeth Labyrinth seal with constant cavity pitch (LSCP5T). For a 5 bar inlet pressure, the model overpredicts the leakage over the range of pressure ratios. The maximum and minimum deviation of 5.5% and 3.5% can be observed at pressure ratios of 2.5 and 1.67 respectively. At 9 bar inlet pressure, the author's model underpredicts leakage by up to 5% at the lowest tested pressure ratio, whereas the deviation for higher pressure ratios is negligible.
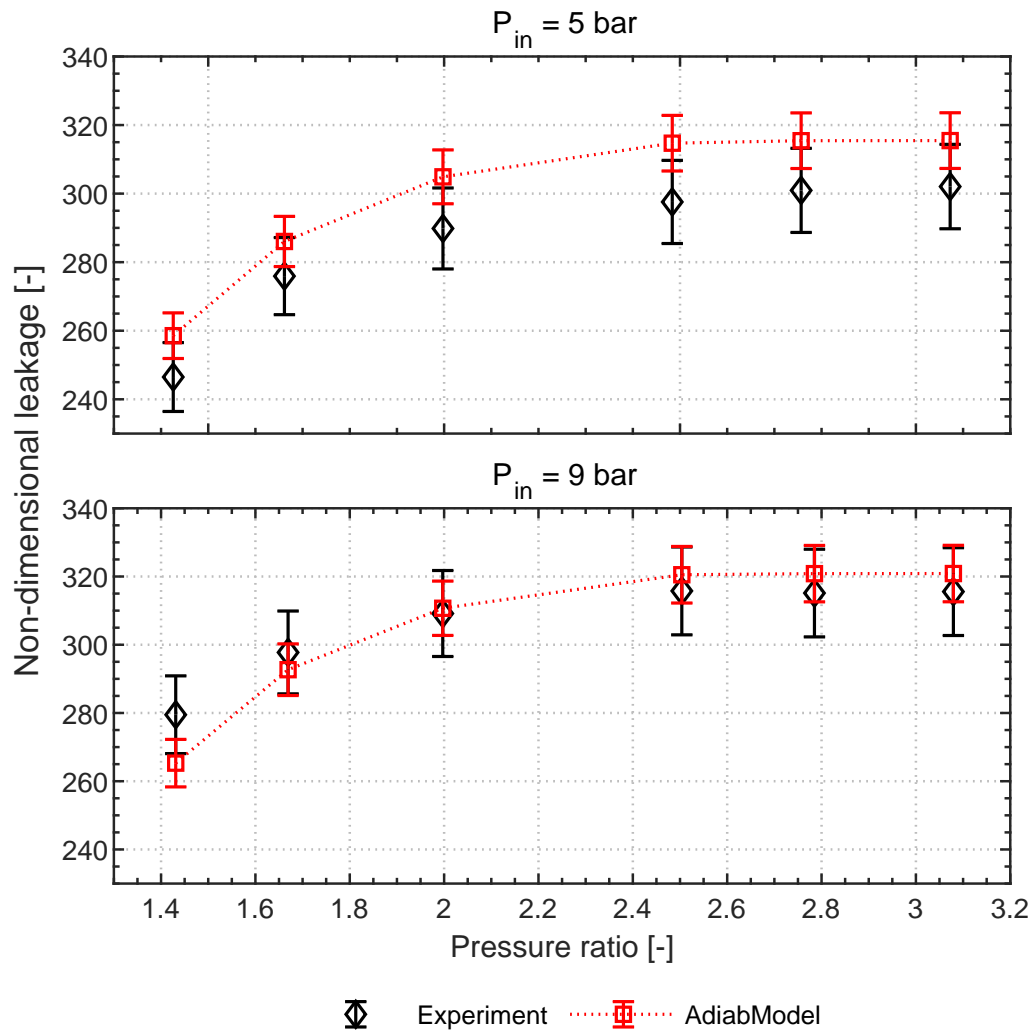
Figure 4.18 – Comparison of non-dimensional leakage between the experiment and the author model on Labyrinth seal (LSCP5T) at inlet pressure of 5 and 9 bar with inlet temperature of 25° and 40° respectively, varying PR and R134a as a working fluid

Labyrinth seal (LSCP4T)

The comparison between the measurement and the author model on 4 teeth Labyrinth seal with constant cavity pitch (LSCP4T) at 5 and 9 bar inlet pressure is shown in figure 4.19. For 5 bar inlet pressure, a maximum deviation of 3.2% is reported at a pressure ratio of 2.5. Similarly, at 9 bar inlet pressure, the author's model highlights overprediction at all pressure ratios. The maximum deviation of 4.5% has been observed at a pressure ratio of 2.5.

The author's model suggests a good agreement with the experimental results in seal leakage prediction at different inlet boundary conditions over the range of pressure ratios irrespective of the seal clearances and seal types. The indication of the higher
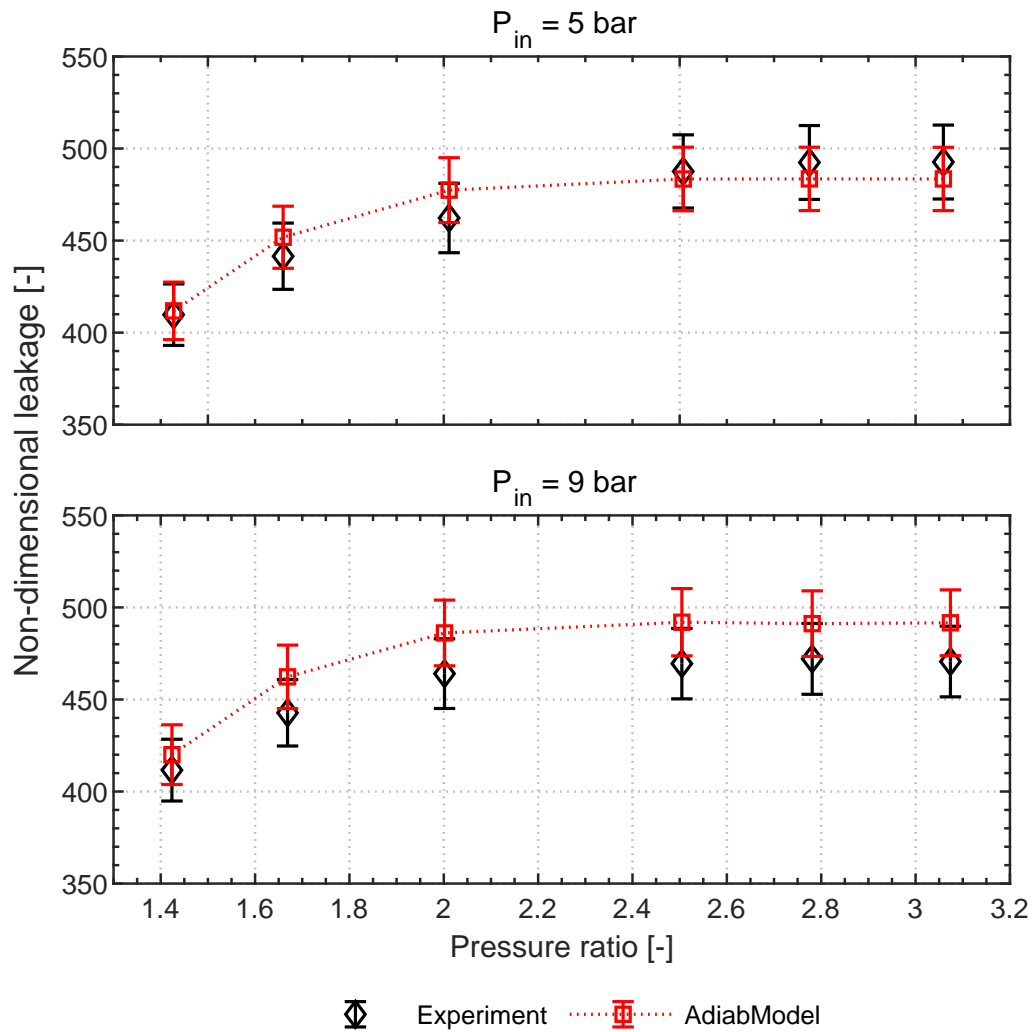
Figure 4.19 – Comparison of non-dimensional leakage between experiment and the author model on Labyrinth seal (LSCP4T) at inlet pressure of 5 and 9 bar with inlet temperature of 25° and 40° respectively, varying PR and R134a as a working fluid

deviation compared to the cylindrical seal can be attributed to the assumptions of linear interpolation in clearances, which may not corresponds to reality. Thus, the validity of the author's model with regards to the leakage is illustrated experimentally on seals with non-constant clearance.

4.4.2 Comparison of cavity pressure distribution

To quantify the performance of the author model regarding the pressure prediction within the seal cavities on irregular seals with non-uniform flow cross-section, the predicted data is compared with the measurement results on labyrinth seals with different geometrical configuration at 5 and 9 bar inlet pressure.

Labyrinth seal (LSVP4T)

Figure 4.20 shows the comparison of cavity pressure distribution between the measured data and the predicted results from the author model for the 4 teeth Labyrinth seal with varying cavity pitch (LSVP4T) at 9 bar inlet pressure. The author's model suggests an accurate prediction quality in the first and the second cavity with a minor underprediction at the high-pressure ratios, whereas up to 11% of underprediction has been observed in the last cavity at high pressure ratios. A similar result has been recorded at 5 bar inlet pressure (refer to the figure D.28 in the appendix).

Figure 4.20 – Comparison of cavity pressure distribution between the experiment and the author model on Labyrinth seal (LSVP4T) at 9 bar inlet pressure, 40°C inlet temperature, varying PR and R134a as a working fluid

Labyrinth seal (LSCP4T)

The prediction quality of the author model with the cavity pressure distribution on the 4 teeth Labyrinth seal with constant cavity pitch (LSCP4T) at 9 bar inlet pressure is shown in figure 4.21. The author's model indicates an underprediction of pressure in all cavities for all the tested pressure ratios. A maximum deviation of 4%, 8.5%, and 12% have been observed in the first, second and third cavity respectively at a pressure ratio of 3.07. A similar prediction quality has been noted at 5 bar inlet pressure with comparatively less deviation in all cavity and all pressure ratios (refer to figure D.29 in appendix).

The comparison of the seal cavity pressure distribution between the numerical results and the measurement data on test seals suggests a reasonable prediction accuracy of the author's model on non-identical irregular conical seals. The existence of increased deviation in cavity pressure compared to the cylindrical seals could be justified due to linear interpolation of the clearance. The author's model indicates the highest deviation to experimental data in the last cavity and on the seal outlet pressure at high pressure ratios where choked flow occurs. At choke flow, flow expansion occurs to match the lower outlet pressure of the seal, which is not implemented in the author model due to the complex flow nature.

Figure 4.21 – Comparison of cavity pressure distribution between the experiment and the author model on Labyrinth seal (LSCP4T) at 9 bar inlet pressure, 40°C inlet temperature, varying PR and R134a as a working fluid

4.4.3   Comparison of cavity temperature distribution

This section presents the results with regards to the seal cavity temperature distribution prediction by the author model versus experimental data. The results for two labyrinth seals tested are shown for the comparison purpose.

Labyrinth seal (LSVP4T)

Figure 4.22 represents the temperature evolution for the labyrinth seal with four teeth and variable cavity pitch (LSVP4T). For all the test conditions, the author's model shows good prediction performance. The highest discrepancy of 1 K on the first cavity and lowest of 0.5 K on the last cavity has been recorded at a pressure ratio of 3.07. Test results at 5 bar inlet pressure shows an opposite trend with a maximum and minimum difference of 1.1 K and 0.2 K on last and first cavity respectively at a pressure ratio of 3.07 (refer figure D.31 in appendix).

Figure 4.22 – Comparison of cavity temperature distribution between the experiment and the author model on Labyrinth seal (LSVP4T) at 9 bar inlet pressure, 40°C inlet temperature and varying PR with R134a as working fluid

Labyrinth seal (LSCP4T)

Figure 4.23 displays the results of cavity temperature profiles on the 4 teeth Labyrinth seal with constant cavity pitch at 9 bar inlet pressure. The maximum and the minimum deviation of 2.3 K and 0.4 K can be observed in the first and the last cavity respectively. Furthermore, in the case of 5 bar inlet pressure, the highest discrepancy of 0.3 K in the last cavity can be observed (see figure 4.23 in appendix).
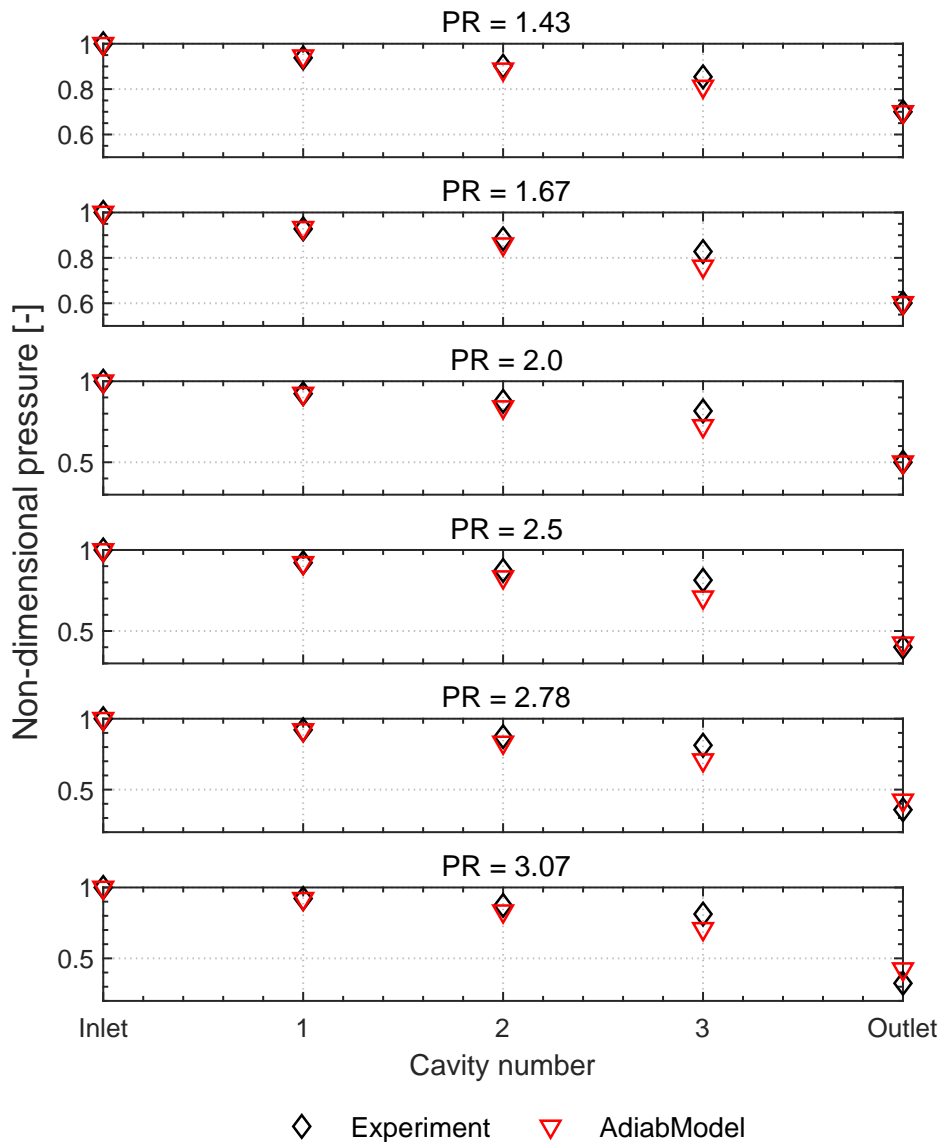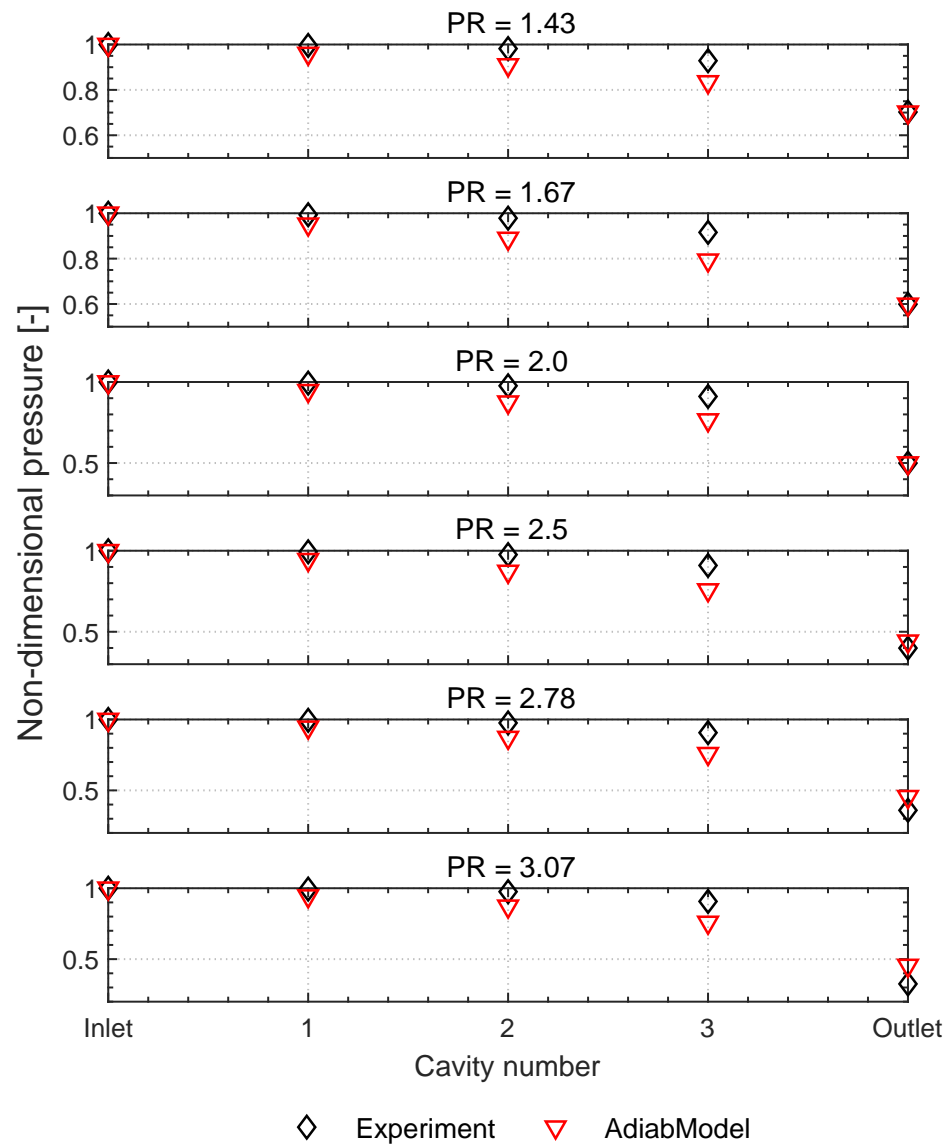

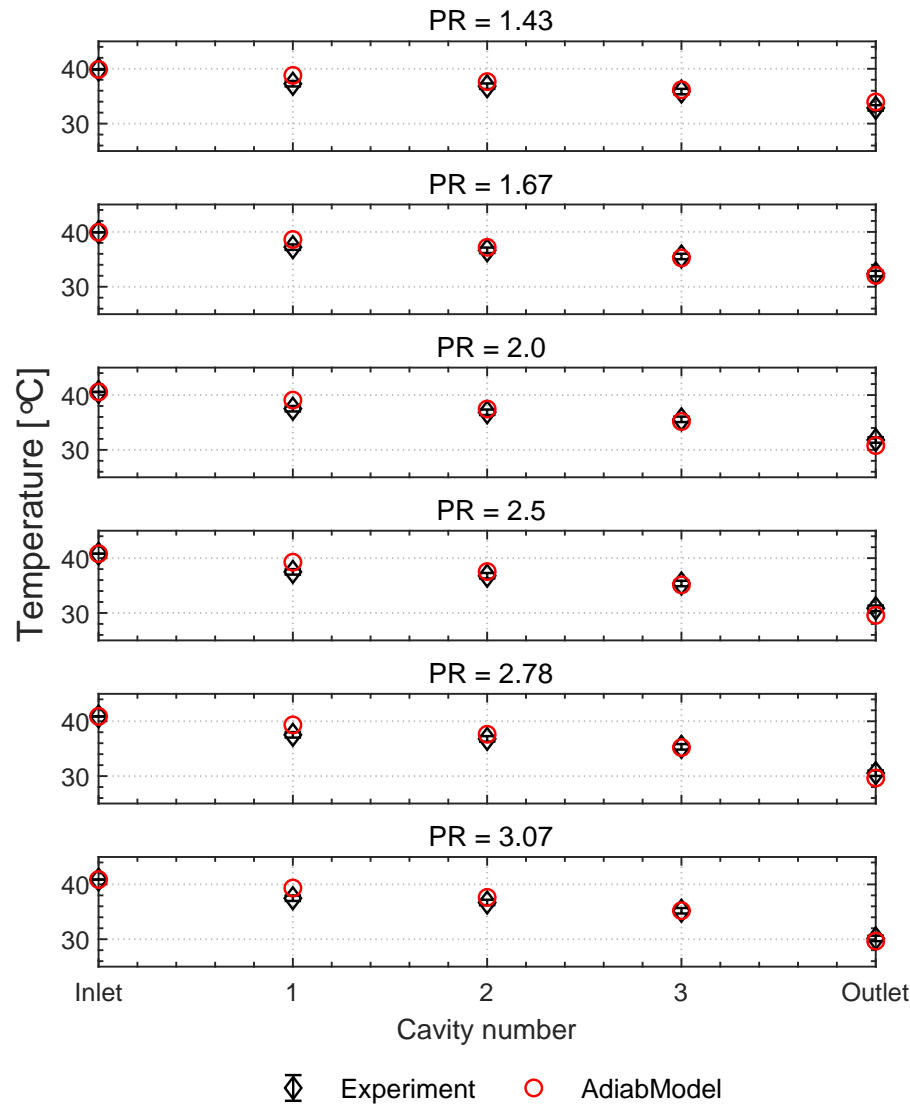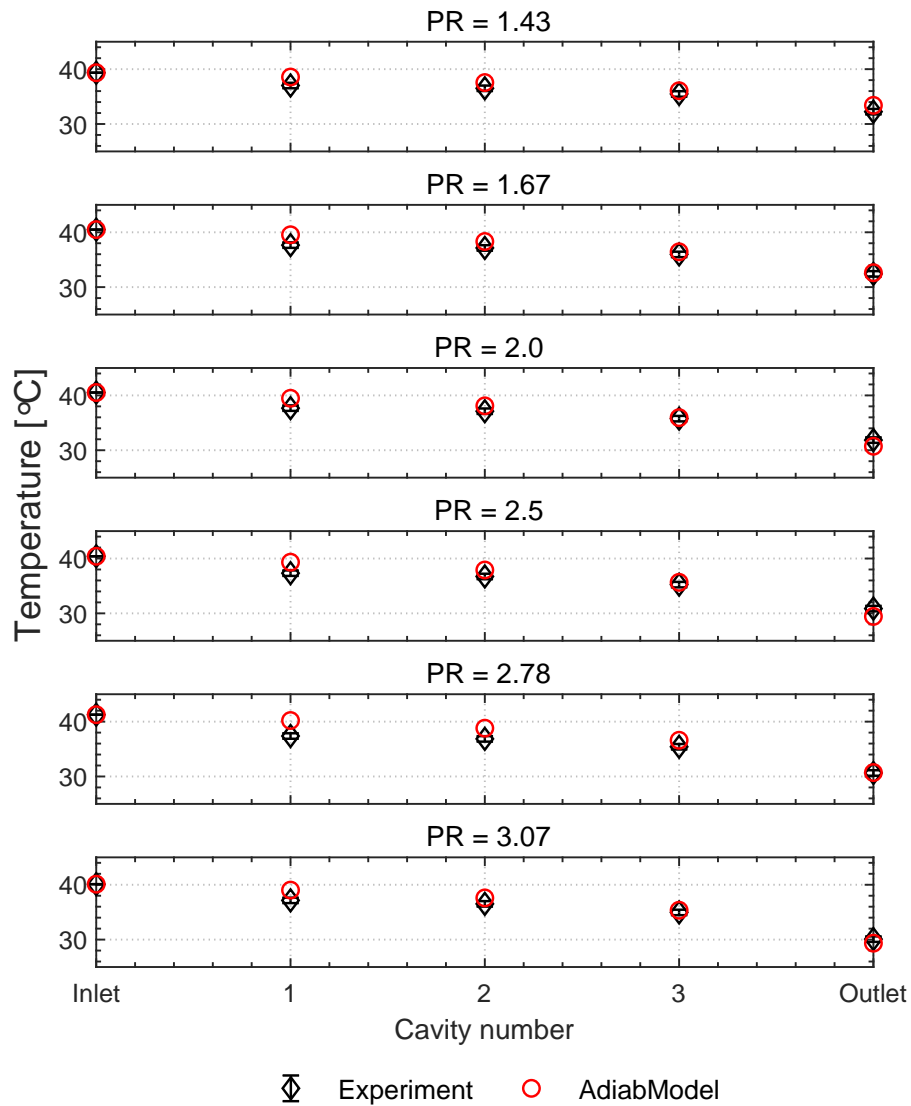Figure 4.23 – Comparison of cavity temperature distribution between experiment and the author model on Labyrinth seal (LSCP4T) at 9 bar inlet pressure, 40°C inlet temperature and varying PR with R134a as working fluid

4.5 Investigations on seals operating to the proximity of the fluid saturation line

In a thermodynamic cycle, the working fluids often operate near the saturation point where commonly practiced perfect gas assumption is not valid and hence real gas properties need to be implemented in the numerical model. The author's research topic focuses on seals for reduced-scale turbomachinery applications working on a fluid, like refrigerant R134a, which are generally operated near the saturation point. A theoretical analysis of real gas properties and their deviation from the perfect gas assumptions on seal leakage has been discussed in Chapter 1.4. To highlight the issue related to real gas effects, all test seals have been experimentally tested at 9 and 12 bar inlet pressure with varying temperatures at a fixed pressure ratio of 2 and R134a as a test fluid. For the sake of visual clarity, the average seal clearance has been used in the-state-of-the-art models. The results are presented for the cylindrical seals (Pocket damper and Hole pattern) and the conical seals (Labyrinth and Smooth).

The measured data are compared with the numerical results of different seal models to evaluate the performance of seal models in the vicinity of the fluid saturation line. For brevity, the average temperature without measurement uncertainty has been considered to present the results.

4.5.1 Pocket damper seal (PDS)

Figure 4.24 presents the comparison of leakage between the experiment and different models at 9 and 12 bar inlet pressure with varying inlet temperature. The experimental data suggests up to 9% increased non-dimensional leakage near the saturation line compared to the tested highest inlet temperature of 59°C (24 K superheat). This clearly suggests a significant effect on leakage resulting from the real gas effect. i.e. the proximity of the inlet conditions to the saturation line. At 9 bar inlet pressure, the author's model shows a good agreement with the experimental results at all degrees of superheat with a maximum deviation of 1.2% at the inlet temperature of 37.2°C (1.8 K superheat). The Neumann model underpredicts leakage over the complete range of inlet temperatures. The maximum deviation has been observed near the saturation point with 1.8 K superheat.

At 12 bar inlet pressure, the author's model underpredicts leakage with a maximum deviation of 3.2% in the vicinity of the saturation line (1 K superheat). Likewise, the Neumann model showed underprediction of leakage for all inlet temperatures with a maximum deviation of 7% at a superheat of 1 K. The measured data suggests up to 10% higher leakage near the saturation line (1 K superheat) compared to the increased degree of superheat of 26 K.

The results highlights the effects of the degree of superheat on seal leakage perfor-

Figure 4.24 – Comparison of different model performance on seal leakage with varying degree of superheat on Pocket damper seal (PDS) at 9 and 12 bar inlet pressure, PR of 2 and R134a as working fluid

mance. Both experimental data as well as the author's model suggest an increase in non-dimensional leakage with a decreasing degree of superheat, which suggests a strong effects related to the real gas effects, i.e. the deviation of the working fluid behavior from a perfect gas. The ability of the author model to capture this effect has been shown. The Neumann model shows a similar trend of leakage with the varying inlet temperature. However, the ideal Neumann and the St. Venant model illustrate their inability to capture the trend compared to the measurements due to the assumption of an ideal gas in their equations. The coincidence of the matching results from the ideal Neumann model can be better understood by referring to the previously presented results (refer to figure 4.3) where the investigated pressure ratio and inlet temperature are aligned.

4.5.2 Labyrinth seal (LSVP4T)

Figure 4.25 represents a superheat test on the four teeth Labyrinth seal with varying cavity pitch (LSVP4T) at 9 and 12 bar inlet pressure. In the case of 9 bar inlet pressure, the author's model suggests an underprediction of leakage with a maximum deviation of 5.2% at a superheat of 2 K. With the increase in inlet temperature the deviation decreases and shows a minor 0.5% overprediction of leakage at 24 K of superheat. The Neumann model displays underprediction of leakage over the entire range of inlet temperature with a maximum deviation of 9% at low superheat of 2 K. In the case of the ideal Neumann and the St. Venant, both models yield nearly the constant leakage with varying inlet temperature. The experimental data reported up to 11% relatively higher leakage near the saturation line with 2 K superheat compared to the 24 K superheat.

At 12 bar inlet pressure, the author's model underpredicts leakage by up to 3% near the saturation point (1.5 K superheat), whereas a negligible deviation of 0.6% has been observed at the highest degree of superheat (26 K). At a low superheat of 1.5 K, the Neumann model underpredicts leakage by 5.2%, whereas, at higher superheat up to 3.5% deviation has been monitored. The ideal Neumann and the St. Venant model displayed no influence on leakage to the degree of superheat due to the hypothesis of an ideal gas. In the vicinity of the fluid saturation line, the measured data indicates up to 10% increase in leakage.

The author's model reveals its better prediction performance at different levels of superheat and demonstrates its ability to capture the experimental trend. Furthermore, the Neumann model underpredicts leakage, yet is able to capture the experimental trend. The ideal Neumann and the St. Venant model show no effects in leakage regardless of the inlet temperature. As discussed in the Pocket damper seal (PDS), the matching results from the ideal Neumann model can be attributed to the selected pressure ratio and temperature range where the model showed good agreement with the measured results (see figure 4.4). The experimental data reveals a pronounced effect on leakage near the saturation region as a function of the level of superheat, i.e.
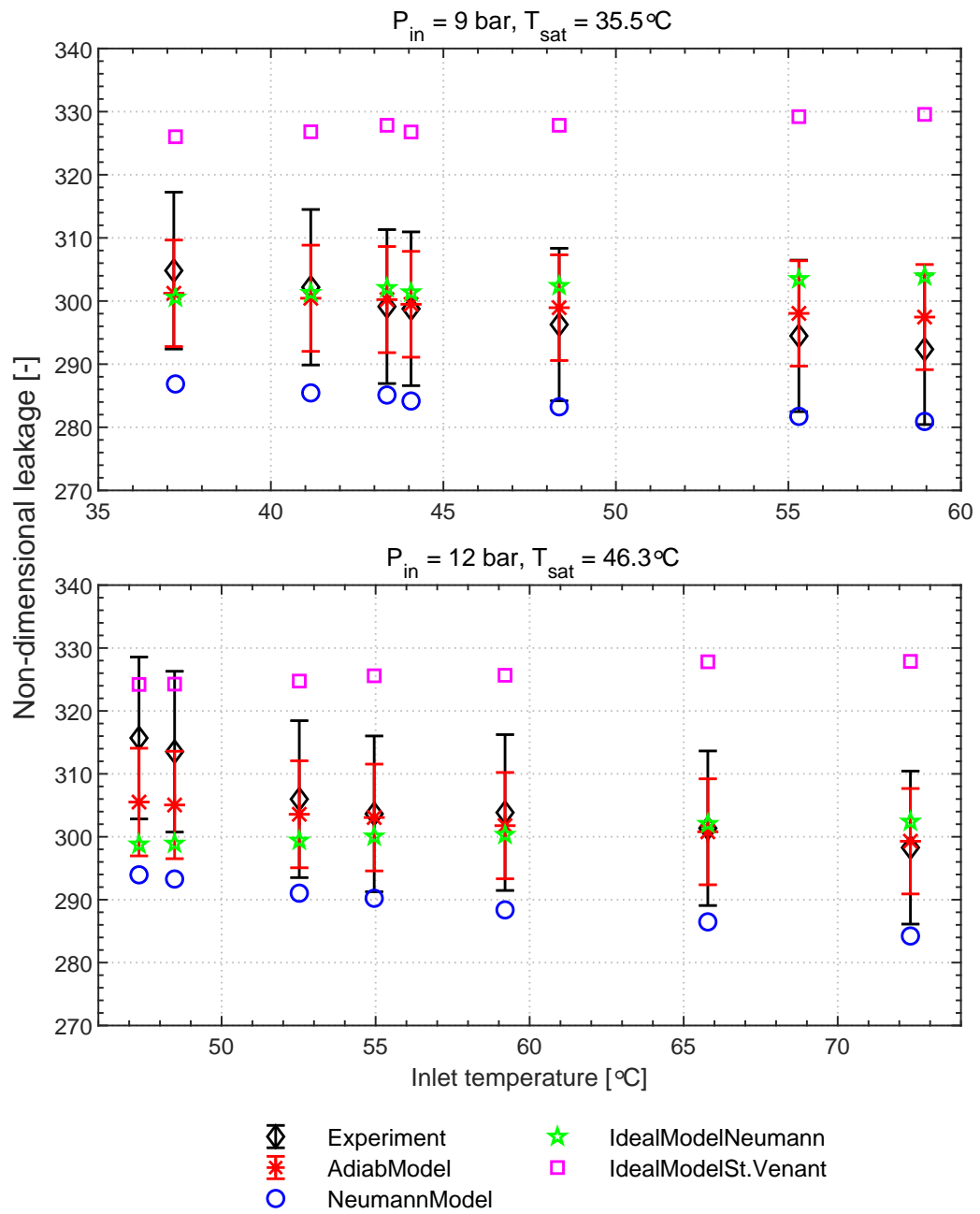
Figure 4.25 – Comparison of different model performance on seal leakage with varying degree of superheat on Labyrinth seal (LSVP4T) at 9 and 12 bar inlet pressure, PR of 2 and R134a as working fluid

the proximity to the saturation line.

4.5.3   Labyrinth seal (LSCP4T)

The comparison between the measurements and the numerical results of different seal models with varying degrees of superheat at 9 and 12 bar inlet pressure is illustrated in figure 4.26 for the 4 teeth Labyrinth seal with constant cavity pitch (LSCP4T). The author's model highlights the underprediction of 3.8% in leakage near the saturation point, however, shows up to 5% overprediction at a high superheat of 25.5 K. The Neumann model shows up to 8% underprediction of leakage at a superheat of 1 K, whereas, a negligible deviation has been observed at a higher degree of superheat. Both, the ideal Neumann and the St. Venant model showed no influence in leakage over the range of investigated inlet temperature. The measurement data suggests elevated leakage extending up to 7% in the vicinity of the saturation point (1 K superheat) compared to 25.5 K superheat.

For 12 bar inlet pressure, the author model suggests a maximum deviation of 2% over the range of superheat. The Neumann model displayed underprediction of leakage in all cases of inlet temperature with a maximum deviation of 6% at a low superheat of 1 K. The ideal and the St. Venant model yields an overprediction of leakage without considerable effects over the range of inlet temperature. Near the saturation point, the experimental results highlighted up to 10% relatively increased in leakage compared to 20 K superheat.

The good agreement between the author's model and the measured data on the 4 teeth Labyrinth seal with constant cavity pitch (LSCP4T) has been highlighted. The effect of superheat on seal leakage has been experimentally and numerically demonstrated by the author's model as well as by the Neumann model. The consequence of ideal gas assumptions on seal leakage performance has been illustrated with reference to the ideal Neumann and the St. Venant model.
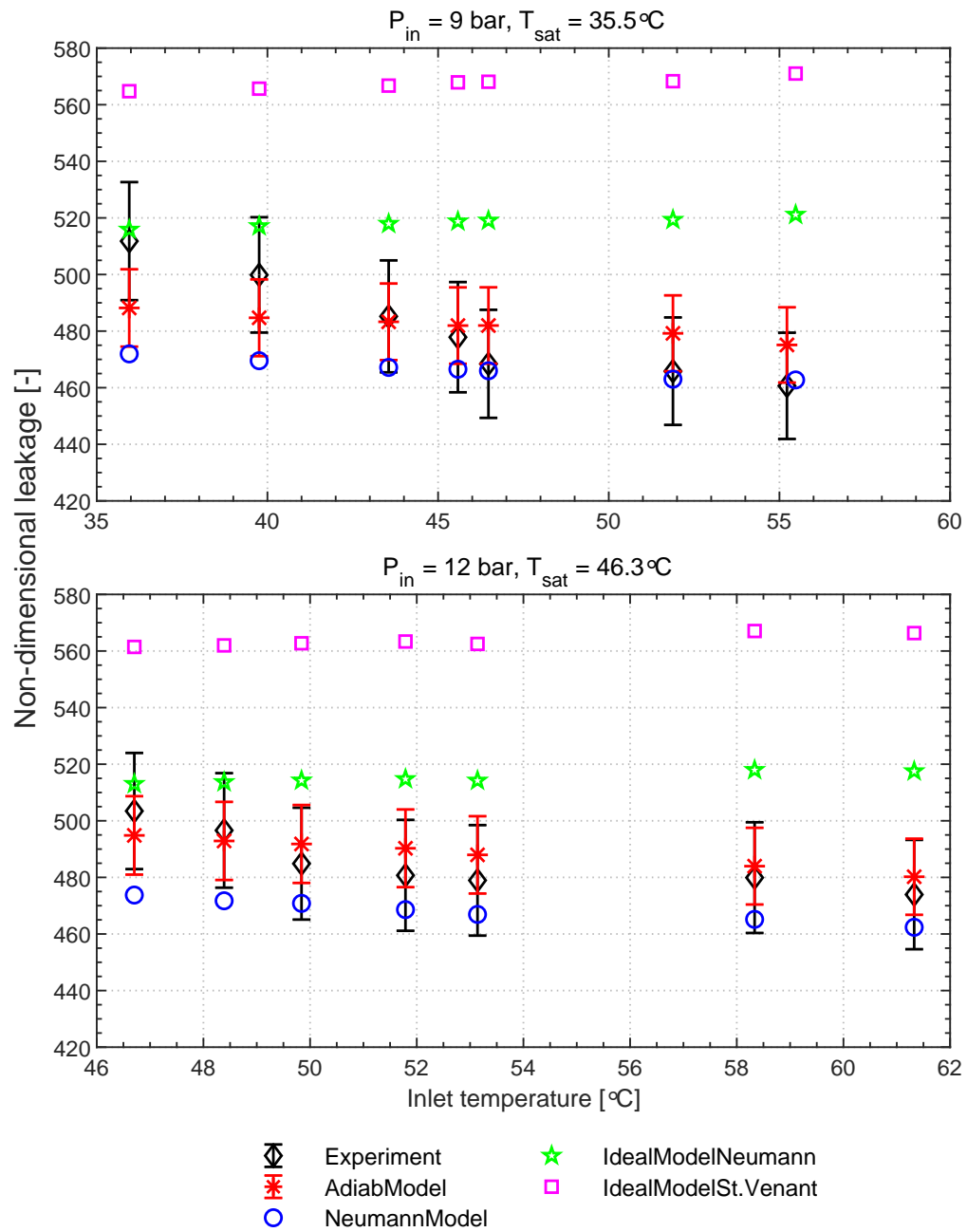
Figure 4.26 – Comparison of different model performance on seal leakage with varying degree of superheat on Labyrinth seal (LSCP4T) at 9 and 12 bar inlet pressure, PR of 2 and R134a as working fluid

4.5.4   Labyrinth seal (LSCP5T)

Figure 4.27 presents the comparison of leakage between the experimental data and different seal models at varying degrees of superheat for the 5 teeth Labyrinth seal with constant cavity pitch (LSCP5T) at 9 and 12 bar. At 9 bar inlet pressure, the author model shows a good agreement with the measurement data over the full range of tested superheat. Near the saturation point with a 1.2 K superheat, a maximum 3% deviation has been recorded whereas at a superheat of about 24 K, a maximum deviation of 9% has been noticed. The Neumann model showed 5% and 2% deviation at 1.2 K and 24 K superheat respectively. The ideal Neumann and the St. Venant model reported overprediction of leakage over the range of superheat with no influence on the degree of superheat. The measurement showed up to 13% of increased leakage at 1.2 K superheat compared to 24 K of superheat.

At 12 bar inlet pressure, the author's model shows a maximum deviation of 3% at low superheat of 2.5 K whereas a negligible deviation at increased superheat. The Neumann model reported up to 7% and 4.5% of deviation at 2.5 K and 27 K superheat respectively. Similar to the other seals, the ideal Neumann and the St. Venant model displayed no effect in leakage irrespective of the degree of superheat. The matching leakage by the ideal Neumann model near the saturation line can be attributed to the coincidence of the investigated pressure ratio and the temperature range as shown in figure 4.5.
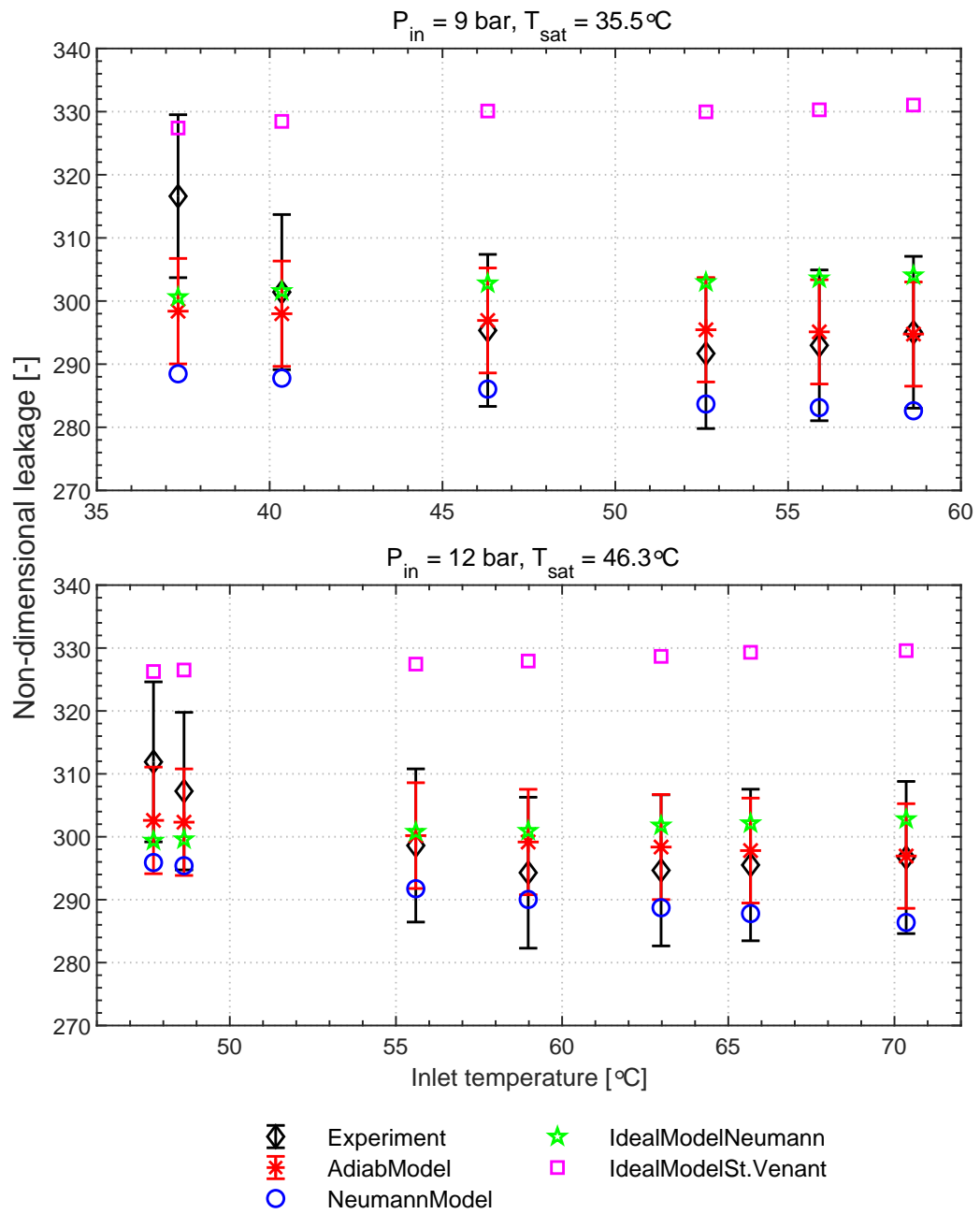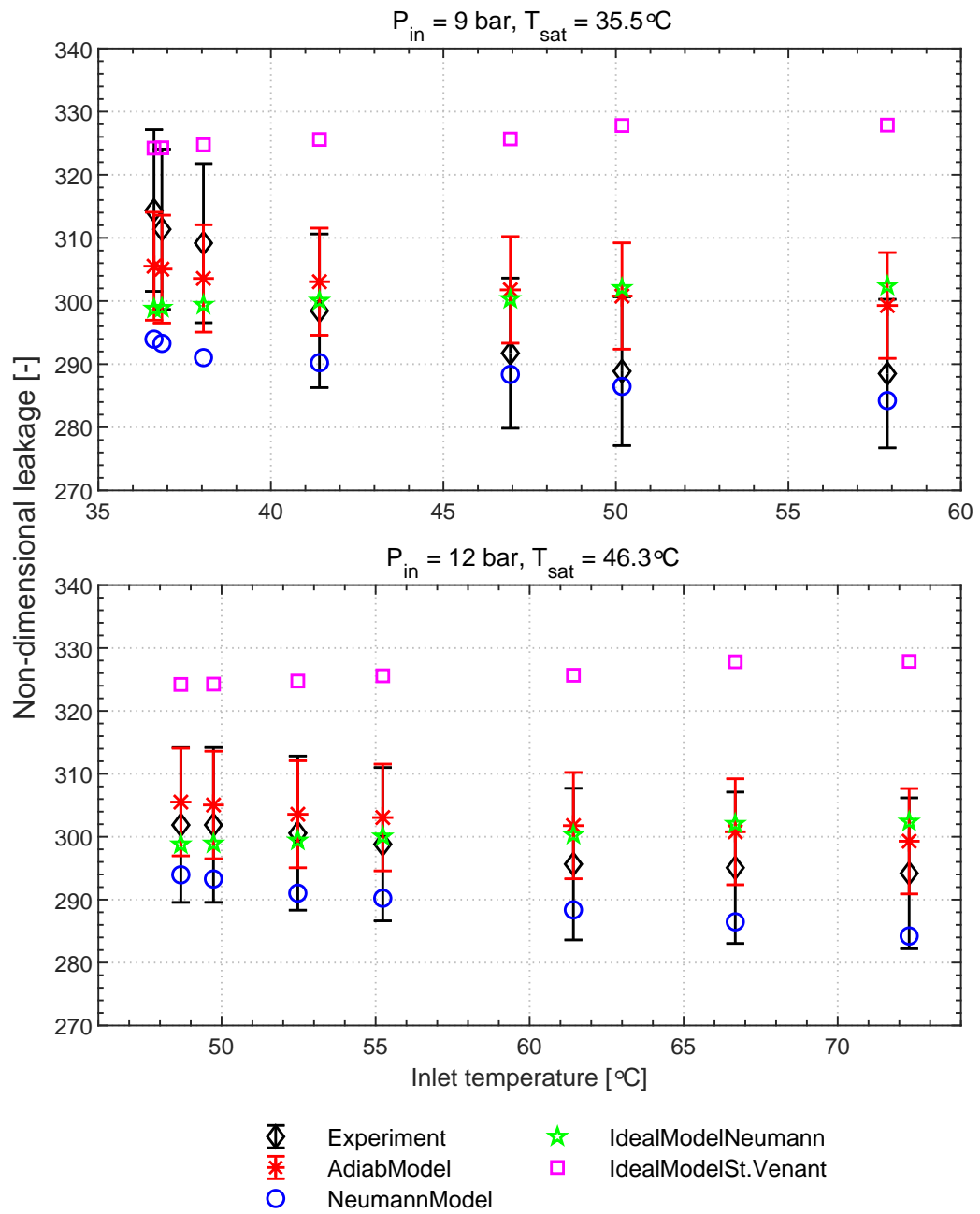
Figure 4.27 – Comparison of different model performance on seal leakage with varying degree of superheat on Labyrinth seal (LSCP5T) at 9 and 12 bar inlet pressure, PR of 2 and R134a as working fluid

Hole pattern seal (HPS)

The experimental investigation on the effect of the varying inlet temperature on leakage has been performed on the Hole pattern seal (HPS) at two different inlet pressures. Figure 4.28 represents the experimental results obtained at 9 and 12 bar inlet pressure against the degree of superheat. At 9 bar inlet pressure, the experimental data shows a higher leakage near the saturation line compared to the high degree of superheat. At a low degree of superheat of 2.4 K, the measurement indicates a 8.2% higher leakage compared to 26 K superheat.
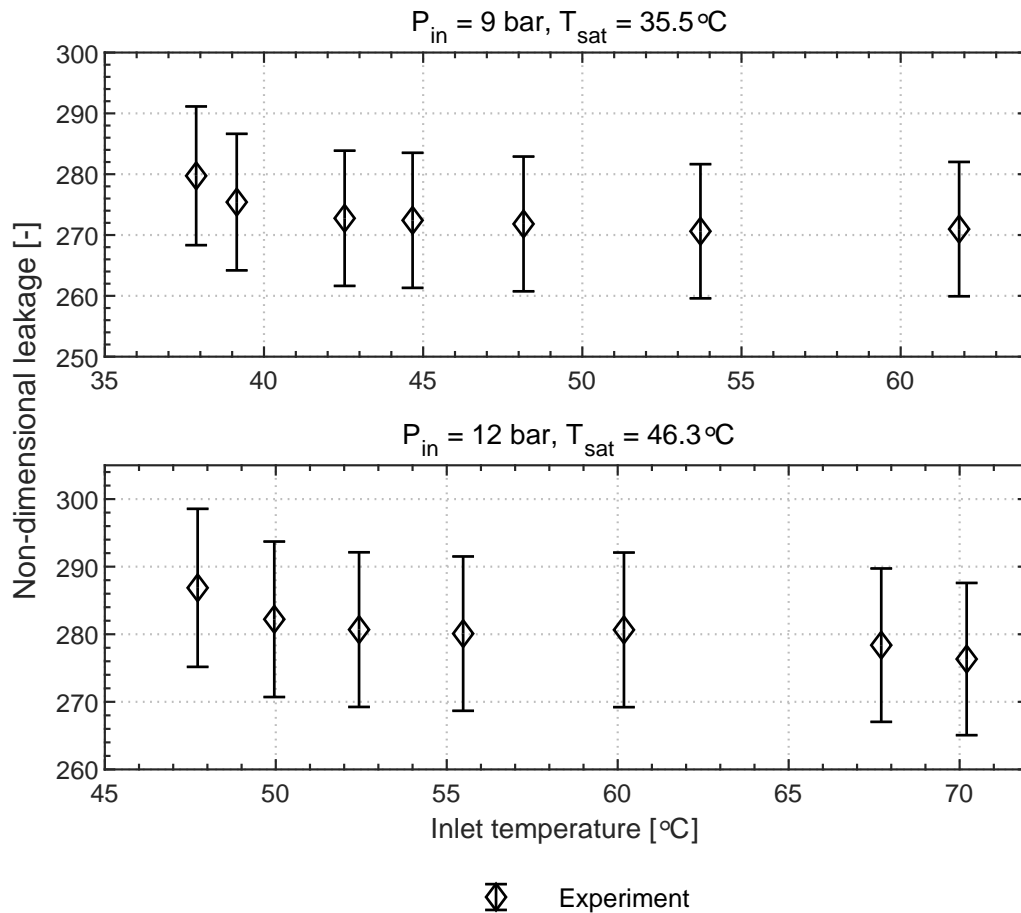
Figure 4.28 – Experimental investigation of leakage with varying degree of superheat on Hole pattern seal (HPS) at 9 and 12 bar inlet pressure, PR of 2 and R134a as working fluid

Similarly, at 12 bar inlet pressure, a leakage increase of 8.8% can be observed with 1.5 K of superheat compared to 24 K superheat. In general, the experimental data clearly highlights the effect of superheat and thus the real gas effect on seal leakage performance.

Smooth seal (SS)

To analyze the effect of superheat on Smooth seal (SS) leakage performance, the experimental investigation has been conducted at 9 and 12 bar inlet pressure. The outcome of the test is shown in figure 4.29. The test results highlight a similar effect of leakage with the degree of superheat resembling the findings on other test seals. For both inlet pressures, the result suggest up to 10% more leakage in the vicinity of the saturation line compared to the higher level of superheat.
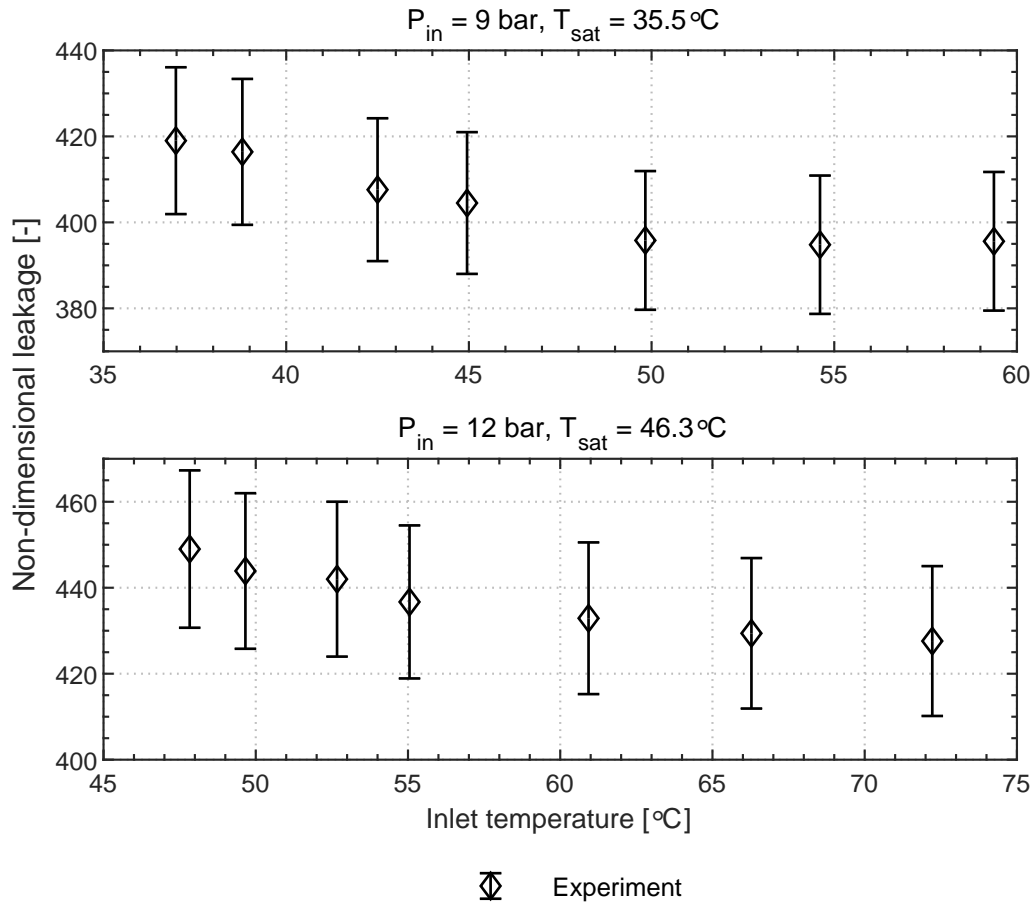
Figure 4.29 – Experimental investigation of leakage with varying degree of superheat on Smooth seal (SS) at 9 and 12 bar inlet pressure, PR of 2 and R134a as working fluid

4.6 Summary and conclusion

In this chapter, a brief summary of the different test seals geometry along with their dimensions is provided for both constant and varying clearance geometries. Initially, the prediction quality of leakage by the different models is assessed for large-scale seals using the experimental data from literature. To evaluate the performance of

the different models at reduced-scale seals, the experimental results obtained within this work are compared with the predicted numerical data from the seal models with R134a and air at different inlet boundary conditions. The effect of the kinetic energy carry-over in seal leakage is investigated within the different seal model using the correlations by Vermes [82] and Neumann [51]. The comparison of cavity pressure and temperature distribution has been carried out between the experiments and the different models. The author model demonstrated better quality compared to the-state-of-the-art models in terms of leakage, pressure, and temperature prediction at reduced-scale cylindrical seals. Furthermore, to examine the robustness of the author model, the conical seals with non-identical clearance have been experimentally tested and compared with the predicted results of the author model. Finally, the non-ideal behavior of the fluid operating in the vicinity of the saturation line and its effect on the seal leakage performance has been experimentally demonstrated. The ability of the author model to capture this non-ideal behavior of the fluid in the proximity of the saturation line has been illustrated. The limitations of the commonly used seal models to predict the non-ideal behavior of the fluid has been identified.

The following conclusions have been drawn from the results acquired in this chapter:

Cylindrical seals

- At large-scale seals ($D_r > 0.1\ m$), different seal models show a good agreement with the experimental data and the reference model of the available literature [35] with nitrogen as a working fluid. The author's model prediction lies within the measurement uncertainty range, hence suggesting the validity of the author's model.

- To evaluate prediction quality of the-state-of-the-art and the author model at reduced-scale, numerical results using empirical kinetic carry-over coefficients by Vermes [82] and Neumann [51], are compared with the experimental measurements.

  With R134a, the author's model with the Vermes kinetic energy carry-over coefficient demonstrated a better quality in terms of leakage prediction with the maximum average deviation of $< 2\%$, whereas, the author model with the Neumann carry-over coefficient reported up to 5% deviation. However, in the case of the 5 teeth Labyrinth seal with constant cavity pitch (LSCP5T), the author's model with the Neumann carry-over coefficient indicates a maximum deviation of 1.2% in leakage compared to 6.8% with the Vermes carry-over coefficient. This suggests an existence of a tradeoff between both carry-over coefficient to the number of teeth in a seal, hence, the need for further investigation in this topic is highlighted. The-state-of-the-art-models yield poor performance compared to the experimental data, with the St. Venant model reaching the highest discrep-

ancy.

With air, the author's model with the Vermes carry-over coefficient suggests good agreement with the experimental data of different seal over the range of pressure ratios showing an overall maximum deviation of 4%. The St. Venant model indicated the highest deviation and followed by the ideal Neumann model whereas the Neumann model with the Neumann carry-over coefficient reported moderate prediction accuracy with an overall maximum deviation of 6%.

- Besides the leakage prediction, the author's model predicts choked flow conditions with a very good agreements to the experimental data, whereas the-state-of-the-art model indicate choked flow at higher pressure ratio compared to the experiments.

- In general, numerical results of all test seals at different operating conditions suggest a $\pm 2.8\%$ deviation in prediction accuracy with the geometrical tolerance of ± 1 μm between seal and rotor, thus highlighting the high sensitivity of the models to the clearance in reduced-scale seals.

- The experimental results reveal the Hole pattern seal (HPS) as the most effective seal with the lowest leakage characteristics indicating up to 20% and 10% reduction in leakage compared to the Smooth seal (SS) and other test seals (PDS, LSVP4T, and LSCP5T) respectively, and therefore recommended for reduced-scale turbomachinery applications. Furthermore, improvement in leakage reduction has been experimentally evidenced with 4 teeth Labyrinth seal with varying cavity pitch (LSVP4T) compared to 5 teeth Labyrinth seal with constant cavity pitch (LSCP5T) for the identical clearance and identical seal axial length. Hence, suggesting the existence of optimum seal geometrical features on the given overall seal length leading not only to the optimum leakage performance but also to a reduction of manufacturing cost and time.

- The cavity pressure distribution predicted by the author model matches the experimental data very well irrespective of the seal types, test fluid, and inlet conditions. The maximum deviation of 5% has been recorded in some specific case, whereas for most of the test cases an average deviation of <3% has been observed. At the outlet of the seal, the highest deviation extending up to 20% has been reported at the high pressure-ratio with a choked flow. The occurrence this high deviation at the exit of the seal can be attributed to the expansion effects which have been neglected in the models due to its complexity in nature to implement in the two-dimensional model.

- The cavity temperature distribution predicted by the author model demonstrates good agreement with the experiments for all test seals and test conditions. In the worst-case scenario, a maximum deviation of about 2.8 K has been monitored. However, on average, this discrepancy has been found out to be <1.2 K.

Conical seals

- The author's model reports a relatively high deviation in leakage ranging up to 5% for the conical seals compared to <2% on the cylindrical seals. The indication of the higher deviation compared to the cylindrical seal can be attributed to the assumptions of linear interpolation in the teeth clearances, which may not corresponds to the reality.

- The comparison of the seal cavity pressure distribution between the numerical and the experimental data suggests a reasonable prediction accuracy of the author's model on irregular conical seals. The existence of increased deviation (up to 10% in worst-case scenario) in cavity pressure compared to the cylindrical seals could be justified due to linear interpolation of the clearance. The author's model yields the highest deviation at the seal outlet when operated under choked flow. The same reason like in the cylindrical seals applies here.

- The comparison of the cavity temperature distribution between the author's model and the measured data shows matching results for all test seals and test conditions. In the worst-case scenario, a maximum deviation of 2.3 K has been monitored. However, on average, this discrepancy has been found out to be <1 K%.

Degree of superheat

- Experimental data suggest an increase in non-dimensional leakage for a decreasing degree of superheat of the inlet state. The comparison between the highest and the lowest degree of superheat suggests a 10% difference, which implies a non-negligible real gas effect, i.e. a significant deviation from the perfect gas assumption. The author's model reveals its better performance quality at different levels of superheat and showed its ability to capture the experimental trend, i.e. the real gas effect. The Neumann model shows a similar trend of leakage with the varying inlet temperature. However, the ideal Neumann and the St. Venant model illustrated their inability to capture the trend compared to the measurements due to the assumption of an ideal gas in their equations.

The good agreement between the experimental results on large-scale and reduced-scale cylindrical and conical seals with nitrogen, R134a, and air at different boundary conditions (inlet pressures and temperatures) highlights the robustness of the author's model. The good agreement on leakage, cavity pressure, and temperature distribution in all test cases experimentally validates the author model.

5 Conclusion and future work

5.1 Summary and conclusion

To achieve reasonable efficiency and lifetime, gas-lubricated bearings are employed in reduced-scale high-speed turbomachinery applications. Dynamic non-contacting seals have been identified as the most appropriate sealing technology for such high-speed rotor-bearing systems since they prevents surface contact during operation. However, any clearance between rotor and seal permits the passage of fluid across regions of unequal pressure as a leakage, which penalizes the system efficiency. The primary function of the non-contacting seal is to reduce leakage and hence increase the system efficiency. Despite the aforementioned advantage, field experiences have revealed significant effects of the seals on the rotor eigenvalues (eigenfrequencies and rotordynamic stability.

In this PhD-thesis, the gap in the literature at reduced-scale seals has been highlighted. One of the objectives of the thesis is to identify the most promising seal technology for reduced-scale applications. Since no work has been reported in sealing technologies for reduced-scale applications, a qualitative approach has been used for the selection procedure of seals, which suggests the pocket damper and the hole pattern seals to be the most promising geometries.

An overview of the different approaches used in seal analysis has been presented and the commonly used bulk-flow modeling techniques to predict the seal performance has been discussed. Based on the bulk-flow theory, the development of an own 2D model with the governing equations, assumptions, and the solving scheme considering the real gas properties is presented. As a benchmarking process, the comparison between developed models and the results from the well-established literature [35, 59, 87] on large-scale seals have been conducted.

The detailed description of the design and development process of the test-rig dedicated to perform the experimental investigations on reduced-scale seals has been

provided. Furthermore, the design and manufacturing of the seals, modular test section, instrumentation, measurement capabilities, and operating procedure has been discussed.

The experimental investigation of different types of reduced-scale seals operated with air and R134a at different boundary conditions have been conducted. The measured leakage, cavity pressure, and temperature distributions have been compared with the results of different seal models to characterize the prediction quality of the individual model. The investigation of the effect of the kinetic energy carry-over in seal leakage has been performed within the different models using the correlations suggested by Vermes [82] and Neumann [51]. A non-dimensional leakage comparison has been performed between different seals, for both on R134a and air. Furthermore, different seals have been experimentally tested and compared with different models at different degrees of superheat on R134a to highlight the real gas effect on seal performance.

The research presented in this thesis allows to draw the following conclusions:

- The scaling analysis highlights leakage as a significant source of losses in reduced-scale turbomachinery systems. For shaft diameters less than 20 mm, the relative leakage mass flow $> 10\%$.

- Using the Qualitative Research Method combined with the Sensitivity Analysis, the Hole Pattern Seal and the Pocket Damper Seals have been identified as the most promising seals for reduced-scale and high-speed turbomachinery application.

- The existence of an optimum number of seal teeth/constrictions has been highlighted experimentally and numerically on labyrinth seals beyond which the effectiveness of the seal drops.

- On large-scale seals, different models yield good agreement with the experimental leakage data published in the literature [35, 59, 87]. Furthermore, the numerical results of cavity pressure and circumferential velocity distribution obtained from the author model suggests a good match with the reference literature [35].

- The comparison between the measured data and the different models has been conducted on cylindrical reduced-scale seals to assess the prediction accuracy using two different empirical kinetic carry-over coefficients of Vermes [82] and Neumann [51].

  With R134a, the author model with the Vermes kinetic energy carry-over coefficient demonstrated the better quality in terms of leakage prediction with the maximum average deviation of $< 2\%$, whereas, the author's model with the Neumann carry-over coefficient yields up to 5% deviation. However, in the case of 5

teeth Labyrinth seal with constant cavity pitch (LSCP5T), the author's model with the Neumann carry-over coefficient indicated a maximum deviation of 1.2% in leakage compared to 6.8% with the Vermes carry-over coefficient. Thus indicated the existence of a tradeoff between both carry-over coefficient to the number of teeth in a seal, hence, the need for further investigation in this topic has been highlighted. The-state-of-the-art-models showed poor performance for the leakage prediction over the range of investigated pressure ratios, with the St. Venant model yielding the highest deviation.

With air, the author model with the Vermes carry-over coefficient demonstrated good agreement with the experimental data of different seal over the range of pressure ratios showing an overall maximum deviation of 4%. The St. Venant model indicated the highest deviation and followed by the ideal Neumann model whereas the Neumann model with the Neumann carry-over coefficient reported moderate prediction accuracy with an overall maximum deviation of 6%.

- The experimental investigations of different seals with air and R134a suggests the Hole pattern seal (HPS) to be the most effective seal in terms of leakage characteristics indicating up to 20% and 10% reduction in leakage compared to the Smooth seal (SS) and other test seals (PDS, LSVP4T, and LSCP5T) respectively. Furthermore, improvement in leakage reduction has been experimentally evidenced with 4 teeth Labyrinth seal with varying cavity pitch (LSVP4T) compared to 5 teeth Labyrinth seal with constant cavity pitch (LSCP5T) for the identical clearance and identical axial length. Thus the existence of optimum seal geometrical features on the given overall length has been highlighted leading not only to the improved leakage performance but also reduction of manufacturing cost and time.

- On the seals with a conical clearance evolution, the author's model demonstrated good agreement with the experimental results in the prediction of leakage at different inlet boundary conditions over the range of pressure ratios irrespective of the seal clearances and seal types. The author's model with the Vermes carry-over correlation reported relatively high deviation in leakage ranging up to 5% in conical seals compared to <2% on the cylindrical seals. The indication of the higher deviation compared to the cylindrical seal can be attributed to the assumptions of linear interpolation in clearances which may not corresponds to the reality.

- The cavity pressure distribution predicted by the author's model on the cylindrical seals suggests matching results to the measurement data irrespective of the seal types, test fluid, and inlet conditions. A maximum deviation of 5% has been recorded in some specific cases, whereas for most of the test cases an average deviation of <3% has been observed.

In the case of conical seals, the comparison of the cavity pressure distribution

on test seals demonstrated a reasonable prediction accuracy by the author's model. The existence of increased deviation (up to 10% in worst case scenario) in cavity pressure compared to the cylindrical seals could be justified due to linear interpolation of the clearance.

At the outlet of the seals, a deviation extending up to 20% has been observed at a pressure ratios with a choked flow. The occurrence of such high deviation at the exit of the seal can be attributed to the expansion effects which have been neglected in the models.

- The cavity temperature distribution predicted by the author's model demonstrated good agreement with the experiments for all test seals and test conditions. The results on the cylindrical seals highlighted up to 2.8 K deviation (worst-case scenario. However, on average, this discrepancy has been found out to be < 1.2 K. On the other hand, the test results of conical seals indicated up to 2.3 K as a maximum deviation, whereas, on average < 1 K has been stated.

- A leakage increase reaching up to 10% for fluid operated in the vicinity of the saturation line compared to an increased level of superheat (distance to the saturation line) has been experimentally demonstrated on different seals. The author's model illustrated its better performance quality at different levels of superheat and demonstrated its ability to capture the experimental trend. The Neumann model indicated a similar trend of leakage with the varying inlet temperature. However, the ideal Neumann and the St. Venant model failed to capture the measurement pattern due to the assumption of an ideal gas in their equations.

5.2   Implications and recommendations

An overview of the suggestions, within the context of this thesis, to the seal practitioners in the field of turbomachinery applications are as follows.

- Commonly used seal models are valid at large-scale seals on fluids with compressibility factor ($Z = PV/RT$) near to unity.

- For the numerical modeling, the approach followed by the author (i.e. adiabatic flow assumption with continuity equation to calculate leakage instead of using the empirical leakage equations, which are validated for large-scale seals with ideal gases) is recommended due to its better prediction quality of seal performance irrespective of fluid, operating boundary conditions, and size.

- At reduced-scale, the-state-of-the-art models show poor performance and are therefore not recommended.

- The accurate measurement of the clearance between the rotor and the seal is pivotal. The prediction accuracy of the seal models are more sensitive for reduced-sized seals due to the higher relative geometrical deviation due to manufacturing errors.

- For the robustness of the experimental data, centering of the shaft and seal, proper insulation, and stable operating conditions with the thermal equilibrium in the test section is recommended.

- For reduced-scale turbomachinery, the Hole Pattern Seal is suggested following the evidence gathered from the experimental campaign.

- For the seals operating within the proximity of the fluid saturation line, the commonly used ideal Neumann and St. Venant modeling approach is not recommended, instead, the author's modeling approach is recommended.

5.3 Further research prospects

The presented research highlights several avenues for the further explorations on the experimental and numerical aspects of turbomachinery seals:

- Due to the condensation effect (as a result of sudden expansion) happening in the seal test section, the present experimental work on test seals was limited to 12 bar inlet pressure for R134a. This limitation can be overcome by placing a heat exchanger coupled with the thermostat near the seal inlet section. By so doing, tests can be conducted at elevated pressure and temperature which serves as a validation tool of the numerical model at a wide spectrum.

- To check the prediction quality of models at large-scale seals with R134a, the manufacturing and the testing of the different sized seals are encouraged.

- To support the experimental findings of the optimum number of teeth and cavity pitch distribution, further tests need to be conducted with varying numbers of teeth and cavity pitch distribution seals while keeping the clearance and the overall axial length constant.

- The experimental investigation of the Hole pattern seal (HPS) and the Pocket damper seal (PDS) in a dynamic test-rig supported on gas lubricated bearings should be performed to examine the influence of these seals on rotor-bearing stability. The findings can be used to assess the reliability of the qualitative selection process of reduced-scale seals.

A Appendix: Selection of seals

A.1 Background

One of the objectives was to select the most promising seal technology for reduced-scale applications. Since no work has been reported in sealing technologies for reduced-scale applications, the selection procedure has been carried out with the help of *Decision-Matrix Method* using qualitative data of different non-contacting gas seals. For this purpose, a Focus Group methodology, a qualitative research tool, was selected as an ideal survey tool for the selection of the non-contacting gas seals.

A.2 Focus group

A Focus Group is a group interaction of approximately six to ten people who share similar characteristics or common interests to collect data on topics of interest to the researcher [102]. It is suitable for exploratory, descriptive and explanatory research with a goal to gain insights from a target group, who has knowledge about the topic of issue, at low cost and with the minimal amount of time [103], [104]. The main objectives of the Focus Group are listed below:

- Identify the characteristics features of non-contacting gas seals
- Define ranking of the characteristics features and weightage points for each feature
- Select promising seal topology based on the above points

A.2.1 Instrument development for Focus Group

Prior to performing the Focus Group, the relevant literature review in non-contacting gas seals has been carried out by the author in order to have the better understanding

of the subject of interest. Further, a short summary of the different types of state-of-the-art non-contacting gas seals was prepared for handing to the participants so as to familiarize them the topic of discussion. This was carried out to provide a framework and a structure for the Focus Group meeting.

A.2.2 Site selection

The Laboratory of Applied Mechanical Design (LAMD), Neuchâtel, focuses on the design and experimental investigation of reduced-scale turbomachinery. The field of expertise of LAMD has the similar body of knowledge and most of the on-going research is inter-related with each other. For this reason, LAMD has been selected as a site for the Focus Group discussion.

A.2.3 Participants selection

The participants for this Focus Group were selected from the working team of LAMD. The selection was based upon the knowledge and experience gained in the field of turbomachinery. For this work, six individuals were selected from the team so as to form a Focus Group.

A.2.4 Focus Group: Outcome

Each participant were handed a material containing a brief summary of different types of non-contacting gas seals. The qualitative parameters of seals were identified which includes leakage resistance, rotordynamic performance (stiffness and damping), overall size, manufacturability, adaptability with the system, design simplicity, cost effective, durability and maneuver simplicity. For the sake of simplicity, these parameters were reduced to the four core characteristics features: leakage resistance, rotordynamics, overall size and other factors (this factor includes all the rest parameters). Finally, participants were asked to provide their own weightage value for each of these core features.

A.3 Results and discussion

This section contains the results from the performed focus group discussion. The topics of discussion and the outcomes of the focus group have been illustrated. Further, core features of non-contacting gas seals identified from the discussion concerned with the reduced-scale machines has been presented. The detailed analysis of the topics discussed, responses received from the participants and overall attitudes of the non-contacting seals gas for reduced-scale turbomachinery are highlighted in

following sections.

A.3.1   Preliminiary results

The participants were allowed to put their individual views and the characteristics features which they think is necessary on reduced-scale non-contacting gas seals. This session of discussion was broad in nature. The collective features which participants highlighted are as follows: Leakage resistance, damping & stiffness (rotordynamics behaviour), manufacturability, overall size, adaptability with the system, design simplicity, cost effective, lifetime (durability) and maneuver simplicity. Further, the discussion was focused on the preliminary features of seals with an aim to select the core features. The identified core features are: Leakage resistance, rotordynamics performance, overall size and other factors (this includes manufacturability, lifetime, cost, adaptability etc.). Taking these four features in considerations, each participant was asked to provide their own weightage value on each feature based upon their priority level. The outcomes of the weightage value for each core feature are discussed below.

Leakage resistance

Leakage was ranked first on the priority feature of the seals and every participant has allocated more weightage value for leakage. The minimum and maximum value from the Focus Group was 30% and 45% respectively.

Rotordynamic performance

This feature was identified as the second most priority feature of seals from the group discussion for the selection process of non-contacting gas seal. The minimum and maximum weightage value for this feature from the Focus Group was 30% and 40% respectively.

Overall size

This feature includes the axial length and outer diameter of the seal. For reduced-scale application, this feature is also a crucial factor as long axial length of seal leads to longer shaft length, hence making shaft heavy which may influence to system stability. This feature was ranked third in priority level. The minimum and maximum weightage value for this feature was 10% and 20% respectively.

Others

This feature comprises all the other remaining features of seals (i.e. manufacturability, lifetime, cost, system adaptability and design simplicity) which were highlighted during group discussion. Though, these features cannot be neglected but in comparison to previous features they plays less effective role in seals selection process. So they were set to lower priority and were assigned less weightage. Collectively, 5% of weightage was allocated for this feature.

A.3.2 Selection of non-contacting gas seals

Referring to the range of weightage value obtained from Focus Group for four core features of non-contacting gas seals, weightage decision matrix was performed. Each of these features were provided with their own range of weights based on the priority level. Different weight configurations have been analyzed in order to assess the robustness of the selection process. The feature *others* with lowest priority level was always kept constant with weightage of 5% during the selection process.

Table A.1 – *Weighted decision matrix of non-contacting gas seals: Leakage and Other variables as constant value with varying Rotordynamic and Axial length variables value*

Var	*W1*	ST	SP	SG	HC	HP	PD	FX	FL	HS	HD	CF	SB
Lke	0.45	1	2	3	3.7	4	3.3	3.6	4	4	3.8	4	3.5
Rdc	0.3	1	1	1	4	4.5	5	3	4	3.5	4	3	3
Alh	0.2	1	2	3	3	4.2	5	2	1	3.5	4	4	3
Ots	0.05	5	4	3	2	4.5	4	3	2	3	2	1	1
Tot	1	1.2	1.8	2.4	3.56	**4.21**	**4.19**	3.07	3.3	3.7	3.81	3.55	3.12

Var	*W2*	ST	SP	SG	HC	HP	PD	FX	FL	HS	HD	CF	SB
Lke	0.45	1	2	3	3.7	4	3.3	3.6	4	4	3.8	4	3.5
Rdc	0.35	1	1	1	4	4.5	5	3	4	3.5	4	3	3
Alh	0.15	1	2	3	3	4.2	5	2	1	3.5	4	4	3
Ots	0.05	5	4	3	2	4.5	4	3	2	3	2	1	1
Tot	1	1.2	1.75	2.3	3.61	**4.23**	**4.19**	3.12	3.45	3.7	3.81	3.5	3.13

Var	*W3*	ST	SP	SG	HC	HP	PD	FX	FL	HS	HD	CF	SB
Lke	0.45	1	2	3	3.7	4	3.3	3.6	4	4	3.8	4	3.5
Rdc	0.4	1	1	1	4	4.5	5	3	4	3.5	4	3	3
Alh	0.1	1	2	3	3	4.2	5	2	1	3.5	4	4	3
Ots	0.05	5	4	3	2	4.5	4	3	2	3	2	1	1
Tot	1	1.2	1.7	2.2	3.66	**4.24**	**4.19**	3.17	3.6	3.7	3.81	3.45	3.12

Table A.2 – *Weighted decision matrix of non-contacting gas seals: Rotordynamic and Other variables as constant value with varying Leakage and Axial length variables value*

Var	*W4*	ST	SP	SG	HC	HP	PD	FX	FL	HS	HD	CF	SB
Lke	0.4	1	2	3	3.7	4	3.3	3.6	4	4	3.8	4	3.5
Rdc	0.4	1	1	1	4	4.5	5	3	4	3.5	4	3	3
Alh	0.15	1	2	3	3	4.2	5	2	1	3.5	4	4	3
Ots	0.05	5	4	3	2	4.5	4	3	2	3	2	1	1
Tot	1	1.2	1.7	2.2	3.63	**4.26**	**4.27**	3.09	3.45	3.67	3.82	3.45	3.1

Var	*W5*	ST	SP	SG	HC	HP	PD	FX	FL	HS	HD	CF	SB
Lke	0.35	1	2	3	3.7	4	3.3	3.6	4	4	3.8	4	3.5
Rdc	0.4	1	1	1	4	4.5	5	3	4	3.5	4	3	3
Alh	0.2	1	2	3	3	4.2	5	2	1	3.5	4	4	3
Ots	0.05	5	4	3	2	4.5	4	3	2	3	2	1	1
Tot	1	1.2	1.7	2.2	3.6	**4.27**	**4.36**	3.01	3.3	3.65	3.83	3.45	3.08

Table A.3 – *Weighted decision matrix of non-contacting gas seals: Axial length and Other variables as constant value with varying Leakage and Rotordynamic variables value*

Var	*W6*	ST	SP	SG	HC	HP	PD	FX	FL	HS	HD	CF	SB
Lke	0.45	1	2	3	3.7	4	3.3	3.6	4	4	3.8	4	3.5
Rdc	0.3	1	1	1	4	4.5	5	3	4	3.5	4	3	3
Alh	0.2	1	2	3	3	4.2	5	2	1	3.5	4	4	3
Ots	0.05	5	4	3	2	4.5	4	3	2	3	2	1	1
Tot	1	1.2	1.8	2.4	3.6	**4.22**	**4.19**	3.07	3.3	3.7	3.81	3.55	3.12

Var	*W7*	ST	SP	SG	HC	HP	PD	FX	FL	HS	HD	CF	SB
Lke	0.4	1	2	3	3.7	4	3.3	3.6	4	4	3.8	4	3.5
Rdc	0.35	1	1	1	4	4.5	5	3	4	3.5	4	3	3
Alh	0.2	1	2	3	3	4.2	5	2	1	3.5	4	4	3
Ots	0.05	5	4	3	2	4.5	4	3	2	3	2	1	1
Tot	1	1.2	1.75	2.3	3.58	**4.24**	**4.27**	3.04	3.3	3.68	3.82	3.5	3.1

A.4   Concluding remark

Focus Group methodology as a qualitative data collection tool was used to select the most promising non-contacting seals for reduced-scale application. For this purpose six participants from the LAMD team were selected. A short summary of the different types of state-of-the-art non-contacting seals was handed to the participants during the discussion session. During the discussion, participants emphasized their individ-

ual features on non-contacting gas seals. The features of non-contacting gas seals which they highlighted are: *leakage resistance, rotordynamics performance (damping & stiffness), manufacturability, overall size, adaptability with the system, design simplicity, cost and lifetime (durability)*. These features were merged into four major features i.e. *leakage, rotordynamics performance, overall size and other factors*. For each feature, range of weightage value was given by each participant. These ranges of value were used for decision matrix and sensitivity analysis for the selection of seals. Finally, the most promising seals, namely, Hole Pattern Seal and Pocket Damper Seal have been selected as an outcome of the Focus Group.

B Appendix: Seal theory and modeling

B.1 Development of mathematical seal model
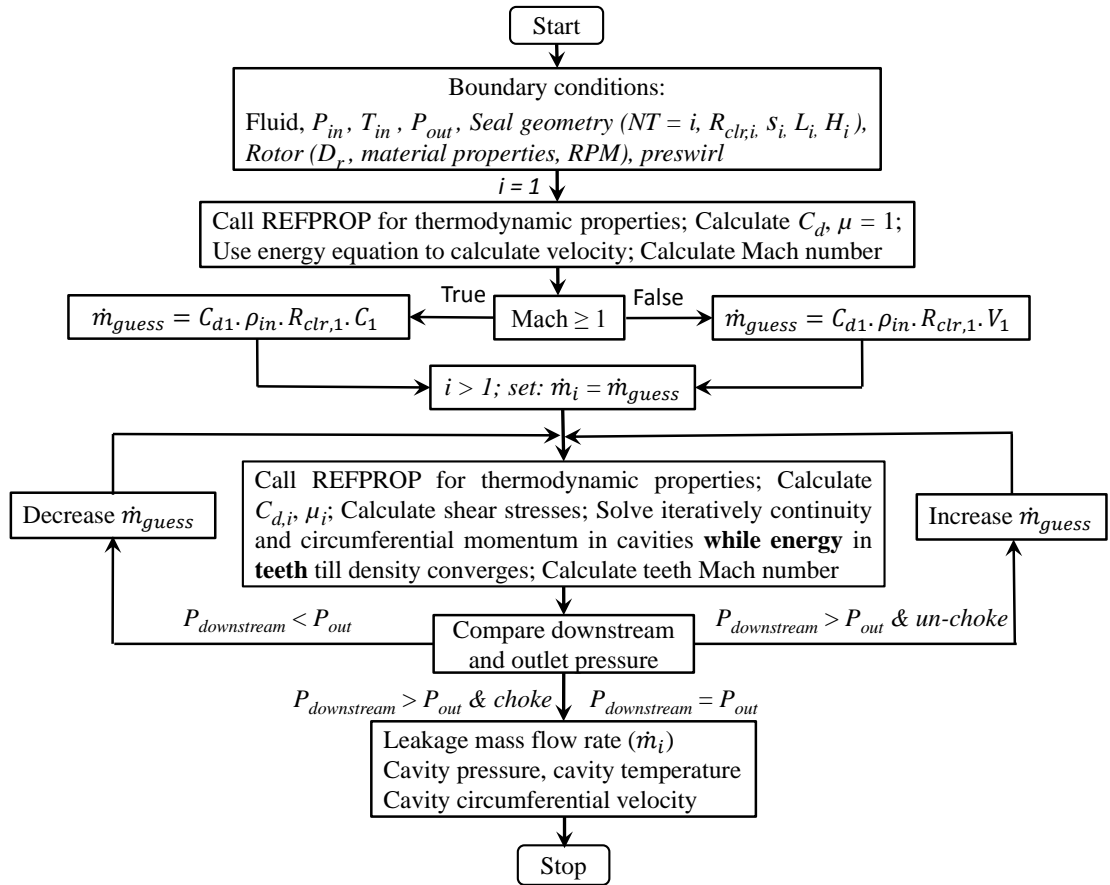
Figure B.1 – Iterative solution scheme of author two control volume bulk-flow model based on isenthalpic flow assumptions

C Appendix: Seal test-rig

C.1 Calibration of probes
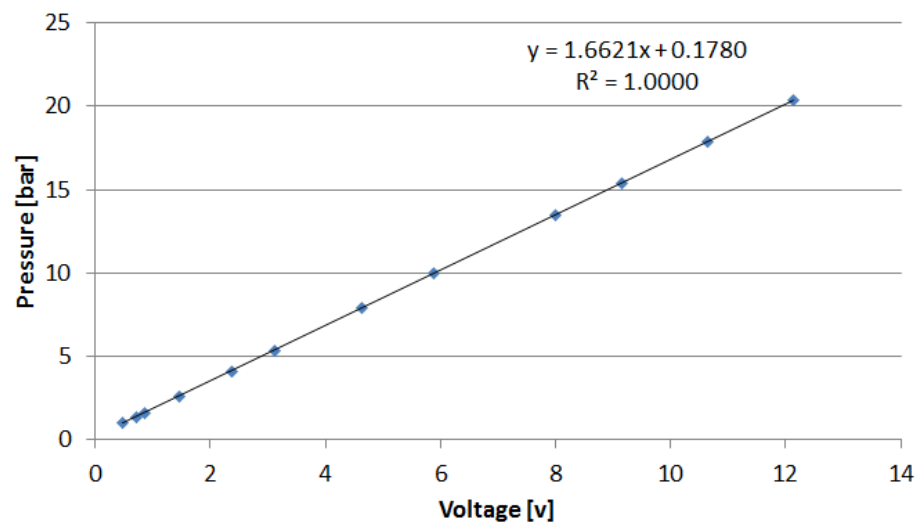
Figure C.1 – Calibration data of Kistler pressure transducer
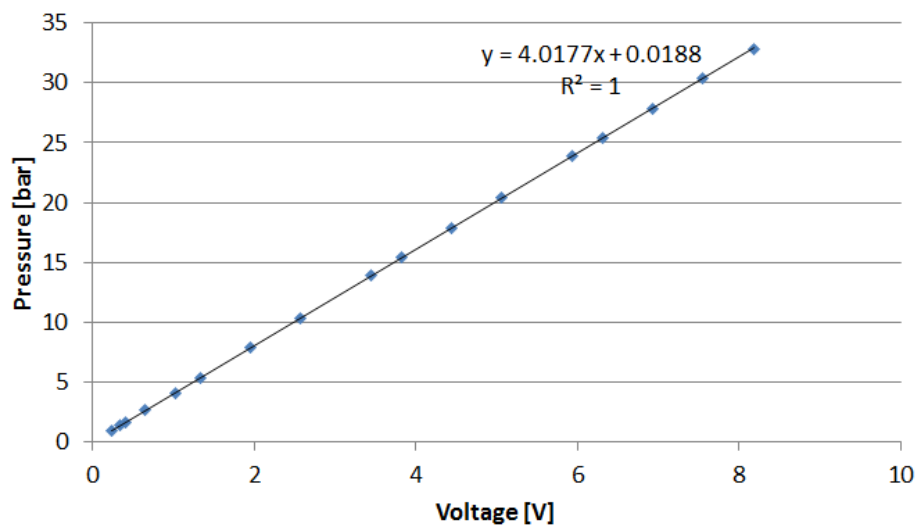
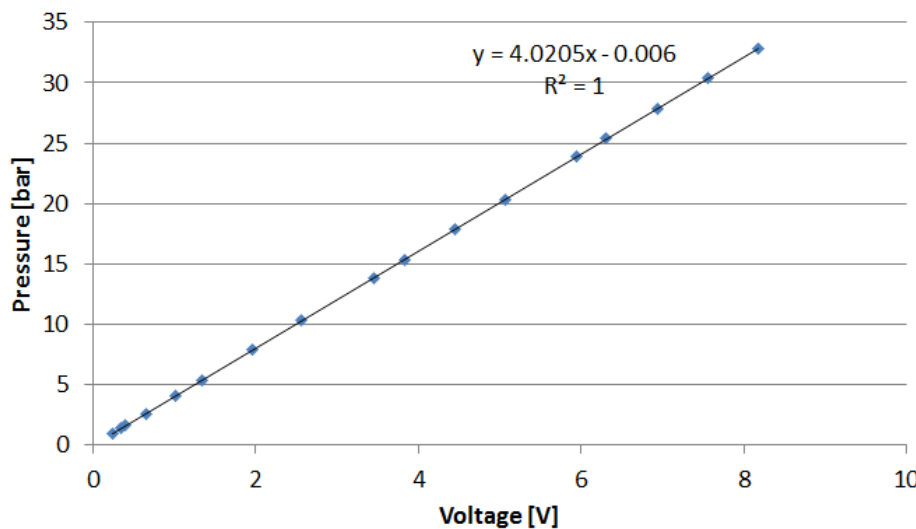Figure C.2 – Calibration data of WIKA pressure transducer: High pressure side

Figure C.3 – Calibration data of WIKA pressure transducer: Low pressure side
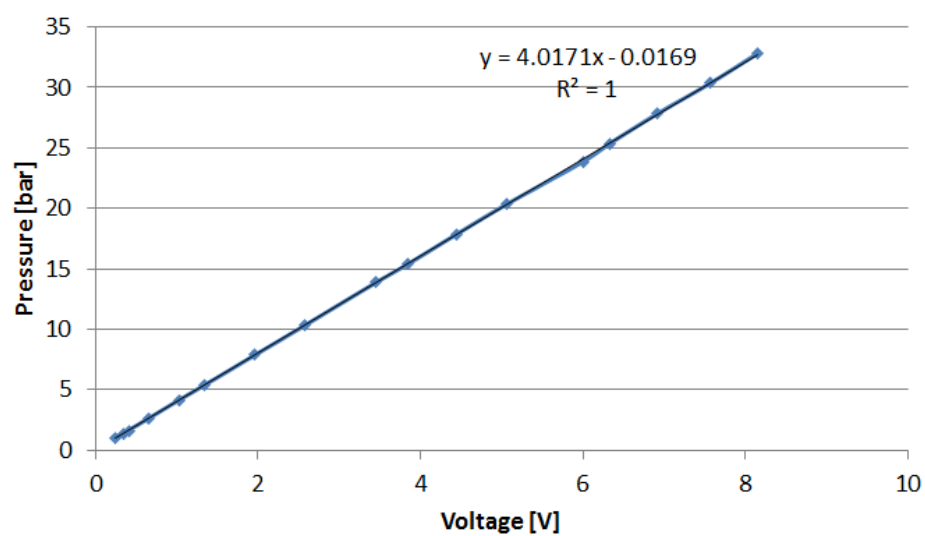
Figure C.4 – Calibration data of WIKA pressure transducer: Bypass side
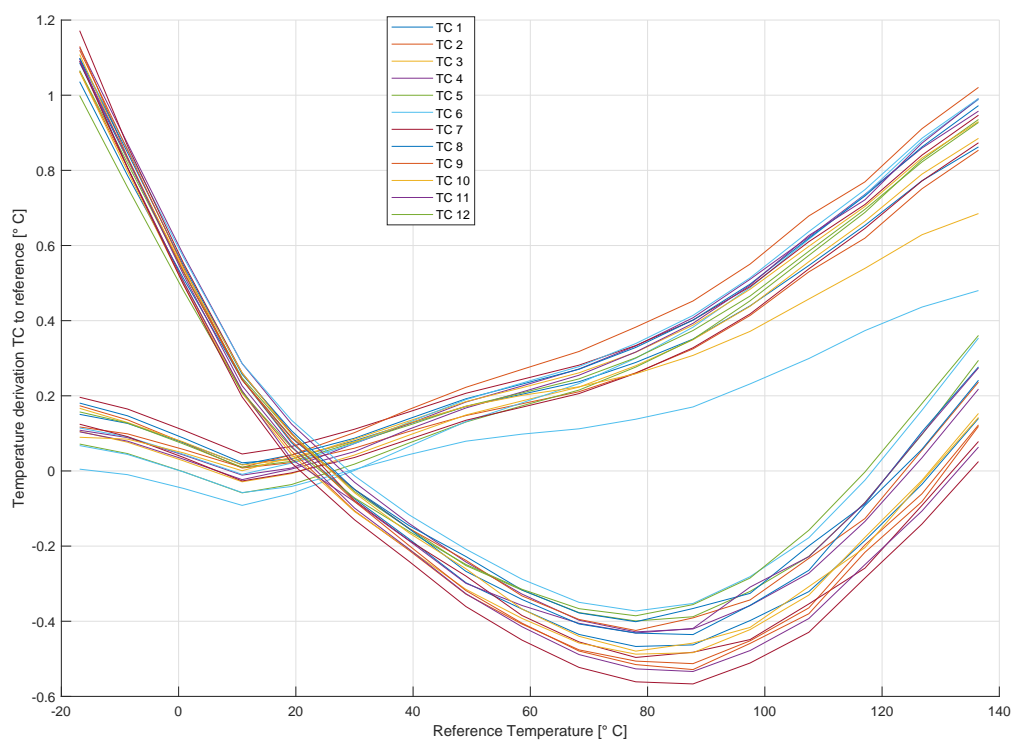
Figure C.5 – Calibration data of thermocouples

C.2 Seal test section
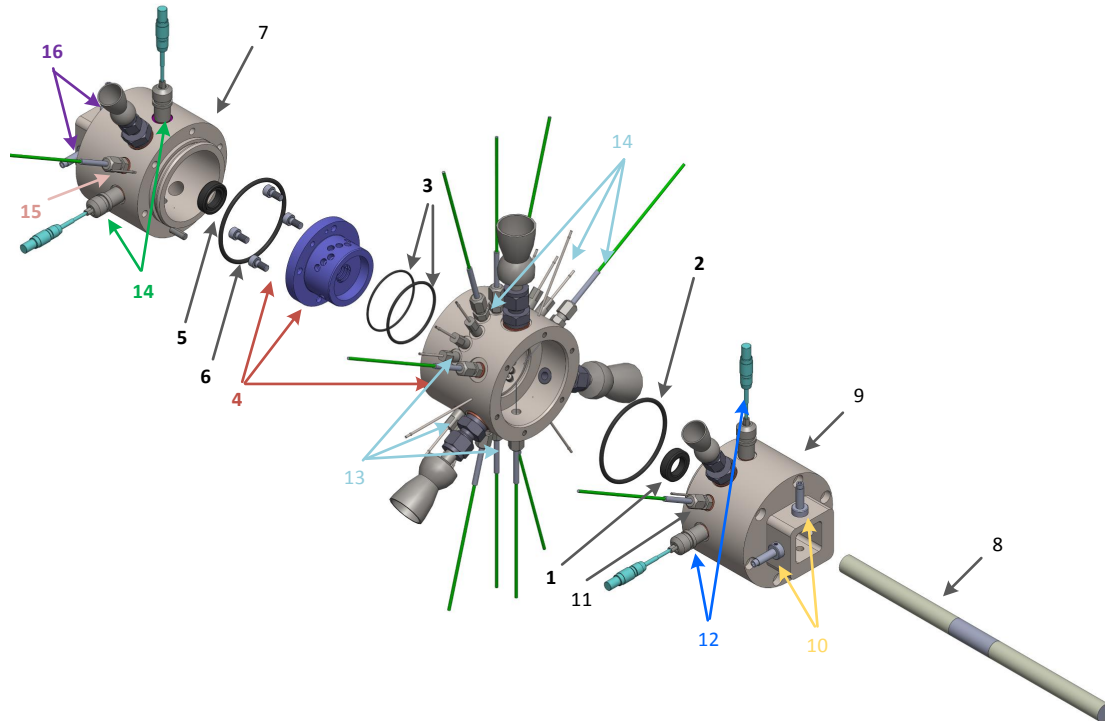
Figure C.6 – Exploded view of the seal test section: assembly steps in a chronological order
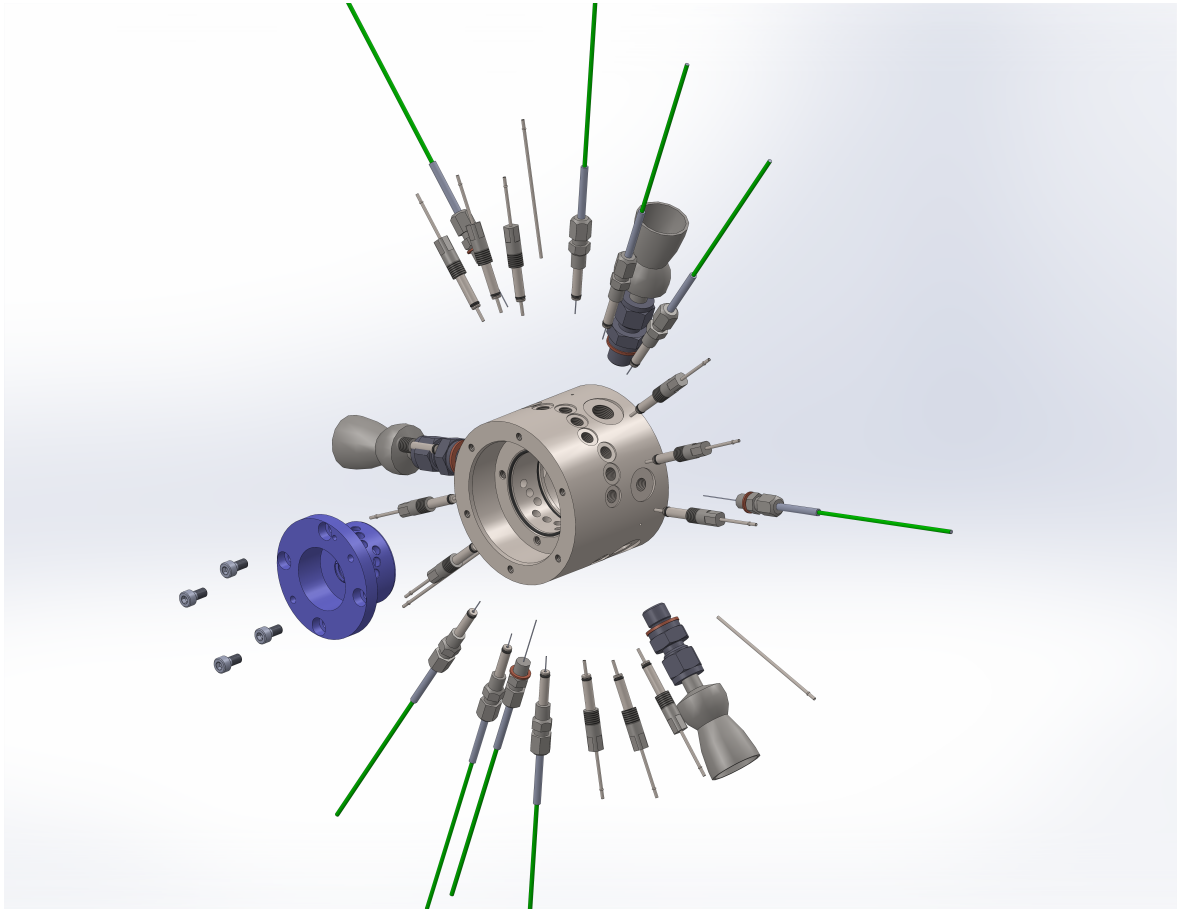
Figure C.7 – Exploded view of the seal housing showing thermocouples, custom made fittings for pressure taps and thermocouples, test seals, O-rings, and scanivalve tubings

D Appendix: Detailed results

D.1 Cylindrical seals

Comparison of leakage
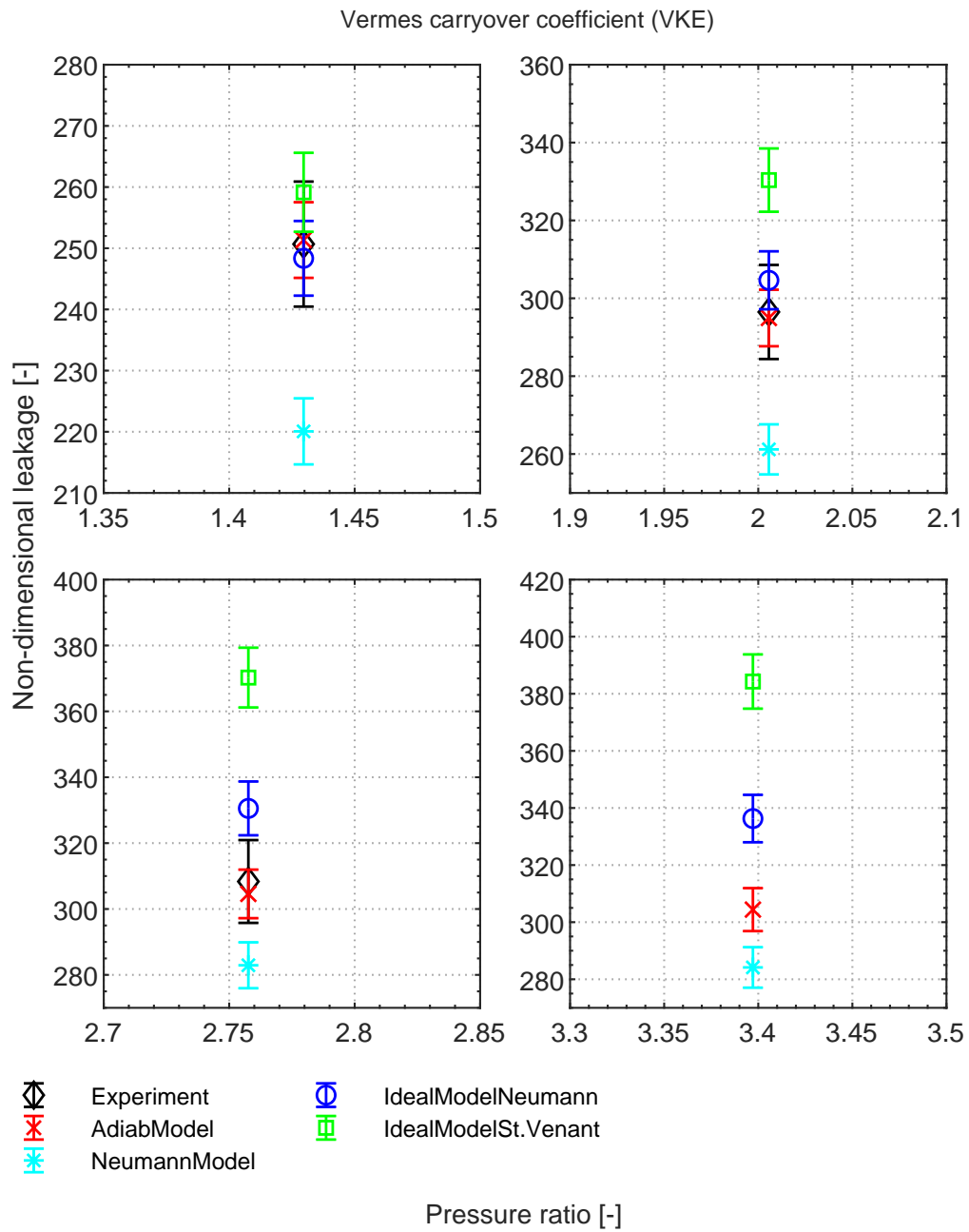
Figure D.1 – Comparison of leakage between the experimental measurements, the author model and state-of-the-art models using Vermes carry-over coefficient on Pocket damper seal (PDS) at 5 bar inlet pressure, 25°C inlet temperature, varying PR and R134a as a working fluid
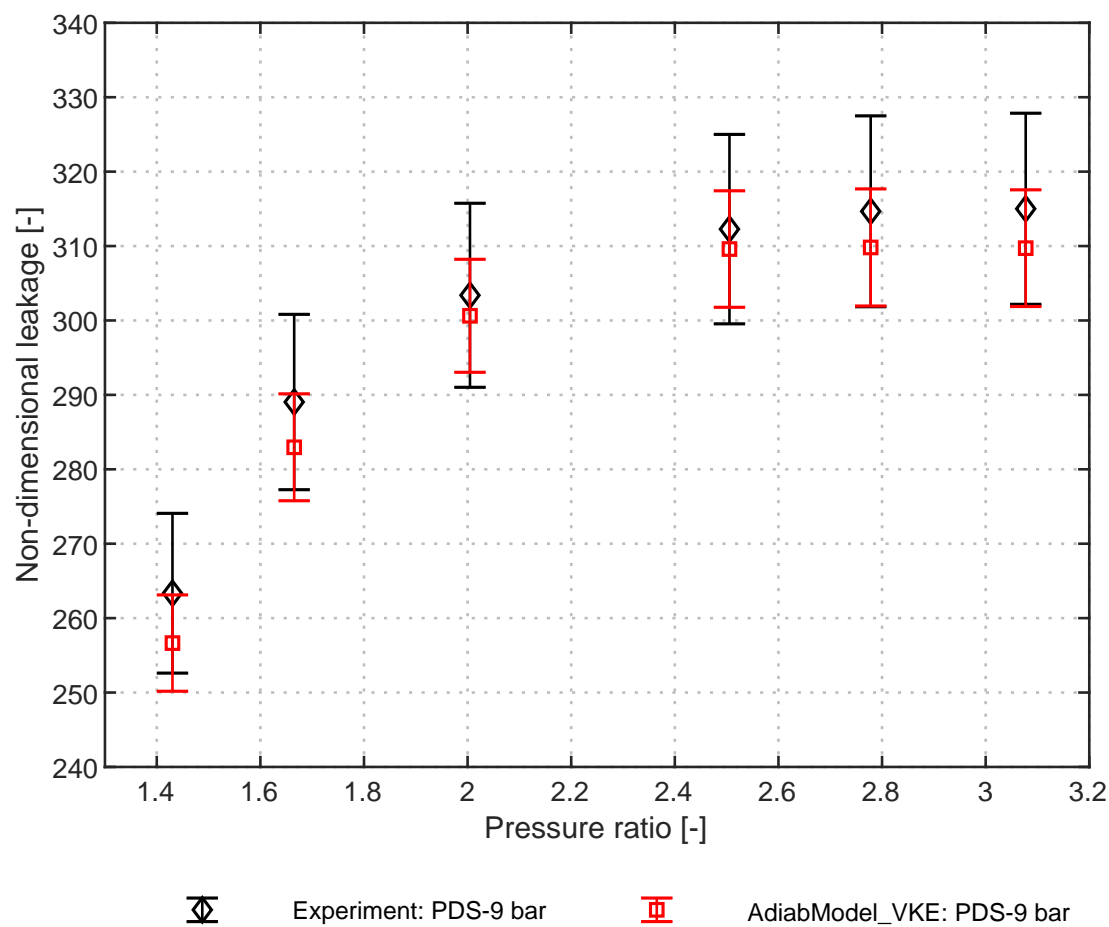
Neumann carryover coefficient (NKE)
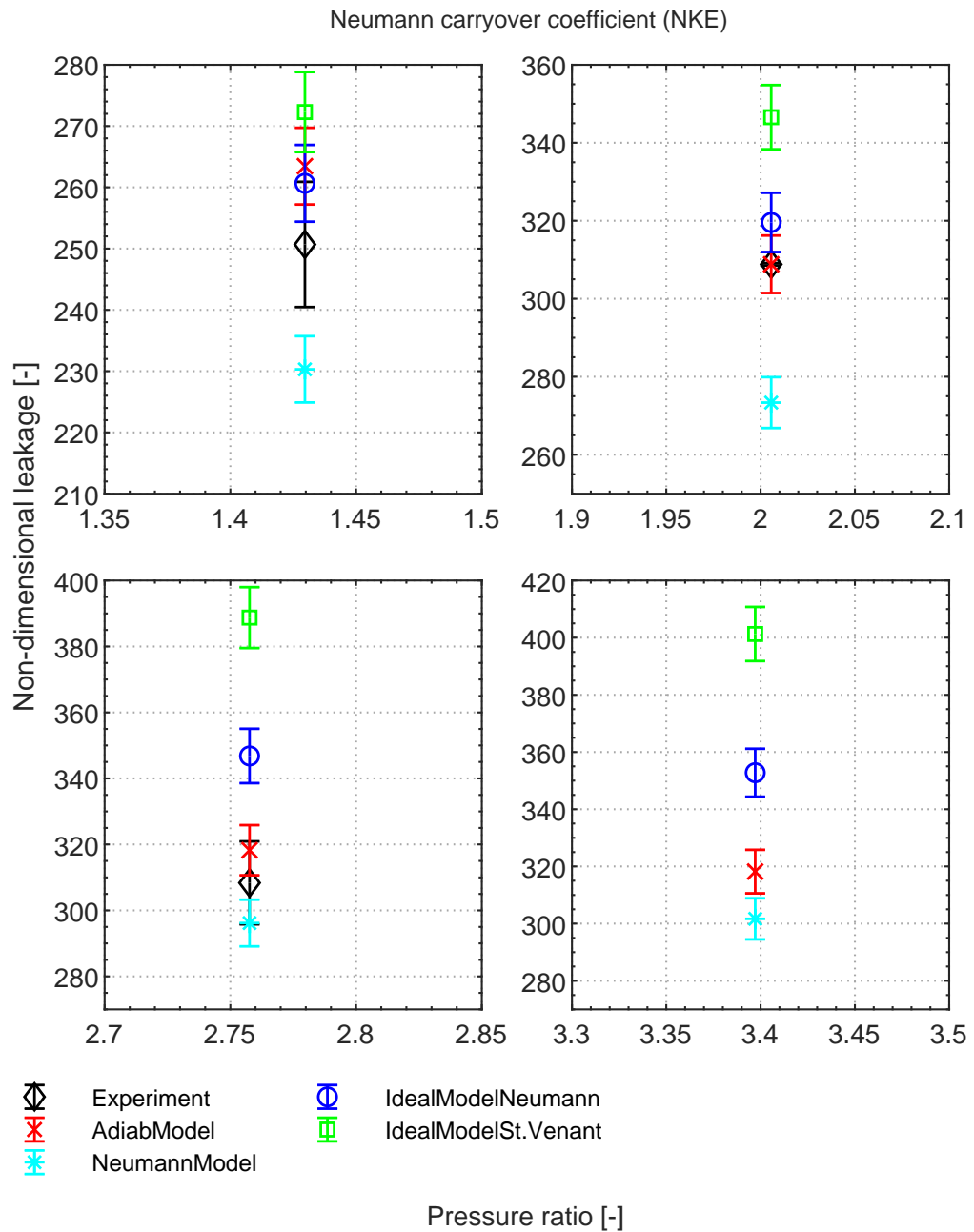
Figure D.2 – Comparison of leakage between the experimental measurements, the author model and state-of-the-art models using Neumann carry-over coefficient on Pocket damper seal (PDS) at 12 bar inlet pressure, 25°C inlet temperature, varying PR and R134a as a working fluid
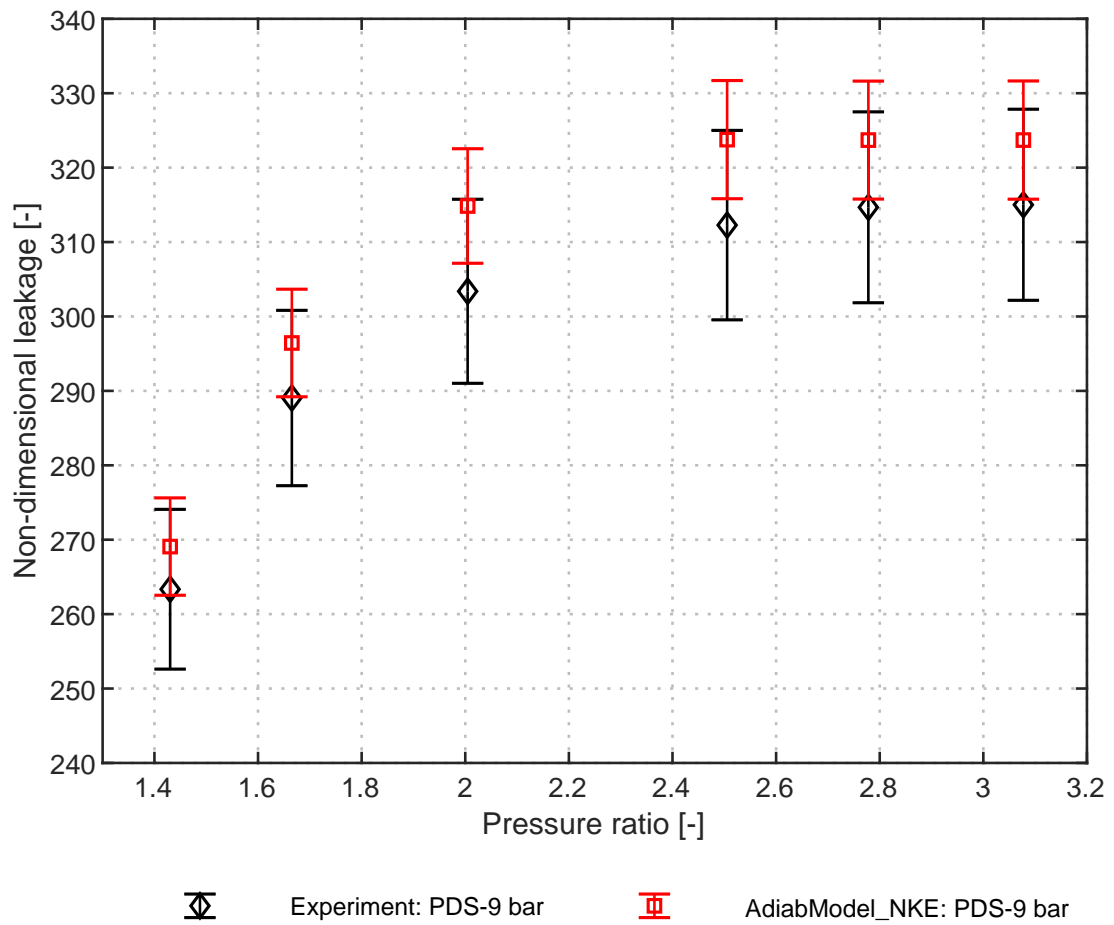
Figure D.3 – Experimental and numerical comparison of PDS seal using Vermes kinetic carry-over coefficient at 9 bar inlet pressure, 40°C inlet temperature, varying PR and R134a as a working fluid

Figure D.4 – Experimental and numerical comparison of PDS seal using Neumann kinetic carry-over coefficient at 9 bar inlet pressure, 40°C inlet temperature, varying PR and R134a as a working fluid
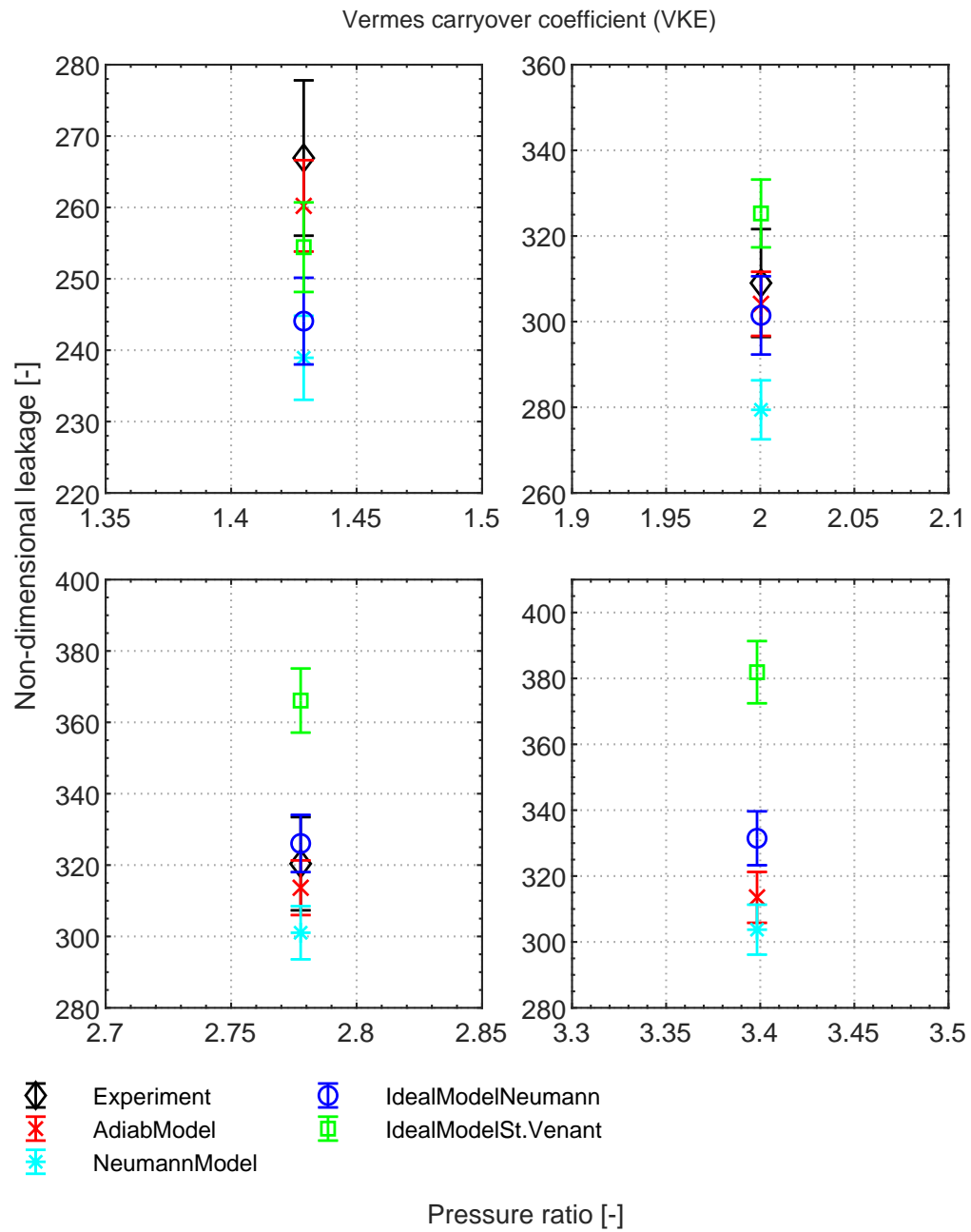
Vermes carryover coefficient (VKE)

Figure D.5 – Experimental and numerical comparison between the author model and state-of-the-art models on PDS seal using Vermes kinetic carry-over coefficient at 12 bar inlet pressure, 50°C inlet temperature, varying PR and R134a as a working fluid
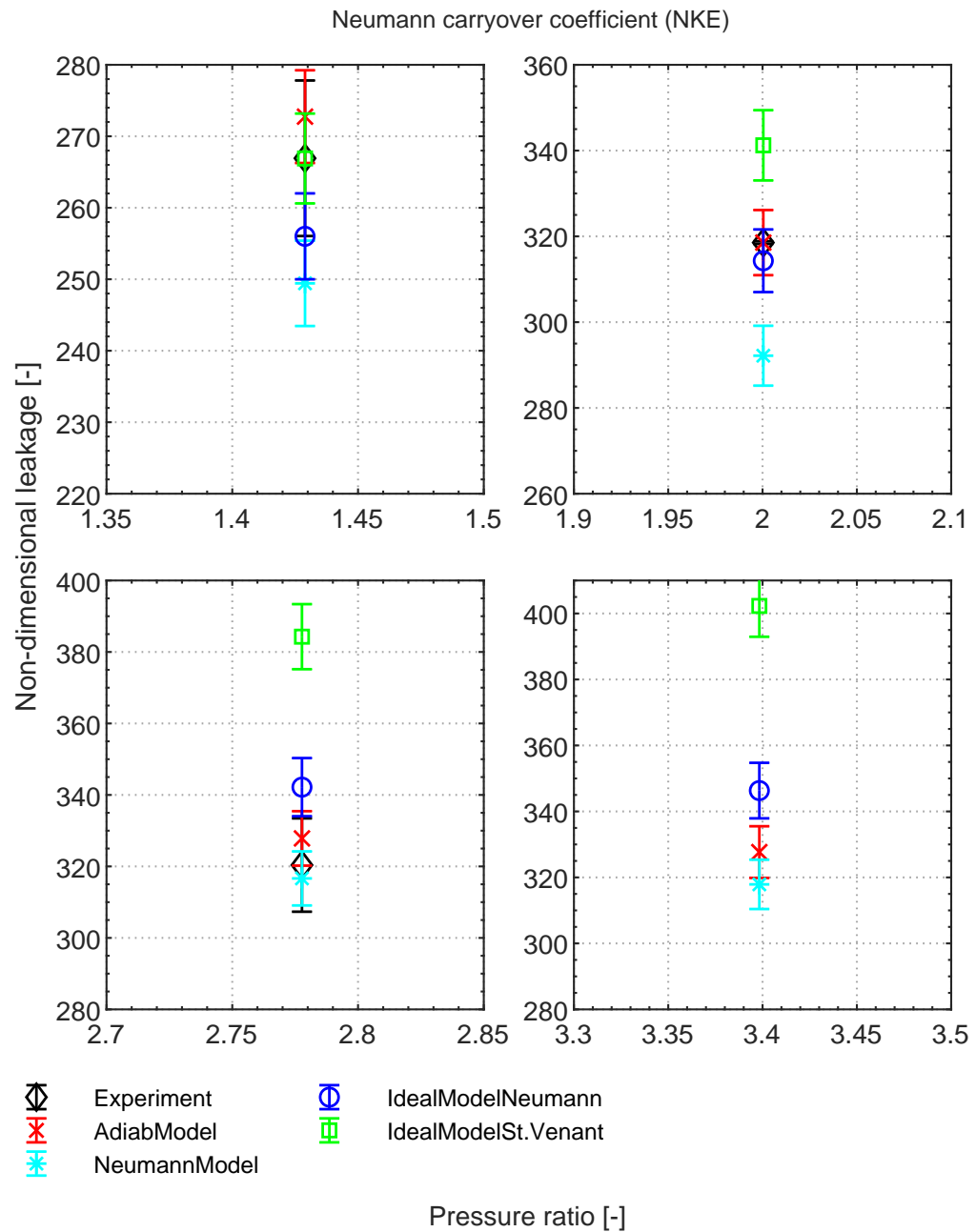
Figure D.6 – Experimental and numerical comparison between the author model and state-of-the-art models on PDS seal using Neumann kinetic carry-over coefficient at 12 bar inlet pressure, 50°C inlet temperature, varying PR and R134a as a working fluid
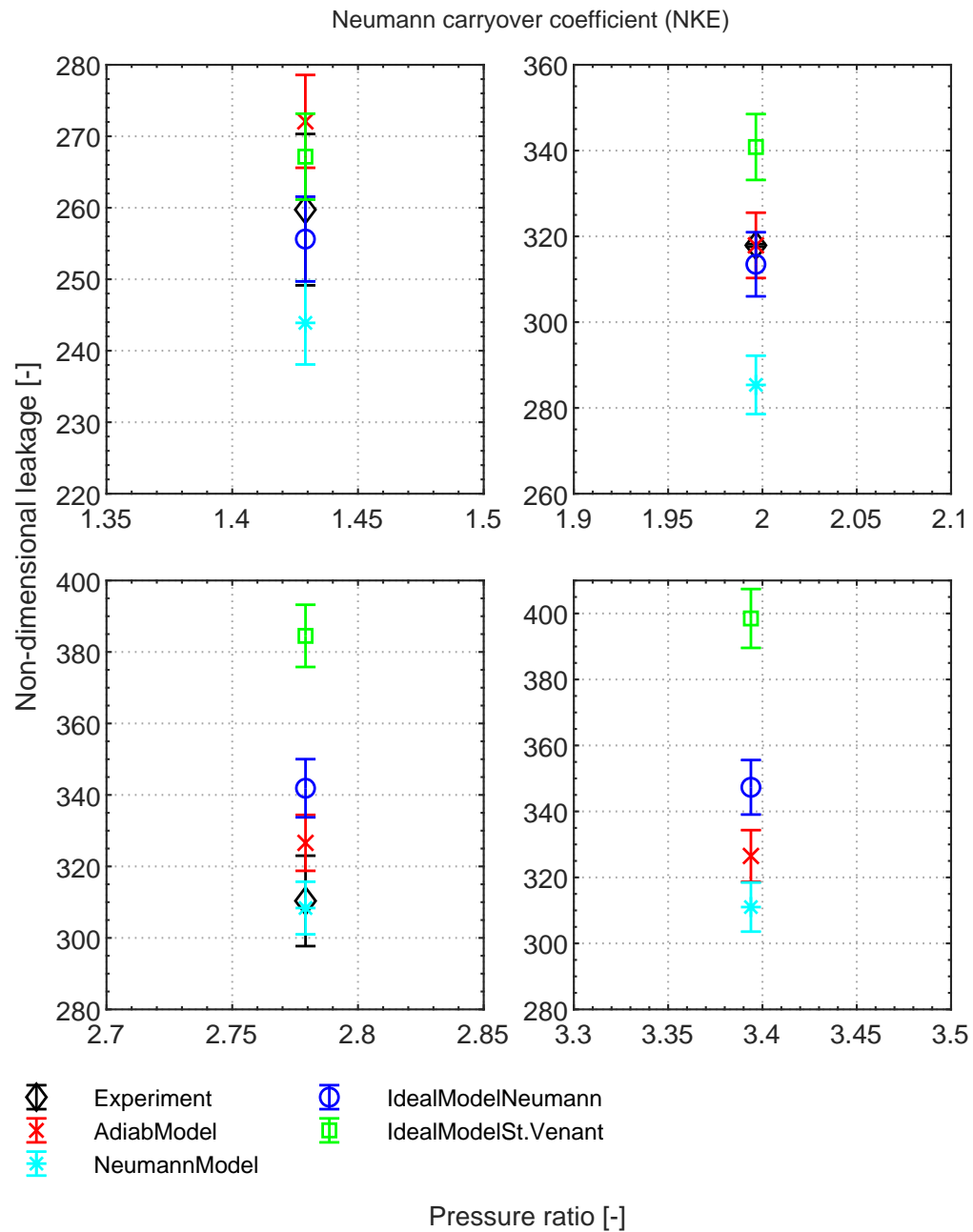
D.1.1   Labyrinth seal (LSVP4T)

Figure D.7 – Experimental and numerical comparison between the author model and state-of-the-art models on Labyrinth seal (LSVP4T) seal using Neumann kinetic carry-over coefficient at 12 bar inlet pressure, 50°C inlet temperature, varying PR and R134a as a working fluid
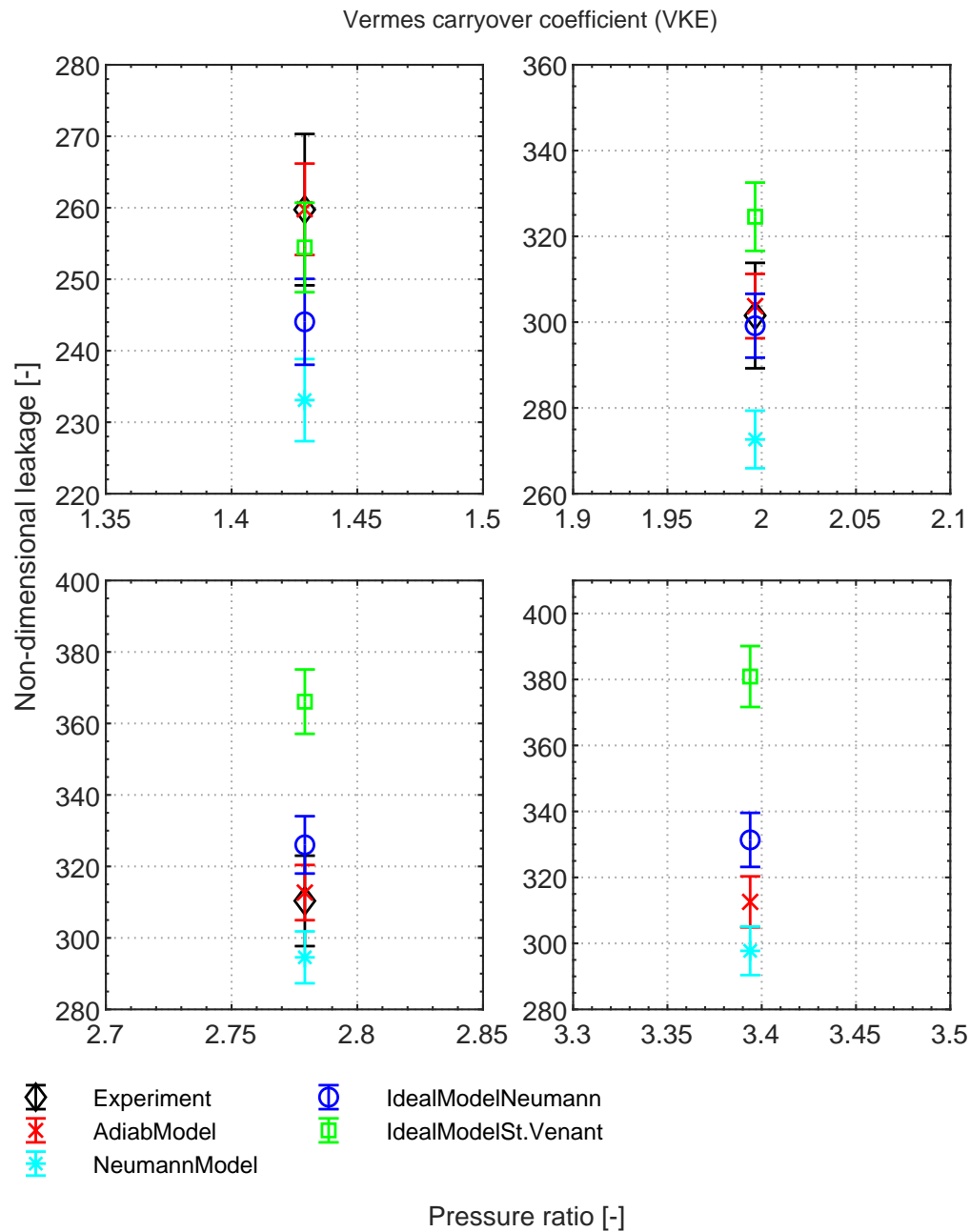
Figure D.8 – Experimental and numerical comparison between the author model and state-of-the-art models on Labyrinth seal (LSVP4T) seal using Vermes kinetic carry-over coefficient at 12 bar inlet pressure, 50°C inlet temperature, varying PR and R134a as a working fluid
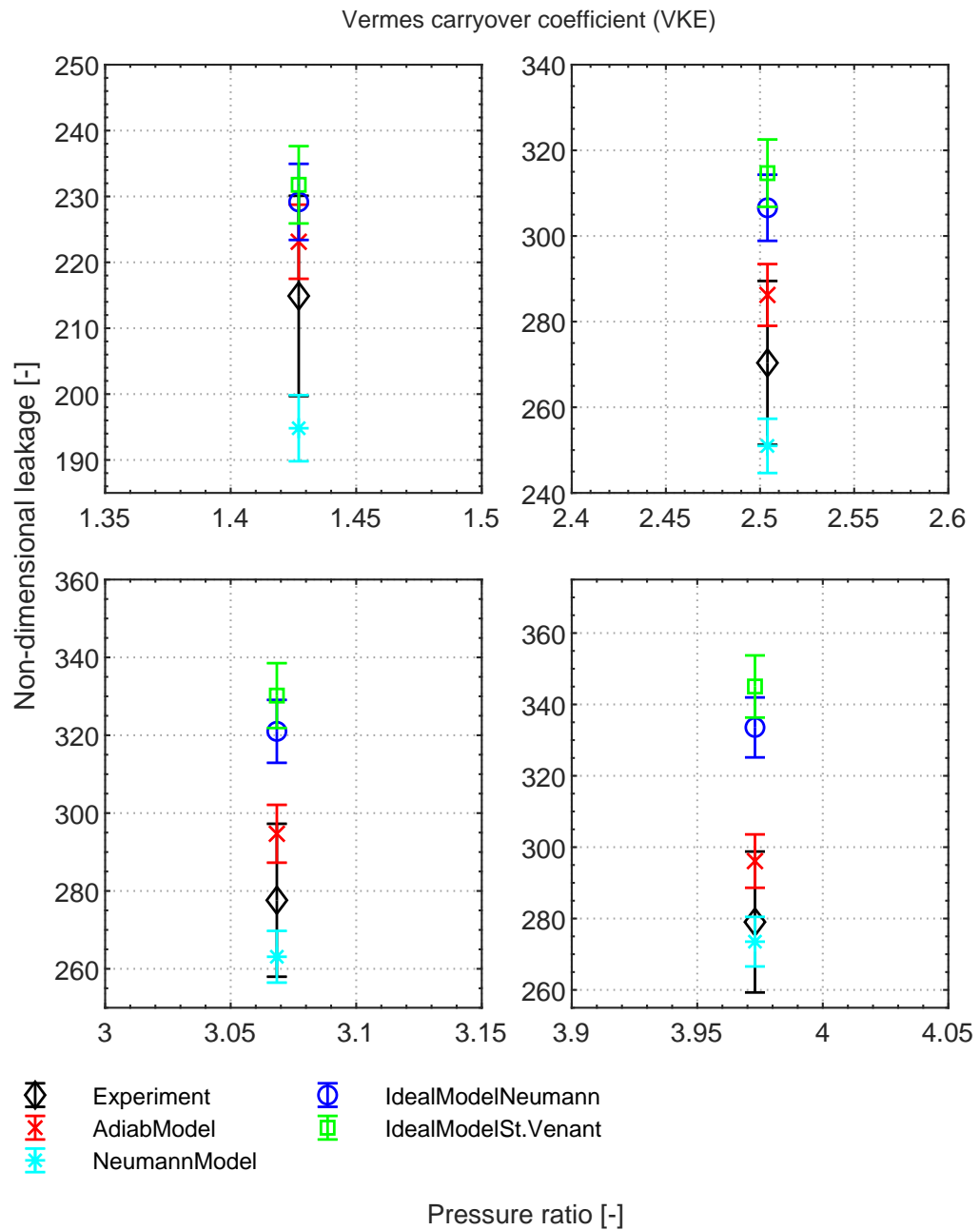
Figure D.9 – Comparison of leakage between experimental measurements, author model and the-state-of-the-art models using Vermes carry-over coefficient on Pocket damper seal (PDS) at 5 bar inlet pressure, 25°C inlet temperature, varying PR and air as a working fluid

Figure D.10 – Comparison of leakage between experimental measurements, author model and the-state-of-the-art models using Neumann carry-over coefficient on Pocket damper seal (PDS) at 5 bar inlet pressure, 25°C inlet temperature, varying PR and air as a working fluid
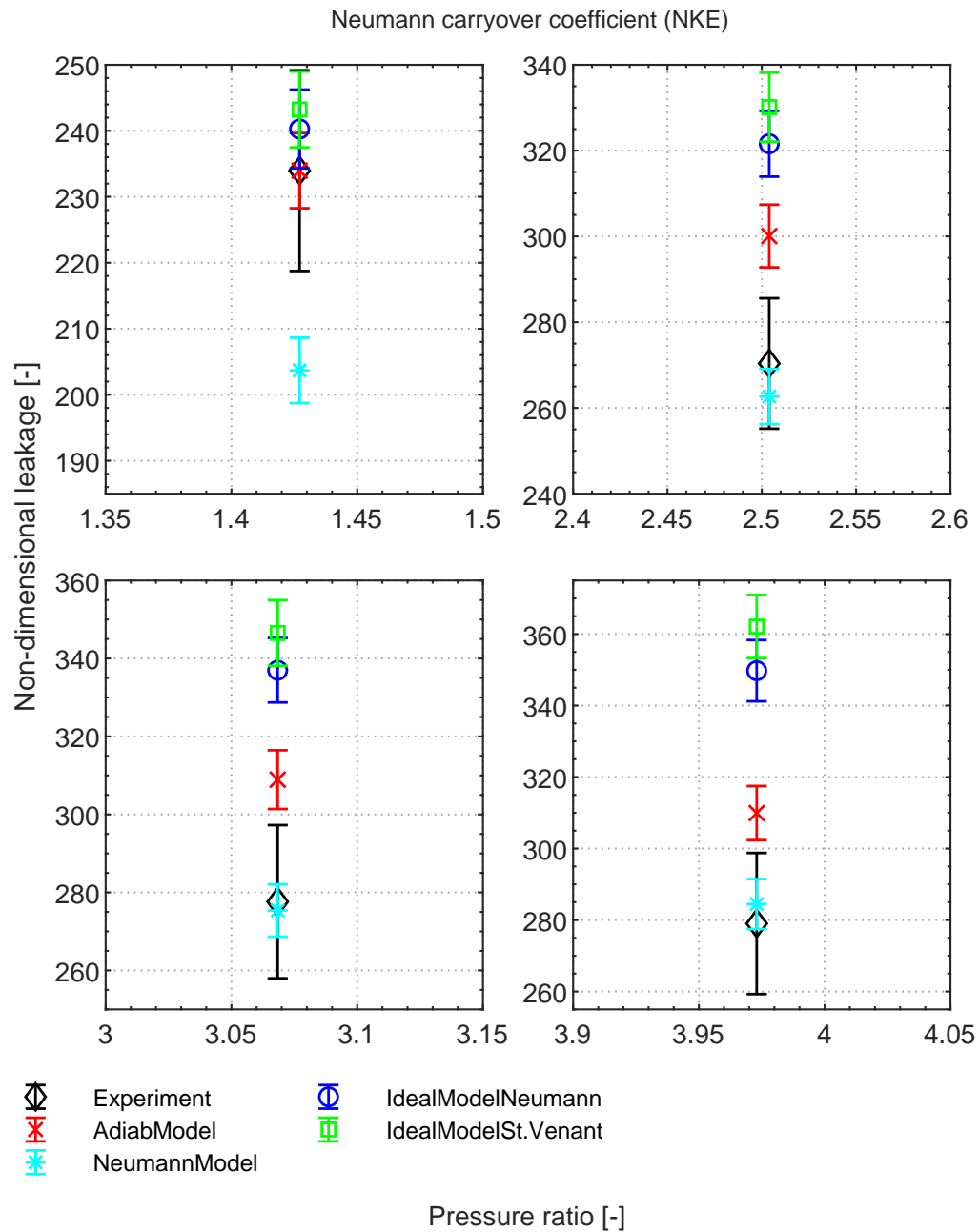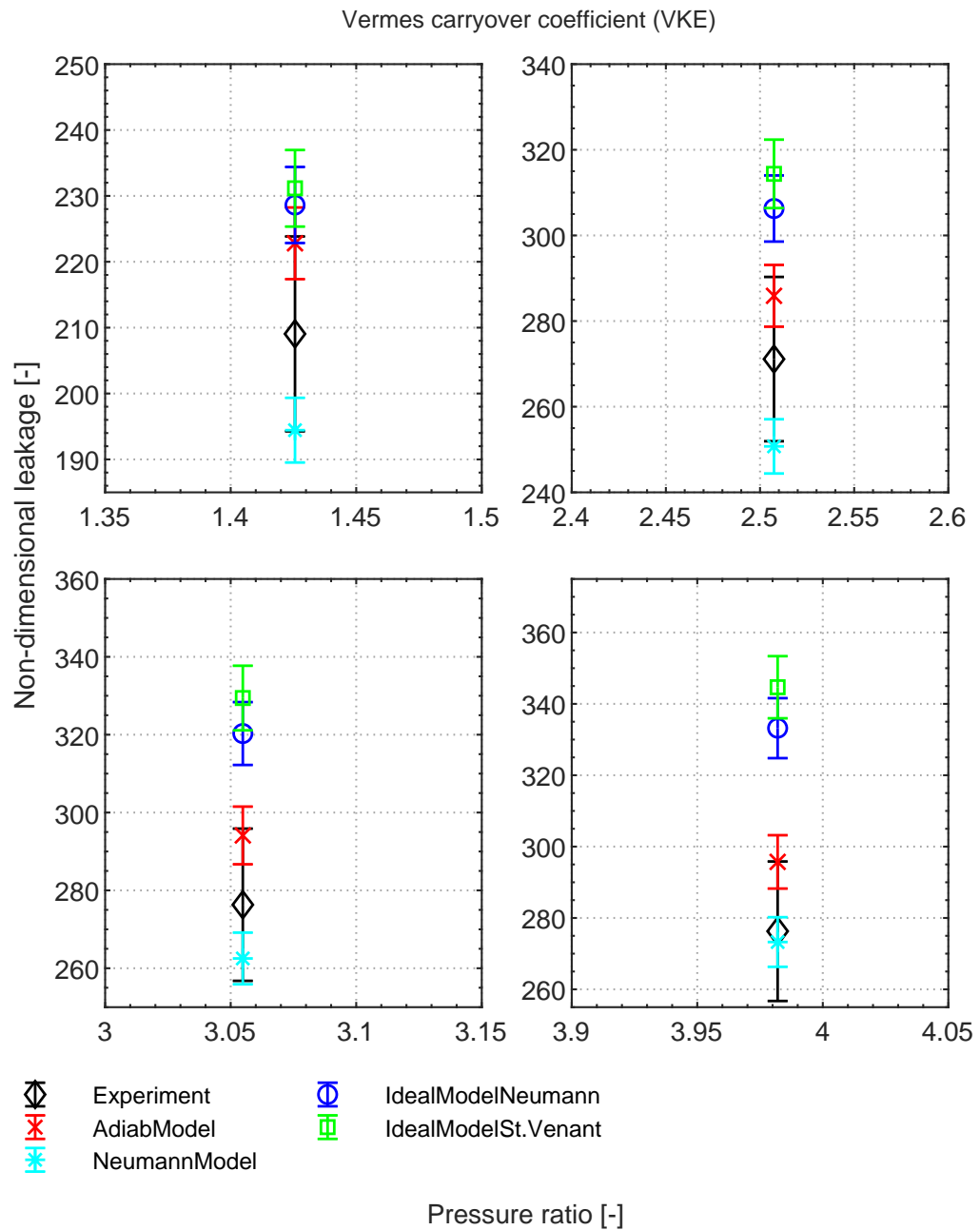
D.1.2 Labyrinth seal (LSVP4T)

Figure D.11 – Comparison of leakage between experimental measurements, author model and the-state-of-the-art models using Vermes carry-over coefficient on Labyrinth seal (LSVP4T) at 5 bar inlet pressure, 25°C inlet temperature, varying PR and air as a working fluid

Vermes carryover coefficient (VKE)

Figure D.12 – Comparison of leakage between experimental measurements, author model and the-state-of-the-art models using Neumann carry-over coefficient on Labyrinth seal (LSVP4T) at 5 bar inlet pressure, 25°C inlet temperature, varying PR and air as a working fluid

D.1.3 Labyrinth seal (LSCP5T)

Figure D.13 – Comparison of leakage between experimental measurements, author model and the-state-of-the-art models using Vermes carry-over coefficient on Labyrinth seal (LSCP5T) at 5 bar inlet pressure, 25°C inlet temperature, varying PR and air as a working fluid
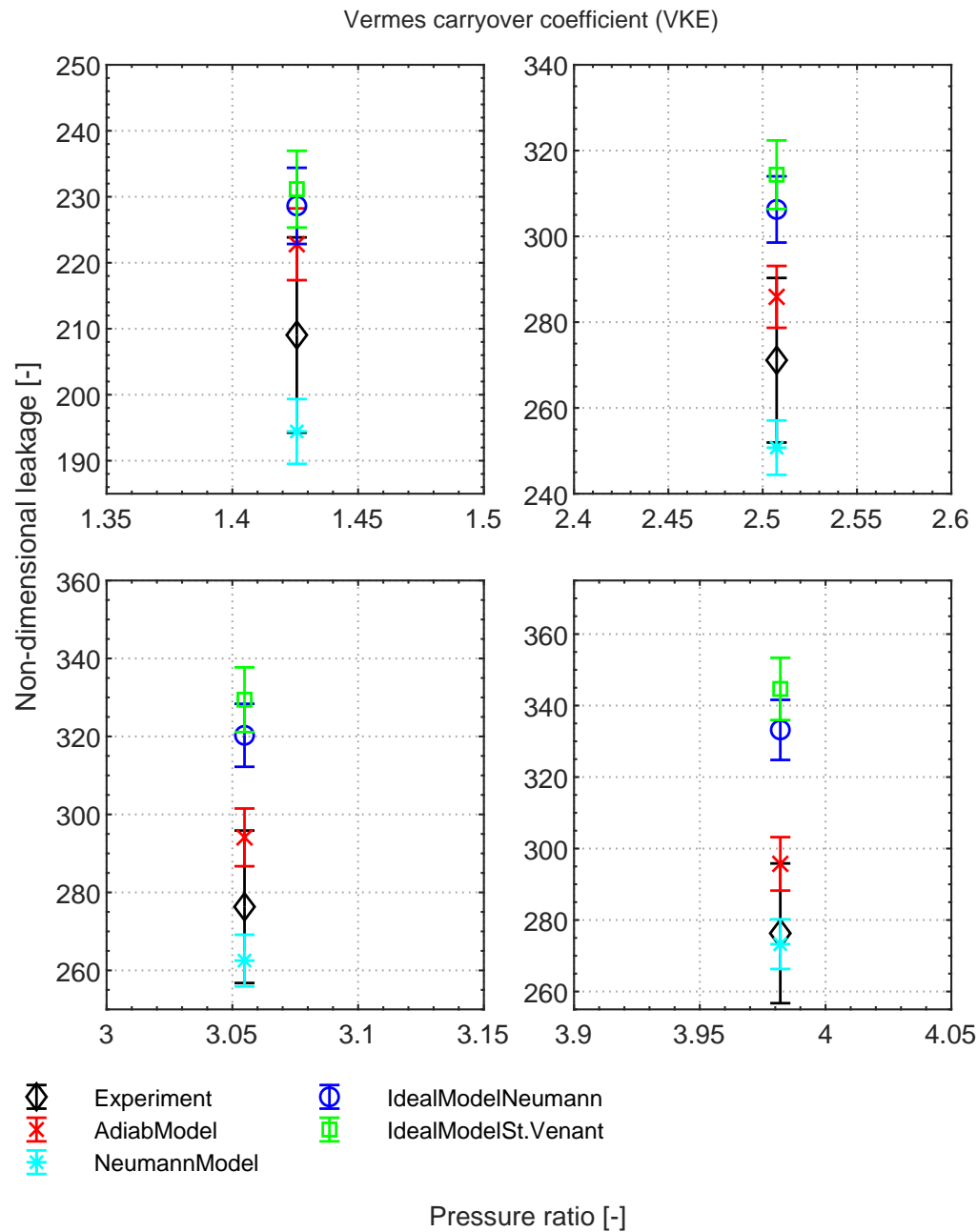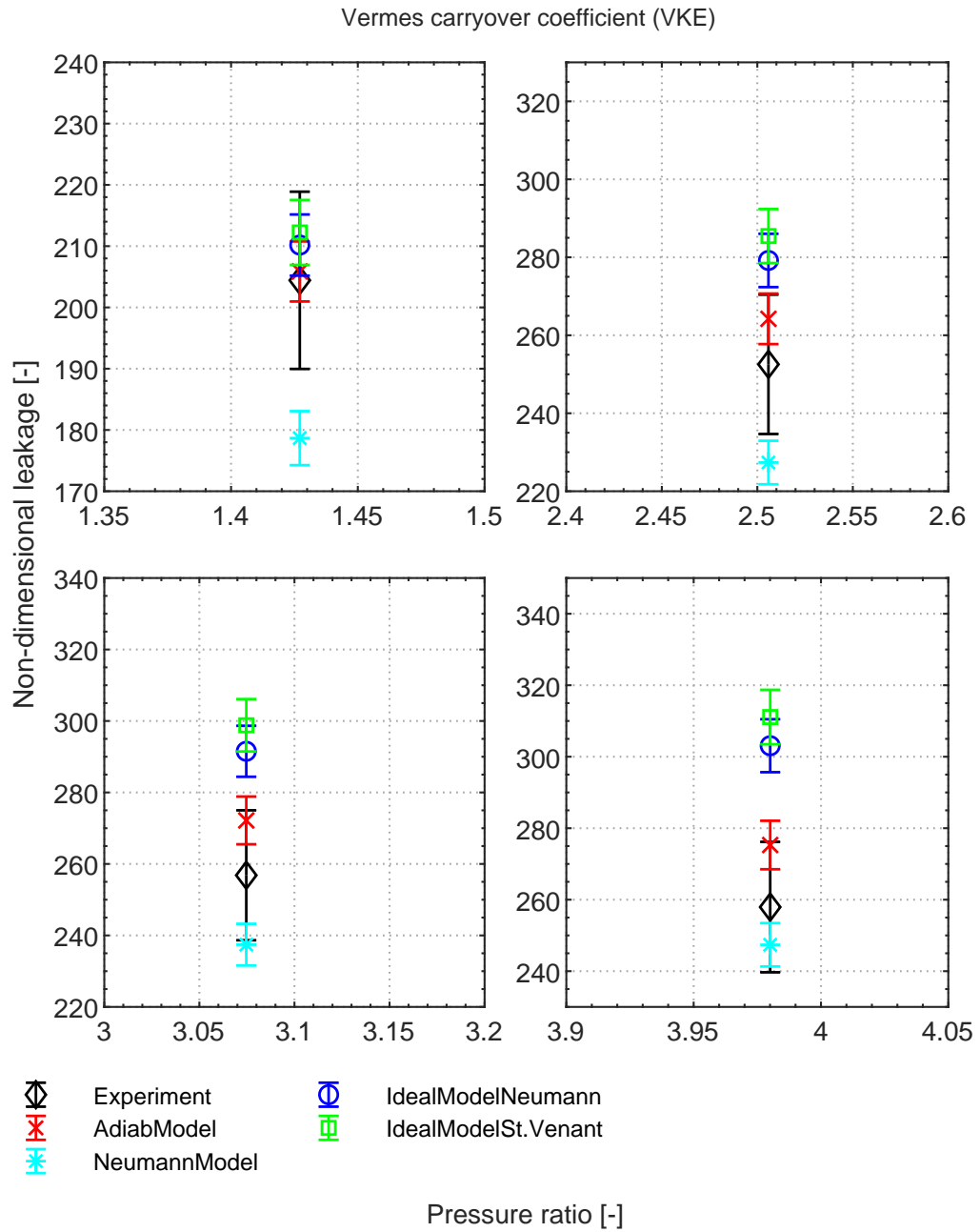
Neumann carryover coefficient (NKE)

Figure D.14 – Comparison of leakage between experimental measurements, author model and the-state-of-the-art models using Neumann carry-over coefficient on Labyrinth seal (LSCP5T) at 5 bar inlet pressure, 25°C inlet temperature, varying PR and air as a working fluid
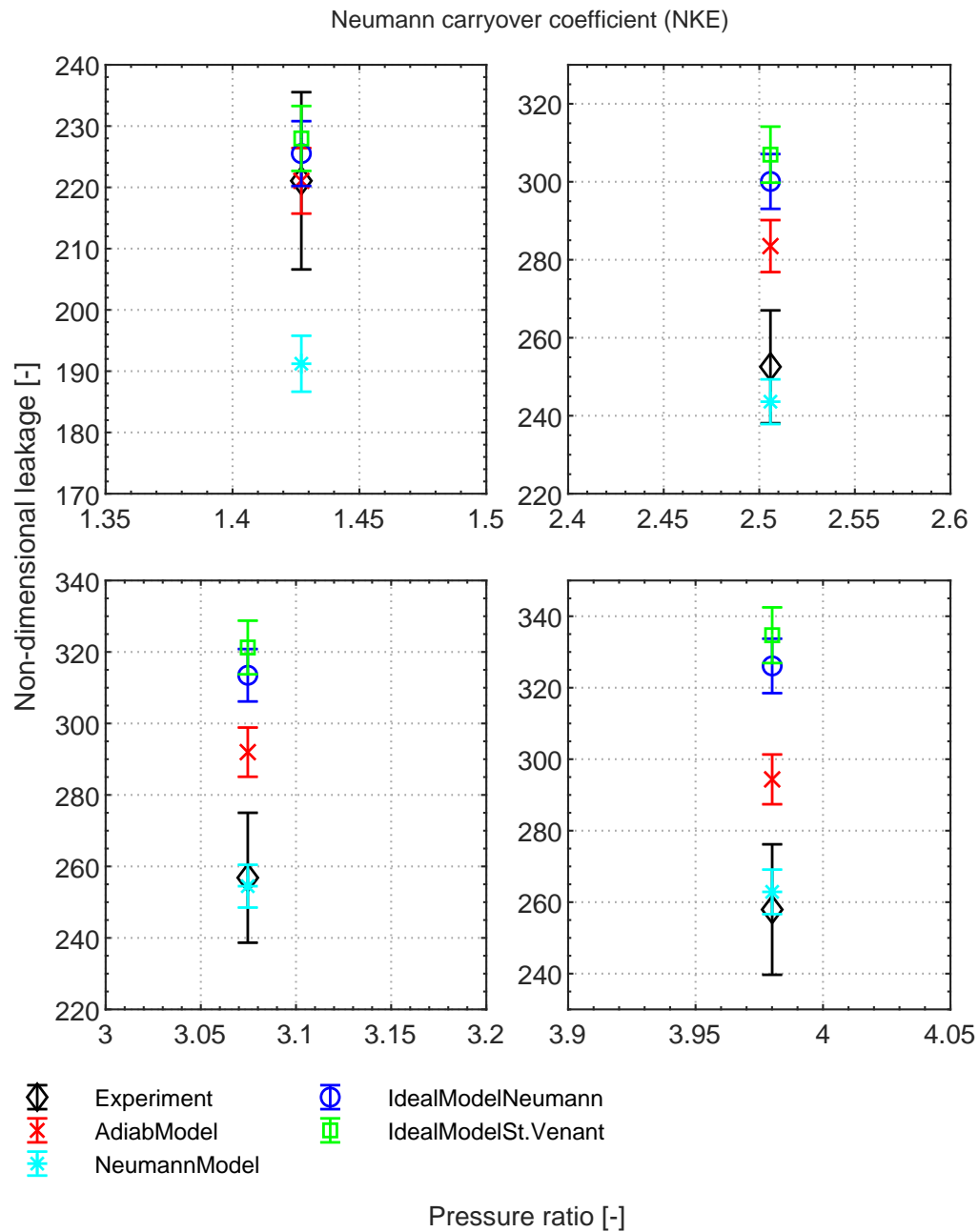
Figure D.15 – Experimental and numerical comparison between the different seals at 12 bar inlet pressure, 50°C inlet temperature, varying PR and R134a as a working fluid
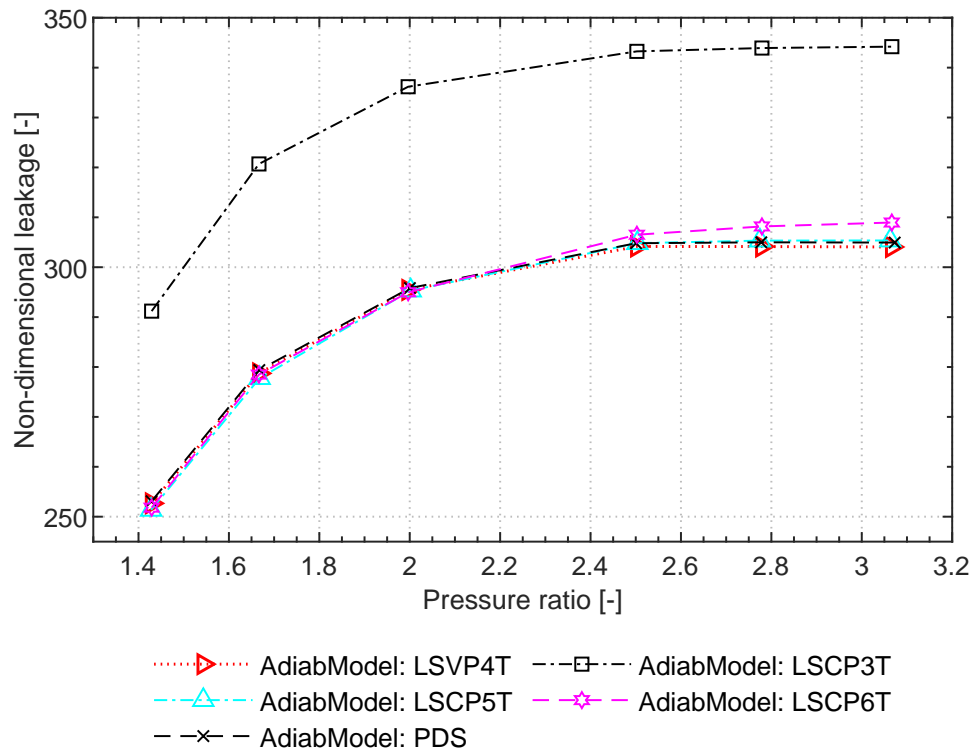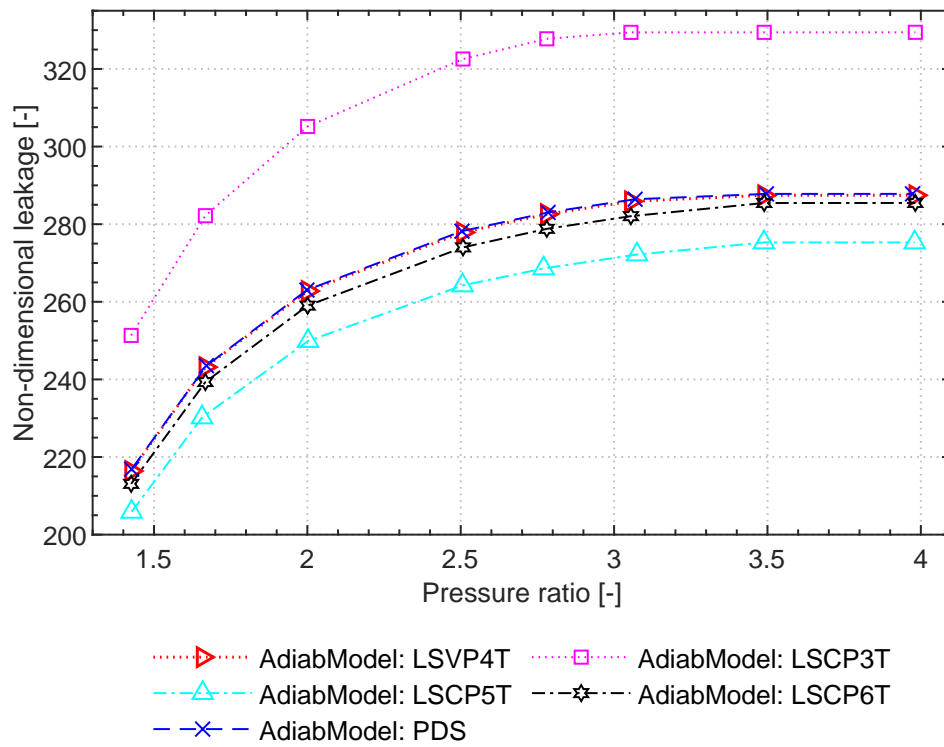
Figure D.16 – Experimental and numerical comparison between the different seals at 12 bar inlet pressure, 50°C inlet temperature, varying PR and R134a as a working fluid

D.1.4   Cavity pressure distribution: R134a
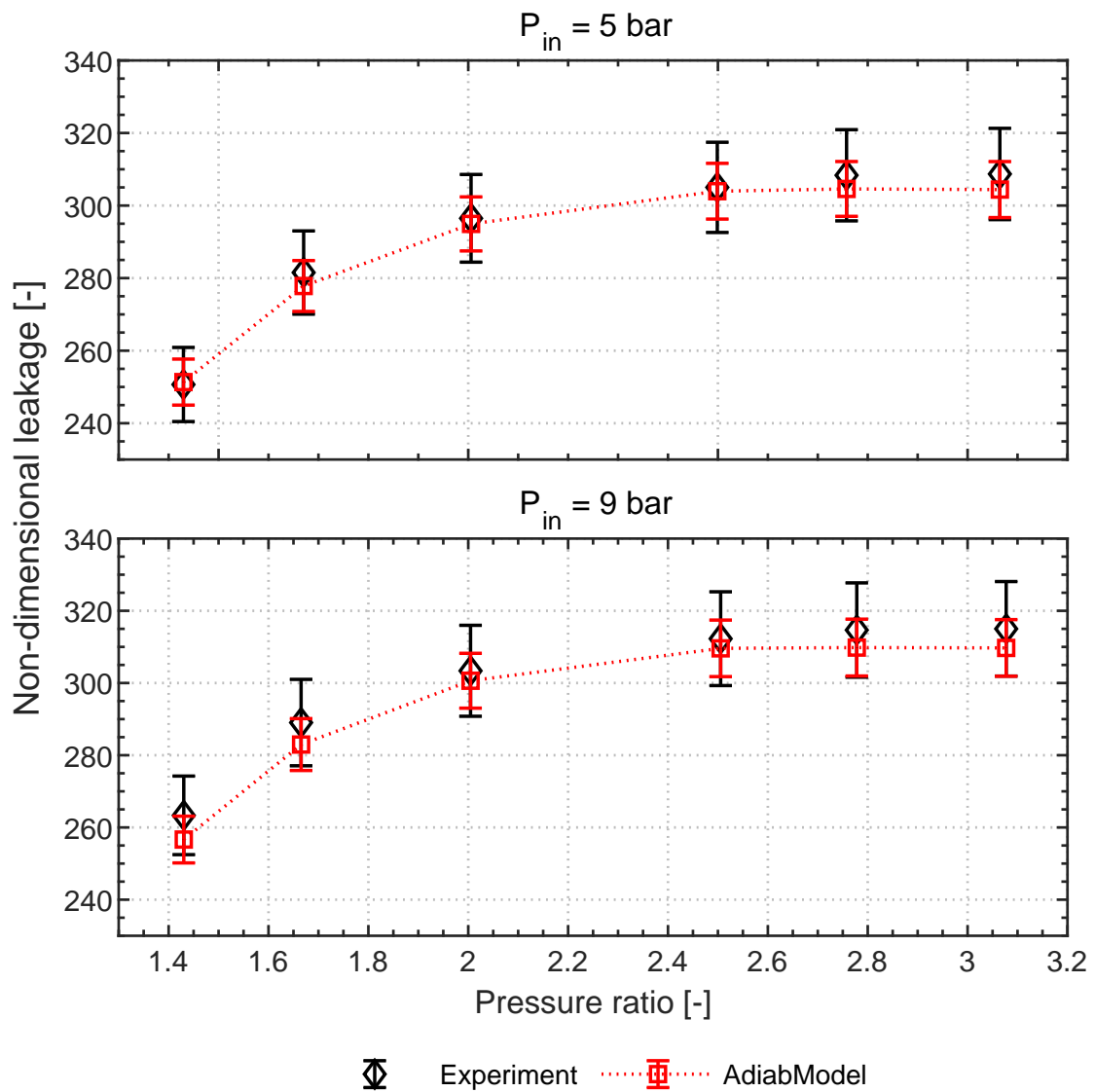
Figure D.17 – Comparison of leakage between the experiment and the author model on Pocket Damper Seal (PDS) at 5 and 9 bar inlet pressure, 25°C and 40°C inlet temperature respectively and varying PR with R134a as working fluid

Figure D.18 – Comparison of cavity pressure distribution between the experiment and the author model on Pocket Damper Seal (PDS) at 5 bar inlet pressure, 25°C inlet temperature and varying PR with R134a as working fluid

Figure D.19 – Comparison of cavity pressure distribution between the experiment and the author model on Pocket Damper Seal (PDS) at 5 bar inlet pressure, 25°C inlet temperature and varying PR with R134a as working fluid

Figure D.20 – Comparison of cavity pressure distribution between the experiment and the author model on Pocket Damper Seal (PDS) at 9 bar inlet pressure, 40°C inlet temperature and varying PR with R134a as working fluid

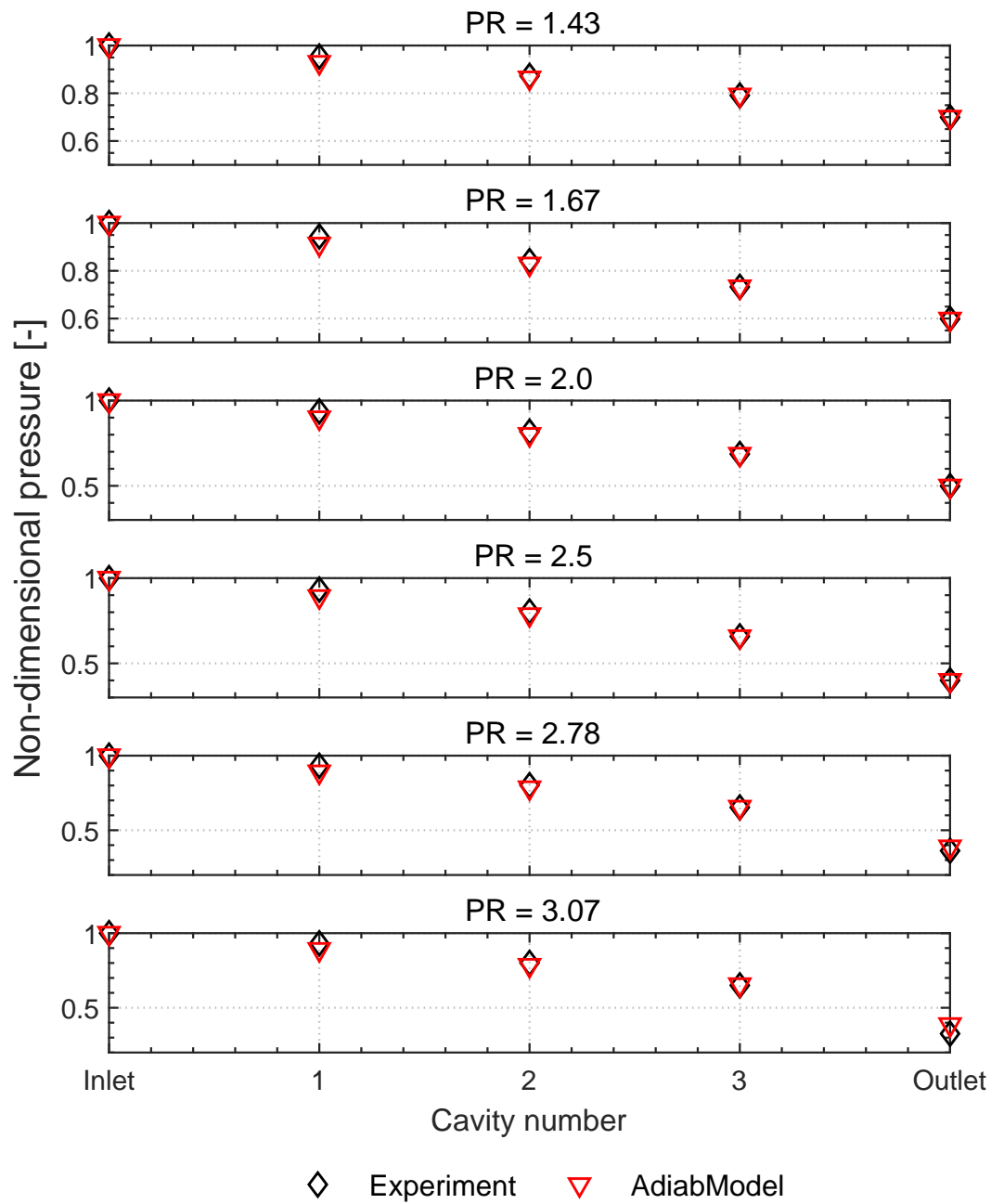Figure D.21 – Comparison of cavity pressure distribution between the experiment and the author model on Pocket Damper Seal (PDS) at 12 bar inlet pressure, 50°C inlet temperature and varying PR with R134a as working fluid

Figure D.22 – Comparison of cavity pressure distribution between the experiment and the ideal Neumann model on Pocket Damper Seal (PDS) at 12 bar inlet pressure, 50°C inlet temperature and varying PR with R134a as working fluid
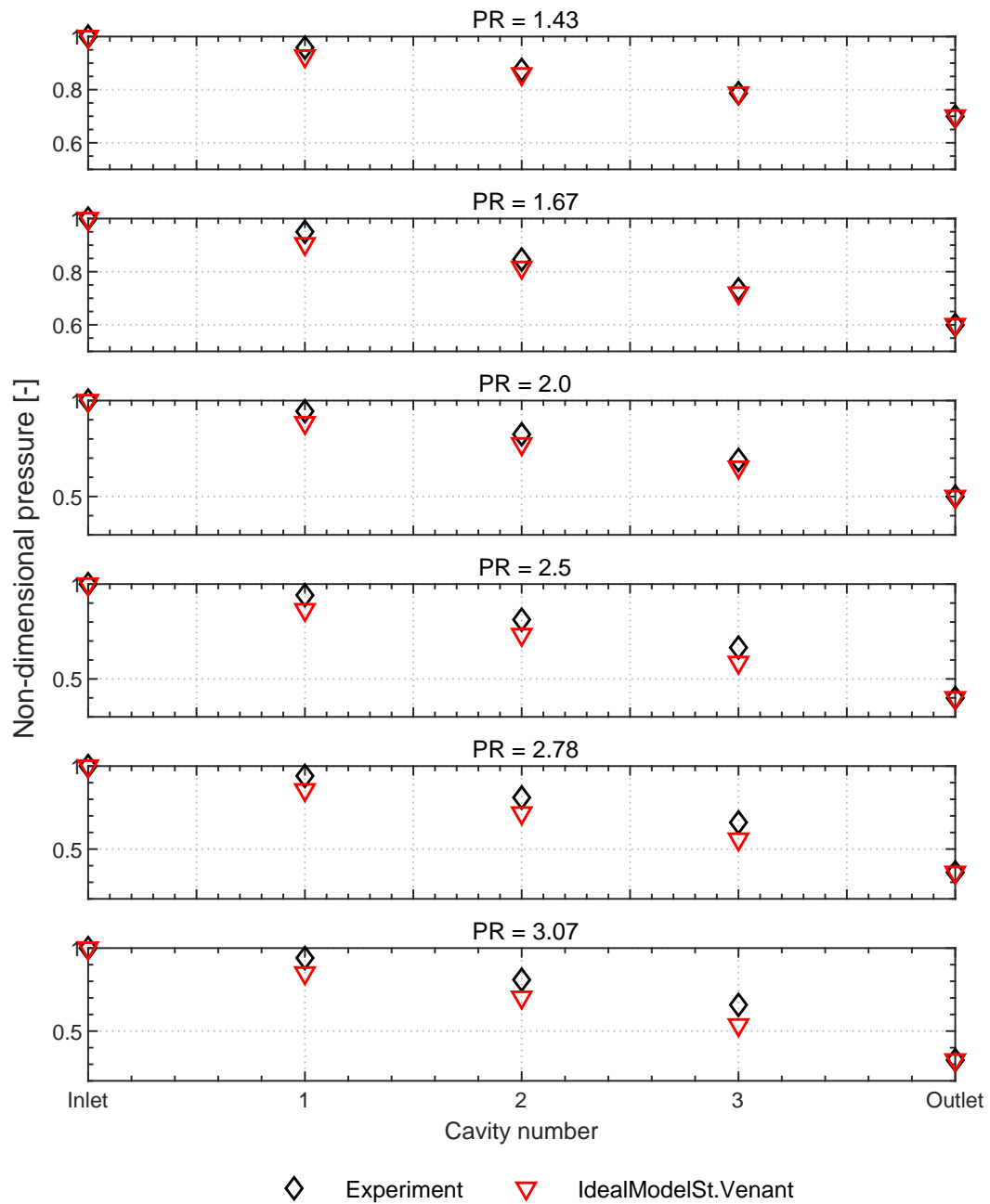
Figure D.23 – Comparison of cavity pressure distribution between the experiment and the ideal St. Venant model on Pocket Damper Seal (PDS) at 12 bar inlet pressure, 50°C inlet temperature and varying PR with R134a as working fluid

D.1.5   Cavity temperature distribution

Figure D.24 – Comparison of cavity temperature distribution between the experiment and the author model on Pocket Damper Seal (PDS) at 5 bar inlet pressure, 25°C inlet temperature and varying PR with R134a as working fluid
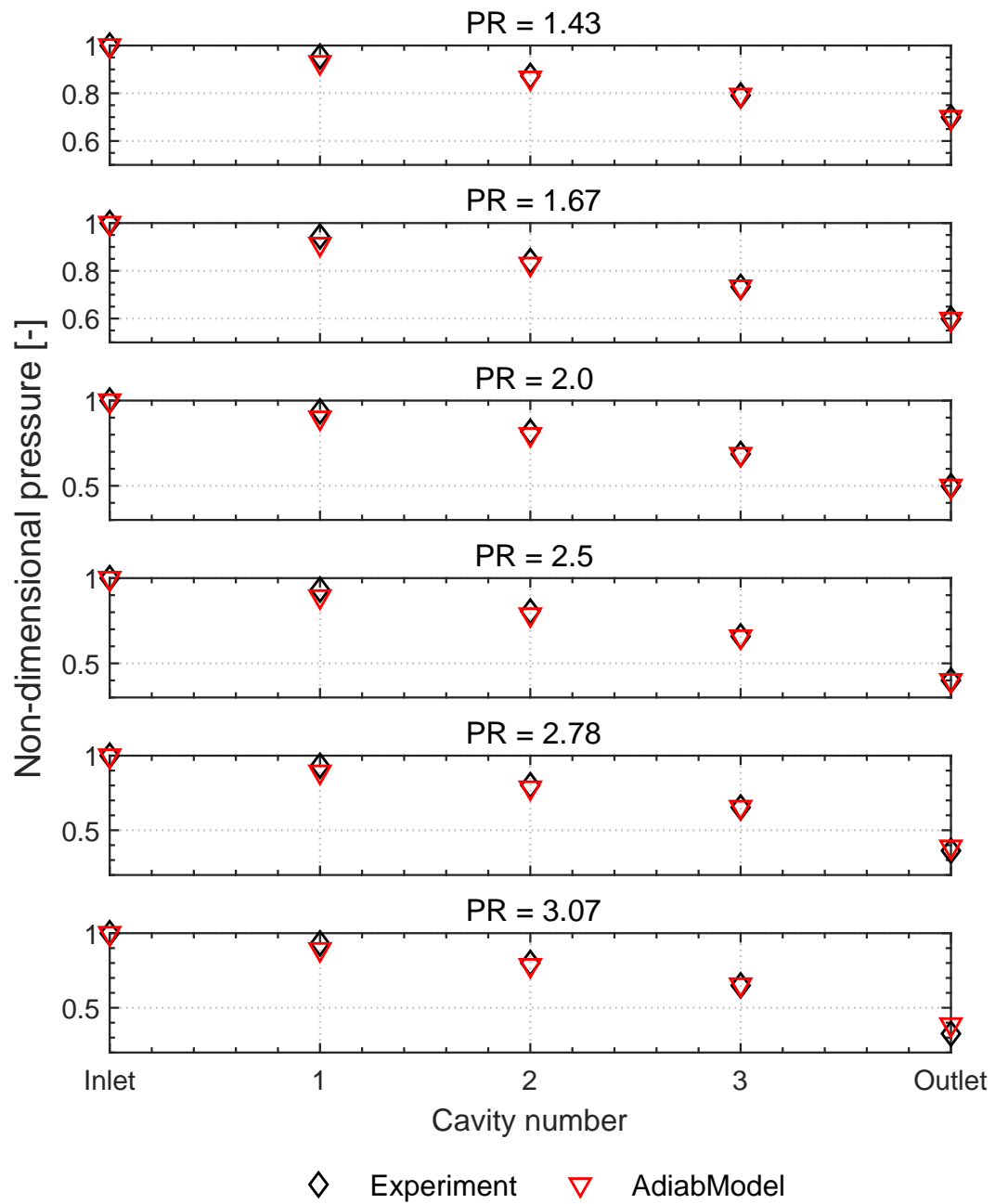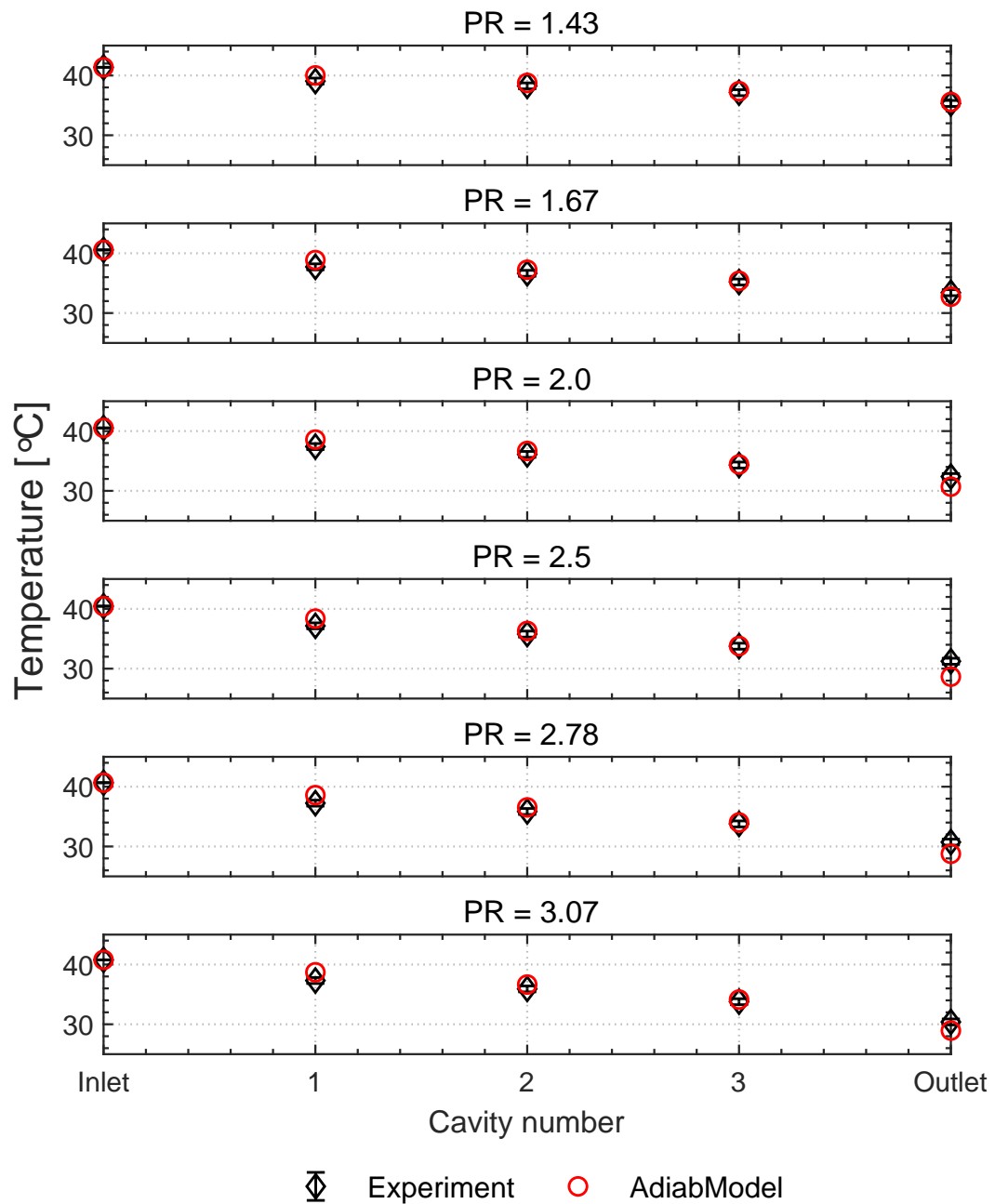
Figure D.25 – Comparison of cavity temperature distribution between the experiment and the author model on Pocket damper seal (PDS) at 9 bar inlet pressure, 40°C inlet temperature and varying PR with R134a as working fluid
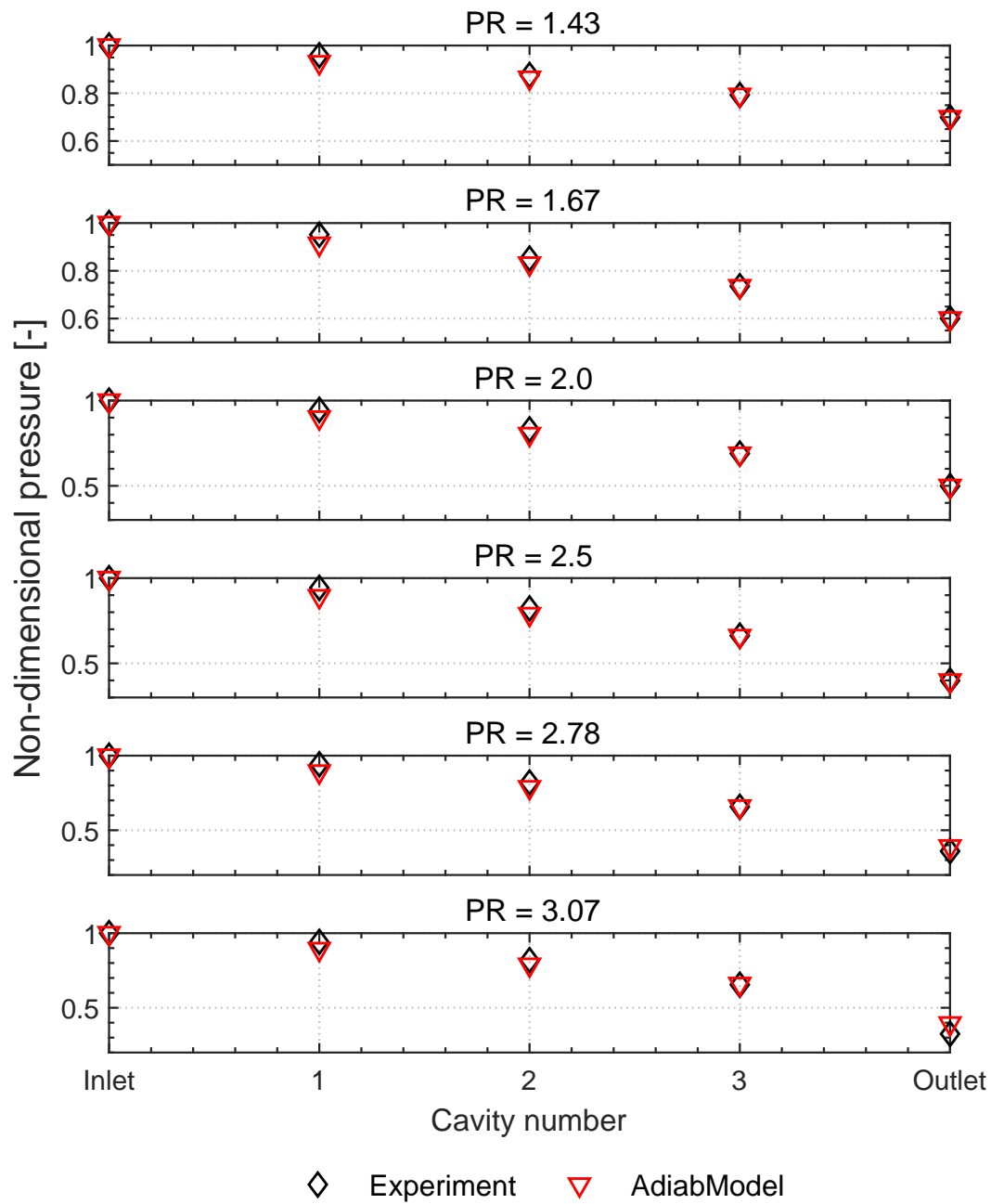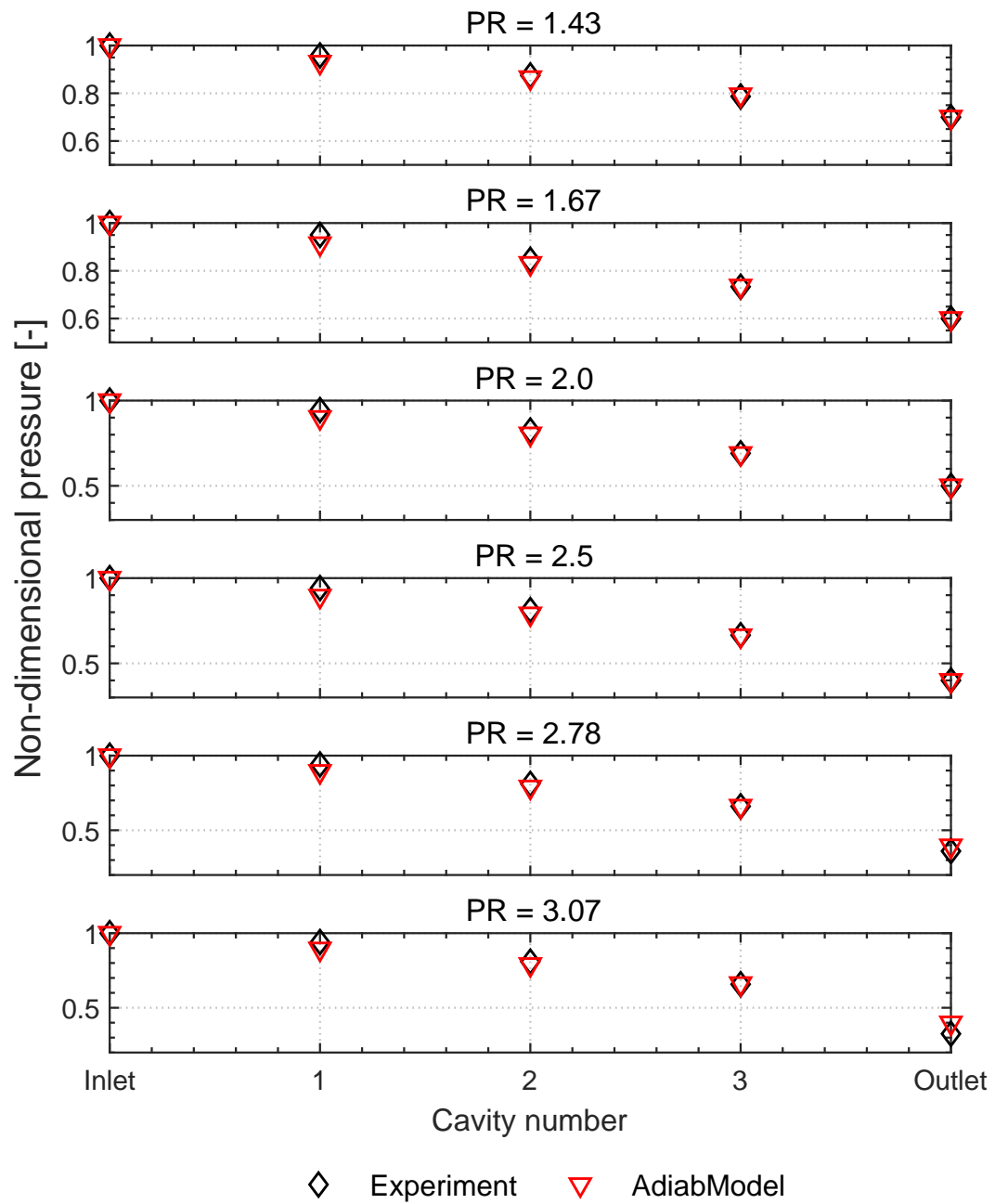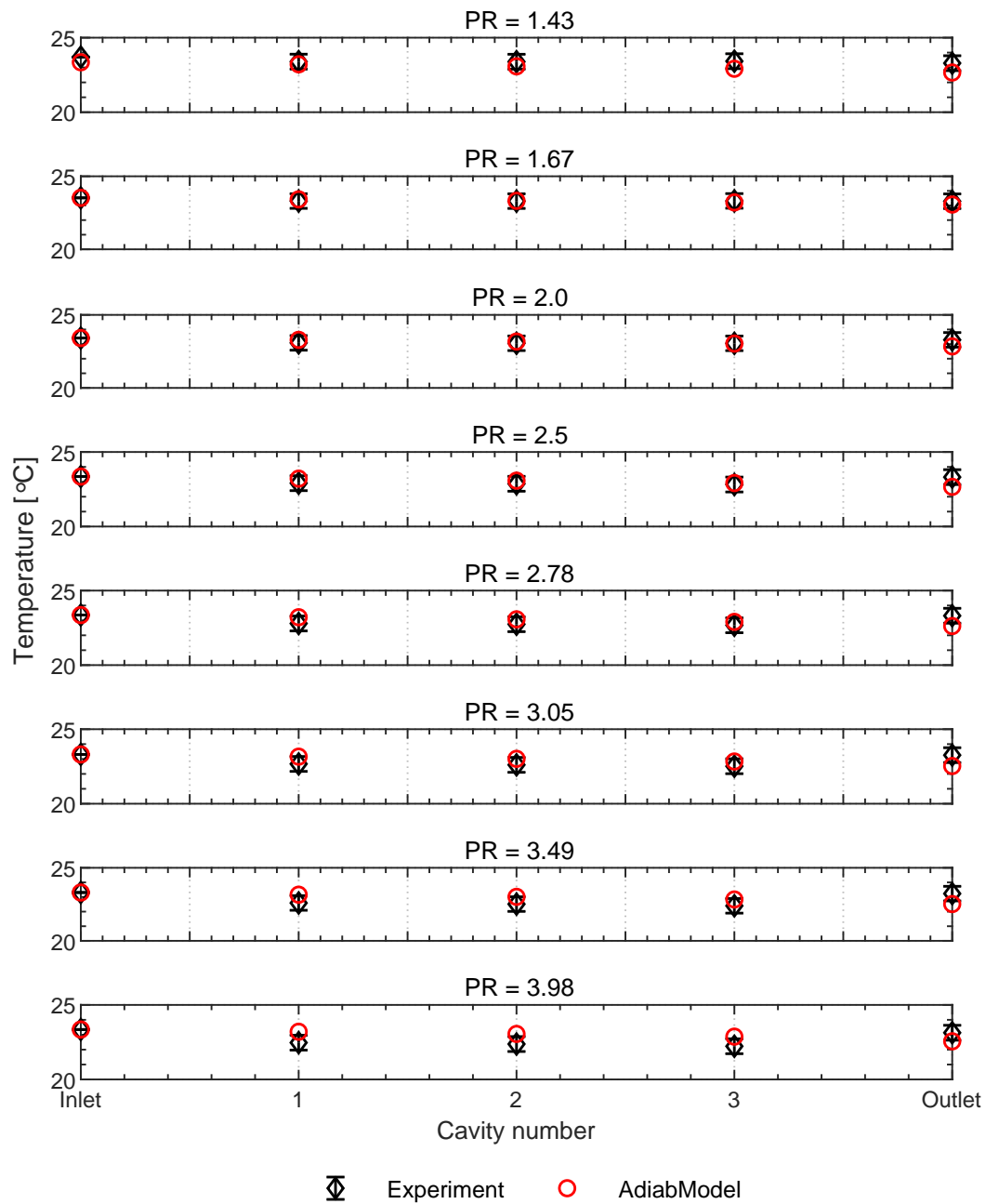
Figure D.26 – Comparison of cavity temperature distribution between experiment and the author model on Pocket Damper Seal (PDS) at 5 bar inlet pressure, 25°C inlet temperature and varying PR with air as working fluid
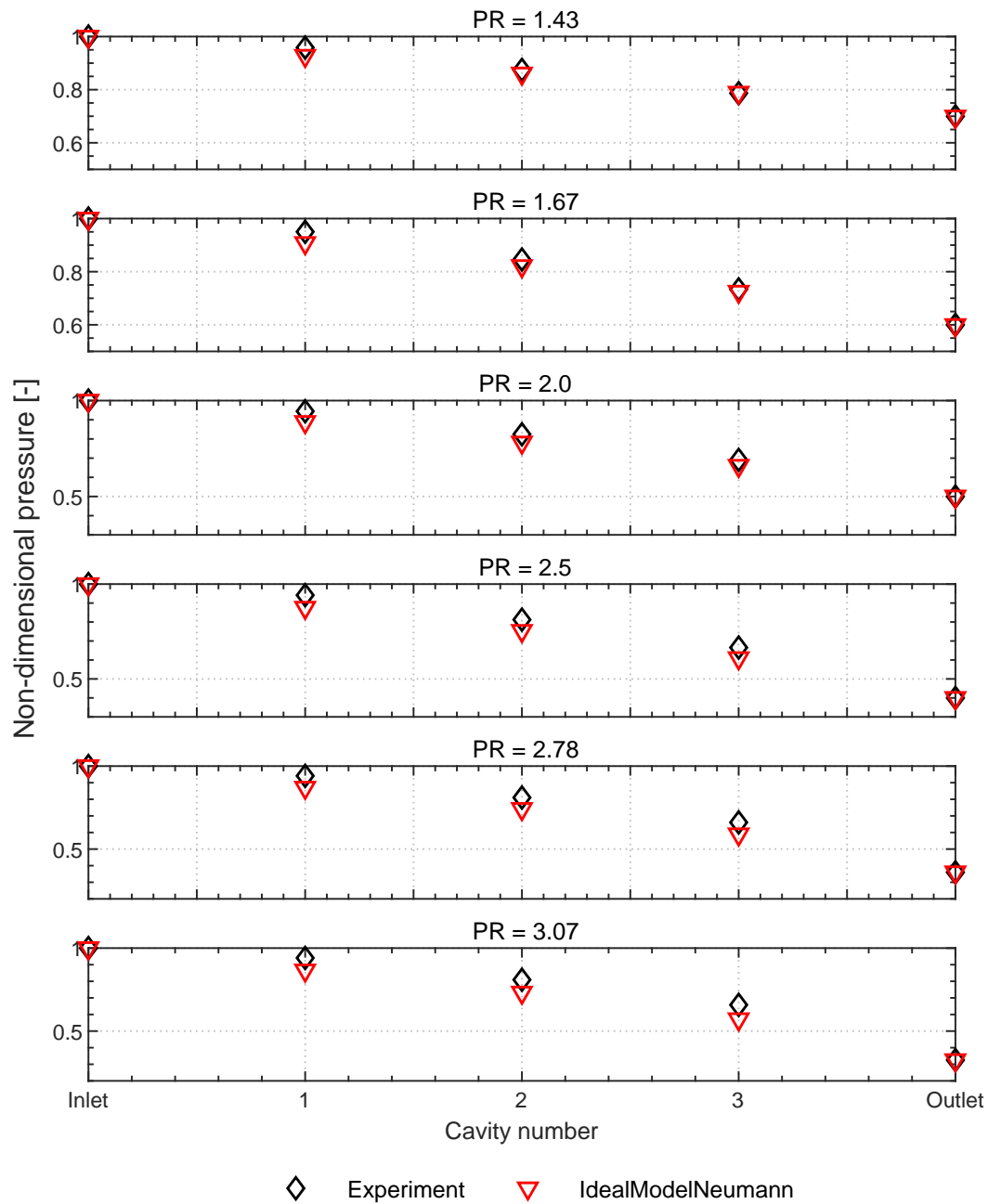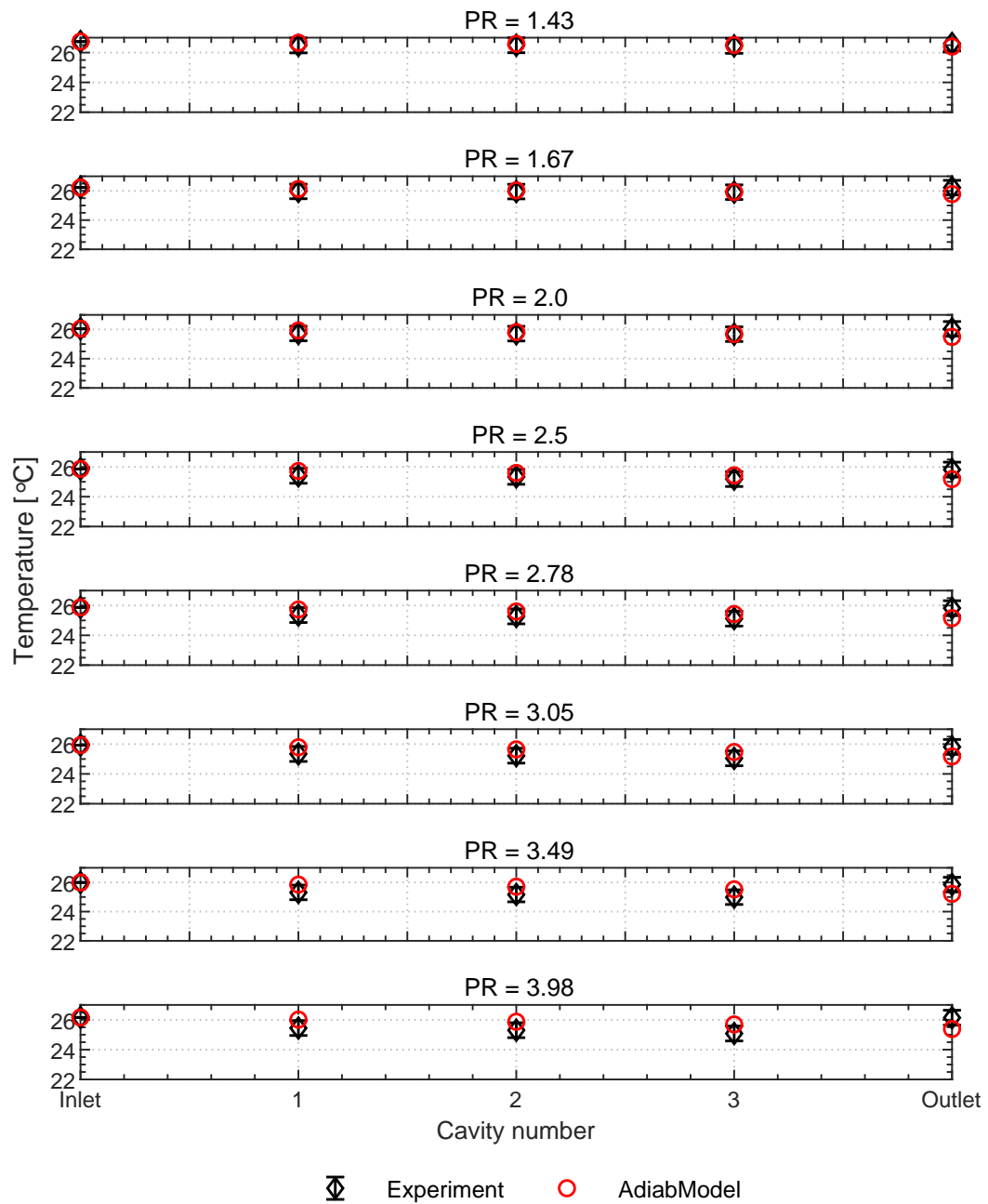
Figure D.27 – Comparison of cavity temperature distribution between experiment and the author model on Labyrinth seal (LSVP4T) at 5 bar inlet pressure, 25°C inlet temperature and varying PR with air as working fluid

D.2 Conical seals

Cavity pressure distribution
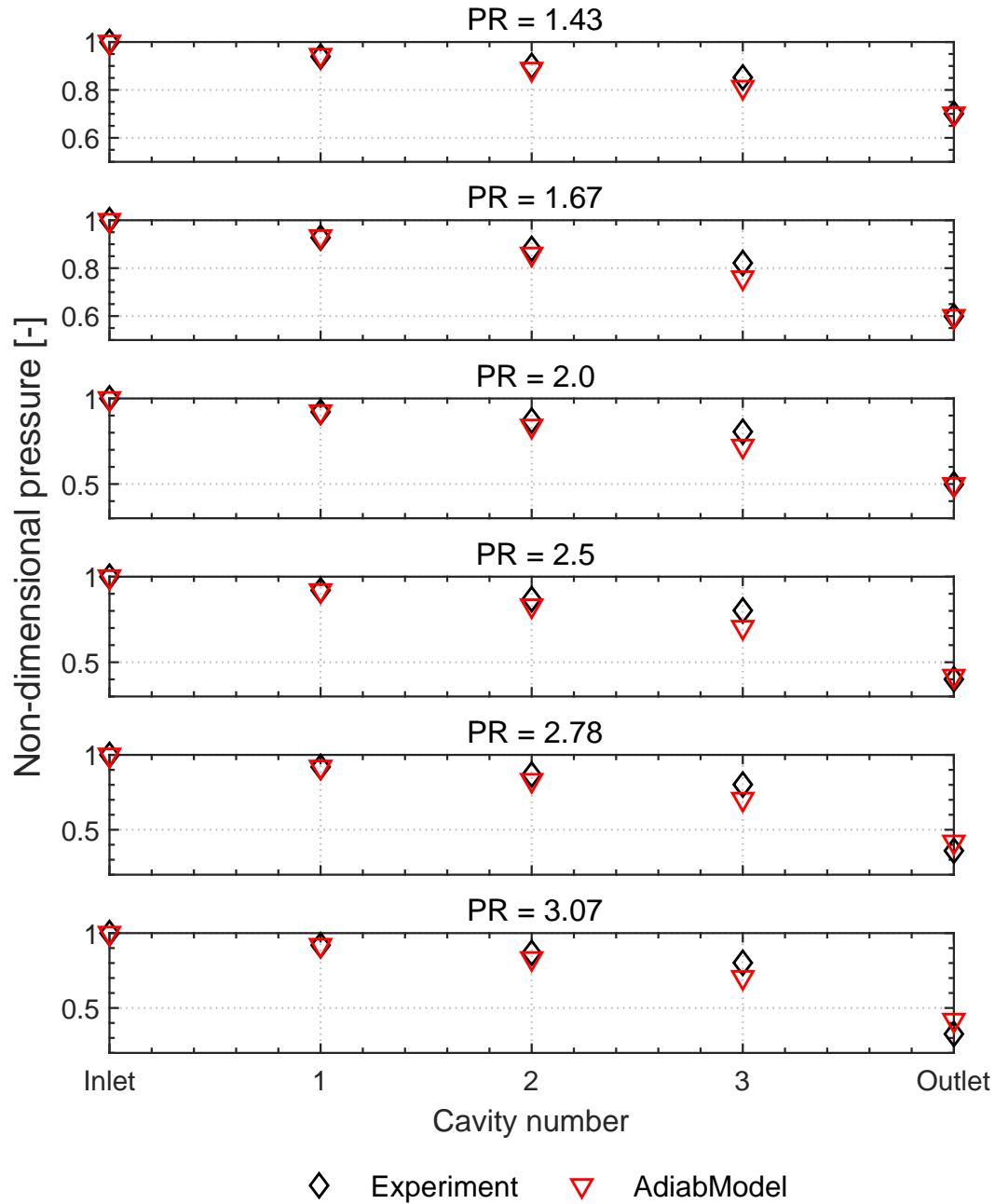
Figure D.28 – Comparison of cavity pressure distribution between the experiment and the author model at 5 bar inlet pressure, 25°C inlet temperature, varying PR and R134a as a working fluid
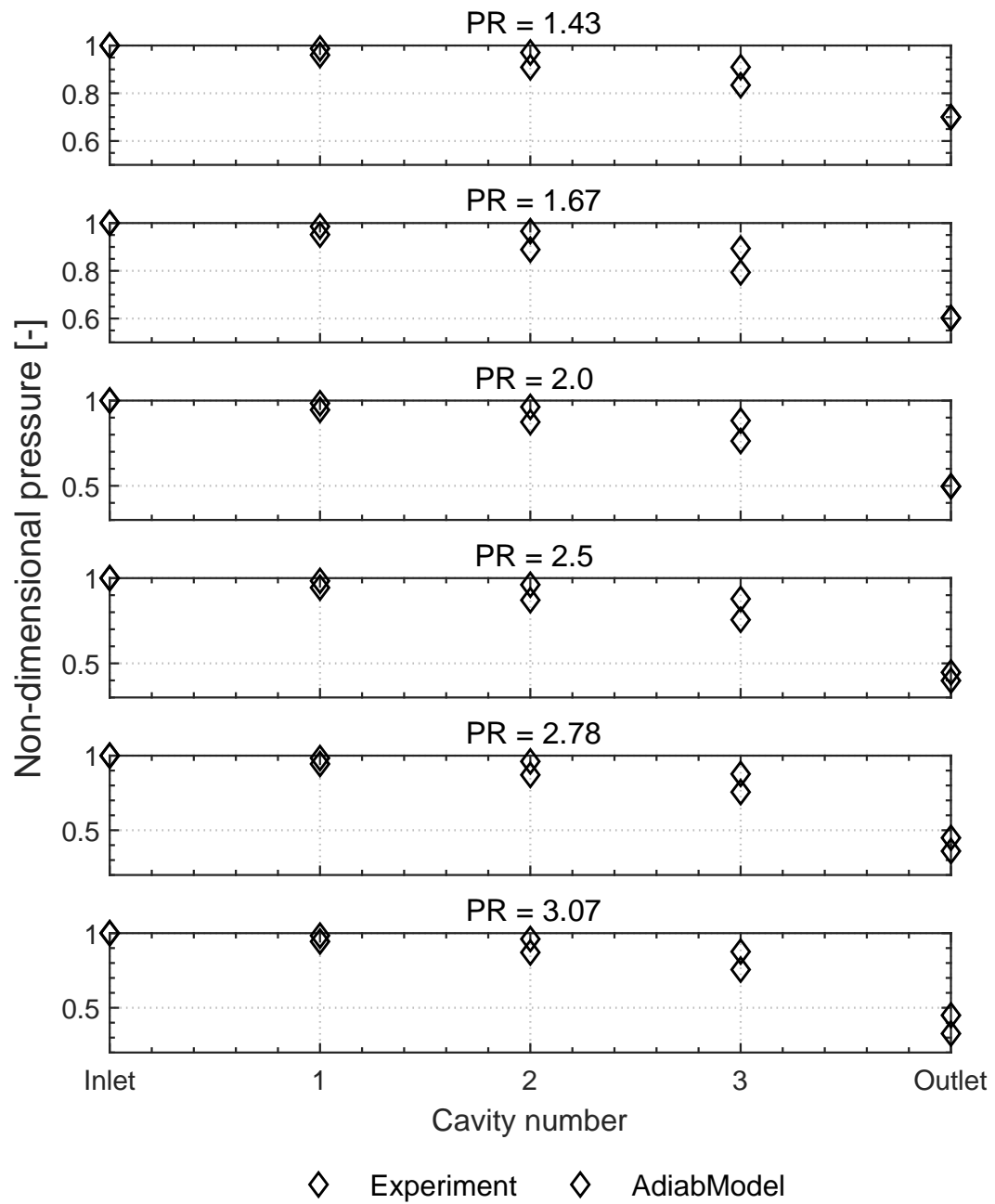
Figure D.29 – Comparison of cavity pressure distribution between the experiment and the author model at 5 bar inlet pressure, 25°C inlet temperature, varying PR and R134a as a working fluid

Cavity temperature distribution
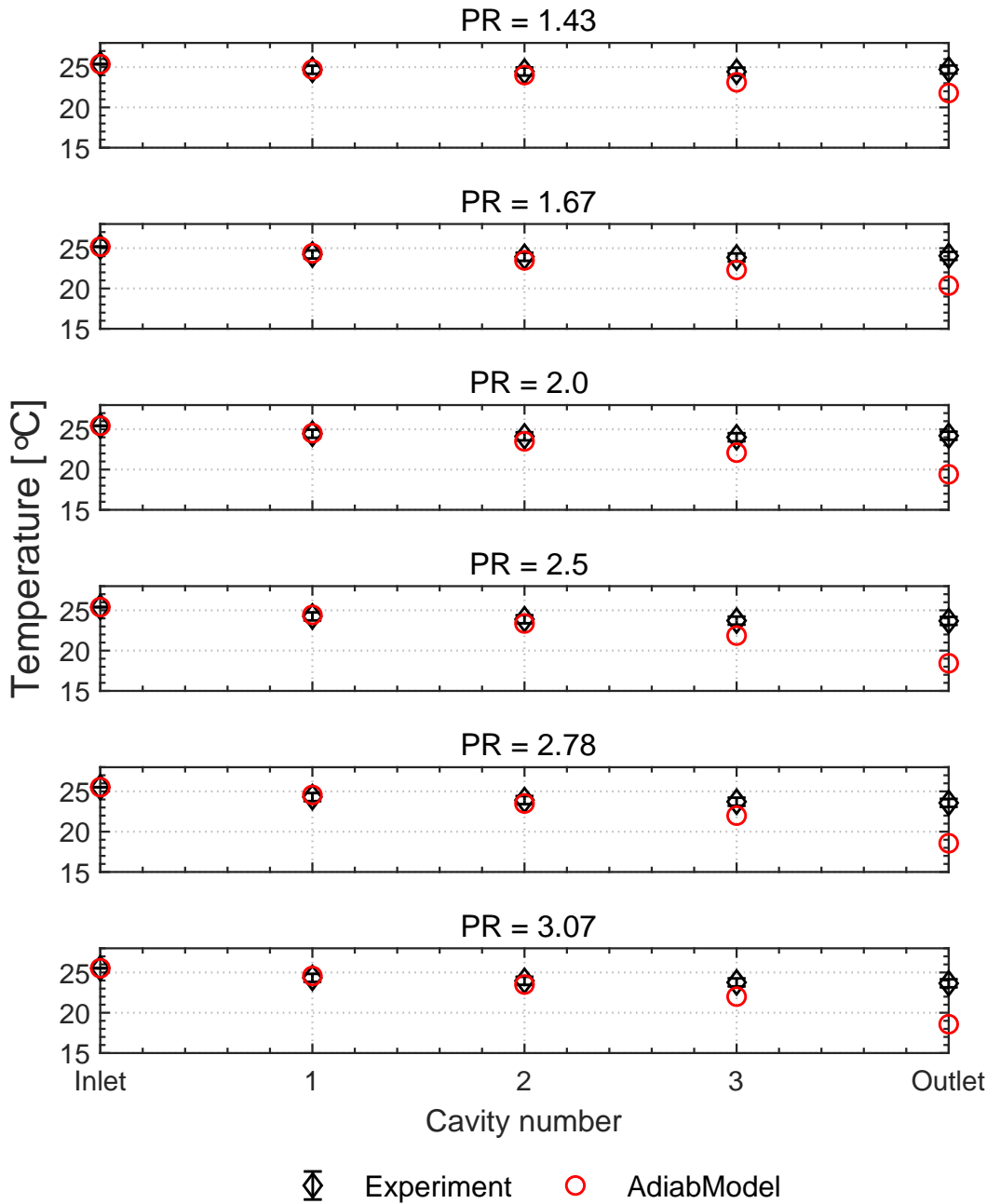
Figure D.30 – Comparison of cavity temperature distribution between experiment and author model on Labyrinth seal (LSVP4T) at 5 bar inlet pressure, 25°C inlet temperature and varying PR with R134a as working fluid
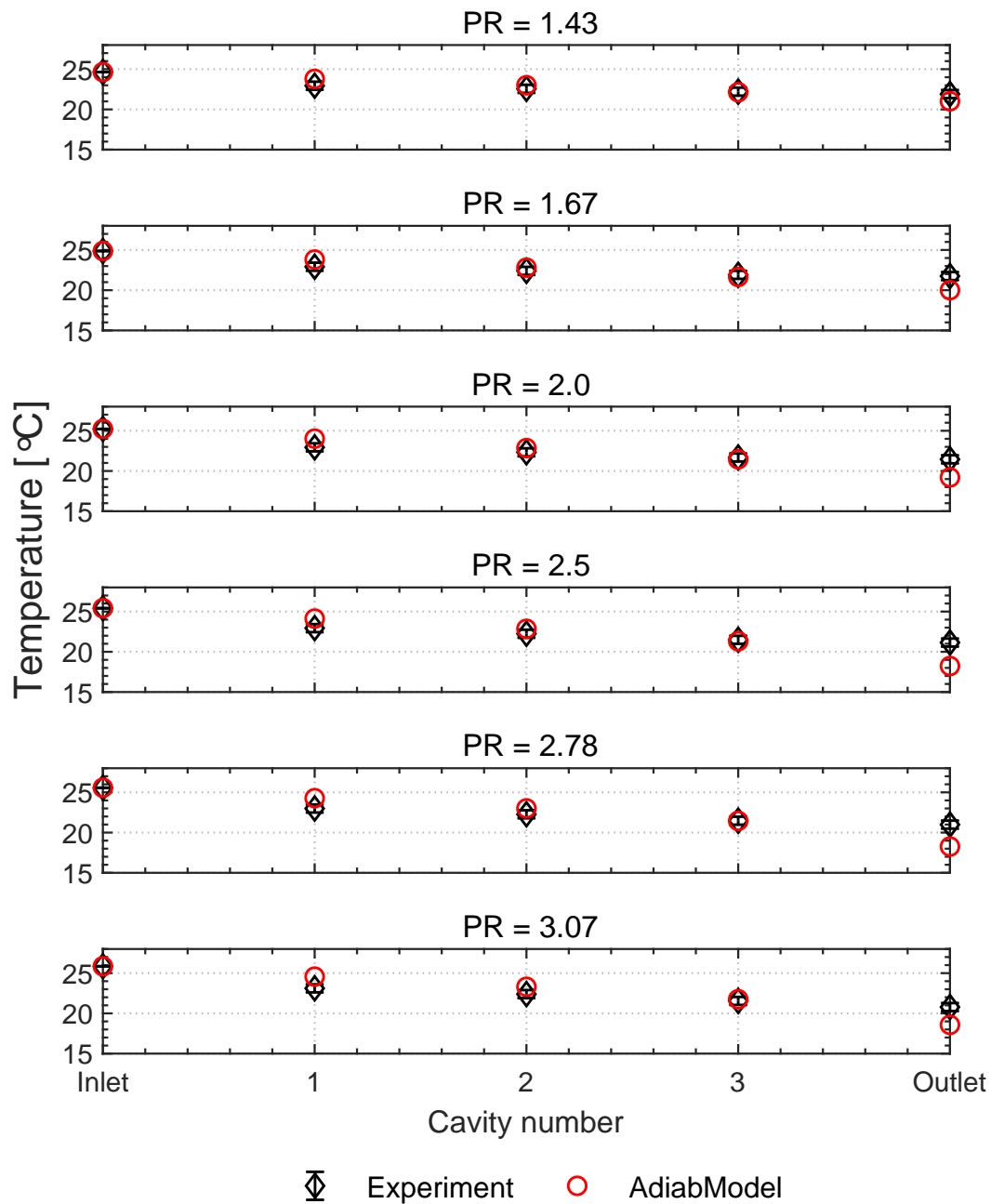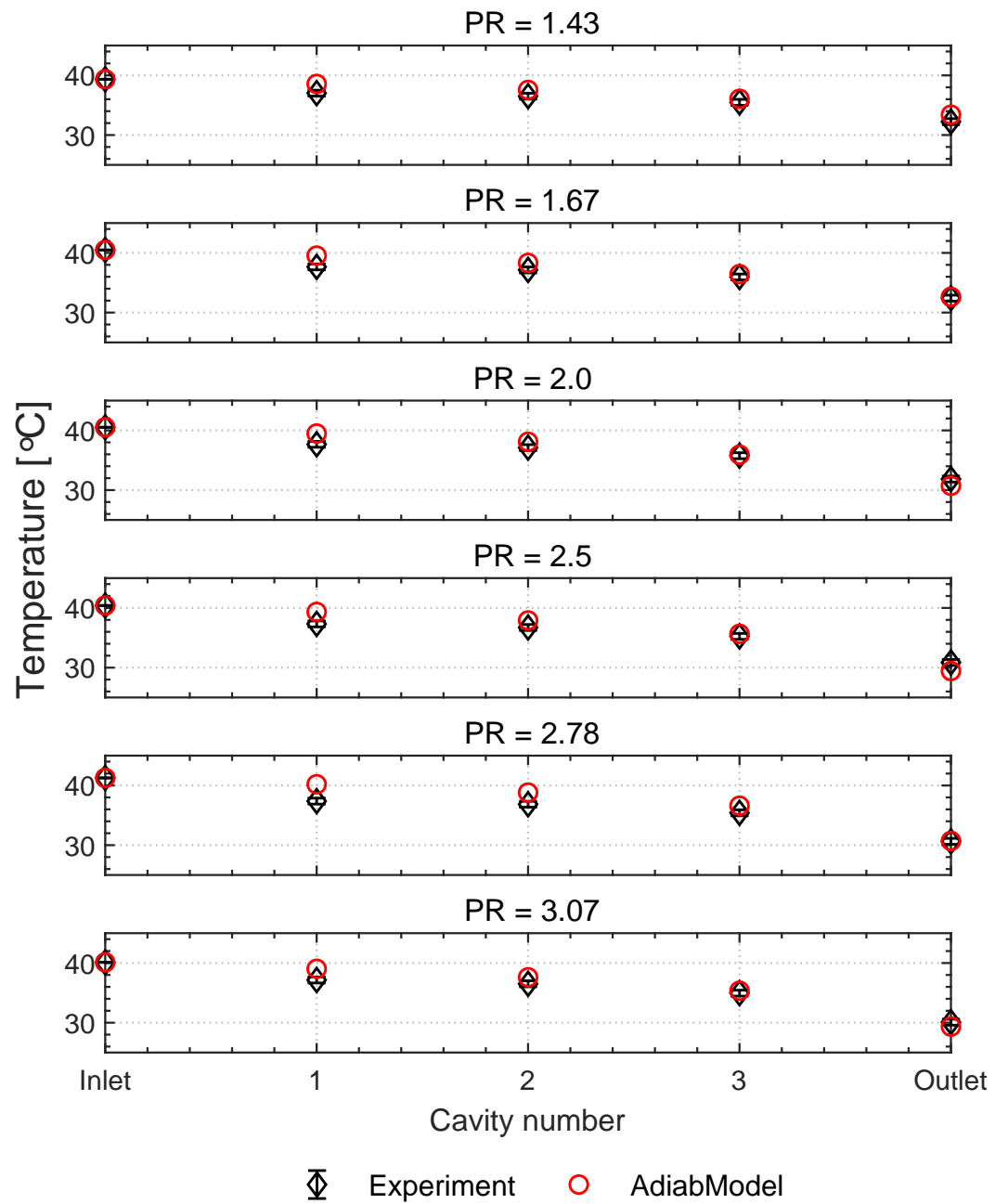
Figure D.31 – Comparison of cavity temperature distribution between experiment and author model on Labyrinth seal (LSCP4T) at 5 bar inlet pressure, 25°C inlet temperature and varying PR with R134a as working fluid

Bibliography

[1] J. Schiffmann and D. Favrat. Experimental Investigation of a Direct Driven Radial Compressor for Domestic Heat Pumps. *International Journal of Refrigeration*, 32:1918 – 1928, 2009.

[2] A. Javed, C. Arpagaus, S. Bertsch, and J. Schiffmann. Small-Scale Turbocompressors for Wide-Range Operation with Large Tip-Clearances for a Two-Stage Heat Pump Concept. *International Journal of Refrigeration*, 69:285 – 302, 2016.

[3] J. Demierre, S. Henchoz, and D. Favrat. Prototype of a Thermally Driven Heat Pump based on Integrated Organic Rankine Cycles (ORC). *Energy*, 41 (1):10 – 17, 2012.

[4] K. Isomura, M. Murayama, S. Teramoto, K. Hikichi, Y. Endo, S. Togo, and S. Tanaka. Experimental Verification of the Feasibility of a 100 W class Micro-Scale Gas Turbine at an Impeller Diameter of 10 mm. *Journal of Micromechanics and Microengineering*, 16 (9):254 – 261, 2006.

[5] A. M. Gamal, B. H. Ertas, and J. M. Vance. High-Pressure Pocket Damper Seals: Leakage Rates and Cavity Pressures. *ASME Journal of Turbomachinery*, 129:826 – 834, 2007.

[6] C. Floyd. Gas Seals for Rotating Shafts. *Tribology International*, 19, no. 4:204 – 211, 1986.

[7] R. K. Flitney. A Description of the Types of High Speed Rotary Shaft Seals in Gas Turbine Engines and the Implications for Cabin Air Quality. *Journal of Biological Physics and Chemistry*, 14:85 – 89, 2014.

[8] S. Florjancic. *Annular Seals of High Energy Centrifugal Pumps: A New Theory and Full Scale Measurement of Rotordynamic Coefficients and Hydraulic Friction Factors*. PhD thesis, Swiss Federal Institute of Technology (ETH) - Zurich, 1990.

[9] D. W. Childs and J. M. Vance. Annular Gas Seals and Rotordynamics of Compressors and Turbines. In *Proceeding of the 26th Turbomachinery Symposium*, College Station, Texas, USA, 1997. Texas A&M University, The Turbomachinery Laboratory.

Bibliography

[10] D. W. Childs. *Turbomachinery Rotordynamics: Phenomena, Modelling, & Analysis.* John Wiley & Sons Inc., New York, 1993.

[11] B. Ertas, A. Gamal, and J. Vance. Rotordynamic Force Coefficients of Pocket Damper Seals. *ASME Journal of Turbomachinery*, 128:725 – 737, 2006.

[12] J. Li, R. Aguilar, L. S. Andres, and J. Vance. Dynamic Force Coefficients of a Multiple-Blade, Multiple-Pocket Gas Damper Seal: Test Results and Predictions. *ASME Journal of Tribology*, 122:317 – 322, 2000.

[13] J. Vance, F. Zeidan, and B. Murphy. *Machinery Vibration and Rotordynamics.* John Wiley & Sons, Ltd, 2010.

[14] A. M. Gamal Eldin. *Leakage and Rotordynamic Effects of Pocket Damper Seals and See-Through Labyrinth Seals.* PhD thesis, Texas A&M University, 2007.

[15] B. K. Srinivas. Development and Validation of an Analytical Model for the notched Pocket Damper Seal. Master's thesis, Texas A&M University, 2003.

[16] D. Joachimiak. Universal Method for Determination of Leakage in Labyrinth Seal. *Journal of Applied Fluid Mechanics*, 13:935 – 943, 2020.

[17] R. E. Burcham. *Liquid Rocket Engine Turbopump Rotating Shaft Seals.* NASA, 1978.

[18] B. H. Ertas. *Rotordynamic Force Coefficients of Pocket Damper Seals.* PhD thesis, Texas A&M University, 2005.

[19] K. K. Nielsen, K. Joenck, and H. Underbakke. Hole-Pattern and Honeycomb Seal Rotordynamic Forces: Validation of CFD-based Prediction Techniques. *ASME J. Eng. Gas Turbines Power*, 134 (12):122505 – 122505–10, 2012.

[20] F. Y. Zeidan, R. X. Perez, and E. M. Stephenson. The Use of Honeycomb Seals in Stabilizing Two Centrifugal Compressors. In *Proceeding of the twenty-second Turbomachinery Symposium.* Texas A&M University, The Turbomachinery Laboratory, College Station, Texas, 1993.

[21] B. H. Ertas and J. M. Vance. Rotordynamic Force Coefficients for a New Damper Seal Design. *Journal of Tribology*, 129:365 – 374, 2007.

[22] B. Facchini, D. Massini, C. Bianchini, M. Micio, A. Ceccherini, and L. Innocenti. Flat Plate Honeycomb Seals Acoustic Analysis. In *Proceeding of 11th European Conference on Turbomachinery Fluid dynamics & Thermodynamics*, Madrid, Spain, 2015. ETC11.

[23] K. Müller, Heinz and S. Nau, Bernard. *Fluid Sealing Technology: Principles and Applications.* Mechanical Engineering. CRC press, New York Basel, first edition, 1998.

172

[24] S.M. Tibos, J.A. Teixeira, and C. Georgakis. Investigation of Effective Groove Types for a Film Riding Seal. *Journal of Engineering for Gas Turbines and Power*, 139:072503–1 – 8, 2017.

[25] J. Munson and G. Pecht. Development of Film Riding Face Seals for a Gas Turbine Engine. *Tribology Transactions*, 35:65 – 70, 1992.

[26] S. Mohsen and H. Hooshang. Performance of a Complaint Foil Seal in a Small Gas Turbine Engine Simulator Employing a Hybrid Foil / Ball Bearing Support System. *Tribology Transactions*, 44:3:458 – 464, 2001.

[27] O. Balje. *Turbomachines: A Guide to Design, Selection and Theory*. John Wiley & Sons Inc., New York, 1981.

[28] W. Wang, Y. Liu, and P. Jiang. Numerical investigation on influence of real gas properties on nonlinear behavior of labyrinth seal-rotor system. *Applied Mathematics and Computation*, 263:12 – 24, 2015.

[29] Z.M. Fairuz and I. Jahn. The influence of real gas effects on the performance of supercritical CO2 dry gas seals. *Tribology International*, 102:333 – 347, 2016.

[30] E. W. Lemmon, Ian H. Bell, M. L. Huber, and M. O. McLinden. NIST standard reference database 23: Reference fluid thermodynamic and transport properties-REFPROP, version 10.0, National Institute of Standards and Technology, 2018.

[31] A. Egli. The leakage of steam through labrinth seals. *Transactions of the ASME*, 57:115 – 122, 1935.

[32] H. Benckert and J. Wachter. Flow Induced Spring Coefficients of Labyrinth Seals for Application in Rotor Dynamics. In *NASA Conf. Pub. 2133 Rotordynamic Instability Problems in High-Performance Turbomachinery*, pages 189 – 212. Texas A&M Workshop, Texas, 1980.

[33] D. W. Childs and J. K. Scharrer. Experimental Rotordynamic Coefficient Results for Teeth-On-Rotor and Teeth-On-Stator Labyrinth Gas Seals. *Transactions of the ASME Journal of Engineering for Gas Turbines and Power*, 108 599:599 – 604, 1986.

[34] A. Picardo and D. W. Childs. Rotordynamic Coefficients for a Tooth-on-Stator Labyrinth Seal at 70 bar Supply Pressures Measurements Versus Theory and Comparisons to a Hole Pattern Stator Seal. In *Proceedings of ASME Turbo Expo 2004 Power for Land, Sea, and Air*, pages GT2004 – 53327, Vienna, Austria, 2004. ASME.

[35] F. Cangioli, P. Pennacchi, G. Vannini, L. Ciuchicchi, G. Riboni, A. Vania, and S. Chatterton. Sensitivity Analysis of the One-Control-Volume Bulk Flow Model for a 14 teeth-on-stator Straight-Through Labyrinth Seal. In *Proceeding of ASME*

Turbo Expo 2017*, Turbomachinery Technical Conference and Exposition*, Charlotte, NC, USA, 2017. ASME.

[36] F. Cangioli, S. Chatterton, P. Pennacchi, and L. Nettis. Thermo-elasto Bulk-flow Model for Labyrinth Seals in Steam Turbines. *Tribology International*, 119:359 – 371, 2018.

[37] F. Cangioli, G. Vannini, and T. Chirathadam. A Novel Bulk-Flow Model for Pocket Damper Seals. In *Proceedings of ASME Turbo Expo 2019 Turbomachinery Technical Conference and Exposition GT 2019*, pages GT2019 – 90059, Phoenix, Arizona, USA, 2019. ASME.

[38] G. Vannini, S. Cioncolini, V. Calicchio, and F. Tedone. Development of a High Pressure Rotordynamic Test Rig for Centrifugal Compressors Internal Seals Characterization. In *Proceedings of the 40th Turbomachinery Symposium*, pages 46 – 59, Houston, Texas, USA, 2011.

[39] V. Mounier. *Potential and Challenges of ORC driven Heat Pumps Based on Gas Bearing Supported Turbomachinery*. PhD thesis, École Polytechnique Fédérale de Lausanne, 2018.

[40] F. Cangioli, P. Pennacchi, G. Vannini, and L. Ciuchicchi. Effect of energy equation in one control-volume bulk-flow model for the prediction of labyrinth seal dynamic coefficients. *Mechanical Systems and Signal Processing*, 98:594 – 612, 2017.

[41] D. Eser and J. K. Kazakia. Air Flow in Cavities of Labyrinth Seals. *International Journal of Engineering Science*, 33:2309 – 2326, 1995.

[42] F. Cangioli, P. Pennacchi, L. Nettis, and L. Ciuchicchi. Design and Analysis of CFD Experiments for the Development of Bulk-Flow Model for Staggered Labyrinth Seal, Article ID 9357249. *International Journal of Rotating Machinery*, 2018.

[43] M. Arghir and A. Mariot. About the Negative Direct Static Stiffness of Highly Eccentric Straight Annular Seals. *Journal of Engineering for Gas Turbines and Power*, 137, 2015.

[44] T. Iwatsubo. Evaluation of Instability Forces of Labyrinth Seals in Turbines or Compressors. In *Proceedings of a workshop held at Texas A&M University, NASA CP No.* 2133, pages 139 – 137, Texas, USA, 1980. Texas A&M University.

[45] H. Black. Effects of Hydraulic Forces on Annular Pressure Seals on the Vibrations of Centrifugal Pump Rotors. *Journal of Mechanical Engineering Science*, 11(2), 1969.

[46] H. Black and D. Jenssen. Dynamic Hybrid Properties of Annular Pressure Seals. *Journal of Mechanical Engineering*, 184:92 – 100, 1970.

[47] R. Tiwari. *Rotor Systems Analysis and Identification.* CRC Press, Taylor & Francis Group, 2018.

[48] A. G. Kostyuk. A Theoretical Analysis of the Aerodynamic Forces in the Labyrinth Glands of Turbomachines. *Teploenergetica*, 419 (11):29 – 33, 1972.

[49] D. W. Childs and J. K. Scharrer. An Iwatsubo-based solution for Labyrinth Seals Comparison to Experimental Results. *Trans. ASME Journal of Engineering for Gas Turbines and Power*, 108:325 – 331, 1986.

[50] M. Kurohashi, Y. Inoue, T. Abe, and T. Fujikawa. Spring and Damping Coefficients of the Labyrinth Seal. In *Paper No C283/80 delivered at the Second International Conference on Vibrations in Rotating Machinery*. The Institute of Mechanical Engineering.

[51] K. Neumann. Zur Frage der Verwendung von Durchblicktungen im Dampfturbinebau. *Maschinentechnik*, 13:4, 1964.

[52] M. I. Gurevich. *The Theory of Jets in an Ideal Fluid.* Pergamon Press, 1966.

[53] H. Blasius. Forschungoarb. *Ing. - Wes*, 131, 1913.

[54] Y. Yamada. Transactions of Japan Society of Mechanical Engineers. 27, No 131:1267, 1961.

[55] T. Iwatsubo, N. Matooka, and R. Kawai. Flow Induced Force and Flow Patterns of Labyrinth Seals. In *NASA CP 2250 Proceedings of a Workshop at Texas A&M University*, pages 205 – 222, Texas, USA, 10 - 12 May 1982. Texas A&M University.

[56] D. Rhode. Simulation of Subsonic Flow Through a Generic Labyrinth Seal Cavity. ASME Paper No. 85-GT-76, 1985.

[57] H. Stoff. Incompressible Flow in a Labyrinth Seal. *Journal of Fluid Mechanics*, 100, part 4:817 – 829, 1980.

[58] S. B. Ahmed, B. A. Abass, and N. A. Hamza. Prediction of Carry-over Coefficient for Fluid Flow through Teeth on Rotor Labyrinth Seals Using Computational Fluid Dynamics. *Mathematical Theory and Modeling*, 3, No. 11:51 – 63, 2013.

[59] J. Scharrer. *A Comparison of Experimental And Theoretical Results For Labyrinth Gas Seals.* PhD thesis, Texas A&M University, 1987.

[60] H. R. Wyssmann, T. C. Pham, and R. J. Jenny. Prediction of Stiffness and Damping Coefficients for Centrifugal Compressor Labyrinth Seals. *ASME Trans. Journal of Engineering for Gas Turbines and Power*, 106:920 – 926, 1984.

[61] Joseph K. Scharrer. Theory Versus Experiment for the Rotordynamic Coefficients of Labyrinth Gas Seals: Part I—A Two Control Volume Model. *Journal of Vibration, Acoustics, Stress, and Reliability in Design*, 110:270 – 280, 1988.

Bibliography

[62] B. P. Williams and R. D. Flack. Calculation of Rotor Dynamic Coefficients for Labyrinth Seals. *International Journal of Rotating Machinery*, 4, No. 4:257 – 269, 1998.

[63] E. Klauk. Berechnung der rotordynamischen Koeffizienten von mit kompressiblen Median durchströmten Labyrinthdichtungen unter Anwendung von Mehr-Volumen-Modellen. Master's thesis, University of Kaiserlautern, 1987.

[64] H. P. Weiser. *Ein Beitrag zur Berechnung der dynamischen Koeffizienten von Labyrinthdichtungssystemen bei turbulenter Durchströmung mit kompressiblen Medien.* PhD thesis, University of Kaiserlautern, 1989.

[65] B. P. Williams and R. D. Flack. Evaluation of Rotordynamic Coefficients of Look-Through Labyrinths by Means of a Three Volume Bulk Model. In *Rotordynamic Instability Problems in High Performance Turbomachinery, proceedings of a workshop held at Texas A&M University*, pages 141 – 157, Texas, USA, 1990. Texas A&M University.

[66] L. F. Moody. Friction Factors for Pipe Flow. *Trans. ASME*, 66:671 – 684, 1944.

[67] C. F. Colebrook and C. M. White. Experiments with Fluid-Friction Roughened Pipes. In *Proc. R. Soc. Ser. A, 161*, page 367, 1937.

[68] P. Swamee and A. Jain. Explicit Equations for Pipe-Flow Problems. *Journal of Hydraulics Division-ASCE*, 102 (HY5):657 – 664, 1976.

[69] Y. Dereli. Comparison of Rotordynamic Coefficents for Labyrinth Seals using a Two-Control Volume Method. *Journal of Power and Energy*, 222 Part A:123 – 135, 2008.

[70] M. Kamouni and S. M. Abdelleh. CFD Predictions of Induced Fluid Forces and Dynamic Coefficients for a Compressor Eye Seal. *International Journal of Scientific & Engineering Research*, 7, 2016.

[71] D. L. Rhode and S. R. Sobolik. Simulation of Subsonic Flow Through a Generic Labyrinth Seal. *Journal of Engineering for Gas Turbines and Power*, 108:674 – 680, 1986.

[72] R. Nordmann, F. J. Dietzen, and H. P. Weiser. Calculation of Rotordynamic Coefficients and Leakage for Annular Gas Seals by Means of Finite-Difference Techniques. In *11th Biennial Conference on Mechanical Techniques*, Boston, USA, Sept. 1987.

[73] R. Nordmann and H. P. Weiser. Rotordynamic Coefficients for Labyrinth Seals Calculated by Means of a Finite-Difference Technique. In *NASA, CP 3026*. NASA, 1988.

[74] B. E. Launder and D. B. Spalding. The Numerical Computation of Turbulent Flows. *Computer Methods in Applied Mechanics and Engineering 3*, pages 269 – 289, 1974.

[75] P. J. Migliorini, A. Untaroiu, H. G. Wood, and P. E. Allaire. A Computational Fluid Dynamics/Bulk-flow Hybrid Method for Determining Rotordynamics Coefficients of Annular Gas Seals. *ASME Journal of Tribology*, 134 (2):0222021 – 9, 2012.

[76] P. J. Migliorini, A. Untaroiu, H. G. Wood, W. C. Witt, and N. R. Morgan. Hybrid Analysis of Gas Annular Seals with Energy Equation. *ASME Journal of Tribology*, 136 (3):0317041 – 9, 2014.

[77] T. Wu and L. San Andrés. Gas labyrinth seals On the effect of clearance and operating conditions on wall friction factors - A CFD investigation. *Tribology International*, 131:363 – 376, 2019.

[78] M. I. Gurevich. *The Theory of Jets in an Ideal Fluid*. Pergamon, New York, 1966.

[79] L. Joubert. Mathematical Modeling of Leakage Flow Through Labyrinth Seals. Master's thesis, Potchefstroom University for Christian Higher Education, 2003.

[80] B. Hodkinson. Estimation of the Leakage through a Labyrinth Gland. In *Proceedings of the Institution of Mechanical Engineers 141*, pages 283 – 288, 1939.

[81] M. Sriti, M. Agouzoul, D. Ouazar, and P. Micheau. Simulation Numerique D'Ecoulement Compressible dans les Joints Labyrinthe. *Journal De Physique*, III, 7 (5):1025 – 1037, 1997.

[82] G. Vermes. A Fluid Mechanics Approach to the Labyrinth Seal Leakage Problem. *Journal of Engineering for Power*, pages 283 – 288, 1961.

[83] J. Kiijarvi. Darcy Friction Factor Formulae in Turbulent Pipe Flow. *Lunowa Fluid Mechanics Paper*, n. 110727, 2011.

[84] Y. Yamada. Resistance of Flow Through an Annulus with an Inner Rotating Cylinder. *Bull J.S.M.E*, 5(8):302 – 310, 1962.

[85] J. K. Vennard and R. L. Street. *Elementary Fluid Mechanics*. John Wiley & Sons, New York, 1982.

[86] F. White. *Fluid Mechanics*. McGraw Hill, 8th edition, 2015.

[87] B.P. Williams. The Calculation of Rotordynamic Coefficients for Labyrinth Seals. Master's thesis, University of Virginia, 1992.

[88] E. Chance, Vipin V., Wesley Z., and Richard H. National Instruments LabVIEW: A Programming Environment for Laboratory Automation and Measurement. *JALA: Journal of the Association for Laboratory Automation*, 12(1):17–24, 2007.

Bibliography

[89] Z. Li, J. Li, and Z. Feng. Numerical Investigations on the Leakage and Rotodynamic Characteristics of Pocket Damper Seals-Part II: Effects of Partition Wall Type, Partition Wall Number, and Cavity Depth. *ASME Journal of Engineering for Gas Turbines and Power*, 137(3):032504, 2015.

[90] D. W. Childs and J. Wade. Rotordynamic-Coefficient and Leakage Characteristics for Hole-Pattern-Stator Annular Gas Seals–Measurements Versus Predictions. *ASME Journal of Tribology*, 126(2):326 – 333, 2004.

[91] D. W. Childs and C. H. Kim. Test Results For Round-Hole-Pattern Damper Seals Optimum Configurations and Dimensions for Maximum Net Damping. *ASME Journal of Tribology*, 108:605 – 609, 1986.

[92] G. L. von Pragenau. Damping Seals for Turbomachinery. In *Marshall Space Flight Center*, pages 438 – 451, Huntsville, Alabama, USA, 1982. NASA.

[93] D. W. Childs and C. H. Kim. Analysis and Testing of Turbulent Annular Seals with Different, Directionally Homogeneous Surface Roughness Treatments for Rotor and Stator Elements. *ASME Journal of Tribology*, 107:296 – 306, 1985.

[94] M. Arghir, F. Billy, G. Pineau, J. Fréne, and A. Texier. Theoretical Analysis of Textured 'Damper' Annular Seals. *ASME Journal of Tribology*, 129:669 – 678, 2007.

[95] D. W. Childs, Y.S. Shin, and B. Steifert. A Design to Improve the Effective Damping Characteristics of Hole-Pattern-Stator Annular Gas Seals. *Journal of Engineering for Gas Turbines and Power*, 130:012505, 2008.

[96] D. Childs, D. Elrod, and K. Hale. Annular Honeycomb Seals Test Results for Leakage and Rotordynamic Coefficients Comparisons to Labyrinth and Smooth Configurations. *Journal of Tribology*, 111:293 – 300, 1989.

[97] D. W. Childs and Z. Yu. Annular Honeycomb Seals Test Results for Leakage and Rotordynamic Coefficients Comparisons to Labyrinth and Smooth Configurations. *ASME Journal of Engineering Gas Turbines Power*, 120(4):778 – 783, 1998.

[98] G. Vannini, S. Cioncoloni, G. Del Vescovo, and M. Rovini. Labyrinth Seal and Pocket Damper Seal High Pressure Rotordynamic Test Data. *ASME Journal of Engineering Gas Turbines Power*, 136(2):022501, 2014.

[99] B. Richards, J.M. Vance, D.J. Paquette, and F.Y. Zeidan. Using a Damper Seal to Eliminate Sub-synchronous Vibrations in Three Back to Back Compressors. In *Proceedings of the 24th Turbomachinery Symposium*, Houston, Texas, September 26 - 28 1995. Texas A&M University, The Turbomachinery Laboratory.

[100] J. Li, P. Choudhury, and R. Tacques. Seal and Bearing Upgrade for Eliminating Rotor Instability Vibration in a High Pressure Natural Gas Compressor. In *Proceedings of the ASME Turbo Expo 2002*, Amsterdam, Netherland, June 3 - 6 2002. ASME.

[101] A. Lomakin. Calculation of Critical Number of Revolutions and the Conditions Necessary for Dynamic Stability of Rotors in High-Pressure Hydraulic Machines when Taking into Account Forces Riginating in Sealings. *Power and Mechanical Engineering (in Russian)*, 1958.

[102] H. Freitas, M. Oliveira, M. Jenkins, and O. Popjoy. The Focus Group, a Qualitative Research Method Reviewing the theory, and Providing Guidelines to Its Planning, ISRC Working Paper 010298. Technical report, Merrick School of Business, University of Baltimore (MD, EUA), 1998.

[103] David L. Morgan. *Focus Groups as Qualitative Research*, volume 16. SAGE publication, Thousand Oaks London, second edition, 1997.

[104] T. Kroll, R. Barbour, and J. Harris. Using Focus Groups in Disability Research. *Qualitative Health Research*, 17(5):690 – 698, 2007.

Suresh KATUWAL CHHETRI

Date/Place of birth	: March 28, 1984/ Nepal
E-mail	: suresh.katuwal.chhetri@gmail.com
Contact address	: Gratte Semelle 9, 2000, Neuchatel
	Switzerland

Education

2014 - 2020	**Doctoral student,** *Laboratory for Applied Mechanical Design (LAMD)* *École Polytechnique Fédérale de Lausanne (EPFL),* Switzerland
2010 - 2013	**Master of Science (M.Sc**.)**,** *University of Duisburg-Essen, Germany*
2002 - 2006	**Bachelor of Engineering (B.Eng.),** *Kathmandu University, Dhulikhel, Nepal*

Professional Experience

2012 - 2013	**Fraunhofer Institute for Solar Energy System,** *Freiburg, Germany*
	Fabrication of the fluid dynamic test facility for pressure loss measurement and flow visualization of heat exchangers
2006 - 2009	**Kathmandu University-Happy House Foundation (Switzerland),** *Nepal*
	Design, build and test of a temperature and humidity controlled solar coolstore system; Modification, installation and testing of pico-scaled axial flow turbines

Academic Experiences

2007 - 2009	**Kathmandu University**, Dhulikhel, Nepal
	'Mechanical Vibration, Sound, Noise and Acoustics', 'Refrigeration and Air-conditioning'

Languages

English	Fluent in speaking and writing
German	Intermediate in speaking and writing
Hindi	Fluent in speaking and writing
Nepali	Mother tongue

Personal interest

Trekking, Football, Billiard, Current affairs, Social service

Neuchàtel, 1 May 2020